UNIVERSITY OF WEST ATTICA

SCHOOL OF ENGINEERING

DEPARTMENT OF MECHANICAL ENGINEERING

TURBOPUMP DESIGN FOR CRYOGENIC ROCKET ENGINE

AUTHOR : EYAGGELOS TSICHLAS, SN:19392155

SUPERVISOR PROFESSOR : IOANNIS SARRIS

ACADEMIC YEAR 2023-2024

ATHENS

July 2024

ΤΡΗΜΕΛΗΣ ΕΞΕΤΑΣΤΙΚΗ ΕΠΙΤΡΟΠΗ

Α/Α	**Ονοματεπώνυμο**	**Βαθμίδα**	**Ψηφιακή υπογραφή**
1	Ιωάννης Σαρρής	Καθηγητής	Ioannis Sarris Digitally signed by Ioannis Sarris Date: 2024.09.26 19:57:01 +03'00'
2	Γεώργιος Σοφιάδης	Μεταδιδακτορικός ερευνητής	GEORGIOS SOFIADIS Digitally signed by GEORGIOS SOFIADIS Date: 2024.09.27 11:14:32 +03'00'
3	Ευάγγελος Καρβέλας	Μεταδιδακτορικός ερευνητής	Evangelos Karvelas Digitally signed by Evangelos Karvelas Date: 2024.09.26 22:25:44 +03'00'

ΔΗΛΩΣΗ ΣΥΓΓΡΑΦΕΑ ΔΙΠΛΩΜΑΤΙΚΗΣ ΕΡΓΑΣΙΑΣ

Ο κάτωθι υπογεγραμμένος Ευάγγελος Τσίχλας του Ιωάννη Τσίχλα, με αριθμό μητρώου 19392155 φοιτητής του Πανεπιστημίου Δυτικής Αττικής της Σχολής Μηχανικών του Τμήματος Μηχανολόγων Μηχανικών, δηλώνω υπεύθυνα ότι:

«Είμαι συγγραφέας αυτής της διπλωματικής εργασίας και ότι κάθε βοήθεια την οποία είχα για την προετοιμασία της είναι πλήρως αναγνωρισμένη και αναφέρεται στην εργασία. Επίσης, οι όποιες πηγές από τις οποίες έκανα χρήση δεδομένων, ιδεών ή λέξεων, είτε ακριβώς είτε παραφρασμένες, αναφέρονται στο σύνολό τους, με πλήρη αναφορά στους συγγραφείς, τον εκδοτικό οίκο ή το περιοδικό, συμπεριλαμβανομένων και των πηγών που ενδεχομένως χρησιμοποιήθηκαν από το διαδίκτυο. Επίσης, βεβαιώνω ότι αυτή η εργασία έχει συγγραφεί από μένα αποκλειστικά και αποτελεί προϊόν πνευματικής ιδιοκτησίας τόσο δικής μου, όσο και του Ιδρύματος.

Παράβαση της ανωτέρω ακαδημαϊκής μου ευθύνης αποτελεί ουσιώδη λόγο για την ανάκληση του πτυχίου μου».

Ο Δηλών

CONTENTS

ACKNOWLEDGEMENTS

I would like to thank my professor for supporting me and letting me try to work on such a difficult project. I would also like to thank the colleagues who freely gave me the CFturbo design program to implement my work, and the people who helped me a lot with the Simscale calculator and gave me extra computational resources and special flows. Finally, I want to thank my friends, family and fellow students who supported me psychologically and practically with my work.

ABSTRACT

In this thesis, a general report is made on the cryogenic rocket engines of spaceships using liquid fuels and a detailed description on the technical characteristics of a turbopump. Simultaneously, studies of various turbopumps that were used in known rockets are reported and the new current developments are analyzed. Next, all the laws of fluid mechanics that apply to a turbopump are described, as well as all the coefficients that determine its geometric characteristics and its durability. Subsequently, the design methodology of a turbopump for pumping liquid hydrogen and oxygen in detail using the CFturbo program. Finally, the CFD analysis for each component of the turbopump is conducted using the Simscale program. The results are evaluated, new suggestions for potential efficiency enhancements are proposed and general conclusions are drawn.

Unit 1: Introduction to liquid rocket engine

1.1 Liquid fuel spacecraft

As known, most spacecraft space missions are implemented using liquid fuels as they present a much higher degree of specific impulse Isp compared to those of solid fuels and hybrids (liquid oxidizer and solid fuel) [55] . In case of cryogenic rocket engine, the oxidizer and fuel are stored in liquid form under low temperature conditions. In this way, a greater amount of fuel is stored and volume is saved [55]. The liquid fuel and oxidizer are pumped and pressurized at high pressure into the combustion chamber of the rocket engine[55]. Before the fuel enters the combustion chamber it first flows through passages at high speed inside the walls of the rocket engine and cools it. After the combustion is done, the exhaust gases are expanded and exit the nozzle at high pressure and speed. With this method, the rocket engine is protected from thermal stress as very high temperatures develop inside the combustion chamber. A classic case is the cryogenic rocket engine that burns liquid hydrogen fuel with liquid oxygen. [1]. Also, there are liquid fuels which aren't in cryogenic state. For example, hydrazine and kerosene (RP-1) [55]. In this case the fuel cools the rocket engine but it isn't cryogenic.

Picture 1: The F-1 engine, with 1.5 million pounds of thrust, was the powerplant for the first stage of the 363-foot long Saturn V launch vehicle that took astronauts to the Moon for six successful landing missions between 1969 and 1972 in the Project Apollo program *[2]*.

Picture 2 The RS-25 engine, which successfully powered the space shuttle, is being modified for America's next great rocket, the Space Launch System *[3]*.

The table below lists the most well-known and widespread fuels and oxidizers used in liquid rocket engines [55].

Chemical properties	**Liquid fuels**			**Liquid oxidizers**	
	Hydrazine	**Liquid natural gas**	**Liquid hydrogen**	**Liquid fluorine**	**Liquid oxygen**
Melting point (^0C)	2	-183	-259	-220	-222
Boiling point (^0C)	104	-162	-253	-188	-183
Heat-producing energy (Kj/Kg)	28.000	55.000	120.000	-	-
Density (Kg/m^3)	1010	422	71	1509	1142
Stability	Toxic & flammable	Toxic & flammable	flammable	Very toxic & flammable	good
storage	normal	cryogenic	cryogenic	cryogenic	cryogenic

Since liquid rocket engines, which are commonly used in launches, have a leading role in international space missions, they are still prone to failure, so the risk and cost remain high[54].

Picture 3 *The space shuttle was NASA's space transportation system. It carried astronauts and cargo to and from Earth orbit. The first space shuttle flight took place April 12, 1981. The shuttle made its final landing July 21, 2011. During those 30 years, the space shuttle launched on 135 mission[4]*

Picture 3 A long March 5B rocket lifts off from the Wenchang launch center May 5. Credit: CASC *[5]*

1.2 Liquid fuel storage systems

Fuel and oxidizer are stored in separate tanks. They should be relatively light. When the fuel and oxidizer are in cryogenic conditions then they must be both durable and insulated [6].They are usually made of aluminum alloys. In order to maintain low temperatures, polyurethane, mud or polystyrene coating is used as thermal insulation. Also, it should be noted that the choice of material for the tanks also depends on the fuel or oxidizer itself that will be stored. The table below show various materials that are conventional for two classic examples, liquid hydrogen and liquid oxygen.

Liquid substance	**Conventional materials of tanks**
Liquid hydrogen	Aluminum allows, Nikel allows, stainless steel
Liquid oxygen	Aluminum allows, Nikel allows, stainless steel, copper, Teflon

[55]

The pictures below show the shape of these tanks and how they are positioned in the spaceships liquid fuel storage system

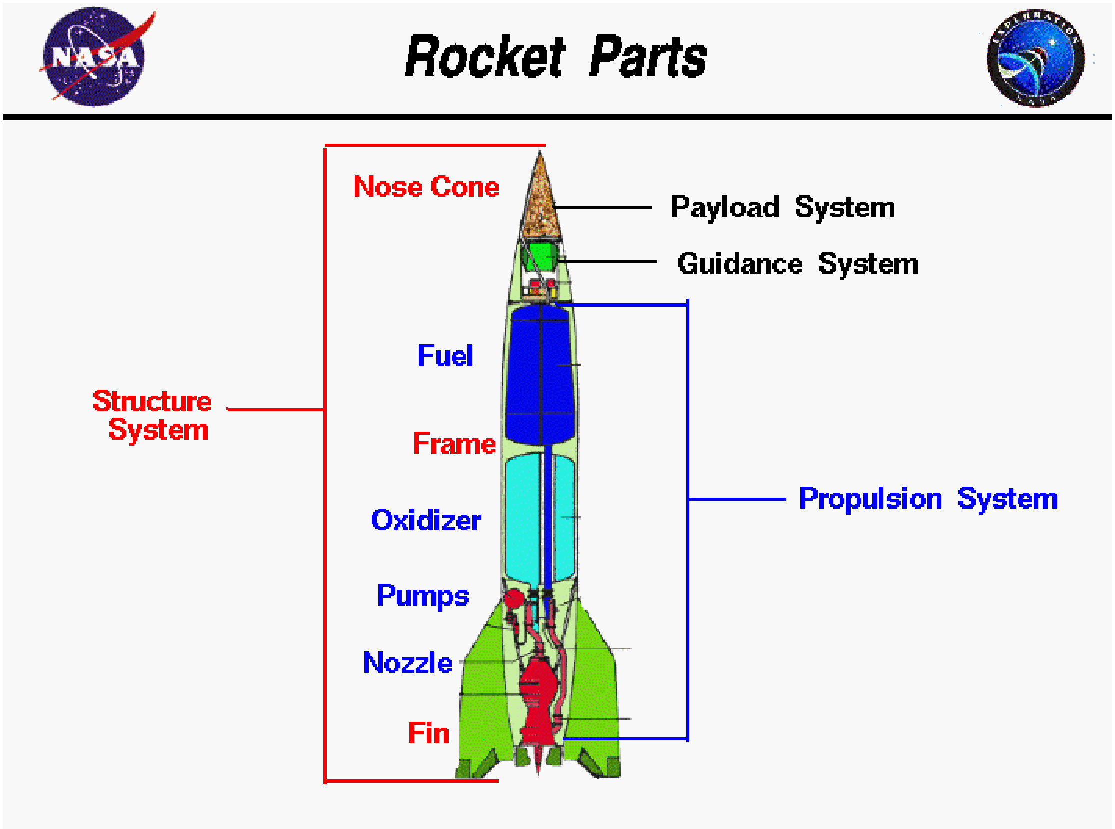

Picture 4 Rocket parts The structure of the V-2 ballistic missile system is presented [7]

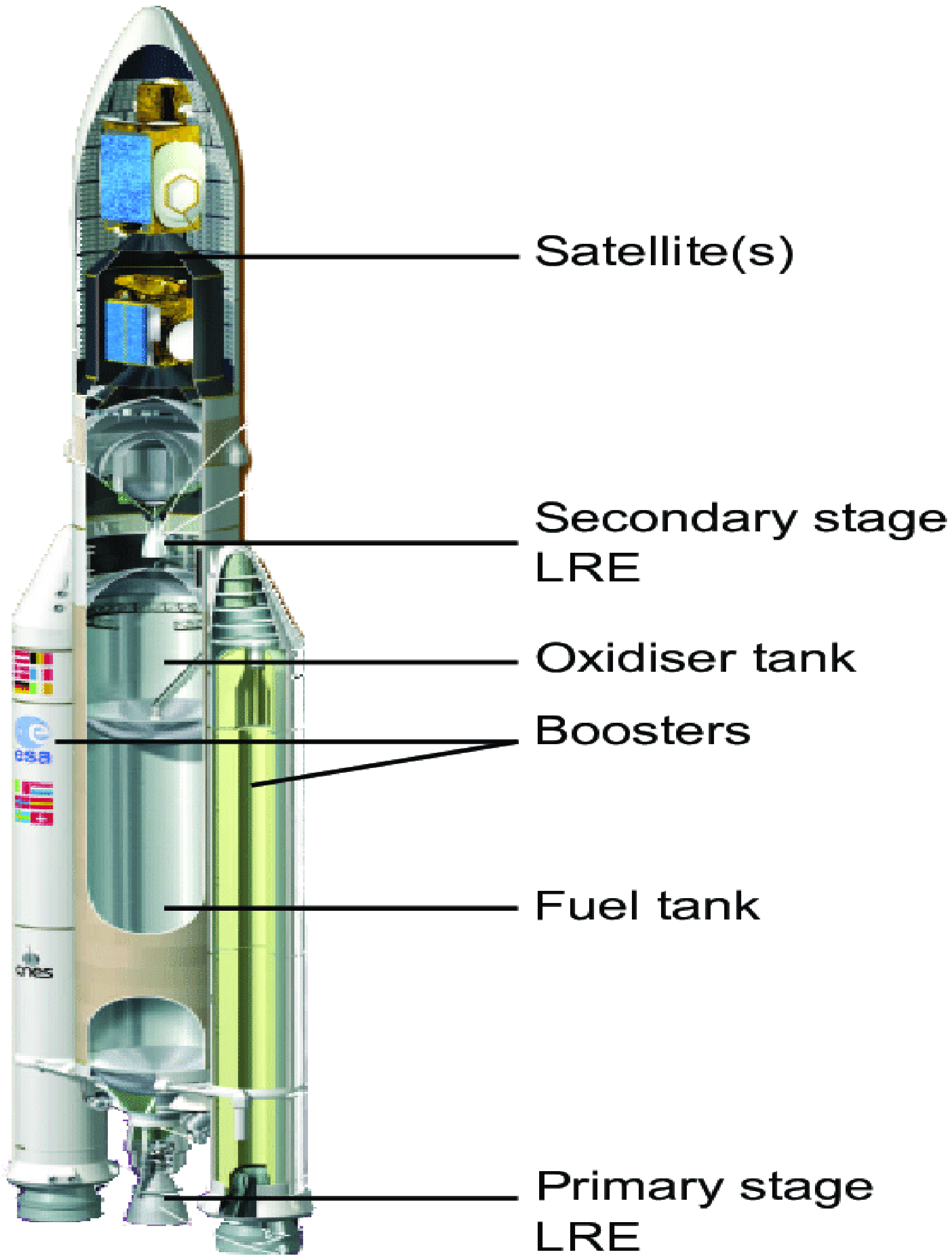

Picture 5 The main components of the Ariane 5 european space launcher [8]

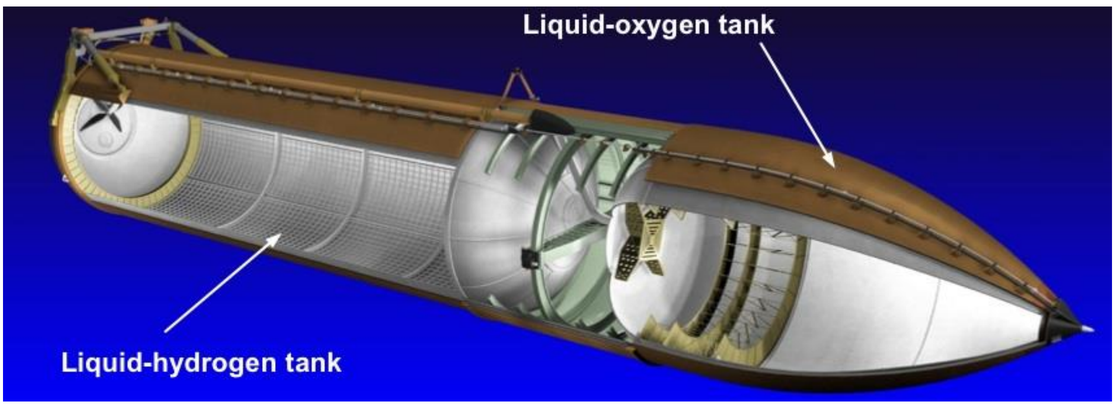

Picture 6 Internal structure of the external space shuttle tank [9]

1.3 Liquid fuel pumping systems

Generally, there are two kinds of pumping systems of liquid fuel in the liquid rocket engines. The pressure vessel system and the turbopump system. In the turbo pump system these is also a pressure vessel but only to prevent cavitation in the pumps[10]. These systems present the following technical characteristics :

- PRESSURE VESSEL SYSTEM : Inert gas is usually stored there, for example nitrogen or helium under very high pressure in a vessel [55]. Typical values of this pressure are from 69 bar to 690 bar [10], depending on the thrust requirements and the hydraulic losses that occur during pumping . The high pressure of the gas pushes the liquid fuel and oxidizer to mix in the combustion chamber of the rocket engine. In this way, the total hydraulic is secured, losses are overcome and the required pressure in the combustion chamber is ensured. The pressure is regulated with the use of special valves. The main advantages of this system are its reliability [55] and that it hasn't got moving parts. But they are not preferred for high-thrust launches or long missions because large pressure vessel sizes will be required. This results in an excessive increase in the weight of the spacecraft [11]. For this reason, these systems are used in the smaller missions of spacecraft which don't have particularly high thrust requirements [55].

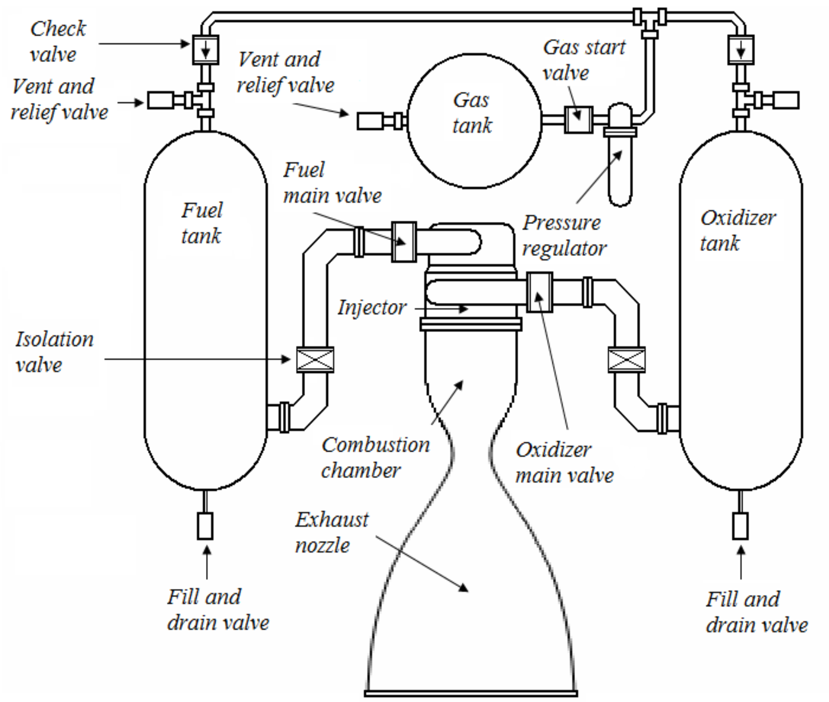

Picture 7 Scheme of a engine with pressurized gas propellant feed system *[10]*

- TURBOPUMP SYSTEM : This system although more complex in construction, plays a dominant role in liquid rocket engines for many reasons. First, it can secure very high pressure in combustion chamber. Second, it is very lightweight, it has small volume and develops a very high thrust relative to its volume[11]. Two centrifugal pumps pump the fuel and the oxidizer from tanks and they press them with high pressure in the combustion chamber. These pumps are rotated by a turbine that runs on a very small amount of fuel in a pre-burner or by exploiting the heat generated by the rocket engine. Furthermore, Turbopump systems are usually also combined with smaller pressure vessels which offer a little assistance .

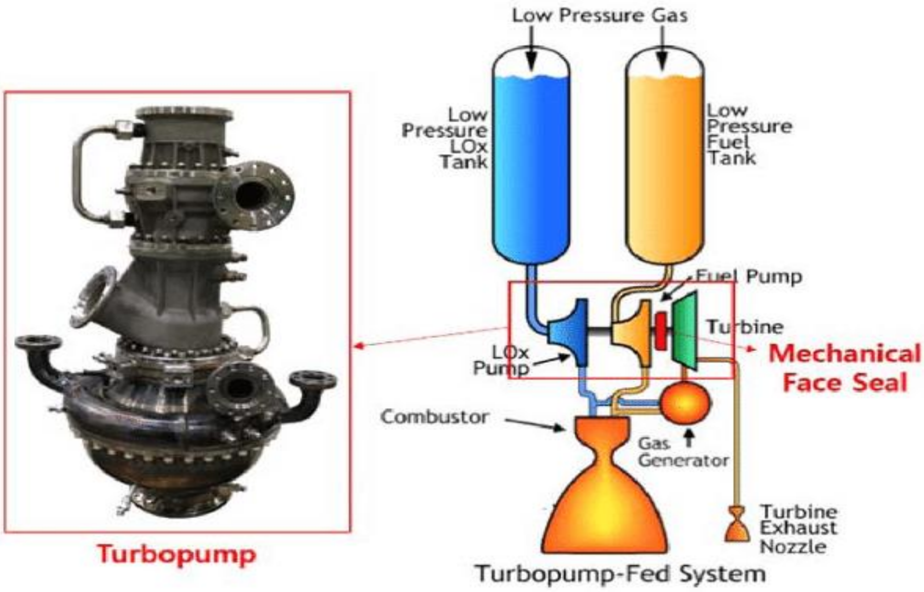

Picture 8 Configuration of 7-ton class turbopump and layout of turbopump type rocket engine *[12]*

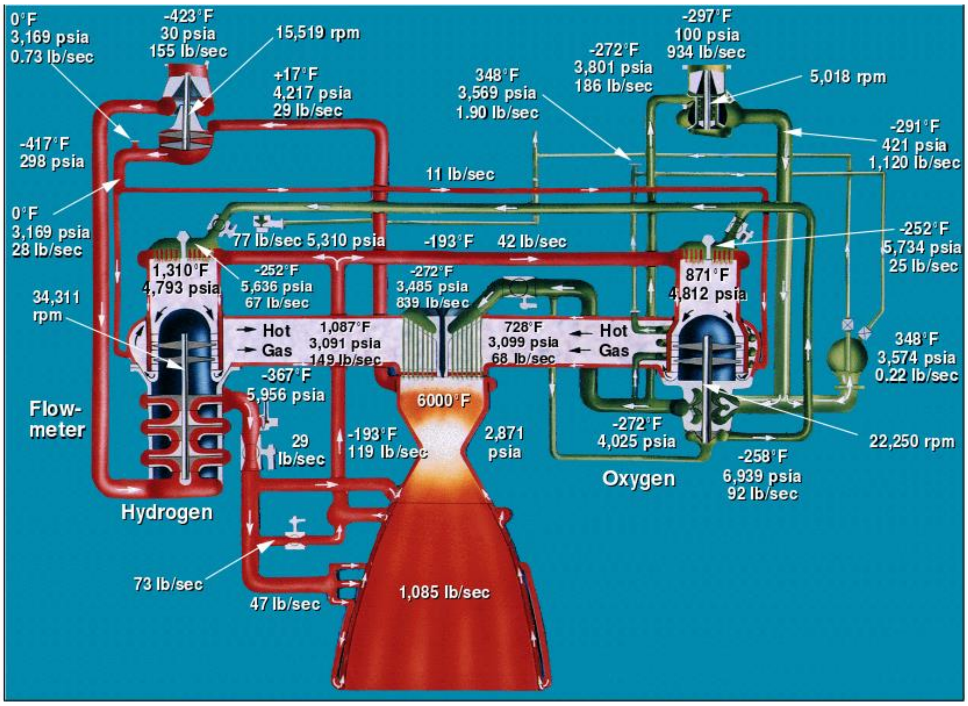

Picture 9 The Space Shuttle Main Engine (SSME) Propellant Flow Schematic *[13]*

Unit 2 General description and the structural parts of a turbopump

2.1 Development history of the turbopump and its current developments

The idea of developing the turbopump came from physics professor Robert Hutchings Gorddad, in 1934. He is considered the father of modern rocket propulsion as he was the one who built and successfully tested the first liquid fuel rocket launch in 1926 [14],[15]. However, the idea the idea that would grow to become the modern rocket turbopump begins life on the design offices in Kummersdorf, Peenemünde and Frankenthal in 1935 in German. Presented by Robert J Dalby. This turbopump was used for program V-2 rockets[16]. Over the years turbopumps evolved and have been used in aerospace for many decades [10]. Nowadays, the 59% of launch failures are attributed to the propulsion system. The main reasons for propulsion system failure are burner instability and turbopump inaccuracy. Due to cavitation instability in pumps, many space missions have failed. Notable examples include NASA's Apollo, Fastrac programs, ESA's Vulcain program, and JAXA's LE-7 program. Unfortunately, cavitation instability in these pumps has not been fully understood to date, and there is no established method for predicting it during the design process [11].

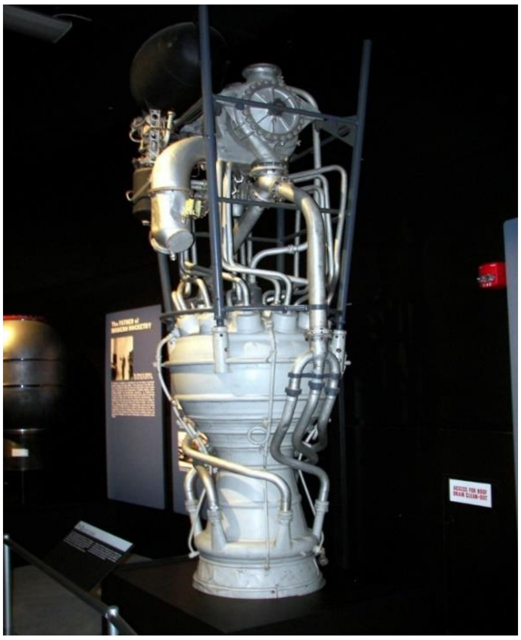

Picture 11 V-2 engine on display at the NationalMuseum of the United States Air Force near Dayton, Ohio *[17]*

Picture 10 The V-2 rocket that was successfully launched on October 3, 1942 *[18]*

2.2 Turbopump structure

The following images show the external form of a turbopump :

Picture 13 This turbopump, intended for the SpaceX Merlin engine, is one of many designs manufactured by Barber-Nichols. The company credits work it did on NASA's Fastrac program with enabling better and cheaper methods of building these machines. Credit: Barber-Nichols Inc [19]

Picture 11 Inducer and impeller and turbine of a rocket engine turbopump [11]

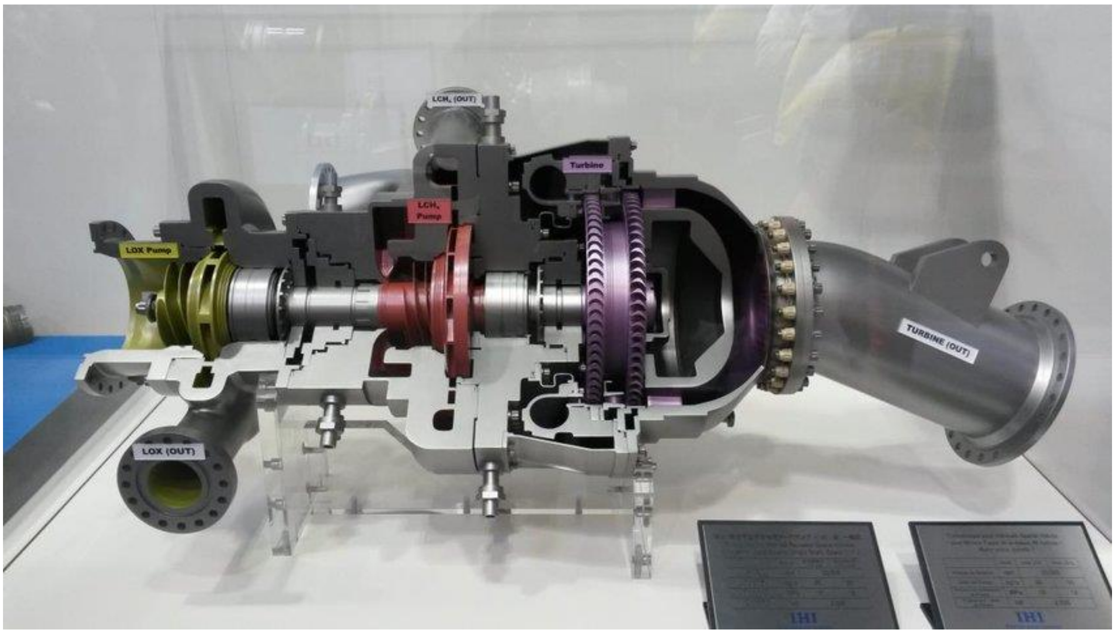

Picture 12 LOX/CH4 single stage single shaft turbopump - Le Bourget 2015 [20]

A simple classical turbopump consists of the following main mechanical components:

1) INDUCER : The inducer essentially is an endless scroll which is positioned in front of the centrifugal pump impeller. It is an integral part of the pump and is necessary to combat cavitation [55]. Cavitation is a phenomenon where vapor bubbles which form

in the flowing fluid collapse suddenly – potentially causing surface damage of the impeller, performance degradation, as well as catastrophic failure. The inductor must be properly designed to protect the pump from cavitation .The number of vanes ranges from 3 to 4 typically [21].

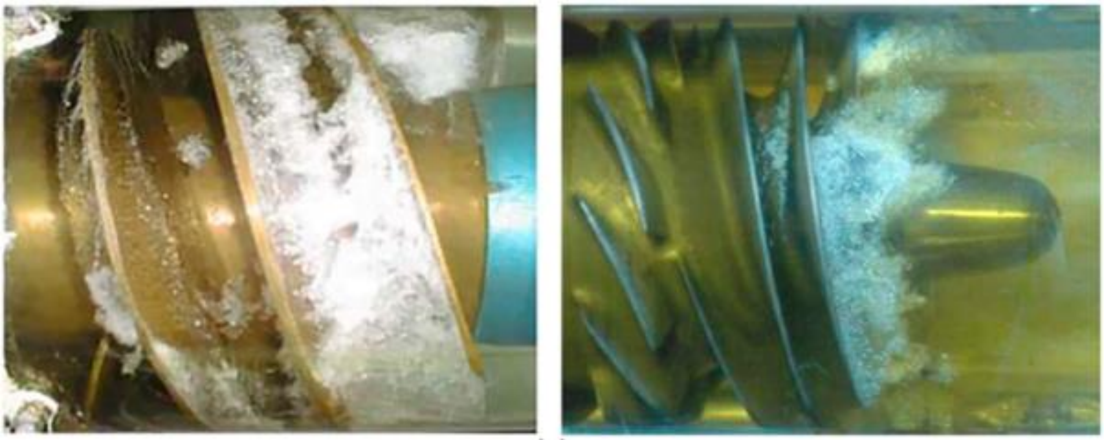

Picture 13 Cavitation is turbopump inducers. Here is shown the vaporization of the fluid that occurs on the vanes of the switch during its operation *[11]*

Picture 14 Model a typical inducer *[22]*

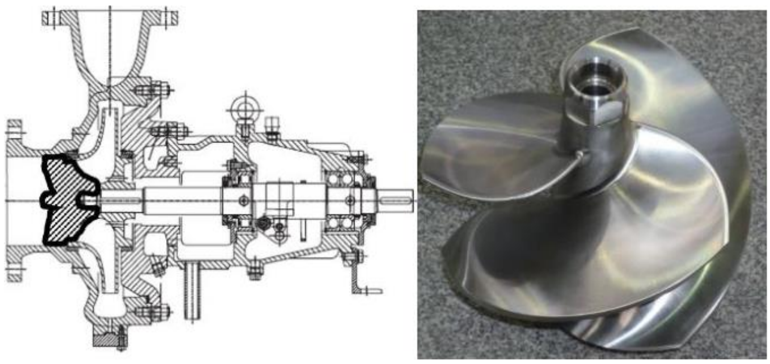

Picture 15 . Inducer (bold black line) placed in front of impeller in centrifugal pump and photo of inducer *[23]*

2) CENTRIFUGAL IMPELLER : In these applications, the pump must be able to significantly increase the pressure of the fuel and oxidizer. The centrifugal pump has been an important element of the history of pump-fed liquid propellant rocket engines. The use of this type of pump is the resultant of its relative simplicity and reliability, wide opcrating flow range, and adequate performance[24]. The hydraulic efficiency can exceed 80% [25].

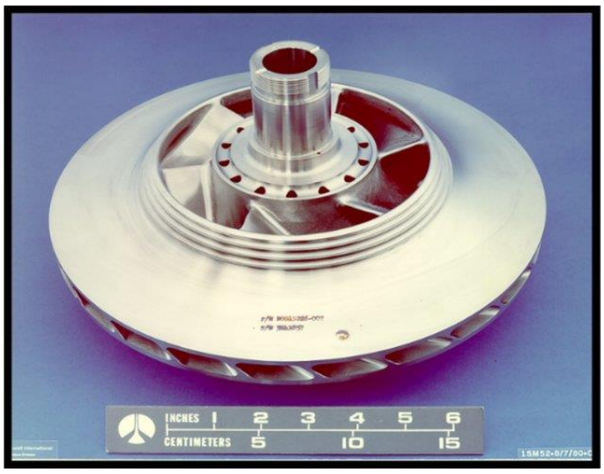

Picture 16 A typical impeller with inducer *[26]*

Picture 17 A Ti-5Al-2.5Sn fuel pump impeller used in the space shuttle main engine *[27]*

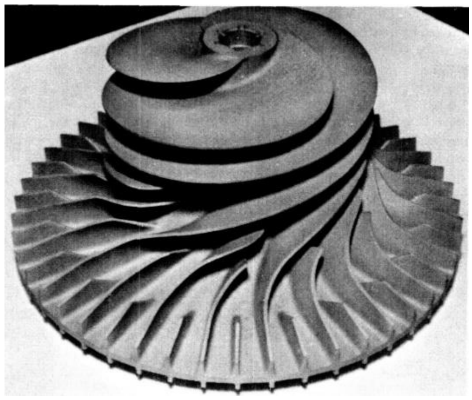

Picture 20 A typical impeller with inducer *[28]*

Picture 18 *typical unshrouded LH_2 pump impeller (NERVA I)[24]*

3) VOLUTE-DIFUSSER : It is the classic volute - diffuser used in centrifugal water pumps as well. It has the geometry of a spiral and ensures an additional increase in the static pressure of the fluid. This is achieved via a gradually increasing cross-sectional area in the volute that increases the fluid's flow-through area, thus increasing the static pressure of the fluid [29]. The diffuser gives an additional pressure increase at the outlet [30].

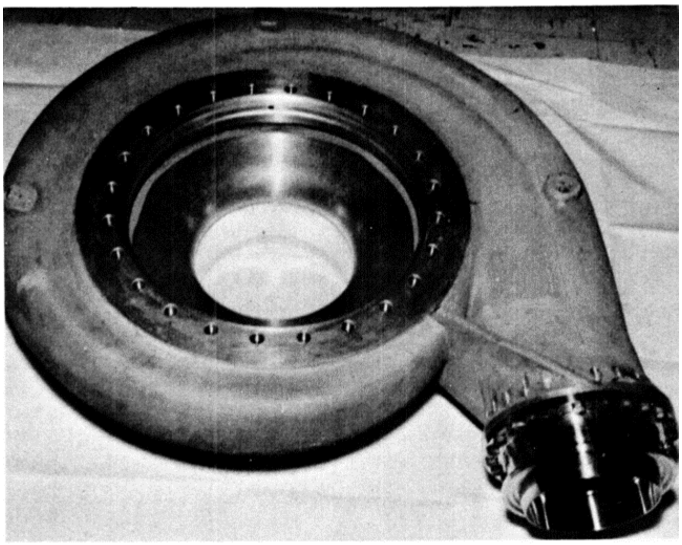

Picture 19 LH_2 pump housing with diffusers (NERVA I) [24]

4) TURBINE: Key role rotates the pumps very quickly. It can operate at various pressures and temperatures.They are usually axial.

Picture 20 Turbine rotor (blisk type) [31]

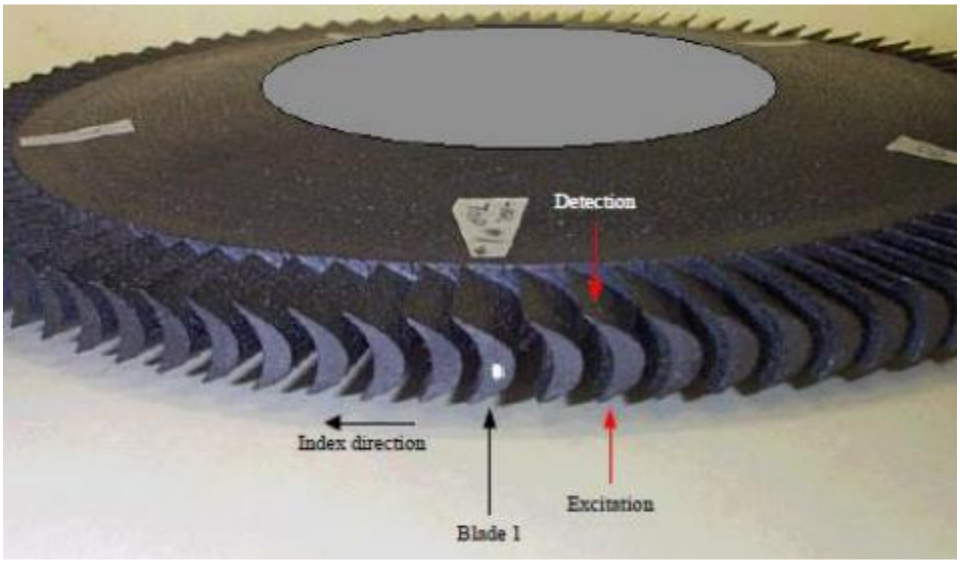

Picture 21 : Photo of SIMPLEX turbopump blisk (Courtesy of NASA MSFC) [32]

In addition to these main components, the centrifugal pump also includes the casing, which houses all the aforementioned parts, specifically bearings for support and sealing, and the inlet and outlet pipes of the system.

Additionally, there are several cases where the fuel pump must operate at different speeds than the oxidizer pump for various technical and design reasons. For this reason, in some cases the oxidizer and fuel pumps work together and rotate with the turbine with a gearbox.

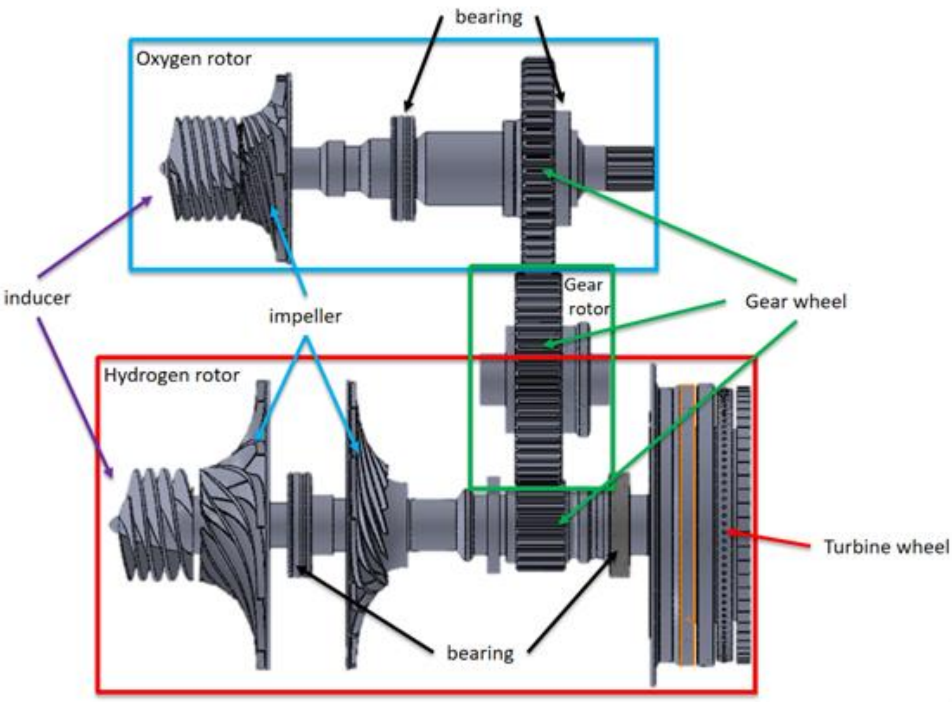

Picture 22 Internally geared turbopump model - A standard schematic of an internally geared turbopump consists of the liquid hydrogen (LH2, fuel) and liquid oxygen (LO2, oxidizer) rotors [33]

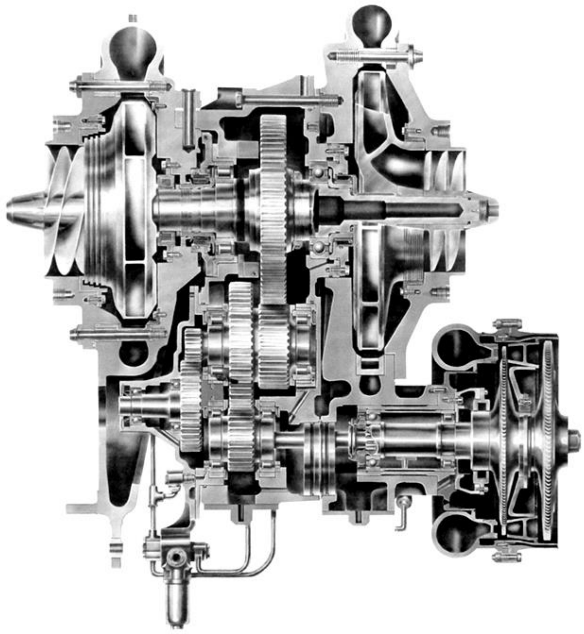

Picture 23 NASA's propulsion-system turbopumps, such as the Rocketdyne Mark-3 turbopump shown here, are sophisticated, complex, and expensive. As part of an effort to develop smaller, simpler, more affordable turbopumps for smaller spacecraft, Marshall Space Flight Center engineers created the Generalized Fluid System Simulation Program (GFSSP) to simultaneously analyze all the interacting flows in these intricate machines [34]

Materials used in turbopumps

For these applications, construction materials must strictly adhere to two basic criteria: high resistance to thermal stress and being very lightweight. Turbopumps are typically made from titanium or nickel alloys or titanium alloys[1]. Also, the gears of gearbox are made from various alloy AISI or AMS [35]. It is very important to select the material of a turbopump because Turbopump weight continues to be a dominant parameter in the trade space for reduction of engine weight . The table below lists some common materials used in these applications.

MATERIAL	$\sigma_{0,2}$	σ_{TS} (Mpa)
99,2Ti	450	525
Ti-5Al-2,5Sn	800	900
Ti-6Al-4V	950	1000
Al2014-T6	430	480
Inconel 718	760	860

[57],[36],[54]

2.3 Analysis of combustion cycles

The method by which a turbopump system is implemented and operated in a liquid rocket engine varies depending on the load and thrust requirements for the launch. For these reasons, certain combustion cycles have been developed with which a turbopump can operate.

1) OPEN CYCLE GAS GENERATION : In this cycle, a small amount of oxidizer and fuel are burned separately in a preburner and the exhaust gases produced are blown into the air turbine and then released into the environment. This cycle satisfies high thrust loads and is reliable but has poor efficiency as extra heat is wasted which is released to the environment and not utilized by the engine. It is simple in design without much complexity[37].

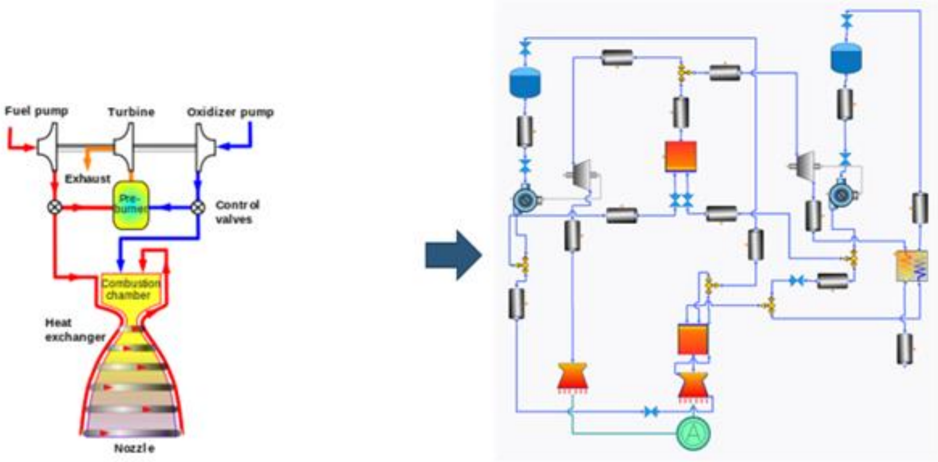

Picture 24 Gas-generator rocket cycle *[37]*

2) CLOSED CYCLE FUEL RICH : In this case, uses the remaining fuel-rich exhaust gases to drive the turbine that powers the propellant pumps. This allows for more efficient use of the propellants, as the remaining exhaust gases burn entirely, and the energy is not wasted. A key advantage of this cycle is the high specific impulse and efficiency, resulting in a greater thrust-to-weight ratio . However, this construction is more expensive and It is a complex and challenging cycle to design and operate, requiring high-precision and high-temperature materials to withstand the harsh combustion environment [37].

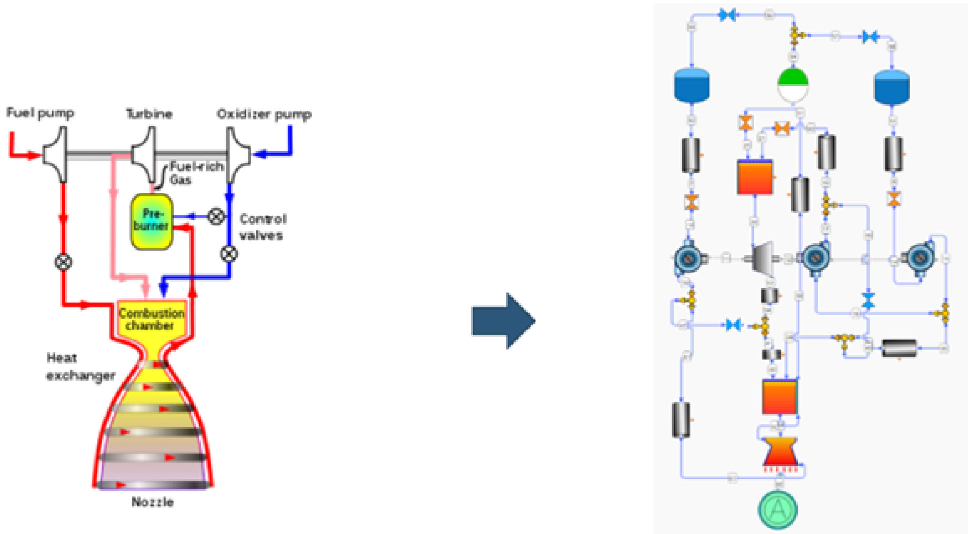

Picture 25 Fuel-rich staged combustion cycle *[37]*

3) FULL FLOW STAGED COMBUSTION CYCLE : This cycle satisfies high thrust loads and is one of the most efficient. The fuel and oxidizer are initially fed into separate pre-burners, where they are partially burned to generate a high-pressure and high-temperature gas mixture. This gas mixture is then fed into the main combustion chamber, which is fully burned to produce high-pressure exhaust gases that exit through the nozzle, providing thrust.. However, a key disadvantage presented by this cycle is manufacturing complexity . This also increases the cost of construction[37].

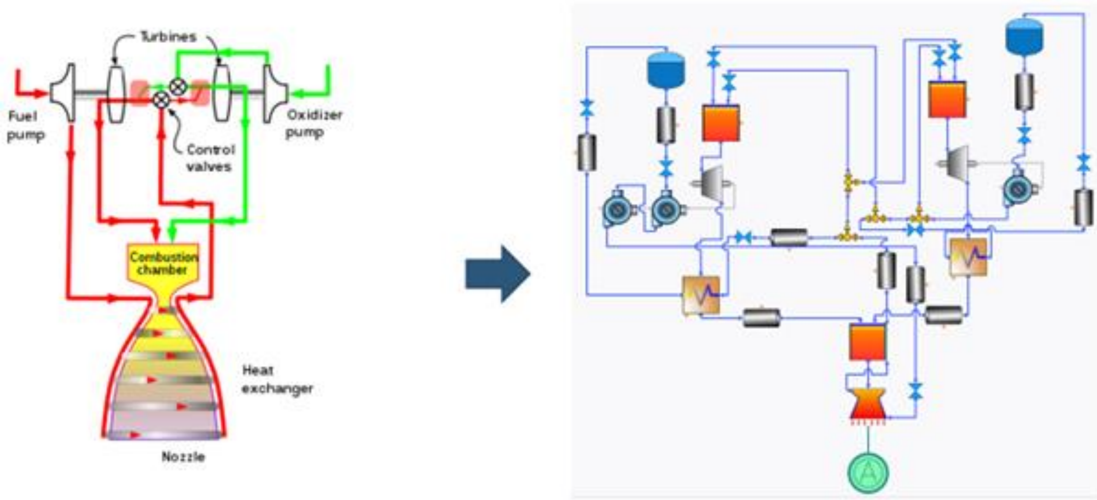

Picture 26 Full-flow staged combustion rocket cycle *[37]*

4) EXPANDER CYCLE : In this cycle, there is no pre-burner which makes it even simpler to design. The fuel that cools the nozzle is used as a working medium for the operation of the air turbine. It essentially takes some of the heat from the walls of the rocket engine. However, this cycle cannot meet high thrust requirements [38].

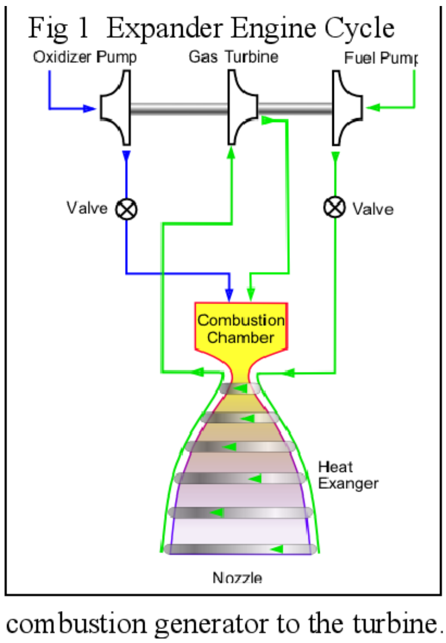

Picture 27 Expander rocket engine (closed cycle) *[38]*

5) ELECTRICAL PUMP : Practical attempts have been made to adapt an electric motor to rotate pumps in aerospace. The fuel and oxidizer are then burned in a combustion chamber, producing exhaust gases that exit through the nozzle to provide thrust. The electric pump-fed cycle has several advantages, including simplicity, reliability, and the ability to use a wide range of fuels. But this method has some disadvantages, such as lower efficiency, high battery weight, and lower thrust-to-weight ratio than the gas generator cycle [37].

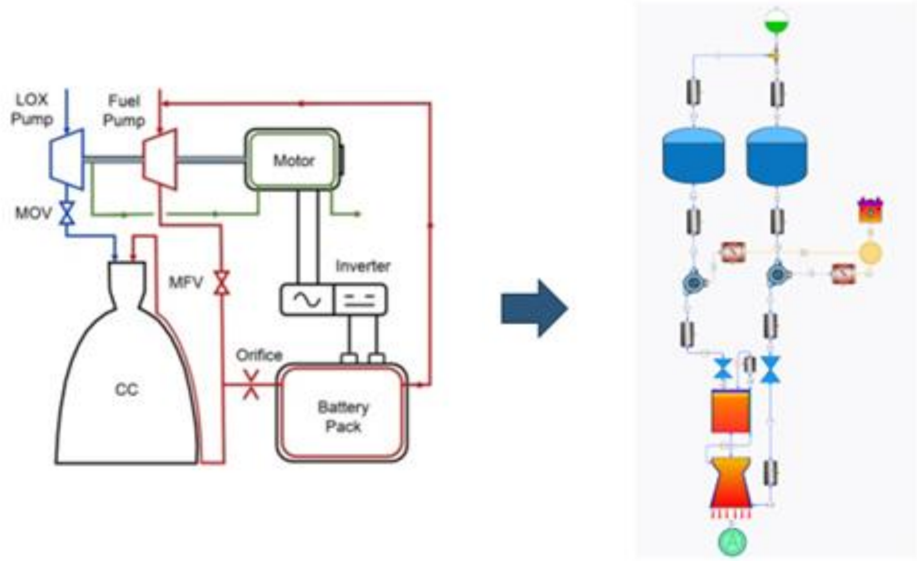

Picture 28 Electric Pump-Fed Engine Cycles *[37]*

2.4 Examples of rocket engines using a turbopump and their technical characteristics

In this subsection, some known rocket engines using turbopump are presented. The familiar liquid hydrogen fueled Space Shuttle rocket engine has two turbines one for the fuel pump and one for the oxidizer pump. They have a power of 54.36 Mw (fuel) and 19.28 Mw (oxidizer). The outlet pressure is 441 bar (fuel pump) and 499.9 bar. Finally the turbine inlet temperature is 838ºC (fuel) and 671.3ºC (oxidizer)[39]. Another well-known rocket engine is that of Space-X called Raptor. It works with liquid methane and liquid oxygen. The fuel supply is 194 Kg/s and 737.2 Kg/s of oxidizer respectively[40]. The picture below shows the RD-170 rocket engine :

Picture 29 The RD-170 rocket engine which was used for the rocket Energia [41]

It is one of the most well-known rocket engines that the Russians have built and is one of the largest in power on a global scale [41]. The RD-170 is designed to run on kerosene(RP-1). Fuel mass delivery 166.2 Kg/s and oxidizer mass delivery 436Kg/s [42]. Below is the H-1 rocket engine with its turbocharger technical characteristics for a specific thrust. It concerns the H-1 C and H-1 D engine version.

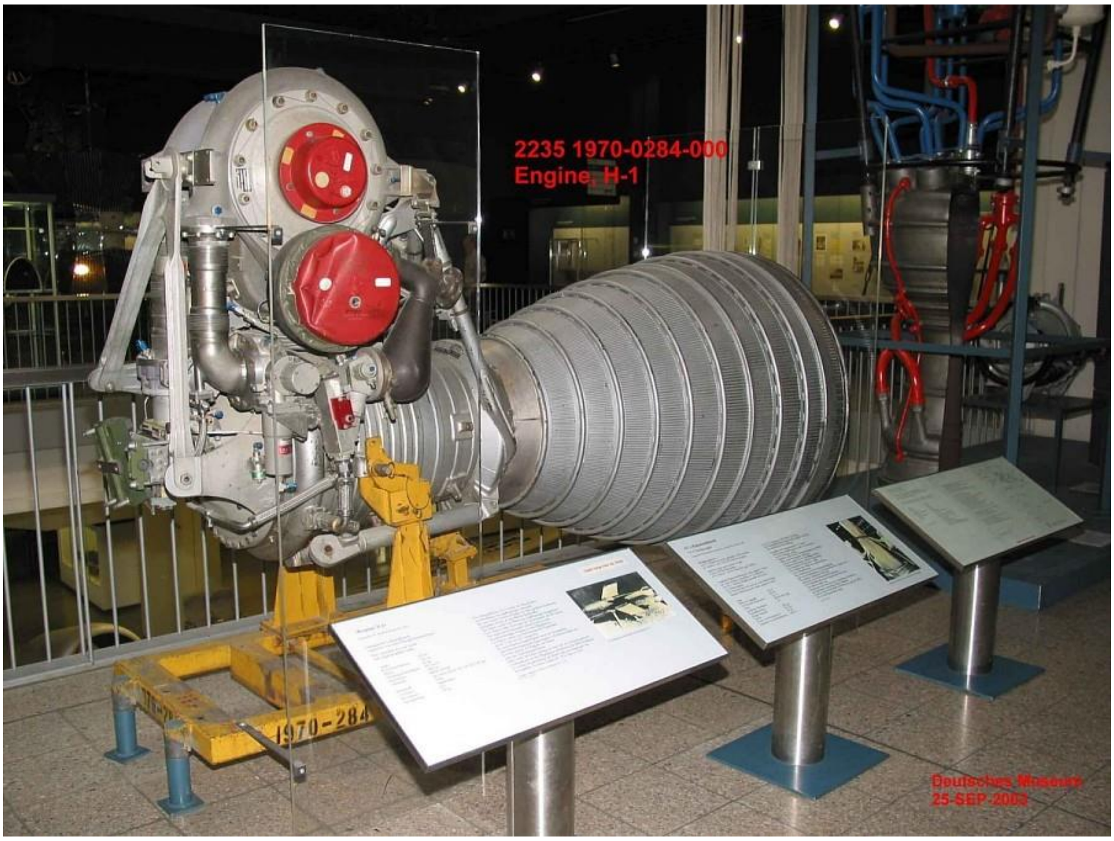

Picture 30 The H-1 liquid-fuel rocket engine was the first stage power plant for the Saturn 1 and Saturn 1B launch vehicles *[43]*

In this case, although the oxidizer pump is on a common shaft with the fuel pump, the air turbine is connected to the pump shaft through a gearbox. This engine has historical value. as it was used in the famous Saturn project in 1961. However, the fuel whichused was kerosene (RP-1) [44] . Some of its technical characteristics of turbopump are listed below .

TECHNICAL CHARACTERISTICS	
Power turbine	3.088 MW
mass flow of oxidizer	247.4 Kg/s
mass flow of fuel	110 Kg/s
Fuel	RP-1
Total effience n_t of turbine	70%
turbine intel Pressure	43 bar
Type turbine	two stage axial
RPM pumps (RP-1 & LO_2)	6680 min^{-1}
hydraulic efficiency pump fuel	71.78%
hydraulic efficiency pump oxidizer	77.88%
Intel pressure total of fuel	3.93 bar
Outlet pressure total of fuel	69.78 bar
Intel pressure total of oxidizer	4.48 bar
Outlet pressure total of oxidizer	66.88 bar

These data is from rocket H-1C and H-1D for thrust 205,000 pounds [45]. Appropriate US to SI unit conversions have been made.

Unit 3. Laws of fluid mechanics in turbine applications and design parameters

3.1 Basic principles of fluid mechanics

1. The continuity equation

$$\frac{D\rho}{Dt} + \nabla(\rho w) = 0$$

For pumps where we have practically incompressible flow the equation becomes:

$$A_1 u_1 = A_2 u_2$$

[55]

But in the case of both axial and radial turbines where we have expansion of the exhaust gases, that is, a reduction in the density of the fluid at their exit, the equation becomes:

$$A_1 u_1 \rho_1 = A_2 u_2 \rho_2$$

[56]

2. The momentum equation (Navier – Stokes & Bernoulli equation)

The most generalized form of this equation considering both compressible flow and temperature change is :

$$\rho \frac{Dw}{Dt} + \rho(w\nabla)w = \rho(\frac{Dw}{Dt} + \nabla \frac{w^2}{2} - wX(\nabla X w))$$

In one-dimensional flow with constant density, it is simplified and the formula takes the following form:

$$\rho u \frac{du}{dx} = -\frac{dp}{dx} + \frac{d}{dx}\left(\mu \frac{du}{dx}\right) + F_2$$

Bernoulli's equation is essentially a specialized and simplified form of the Navier-Stokes equation.

$$\rho \frac{u1^2}{2} + p1 + \rho g z1 = \rho \frac{u2^2}{2} + p2 + \rho g z2$$

[55]

3. The energy equation

It is known that the energy equation results from the balance of motion, pressure, friction and field energy. Therefore, we have the following form:

$$\rho \frac{Dh}{Dt} = \frac{Dp}{Dt} + \nabla(\kappa \nabla T) + \mu \Phi$$

Where Φ is the irreversible loss function and is given below :

$$\Phi = (rotw)^2 + 2div\left(grad\frac{w^2}{2} - wXrotw\right) - 2wgraddivw - \frac{2}{3}(divw)^2$$

Accordingly, in a one-dimensional form where we have no field forces, the energy equation takes the following form :

$$\rho u \frac{dh}{dx} = u \frac{dp}{dx} + \frac{d}{dx}\left(k \frac{dT}{dx}\right) + \frac{4}{3}\mu\left(\frac{du}{dx}\right)^2$$

An even more simplified form where we have a one-dimensional form and incompressible flow :

$$\frac{{u_1}^2}{2} + \frac{p_1}{\rho} + gz_1 = \frac{{u_2}^2}{2} + \frac{p_2}{\rho} + gz_2 + \frac{\Delta pv}{\rho}$$

Where Δpv the total hydraulic losses.

Correspondingly for air turbines where compressible flow prevails the form of this energy equation is :

$$\frac{{u_1}^2}{2} + \frac{\gamma}{\gamma - 1}\frac{p_1}{\rho_1} = \frac{{u_2}^2}{2} + \frac{\gamma}{\gamma - 1}\frac{p_2}{\rho_2}$$

These equations have a similar form to Bernoulli's [52]

4. 1st Thermodynamic axiom

The first law of thermodynamics states that if a system completes a complete thermodynamic cycle during which there is heat input and work output then:

$$\oint dQ - dW = 0$$

In this relation heat and work are the same. For a change of state from 1 to 2 there is the energy change of the system:

$$E_2 - E_1 = \oint_1^2 dQ - dW$$

Where : $E = U + \frac{1}{2}mC^2 + mgz$

For elementary change :

$$dE = dQ - dW$$

From the first law of thermodynamics, the steady flow energy equation is proved::

$$\dot{Q} - \dot{W}x = \dot{m}[(h_1 - h_2) + \frac{1}{2}({c_1}^2 - {c_2}^2) + g(z_2 - z_1)]$$

Because the contribution of the kinetic energy and the dynamic energy of the fluid is usually very small, they are considered negligible and the relationship becomes :

$$\dot{Q} - \dot{W}_x = \dot{m}(h_{02} - h_{01}) \text{ [56]}$$

5. 2nd thermodynamic axiom

Included in this axiom is the concept of entropy and ideal thermodynamic processes. A well-known consequence of this law is the Clausius inequality:

$$\oint \frac{dQ}{T} \leq 0$$

If the processes were reversible then :

$$dQ = dQ_R$$

For a finite change of state the entropy change is :

$$S_2 - S_1 = \int_1^2 \frac{dQ_R}{T}$$

But in reality there are no reversible processes so the relationship becomes :

$$\dot{m}(S_2 - S_1) = \int_1^2 \frac{d\dot{Q}}{T} + \Delta S_{irrev}$$

In case where we have an adiabatic change (dQ = 0) we have :

$$S_2 \geq S_1$$

If hypothetically there was a reversible process then :

$$S_2 = S_1 \quad [56]$$

6. Euler's law

First, state the torque law applied to a control volume of a centrifugal pump. Let it be fluid entering the control volume with a twist with radius r_1 and tangential velocity $C_{\theta 1}$ and exiting with radius r_2 and tangential velocity $C_{\theta 2}$. In one-dimensional steady flow, the torque will be :

$$T_A = \dot{m}(r_2 C_{\theta 2} - r_1 C_{\theta 1})$$

The pump rotating at an angular velocity Ω imparts mechanical work to the fluid in order to convert it into hydraulic work. The mechanical work given through the rotary motion of the rotor is :

$$\dot{W}_c = T_A \Omega = \dot{m}(U_2 C_{\theta 2} - U_1 C_{\theta 1})$$

Therefore, the special project will be :

$$\Delta Wc = \frac{\dot{W}_c}{\dot{m}} = T_A \Omega = (U_2 C_{\theta 2} - U_1 C_{\theta 1})$$

Correspondingly, for the radial air turbine where the fluid gives mechanical work to the rotor, it will be :

$$\Delta Wt = \frac{\dot{W}_t}{\dot{m}} = T_A \Omega = (U_1 C_{\theta 1} - U_2 C_{\theta 2})$$

But in the axial air turbine, where we have a constant radius in the rotor body, there is a constant peripheral speed U, and the specific work is :

$$\Delta Wt = \frac{\dot{W}_t}{\dot{m}} = T_A \Omega = U(C_{\theta 1} - C_{\theta 2})$$

In general, in turbine engines, the energy equation of the steady flow, which is also known as Euler's equation, is written in this form :

$$\Delta W_x = (h_2 - h_1) = (U_1 C_{\theta 1} - U_2 C_{\theta 2}) \text{ or } \Delta h0 = \Delta(U C_\theta) \text{ [55]}$$

7. All sizes & perfect gases

For perfect gases the well-known constitutive equation applies :

$$pv = mRT$$

Accordingly, we also have the heat capacities under constant pressure Cp and volume Cv and the relationship that connects them :

$$\mathrm{R} = C_p - C_v$$

Total enthalpy : $h_{01} = h_1 + \frac{{C_1}^2}{2}$

Total temperature : $T_{01} = T_1 + \frac{{C_1}^2}{2Cp}$

Total pressure : $P_{01} = P_1(1 + \frac{\gamma-1}{2}{M_1}^2)^{\frac{\gamma}{\gamma-1}}$

Total density : $\rho_{01} = \rho_1(1 + \frac{\gamma-1}{2}{M_1}^2)^{\frac{1}{\gamma-1}}$

Total rotational enthalpy: $I_{01} = h_1 + \frac{{w_1}^2}{2} - \frac{U^2}{2}$

8. Relationships from Velocity triangles

Radial Pump :

$$C^2 = C_r^2 + C_\theta^2 + C_x^2 \;\&\; C_\theta - U = W_\theta$$

Axial turbine :

$$C_{\theta 2} - U = W_{\theta 2} \;\&\; C_{\theta 3} + U = W_{\theta 3}$$

$$h_2 + \frac{W_2^2}{2} = h_3 + \frac{W_3^2}{2}$$

Radial turbine :

$$C_{m2} = C_{r2} = W_2 \;\&\; C_{m3} = C_{x3} = W_3$$

$$h_2 + \frac{W_2^2}{2} - \frac{U_2^2}{2} = h_3 + \frac{W_3^2}{2} - \frac{U_3^2}{2} \text{ [56]}$$

3.2 Inducer design

One of the key factors considered in both conventional pumps and inducers is the suction specific speed coefficient Ss.

$$S_s = \frac{N\sqrt{Q}}{NPSHR^{\frac{3}{4}}}$$

There is also the corrected suction specific speed coefficient, which is a number that appears in a hypothetical impeller with zero shroud diameter at the inlet, operating at the same speed and axial velocity. In this way, correction is made by increasing the flow rate at the inlet to counteract the area blocked by the shroud.

$$S_s^* = \frac{S_s}{(1-v^2)^{1/2}}$$

Where is v the ratio of the diameter of the hub to the diameter of the inducer (the tip of the fin) [36]

$$v = \frac{D_h}{D_t}[36]$$

Typical values of this ratio range from 0.2 to 0.4 [46]

Another equally important parameter is the flow coffencient Φ and it usually takes values from 0.07 to 0.14[21].

$$\Phi_m = \frac{C_x}{U}$$

Similarly, we have for the loading factor ψ

$$\Psi = \frac{\Delta C_\theta}{U} = \frac{2gH}{U^2}$$

Correspondingly, there is also the flow coefficient at the edge of the blade which is also often used in design.

$$\Phi = \frac{C_x}{U_t}$$

Similarly, we have for the loading factor ψ

$$\Psi = \frac{2gH}{{U_t}^2}$$

3.2.1 Inducer blade design

The most effective method preferred by designers for shaping the impeller geometry is the method of free vortex. Essentially, the blade is shaped in such a way that the product rC_θ remains constant from the base to the tip of the blade. Although it is a reliable method, it presents manufacturing difficulties.

Usually in inductors the radial lead is constant for flat blades but in practice it is not done by construction with method of free vortex :

$$r tan(\beta) = R_t \tan(\beta_t)$$

Where Rt and βt are the inducer radius and the vane tip angle β respectively.

Radial lead : $\lambda = 2\pi r tan(\beta)$

Another characteristic element for impeller design is the aspect ratio of the blade, defined as the chord length of the blade divided by the axial distance of the blade. It is known as the solidity ratio and significantly contributes to the effectiveness of cavitation reduction. The larger the value, the greater the protection against cavitation. Typical values for better suction performance from 2 to 2.5 at all blade sections from tip to hub[46]. Solidity is given by:

$$\sigma = \frac{C}{S}$$

Where C chord length and S spacing blade[46].

The blade profile must not interfere with the free boundary of the cavitation flow, i.e., the blade must remain within the cavity and operating conditions. The figure below shows the wedge, wing and βw angles.

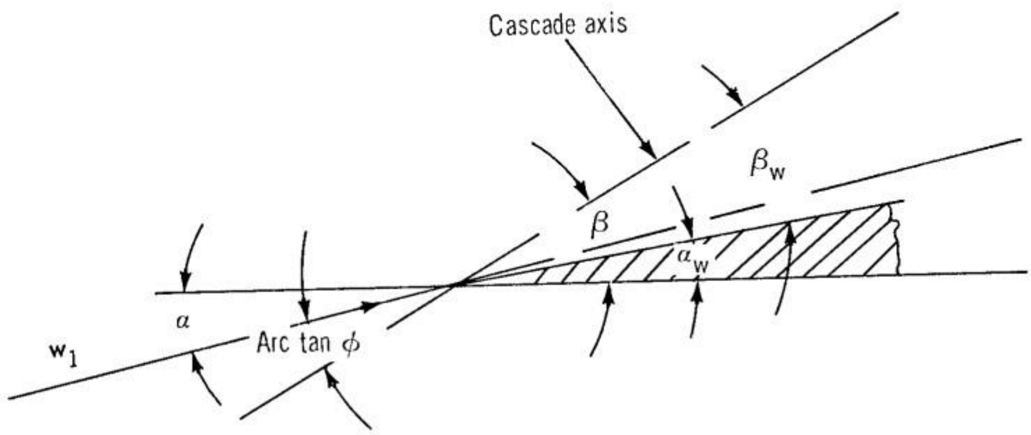

Picture 31 Here are the fluid flow angle, the wedge angle and the vane angle [46]

The wedge angle is calculated from the following relationship :

$$a_w = \beta - \beta_w$$

The angle βw respectively :

$$\beta_w = \arctan(1{,}1\Phi_d)$$

Where Φ_d the design flow coeffient [46].

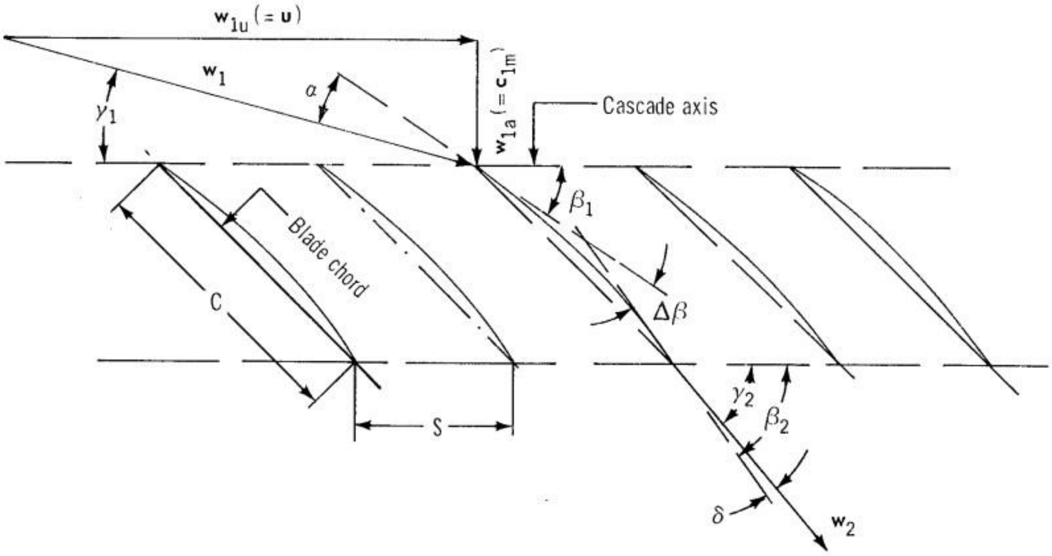

Picture 32 Velocity triangles, fluid flow angles, vane angles and inducer inlet and outlet recall angles*[46]*

3.2.2 Cavitation

Normally the allowable suction head should be less than the available suction head NPSH prevailing at the inlet of the inducer.

$$NPSH_{required} \leq NPSH_{available}$$

Then follows the required suction head which is determined by a pump running an ideal flow (approximate from cold water) and suction coefficient S_S^* :

$$NPSH_{required} = (\frac{n\sqrt{Q'}}{S_S^*})^{4/3}$$

Where Q' is a corrected flowrate

The available tank height is at the inducer inlet is calculated from the following relationship :

$$NPSH_{available} = \frac{P_{total} - P_v}{g\rho_F}$$

Forthermore, where is thermodynamic suppression head TSH

The thermodynamic suppression height can be estimated from the equation below :

$$TSH = NPSH_{available} - NPSH_{ideal\ fluid}$$

Where $NPSH_{ideal\ fluid}$ is the net height of the tank without the hydraulic losses

$$NPSH_{ideal\ fluid} = \left(\frac{P_{total} - P_v}{g\rho_F}\right) tank - H_{loss}$$

In addition, the estimate of TSH can be estimated by a coefficient called the NPSH coefficient and denoted by Z. To calculate it, the following relationship is given :

$$Z = \frac{2g(NSPH)_{tank}}{C_m^2}$$

Average of this coefficient of TSH height is calculated from the following relationship :

$$(TSH) = \frac{(Z_{opt} - Z)C_m^2}{2g}$$

Where Zopt is the optimal NPSH factor. In this way, the $NPSH_{required}$ can be calculated accordingly :

$$NPSH_{required} = \mathrm{NPSH}_{tank} + (TSH) = \frac{Z_{opt}C_m^2}{2g}$$

Where :

$$Z_{opt} = 3(1 - 2\Phi_{opt}^2)$$

For very small Φ_{opt} we consider $Z_{opt} \approx 3$[46].

In order to analyze in greater depth the phenomenon of cavitation in the inducer blades, models and empirical relationships have been developed to describe the geometry and dimensions of the bubbles and the frequency with which they appear and destroy.

The relationship that describes the growth rate of the bubble radius is a well-known equation Rayleigh – Plesset :

$$\rho\left[R\ddot{R} + \frac{3}{2}\dot{R}^2\right] = [p_v - p_\infty(t)] + p_{go}(\frac{R_0}{R})^{3k} - \frac{2S}{R} - 4\mu\frac{\dot{R}}{R}$$

where k is the multimodal coefficient. It takes the value 1 in case of isothermal change. Below is the law relating the pressure of the gas inside the bubble and its radius.

$$p_g R^{3k} = p_{g0} R_0^{3k}$$

This relationship essentially presents the thermodynamic behavior of the gas prevailing inside the bubble. Usually, this law contributes greatly to the increase of the bubble radius in cases where we have heat transfer which does not practically occur in the pump switch. However, there are two factors in the Rayleigh–Plesset equation that reduce bubble growth. The first is the surface tension that develops on the surface of the bubble. These stresses are described by a stress coefficient denoted S and measured in units of N/m. The second is forces due to the potential viscosity of the liquid itself.

The aforementioned forces contribute effectively to reducing the bubble for small radii. For sufficiently large bubbles these forces are considered negligible. Therefore the Rayleigh – Plesset equation is simplified and takes the following form :

$$\rho\left[R\ddot{R} + \frac{3}{2}\dot{R}^2\right] = [p_v - p_\infty(t)]$$

If the static pressure is also considered constant with respect to time, the following relationship results :

$$\dot{R}^2 = \frac{2}{3}\frac{p_v - p_\infty}{\rho}[1 - \left(\frac{R}{R_0}\right)^3]$$

In addition, there are other possibilities and conditions in which cavitation in the inducer can prevail which simplify the Rayleigh – Plesset equation. A characteristic case is bubble equilibrium where the rate of increase of the bubble radius is zero ($\dot{R}$=0), the pressure is constant with respect to time and we have isothermal gas transport. With these conditions the Rayleigh – Plesset equation takes the following form :

$$p_\infty = p_{g0}[\frac{R_0}{R}]^3 + p_v - \frac{2S}{R}$$

But the pressure resulting from this relationship differs inside and outside the bubble as different surface tensions prevail. It is very important to mention that the bubble equilibrium is not always stable. There is a minimum pressure that the liquid can reach and it is below the pressure pv. This pressure is called critical pressure and is denoted pc. Corresponding to this pressure we also have the corresponding radius of the bubble Rc.

$$p_c = p_v - \frac{4S}{3R_c}$$

$$R_c = \sqrt{\frac{3p_{g0}{R_0}^3}{2S}}$$

Bubble development

The rapid growth of bubbles requires the condition p∞ <pv , i.e. the static applied pressure is less than the vapor pressure. In this case R>R0 will hold and the bubbles will be so large enough in size that shear stresses and viscous forces are considered negligible. With these conditions the growth rate of the bubble will be:

$$\dot{R} \cong \sqrt{\frac{2(p_v - p_\infty)}{3\rho}}$$

This relationship shows 2% less error than the original one.

Collapse of bubbles

In a turbopump where bubble collapse is required, the static applied flow pressure must be greater than the vapor pressure (p∞ >pv). In this case we have the destruction of the bubble and R<R0. If viscous forces and shear stresses are neglected the rate of bubble reduction will be :

$$\dot{R} \cong \sqrt{\frac{2(p_v - p_\infty)}{3\rho}[(\frac{R_0}{R})^3 - 1]}$$

Until the bubble is completely destroyed, it takes a certain amount of time, which is called the Rayleigh time. It is the time where R=0. This is estimated from the following relation:

$$\tau_p \cong 0{,}915 R_0 \sqrt{\frac{\rho}{p_\infty - p_v}} \, [57]$$

A cavitation number Kc, based on the cavity pressure instead of the liquid bulk vapor pressure, has been defined :

$$K_c = \frac{p_s - p_v}{\frac{1}{2}\rho w_1^2}$$

where p_s fluid static pressure, p_v fluid vapor pressure in cavity at leading edge, ρ fluid density, w_1 fluid velocity relative to blade at tip and g gravitational constant.

he cavity velocity w_c, follows from Bernoulli's law and the definition of the cavitation number, giving :

$$w_c = w_1\sqrt{1 + K_c}$$

Next, the relative speed at the output of the inducer is calculated :

$$w_2 = \frac{w_c}{F + (F^2 - 1)^{1/2}}$$

Where F is a coefficient calculated from the following relationship :

$$F = \frac{(1 + K_c)^{1/2}\sin(\beta) + (1 + K_c)^{-1/2}\sin(\beta - 2\alpha)}{2\sin(\beta - \alpha)}$$

To find the cavity height that develops above the fin the cavitation ratio the following relationship is used :

$$\frac{h_c}{S} = sin\beta - \frac{w_1}{w_2}\sin(\beta - \alpha)$$

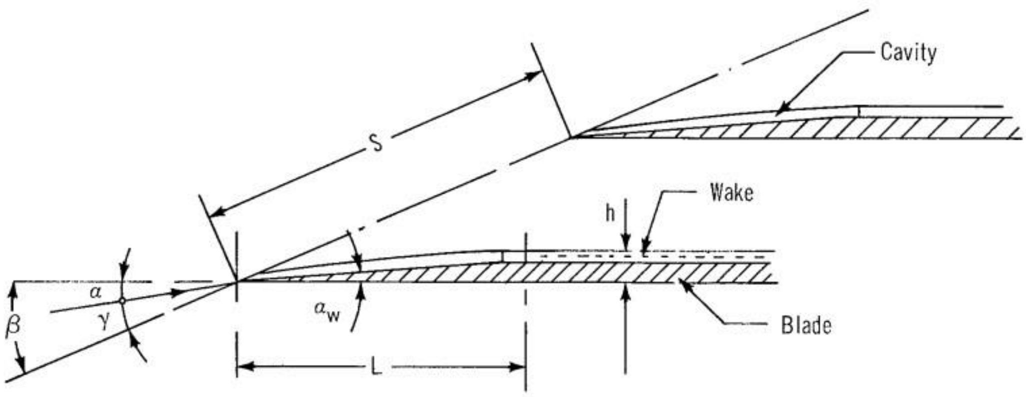

Picture 33 Blade in cavity. Cavitation develops on the flap*[46]*

The minimum value of the cavitation coefficient K can be estimated from the following equation :

$$K_{min} = \frac{2sinasin(\beta-\alpha)}{1+cos\beta} \ [46]$$

3.3 Impeller design

There are 2 types of fenders, open and padded. The hydraulic efficiency of the jacketed impellers is generally higher as the deformations in the shell are more tolerable and smooth without causing particular problems in the gap between the impeller and the wall[47]. In general, although the geometric characteristics of an impeller contribute significantly to the hydraulic degree of efficiency, the most basic quantity by which the efficiency is determined is the specific number of revolutions Ns [25].

$$N_s = \frac{N\sqrt{Q}}{H^{3/4}} \ (rpm, gpm, ft) \text{ or } n_q = \frac{N\sqrt{Q}}{H^{3/4}} \ (\frac{1}{min}, \frac{m\hat{}3}{s}, m) \ [48]$$

Below is a graph of hydraulic efficiency for turbopumps as a function of specific speed nq

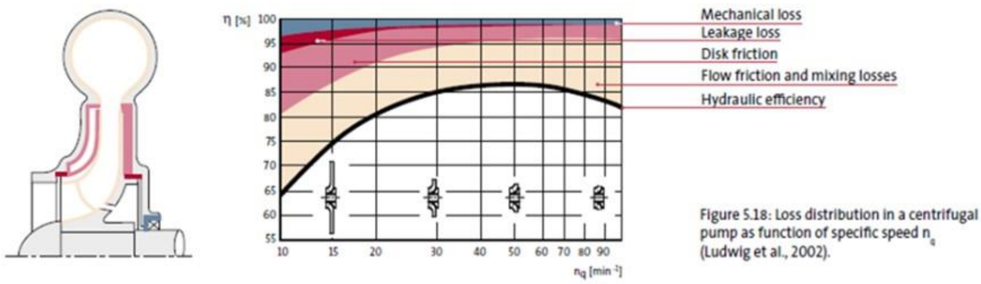

Picture 34 Loss breakdown in centrifugal pumps. From this diagram it is easy to start the design of a centrifugal pump or an impeller-converter system based on the degree of efficiency*[49]*

Another equally important parameter is the specific diameter Ds of the impeller

$$D_s = \frac{DH^{1/4}}{\sqrt{Q}} \quad \text{or} \quad \delta = \frac{\psi^{1/4}}{\Phi^{1/2}} \ [48], [25]$$

Also, as with the commutator, we also have the loading factor ψ in the impeller

$$\psi = \frac{2gH}{U^2}$$

Accordingly, we also have the flow coefficient Φ

$$\Phi = \frac{C_x}{U}$$

In this case the flow coefficient can take values usually from 0.05 to 0.3. The criteria for selecting the flow coefficient at the inlet and outlet are different. At the inlet the flow coefficient Φ1 depends on the required suction while the flow coefficient Φ2 is determined by the vane angle at the outlet and the head coefficient[36]. Typicals value head coefficient is 0,5 to 0,8 [50].

Other design parameters that are known and common in radial pumps are:

1) $\frac{D_{h1}}{D_{S1}}$: The ratio of hub diameter to vane diameter at the impeller inlet.

2) $\frac{b_2}{D_2}$: The ratio of vane height in the discharge area to the impeller outlet diameter.

3) $\frac{D_{S1}}{D_2}$: The ratio of vane diameter to the impeller outlet diameter [48].

3.3.1 Number of blades

The number of blades in an impeller is highly dependent on the head coefficient. Usually for small head coefficients the number of blades is from 3 to 5 and for large coefficients the number of blades exceeds 20. Of course, the number of blades varies depending on the geometric characteristics of the impeller and the slip coefficient M which will be mentioned below . Another factor for the number of vanes is the flow coefficient as the diffusion limits of the impeller (surface dial velocity) must be respected[36]. Alternatively the number of vanes can be calculated from the following formula generally used in pumps:

$$Z = K_z \frac{d_2 + d_1}{d_2 - d_1} sin(\frac{\beta_1 + \beta_2}{2})$$

Where K_z is from 5 to 6,5[48].

It was mentioned above that an equally important factor for the number of blades is the slip coefficient M. This essentially represents in percentage terms how close the actual speed of the C_θ fluid is to the theoretical one.

$$M = \frac{C_\theta}{C_{\theta\infty}} \text{ [48]}$$

Theoretically, if we had an infinite number of blades, we would have the theoretical speed, that is, the coefficient would be M = 1.

There is no universal equation that is widely applicable to calculate the drag coefficient in every turbine. However, several empirical equations that are acceptable have been developed and used to calculate the M factor[36].

3.3.2 Wing design

The blade design for a centrifugal impeller is known to be based on the single circular arc :

$$R = \frac{1}{2} \frac{r_2^2 - r_1^2}{2r_2 COS(\beta_2) - 2r_1 COS(\beta_1)}$$

There is also the method with the double circular arc, but it is not preferred as with this method we have a discontinuity in the geometry and a lower efficiency of the wing.

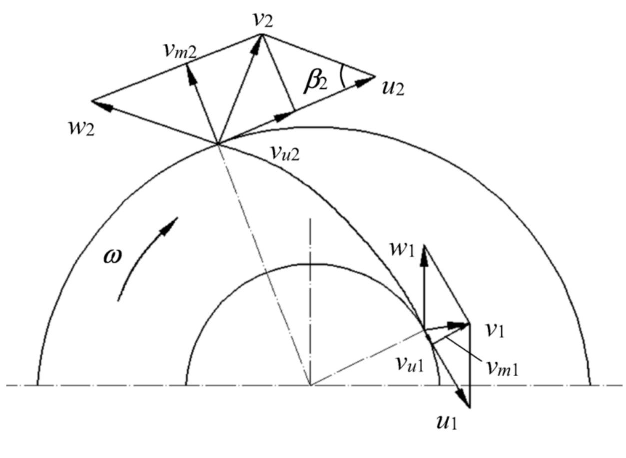

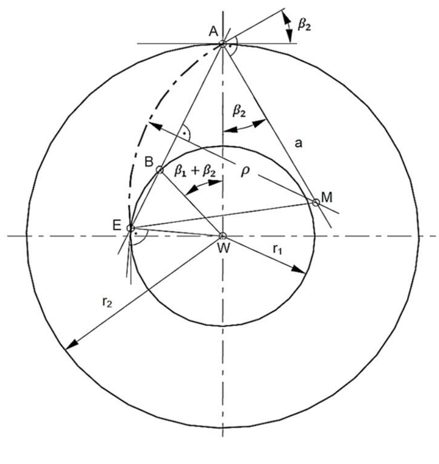

Picture 35 The gear triangles at the inlet and outlet of the centrifugal impeller*[31]*

Picture 36 The arc with which the impeller blade is formed *[51]*

Usually for centrifugal liquid pumps the method by which the vane is designed is by the linear distribution of the relative velocity W = W(r) with respect to the radial position r.

$$W = W_1 + (W_2 - W_1)\frac{r-r_1}{r_1-r_2} \text{ [55]}$$

3.4 Volute – Diffuser design

The volute - diffuser in the pumps essentially helps to smooth out and increase the pressure at the exit of the flow. An asymmetric volute cross section is preferred because it produces a single vortex thut is stable and that improves the efficiency of the conical diffuser at the exit. The conical diffuser at the volute exit will operate efficiently when the included angle forcircular cross sections is between 7° and 9°; for square cross sections, 6°; and for two parallel walls, 11 °[36]. The diffuser depending on the design of the turbopump takes the following forms:

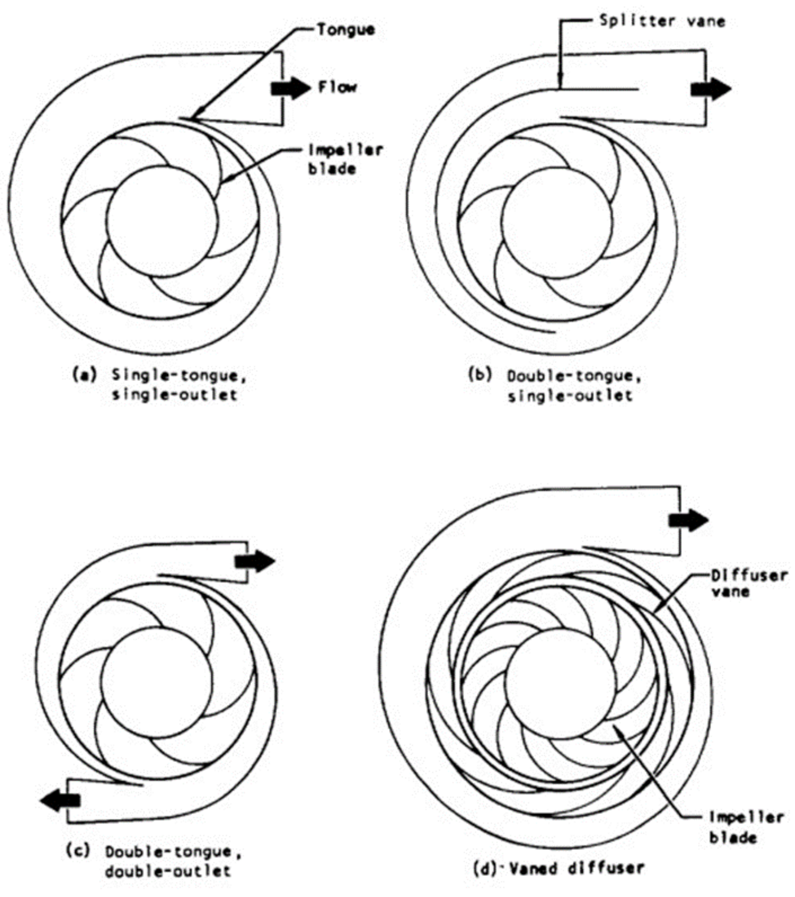

Picture 37 Types of diffusers *[36]*

Generally, a good method for spiral design is with principle of conservation of angular momentum ($C_\theta r$ = constant). In a classic diffuser without static vanes with a single outlet the flow is calculated from the following relation:

$$Q = aNA_{th}C_{th}$$

Where α is a correction factor associated with the boundary layer displacement and a typical value is close to 0.9. The number N is the number of outputs of the diffuser or otherwise bulbs. The velocity C_{th} at the diffuser throat can be related to other velocities by the constant momentum law.

$$C_{th}r_{th} = C_{\theta,0}r_{\theta,0} \text{ [47]}$$

In all spiral diffusers, regardless of their type, there is a limit to the diffusion coefficient D. For single-stage diffusion, D≤0.6 applies and is calculated from the relationship:

$$D = \frac{P_s - P_{min}}{P_t - P_{min}} \text{ [36]}$$

3.4.1 Logarithmic spiral design

This is how the static fins of the diffuser analyzed below are formed :

$$\varphi - \varphi_1 = tan\beta \ln\left(\frac{r}{r_1}\right)$$

Where $tan\beta = \frac{C_\theta}{C_r}$ [47].

3.4.2 Volute -Diffuser with fins

In order to increase the overall efficiency of the pump inside the diffuser, special static vanes are added which further increase the pressure in the fluid discharge area. The pressure distribution at the outlet is also normalized and eddies and vortices are reduced. Another additional purpose of using static vanes is to avoid the amplification of wave pressure caused between the diffuser and the impeller blade. The superposition of these waves may cause large swings in the discharge pressure. Therefore, for a vane diffuser to be effective, it must have a certain number of vanes Zb that corresponds correctly to that of the vane Z2 taking into account as parameters the mean distance Dv and the relatively low flows. In order to identify these amplifications, a special index m is used. When it becomes an integer, then we have a wave amplification. This indicator is calculated in 2 cases.

I. Case : Av $Z_2 > Z_b$

$$m = j\frac{Z_2}{Z_b}\left\{\frac{Z_b - Z_2}{Z_2} + \frac{\pi D_v N}{(a+W)}\right\}$$

II. Case : Av $Z_b > Z_2$

$$m = j\frac{Z_2}{Z_b}\left\{\frac{Z_b - Z_2}{Z_2} - \frac{\pi D_v N}{(a+W)}\right\}$$

Where :

j : order of the harmonic of the fundamental wave frequency

Dv : average distance from center of pump to center of volute passage

a : velocity of sound in liquid

W :average relative velocity of fluid in volute passag

However, the main disadvantage of the diffuser with static vanes is that at large changes in the flow, the efficiency decreases sharply and the operating range is very small. In contrast to the classic diffuser that does not have fins, it shows high performance in a wider range of supply operation [36].

3.4.3 Force due to uneven pressure distribution

Precisely because there are heterogeneities in the pressure and momentum peripherally, we have a logarithmic spiral shape in the diffuser. But these heterogeneities cause unequal radial forces on the impeller. Diffusers with one bulb (output duct) usually have this effect. For this reason, in the design, some diffusers may have 2 or more bulbs in order to achieve the balancing of the radial forces. This radial force is calculated from the following relationship:

$$F = k_F g_0 \rho H D_0 b_0$$

Where k_F is a ratio factor and is determined theoretically and experimentally. Studies have shown that for a single bulb diffuser near shutdown conditions the highest values are from 0.3 to 0.65. However, during the operation of the pump we have values of the order of 0.1. This factor may be constant throughout its operating range [47].

3.5 Turbine design

The air turbine is the one that ensures the necessary rotational work so that the pumps operate at the desired speeds. Although in recent years electric motors have also been developed for this work, they are still in the preliminary stage and are not so prioritized as the weight of the batteries and the electric motor are too high for space applications. Usually air turbines are axial single-stage or two-stage. But there are rarer cases where we have radial turbines which are also very efficient. The inlet operating temperature varies according to the load and the material of which the air turbine is made.

As in pumps, in air turbines we have the flow coefficient and the loading coefficient respectively :

$$\Phi = \frac{C_x}{U}$$

$$\Psi = \frac{\Delta C_\theta}{U}$$

Next, we have the degree of reaction R which represents the rate of reduction of the enthalpy of the fluid where it is done by the rotor. Usually for this application we have prices of 50% and above.

$$R = \frac{h_2 - h_3}{h_1 - h_3} = 1 - \frac{\Phi}{2}(tana_2 - tana_1) \text{ [2]}$$

Other equally important design parameters are the total pressure ratio :

$$\Pi_{tt} = \frac{P_{02}}{P_{03}} \text{ [48]}$$

The total temperature intel T_{02} and the total pressure intel P_{02} . Also another quantity used in the design of a turbine is the isentropic speed ratio :

$$v_{tt} = \frac{U}{C_o} \text{ [48]}$$

3.5.1 Turbine losses and efficiency ratings

The turbine losses are mainly due to the geometrical characteristics of the blade, the boundary layers developed on the walls and the enthalpy losses. These losses are expressed by a factor ζ. We have losses in the stator and the rotor of the turbine therefore we have the factors ζ_N and ζ_R respectively. The following relations state the enthalpy losses :

- For the stator

$$h_2 - h_{2s} = \zeta_N \frac{1}{2} C_2^2$$

- For the rotor

$$h_3 - h_{3s} = \zeta_R \frac{1}{2} W_3^2$$

In air turbines, as in any turbine engine, three different degrees of efficiency can be distinguished :

- Isentropic degree of efficiency total to total

  The isentropic overall efficiency of the turbine depends on the aforementioned losses.

$$n_{tt} = \frac{h_{01} - h_{03}}{h_{01} - h_{03ss}} \cong \left[1 + \frac{T_{03}}{T_3} \frac{\frac{\zeta_N C_2^2 T_3}{T_2} + \zeta_R W_3^2}{2(h_{01} - h_{03})} \right]^{-1}$$

  This essentially represents the actual work produced relative to the theoretical enthalpy change of the fluid.

- Isentropic overall to static efficiency

  The overall to static efficiency of the turbine is calculated respectively from the following relationship :

$$n_{ts} = \frac{h_{01} - h_{03}}{h_{01} - h_{3ss}} \cong \left[1 + \frac{\frac{\zeta_N C_2^2 T_3}{T_2} + \zeta_R W_3^2 + C_3^2}{2(h_{01} - h_{03})} \right]^{-1}$$

  However, this degree of efficiency is not particularly interesting for air turbines in general, but more so for compressors.

- Multimodal efficiency

  The multimode efficiency represents the efficiency of a hypothetical very small air turbine stage regardless of how many stages the actual air turbine has. Essentially, it is the degree of efficiency of an elementary change during the expansion of the fluid. It is different from the isentropic degree of efficiency and is due to the pressure ratio of the air turbine.

$$n_p = \frac{\delta W_{min}}{\delta W}$$

$$n_p = \frac{dh}{dh_{th}} = \frac{vdp}{C_P dT}$$

In the air turbine in an adiabatic change taking into account the multimodal degree of efficiency has the following form:

$$\frac{T_2}{T_1} = \left(\frac{p_2}{p_1}\right)^{n_p(\gamma-1)/\gamma}$$

Accordingly, the equation that connects the isentropic degree of efficiency of the turbine with the multimodal degree of efficiency is derived.

$$n_t = \frac{1 - \left(\frac{p_2}{p_1}\right)^{n_p(\gamma-1)/\gamma}}{1 - \left(\frac{p_2}{p_1}\right)^{(\gamma-1)/\gamma}}$$

3.5.2 Design blades

Depending on the geometrical dimensions of the turbine and the construction requirements, certain blade design methods have been developed for axial turbines which are applicable to compressor and fan blades respectively. These methods are used with the main goal of achieving the radial balance of the fluid, i.e. all constitutive centrifugal forces exerted on an elementary rotating fluid are balanced by the pressure forces.

$$(p + dp)(r + dr)d\theta - prd\theta - \left(p + \frac{1}{2}dp\right)drd\theta = \frac{dmC_\theta^2}{r}$$

For dm = ρrdθdr and ignoring the second-order terms the relationship is simplified :

$$\frac{1}{\rho}\frac{dp}{dr} = \frac{C_\theta^2}{r}$$

Assuming that the C_θ velocity and density are known and with the following assumptions,

- ✓ $h_0 = h + \frac{1}{2}(C_\theta^2 + C_\chi^2)$: Radially stable (dho/dr=0)
- ✓ S : Radially stable (ds/dr=0)

and combining the radial equilibrium equations with enthalpy, with entropy and with the original equation the following radial equilibrium relation for adiabatic and ideal machines is obtained :

$$C_x\frac{dC_x}{dr} + \frac{C_\theta}{r}\frac{d}{dr}(rC_\theta) = 0$$

1) FREE VORTEX METHOD : With this method, practically along the wing from its base to the top, the product Cθr is constant at the inlet and outlet. This method has high manufacturing accuracy and is reliable. However, the main disadvantage of this method is that for very low foot-head ratios (very long fins) sharp changes in the fluid exit angle are caused. Additionally at flows outside the design operating range twist flows can be induced. Thus, construction becomes more difficult and expensive, and significant pressure losses occur. Suppose there is a circulation of fluid C.

$$\Gamma = \oint Cds$$

Turbulence is defined as the elementary circulation δC toward an elementary surface δA to which it is applied.

$$\omega = \frac{d\Gamma}{dA}$$

Where dΓ is :

$$d\Gamma = (C_\theta - dC_\theta)(r - dr)d\theta - C_\theta r d\theta = \left(\frac{dC_\theta}{dr} + \frac{C_\theta}{r}\right) r d\theta dr$$

If the lower order terms are ignored, the following relationship will result:

$$\frac{d\Gamma}{dA} = \frac{1}{r}\frac{dC_\theta r}{dr}$$

Therefore we have :

$$\frac{dC_\theta r}{dr} = 0 => C_\theta r = K$$

Where K constant term.

2) FORCED VORTEX METHOD: In this case the speed Cθ varies proportionally with the radius r.

$$C_\theta = K_1 r$$

By substitution in the last radial equilibrium relation we have :

$$\frac{d}{dr}\left(\frac{C_{x1}^2}{2}\right) = -K_1 \frac{d}{dr}(K_1 r^2)$$

It results from integration

$$C_{x1}^2 = \alpha - 2{K_1}^2 r^2$$

Where a constant term. We have a fixed distribution of work radially.

3) VORTEX VARIABLE METHOD: With this method the tangential velocity of the fluid has the following distribution at the entrance and exit of the rotor :

$$C_{\theta 1} = ar^n - \frac{b}{r}$$

$$C_{\theta 2} = ar^n + \frac{b}{r}$$

For a value of n = 1, a constant degree of radial reaction R is practically achieved.

4) MIXED VORTEX METHOD: With this way of design, the disadvantages and difficulties presented by the free vorticity mentioned above are dealt with. Essentially, it is a method that combines free vorticity with forced vorticity.

$$C_{\theta 2} = \frac{a}{r} + br$$

In this case the vorticity Cθr varies parabolically with the radius r [56].

3.5.3 Rotor and stator flow in an axial flow turbine

The following images describe the flow of the fluid and how the speed relationships are connected to the calls of the vanes at the inlet and outlet.

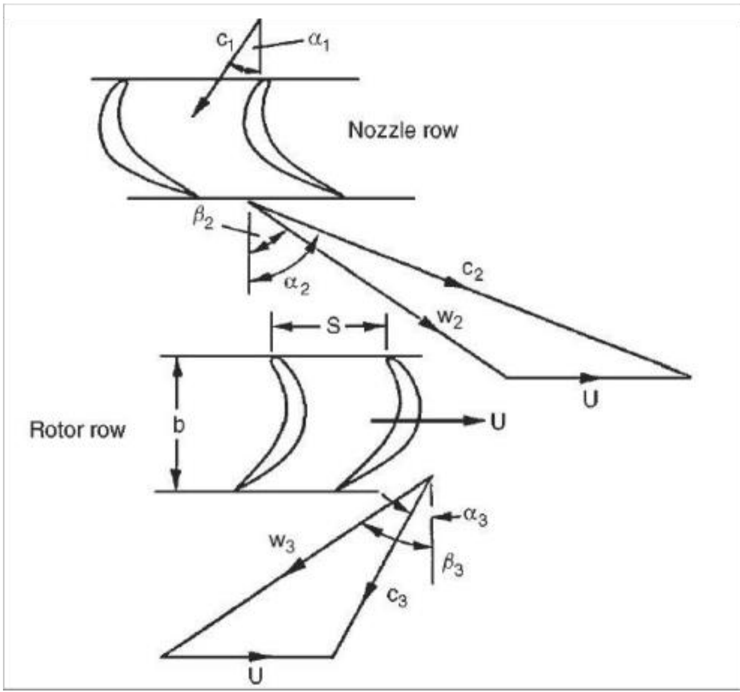

Picture 38 Velocity triangles at the inlet and outlet of an axial turbine [52]

3.5.4 Rotor and stator flow in a radial air turbine

Below it is shown that the exhaust gases get the proper call from the static diffuser vanes to enter the radial air turbine and are removed from them.

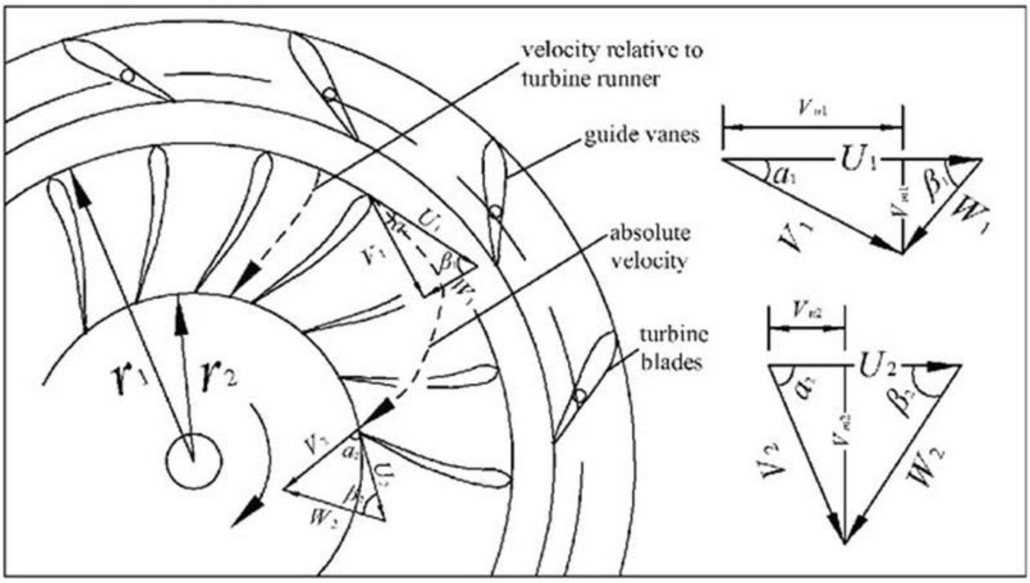

Picture 39 Velocity triangles at the inlet and outlet of an radial turbine[53]

3.6 Endurance and stress

In these applications the pressures and forces are very high strength relationships for tension and bending are given below.

$$\sigma = E\varepsilon$$

Where $\varepsilon = \frac{\Delta l}{l}$ and E the modulus of elasticity

$$T = G\gamma$$

Where γ shear angle and G the modulus of shear

[57]

For an axial turbine blade the elemental force is:

$$dF_c = -\Omega^2 r dm$$

Where : $dm = \rho_m A dr$

Accordingly the elementary voltage will be :

$$\frac{d\sigma_c}{\rho_m} = \frac{dF_c}{\rho_m A} = -\Omega^2 r dm$$

For fins of fixed and conical cross-section the developing stresses are:

- $\frac{\sigma_c}{\rho_m} = \Omega^2 \int_{r_h}^{r_t} r dr = \frac{U_t^2}{2}[1 - \left(\frac{r_h}{r_t}\right)^2]$

- $\frac{\sigma_c}{\rho_m} = \frac{KU_t^2}{2}[1 - \left(\frac{r_h}{r_t}\right)^2]$

Where K is stress factor ratio of cross-sectional reduction [56].

Unit 4 Turbopump design

4.1 Fuel pump design

The fuel is liquid hydrogen in cryogenic stability. With the criterion that the specific speed should be in the range of 1000 to 2000 to have a high efficiency and the difference of total pressure revs and supply were adjusted. The following images show the design point.

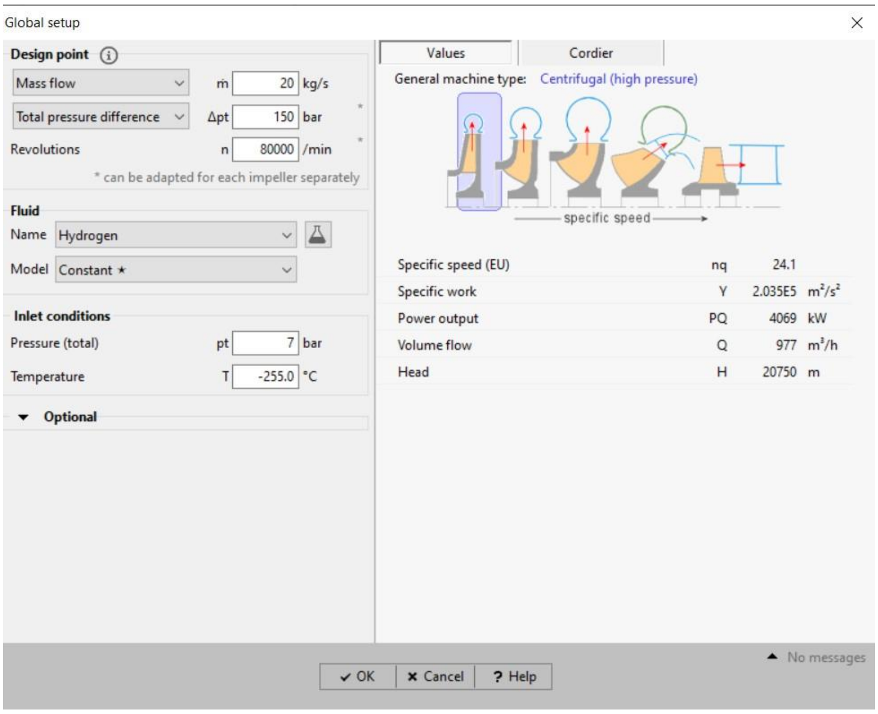

Picture 40 The design point of the LH₂ pump CFturbo program

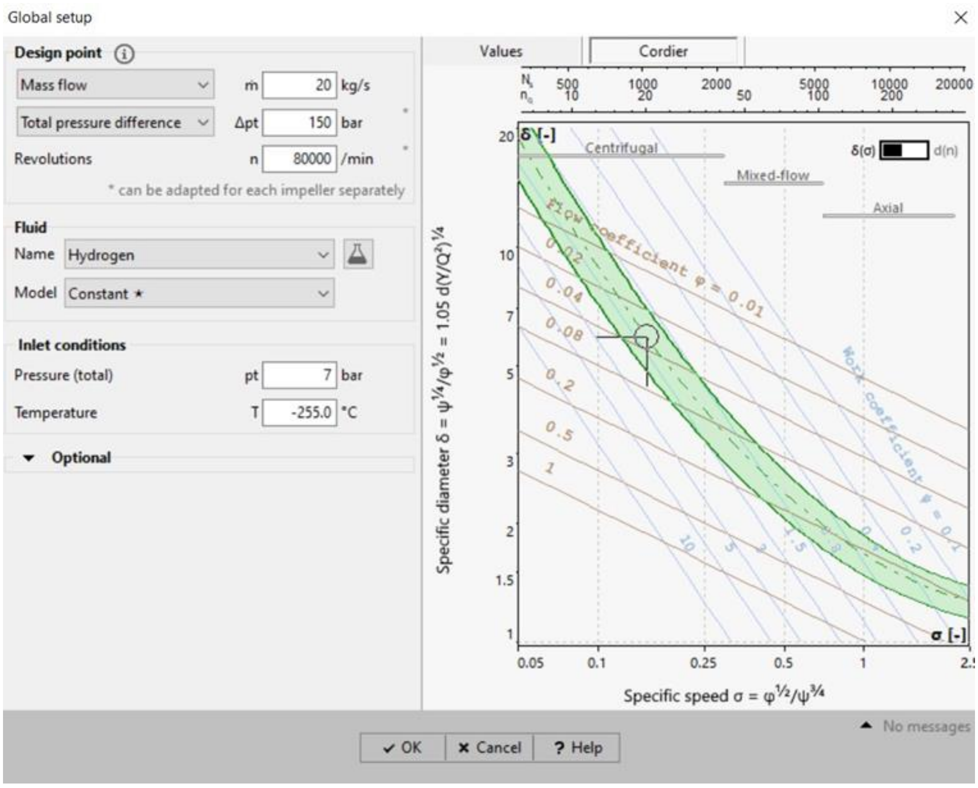

Picture 41 The design point of the LH₂ pump CFturbo program

The next step is determining the percentage pressure difference of the inducer and the impeller.

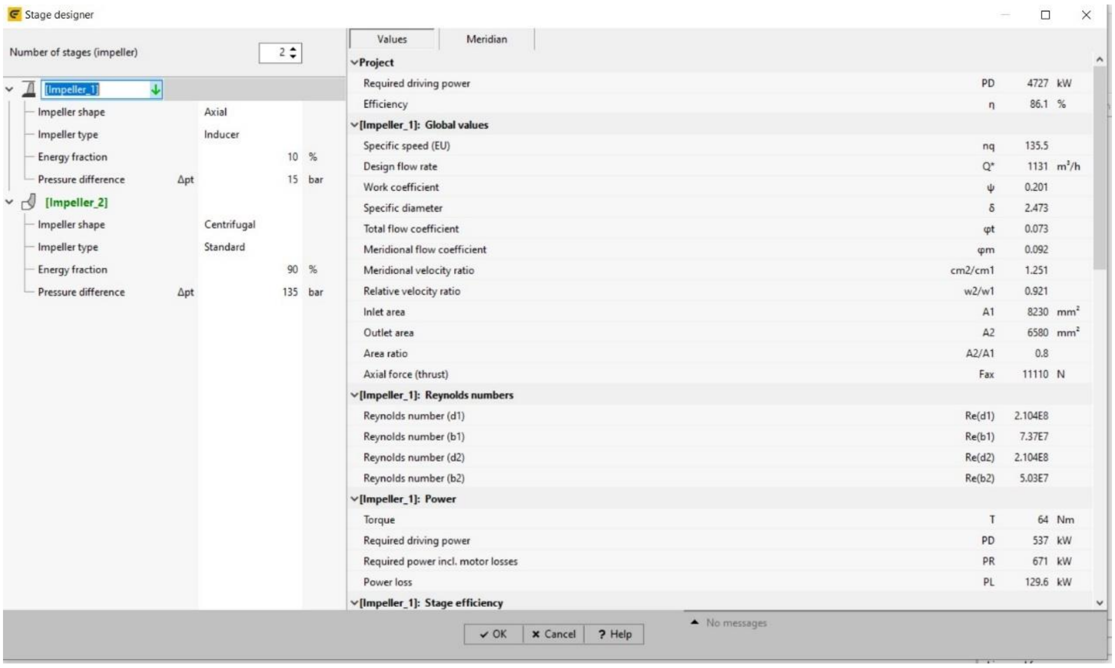

Picture 42 Pressure differential rates of the inducer and the impeller CFturbo program

The 10% of total pressure is from inducer and the 90% from impeller. After the design point of the turbopump has been properly defined, the design of the inducer begins.

4.1.1 Inducer

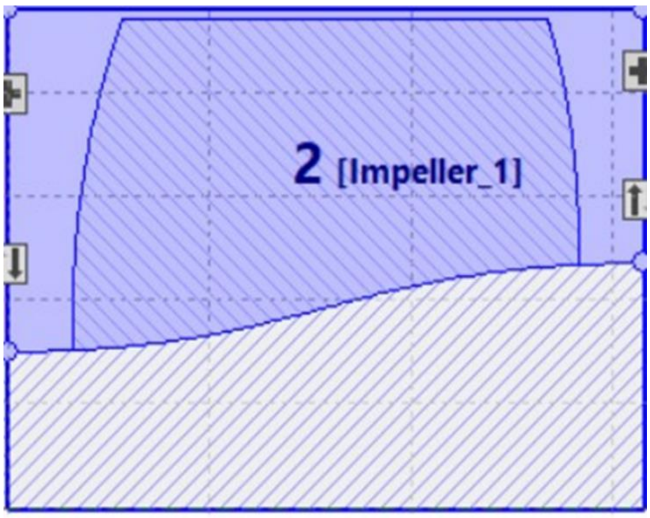

Picture 43 Inducer CFturbo program

The Design of inducer was based the coffecient flow, the ration v_1 and the ration of axial velocities. The tip clearance will be considered 0.1mm but the price is 1mm because to make the CFD analysis easier.

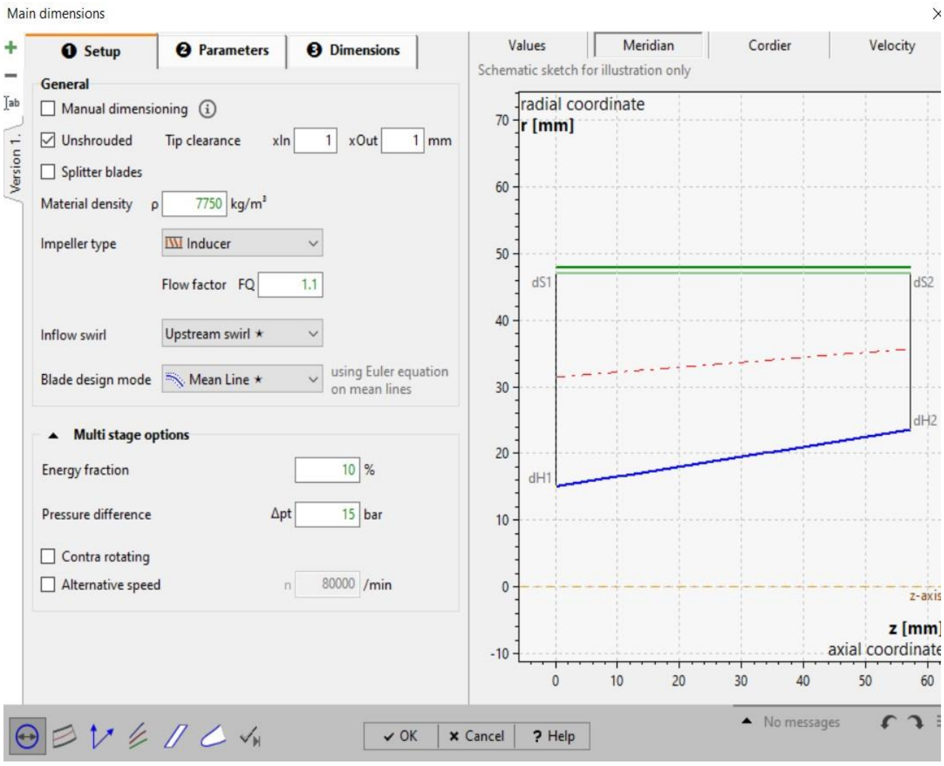

Picture 44 Start of set up of inducer CFturbo program

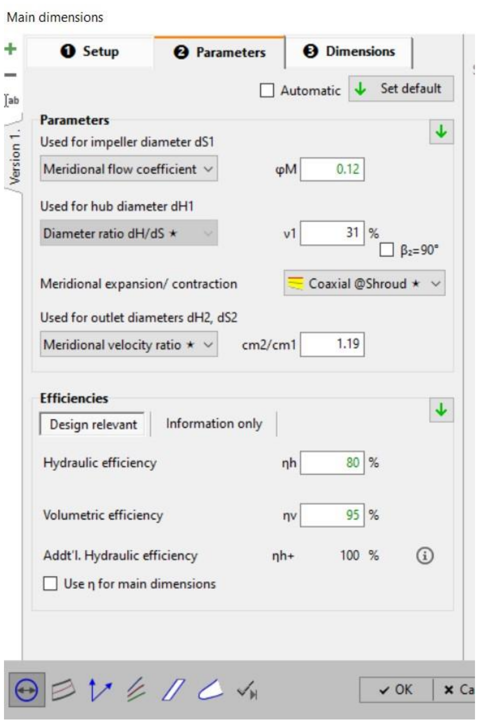

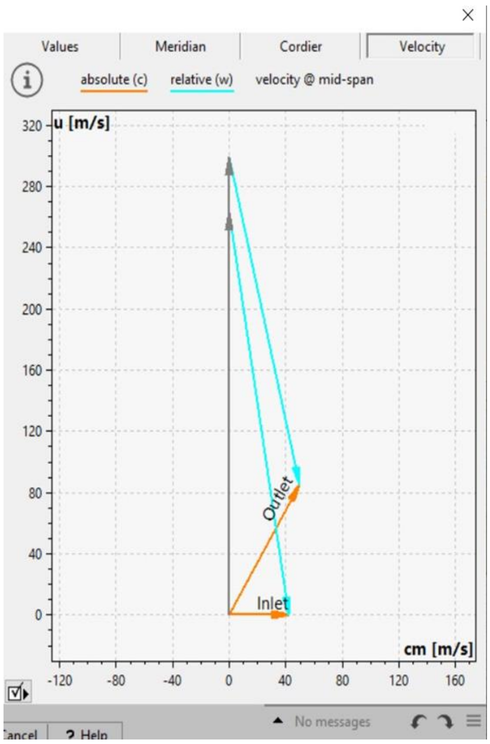

Picture 45 The design parameters CFturbo program

Picture 46 Inducer input and output speed triangles CFturbo program

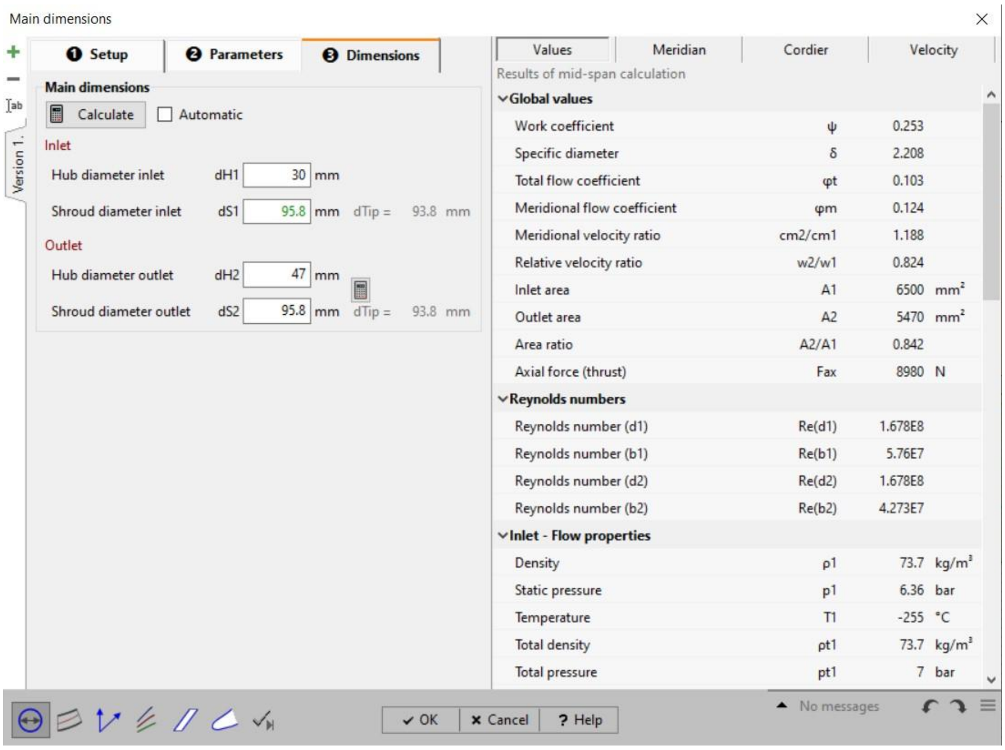

Picture 47 Input and output dimensions of the inducer and the all values CFturbo program

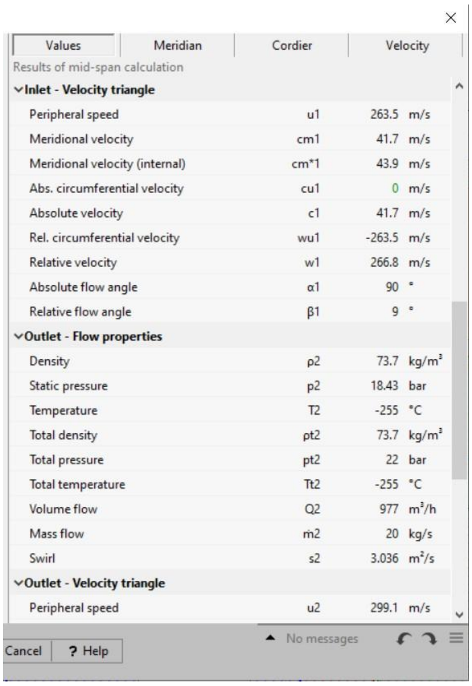

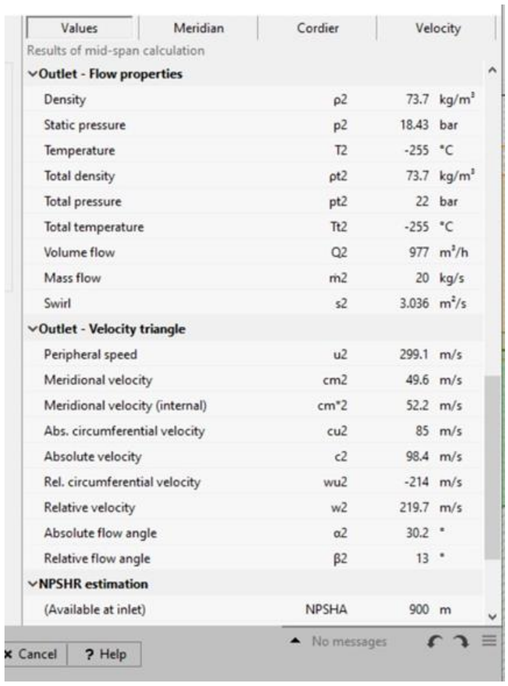

Picture 48 The values of all velocities, pressures and flow angles at the inlet and outlet of the inducer CFturbo program

Picture 49 The values of all velocities, pressures and flow angles at the inlet and outlet of the inducer CFturbo program

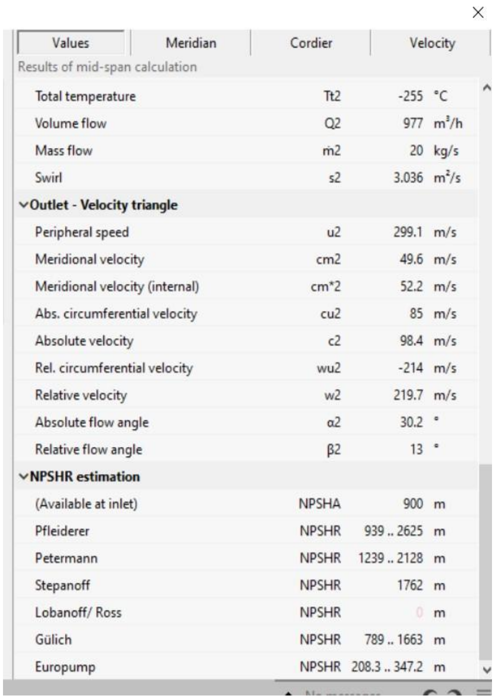

Values | Meridian | Cordier | Velocity

Results of mid-span calculation

Total temperature	Tt2	-255	°C
Volume flow	Q2	977	m³/h
Mass flow	m2	20	kg/s
Swirl	s2	3.036	m²/s
Outlet - Velocity triangle			
Peripheral speed	u2	299.1	m/s
Meridional velocity	cm2	49.6	m/s
Meridional velocity (internal)	cm*2	52.2	m/s
Abs. circumferential velocity	cu2	85	m/s
Absolute velocity	c2	98.4	m/s
Rel. circumferential velocity	wu2	-214	m/s
Relative velocity	w2	219.7	m/s
Absolute flow angle	α2	30.2	°
Relative flow angle	β2	13	°
NPSHR estimation			
(Available at inlet)	NPSHA	900	m
Pfleiderer	NPSHR	939 .. 2625	m
Petermann	NPSHR	1239 .. 2128	m
Stepanoff	NPSHR	1762	m
Lobanoff/ Ross	NPSHR	0	m
Gülich	NPSHR	789 .. 1663	m
Europump	NPSHR	208.3 .. 347.2	m

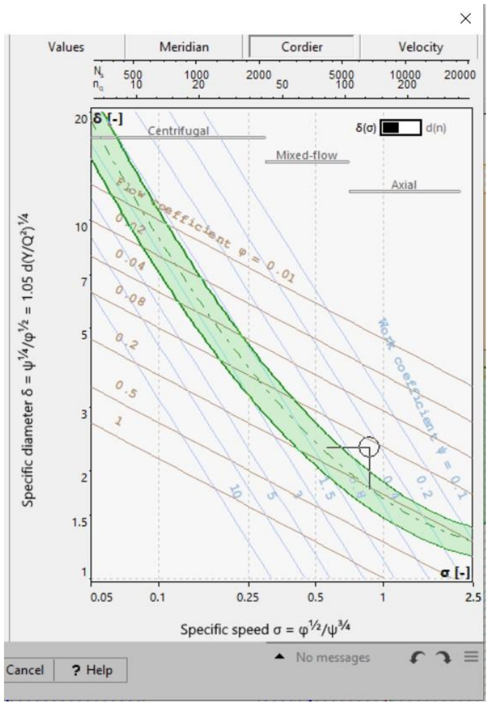

Picture 50 The values of all velocities, pressures and flow angles at the inlet and outlet of the inducer CFturbo program

Picture 51 Inducer design point CFturbo program

In the set up for pump according the Pfleiderer the NPSHR is bigger than NPSHA but for inducer the NPSHR is smaller and below an estimate is made for the NPHR calculation from the set up data and from the flow coefficient curve.

$$\text{NPSHR} = \lambda_c \frac{C_{m1}^2}{2g} + \lambda_w \frac{W_1^2}{2g}$$

- For C_{m1} = 41.7m/s , λ_c = 1.1 , , λ_w = 0.03 and W_1 = 266.8m/s : NPSHR = 206 m
- For C_{m1} = 41.7m/s , λ_c = 1.35, , λ_w = 0.06 and W_1 = 266.8m/s : NPSHR = 337 m

A range of NPSHR height was estimated for all cases. The available suction height is above these values. Therefore, the possibility of cavitation is very small. Below is the curve of nss versus flow coefficient φm.

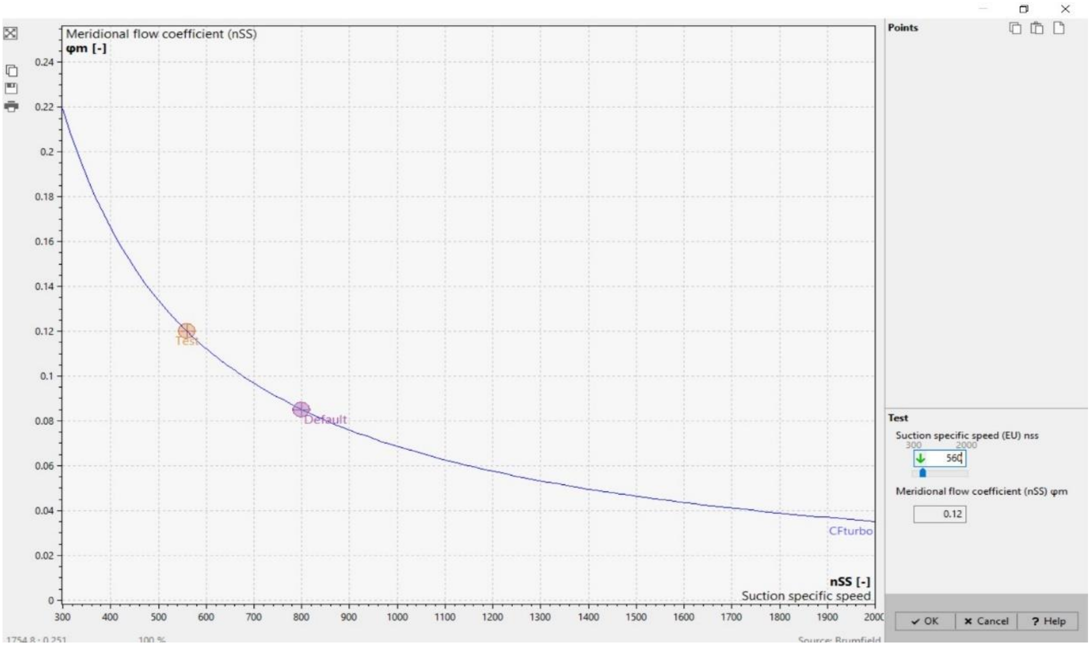

Picture 52 Flow coefficient function curve with specific speed number CFturbo program

For φ_m = 0,12 the n_{ss} = 560. The suction specific speed n_{ss} is calculated from the following relationship :

$$n_{ss} = \frac{n\sqrt{Q}}{NPSHR^{3/4}}$$

From data and the function the NPSHR = 313 m < NPSHA = 900 m

Below is the meridional contour. Minimal changes have been made with B-spline curves. The axial coordinate adjusted to be 63 mm. The last diagramma shows the the axial velocity distribution over the wing.

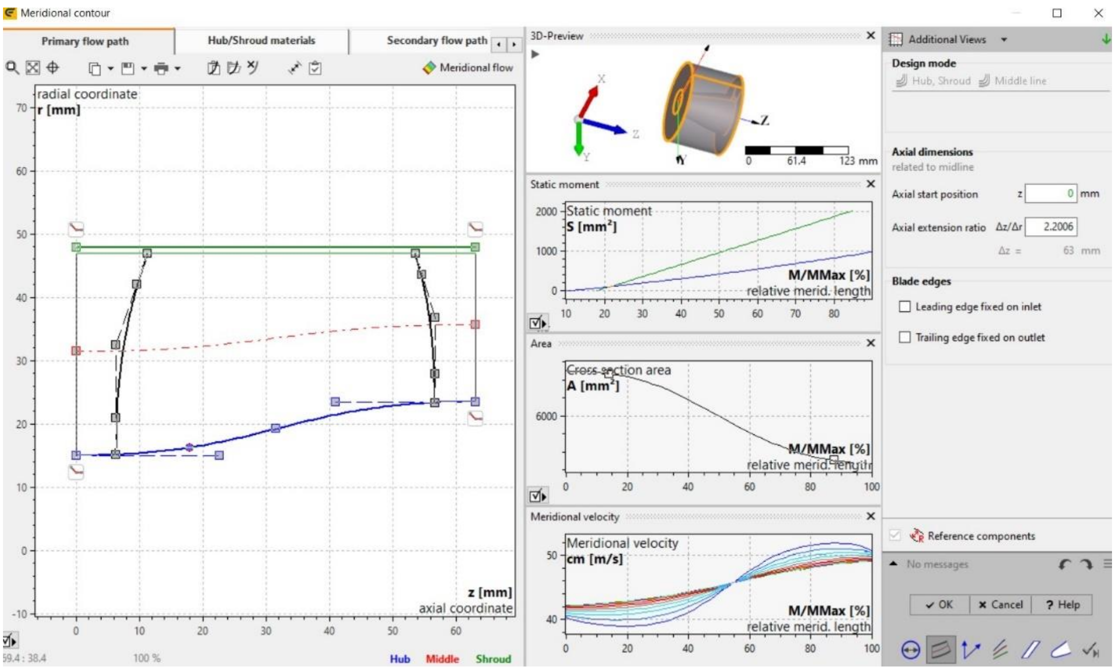

Picture 53 Meridian contour and B-spline configuration CFturbo program

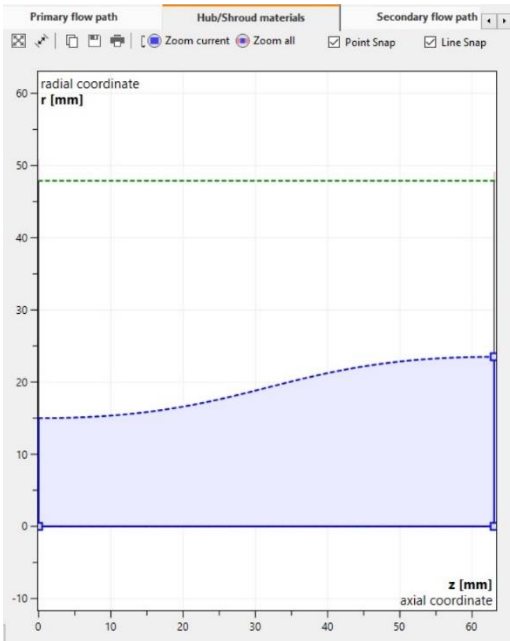

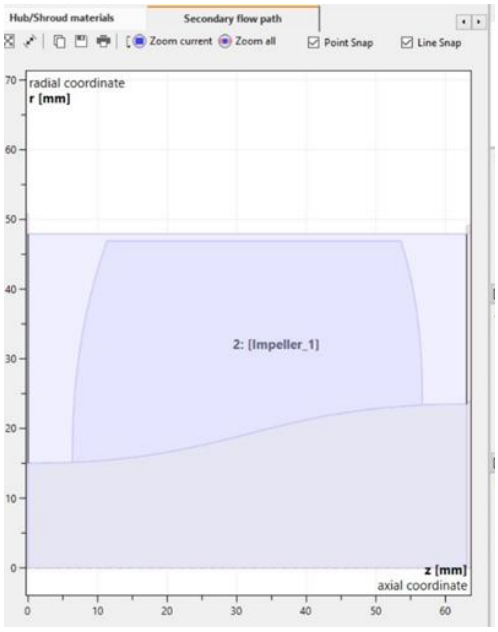

Picture 54 The shaft material (shaft shape) CFturbo program

Picture 55 Picture of inducer CFturbo program

The blade shape was made with base the methods Radial elements 3D. The thickness is 1mm, 0,1mm higher than default. The number of blades in an inducer, usually, 3. The iRelhub is default and the appeal δ is corrected from the number solidy l/t, which will be analyzed below.

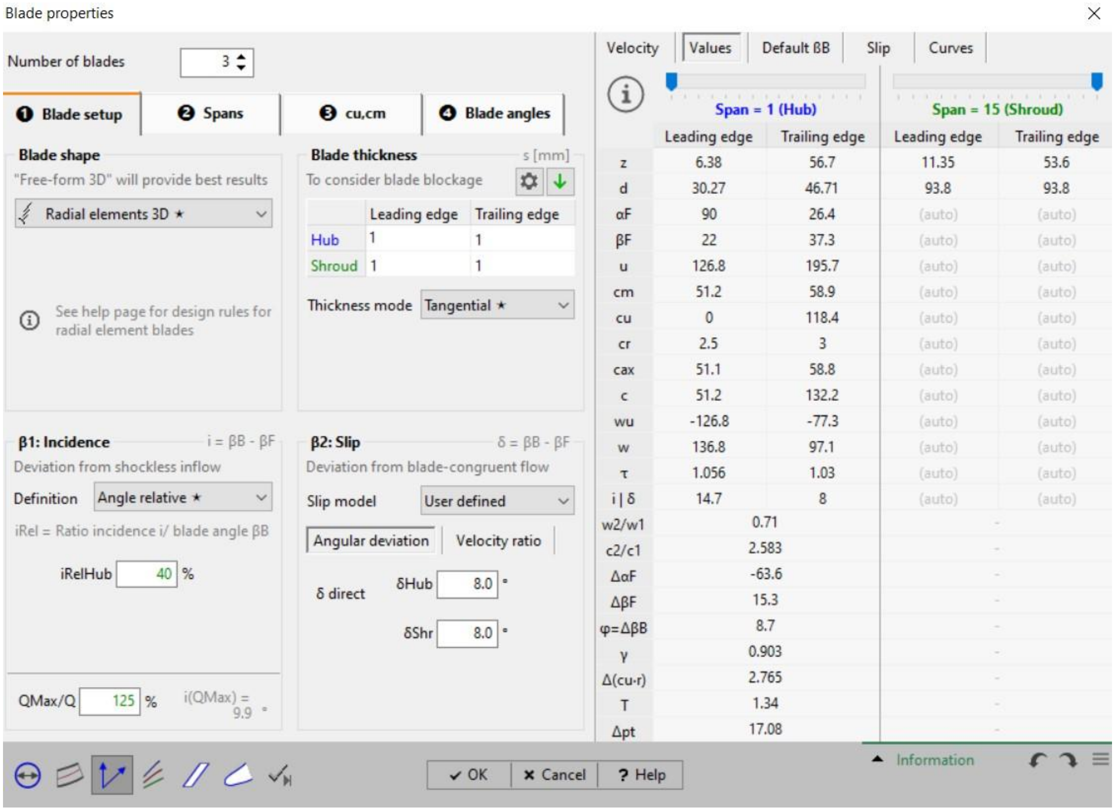

Picture 56 Space for shape and wing design settings and corner deviations CFturbo program

These pictures present the real velocities, the appeal and the corrected fin angles

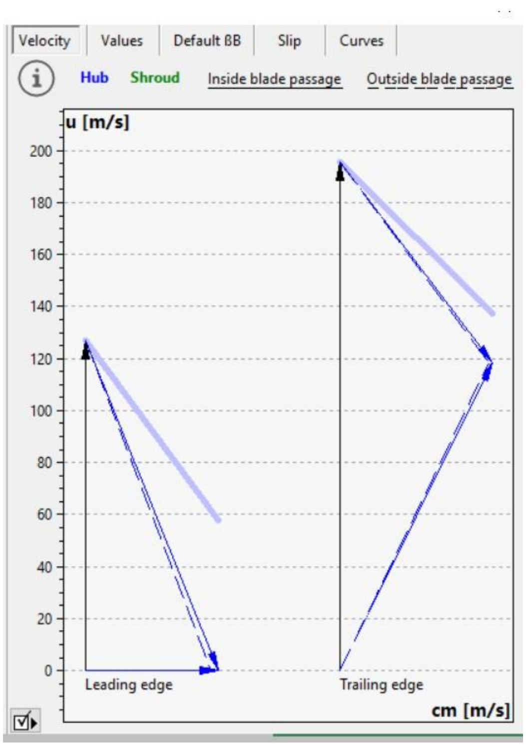


Velocity | Values | Default βB | Slip | Curves

Default blade angles βB [°] for main blade using "Free-form 3D" blade shape.
Based on:
- Shockless inflow for βB1 at leading edge
- Euler equation for βB2 at trailing edge

	βB1 [°]			βB2 [°]		
	optimal	current	ΔβB [°]	optimal	current	ΔβB [°]
1	22.6	36.6	14.0	43.4	45.3	2.0
2	19.8	32.1	12.2	35.6	43.3	7.7
3	17.7	28.9	11.2	30.3	41.4	11.0
4	15.9	26.0	10.1	26.6	39.6	13.0
5	14.5	23.2	8.8	23.8	37.8	14.1
6	13.2	20.7	7.4	21.6	36.1	14.6
7	12.2	18.7	6.5	19.8	34.4	14.6
8	11.4	17.1	5.8	18.4	32.8	14.5
9	10.6	15.8	5.2	17.2	31.3	14.1
10	9.9	14.6	4.7	16.2	29.8	13.7
11	9.4	13.7	4.3	15.3	28.4	13.1
12	8.8	12.8	4.0	14.5	27.0	12.5
13	8.4	12.1	3.7	13.9	25.7	11.9
14	8.0	11.5	3.5	13.3	24.5	11.2
15	7.6	11.0	3.3	12.7	23.3	10.6

Some blade angle values result from mean line constraints for simple blade shapes.

Picture 57 Velocity triangles at the inlet and outlet of the inductor with the deviation angles

Picture 58 The corrected inlet and outlet vane angle values

This is where slippage occurs. The curves that show how the angle changes are not displayed because of the Radial elements 3D command.

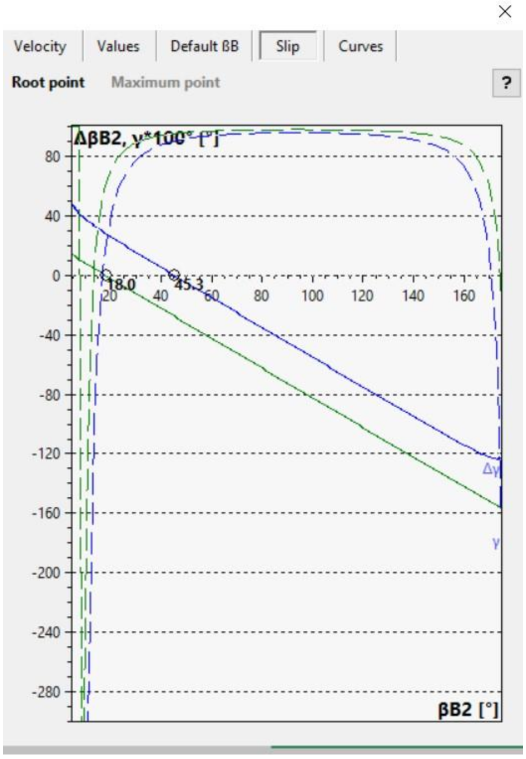

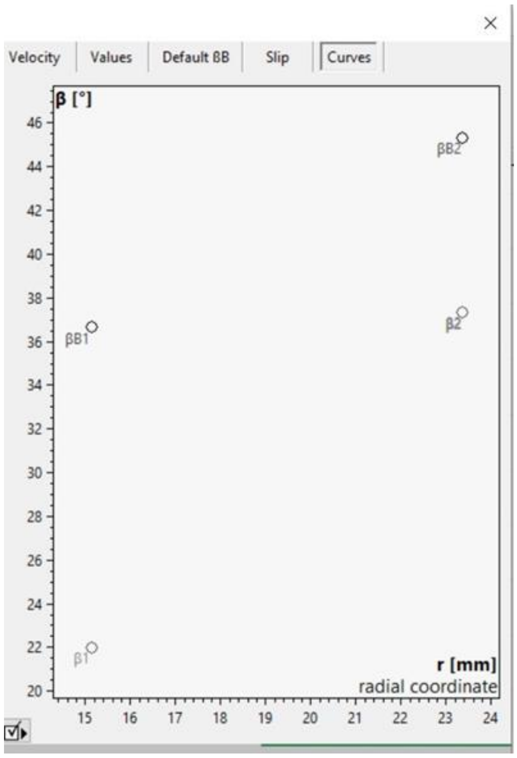

Picture 59 The slip of flow on blade CFturbo program

Picture 60 Angle distribution CFturbo program

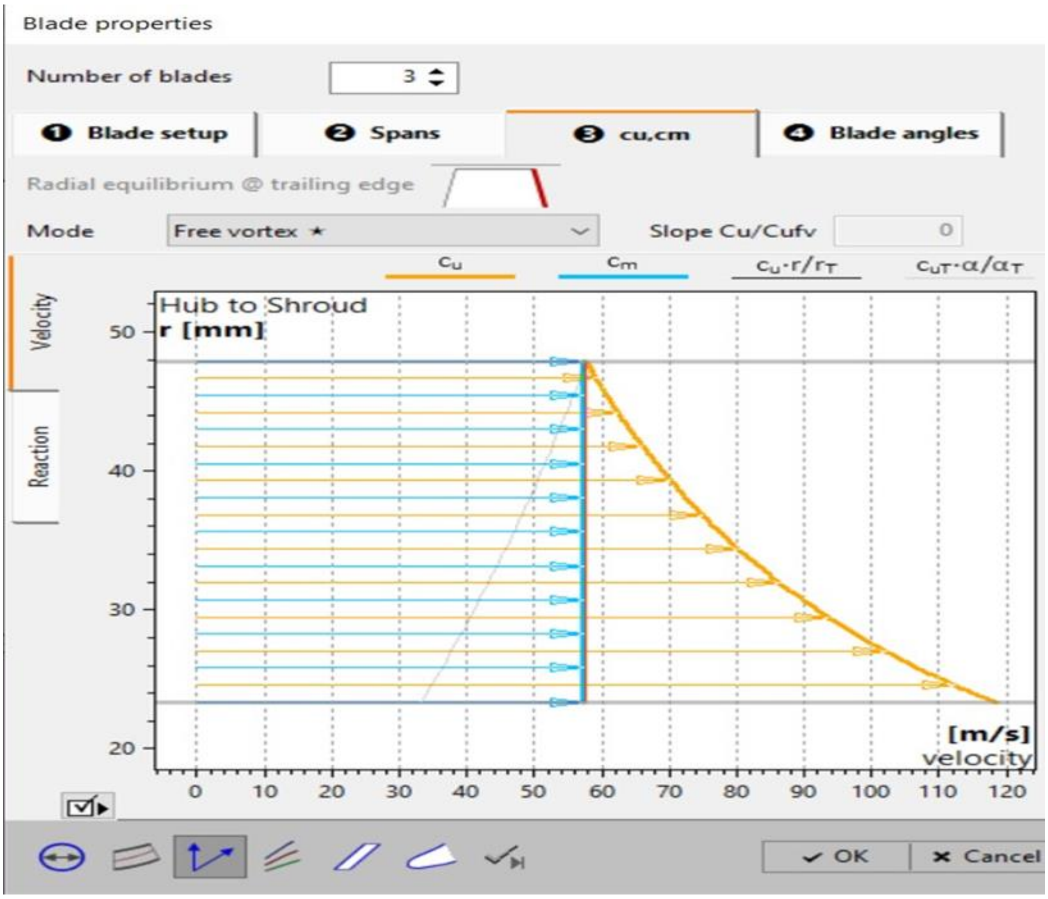

Picture 61 The radial distribution of Cu velocity with the free vorticity method CFturbo program

The methods which were used for blade design hub to shroud is free vortex. This method is considered the most suitable for the design of the inducer. Below, the blades angle aren't present in the picture from Radial elements 3D . The ratio R from the hub to the top of the wing shroud.

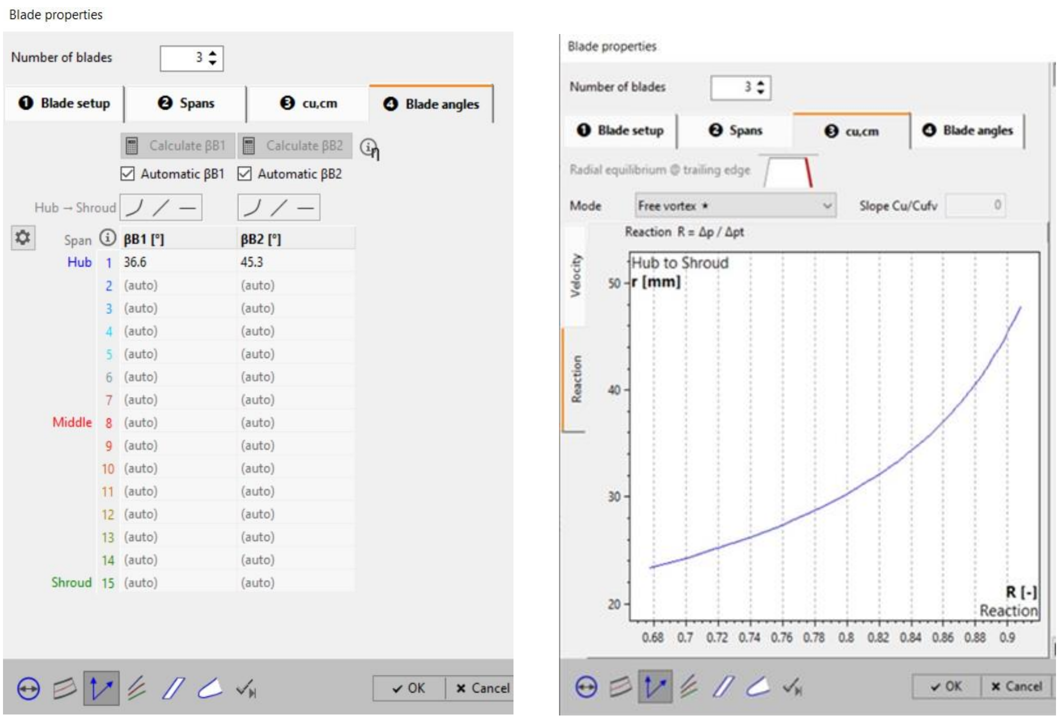

Picture 62 Automatic angle adjustment CFturbo program

Picture 63 The R ratio CFturbo program

The curvature of the wing lines and the wrap angle $\Delta\Phi$ = 240° were adjusted with static pressure as the main criterion. It is noted that in the indicative diagrams for Cm and Cu velocities, there are large exclusions.

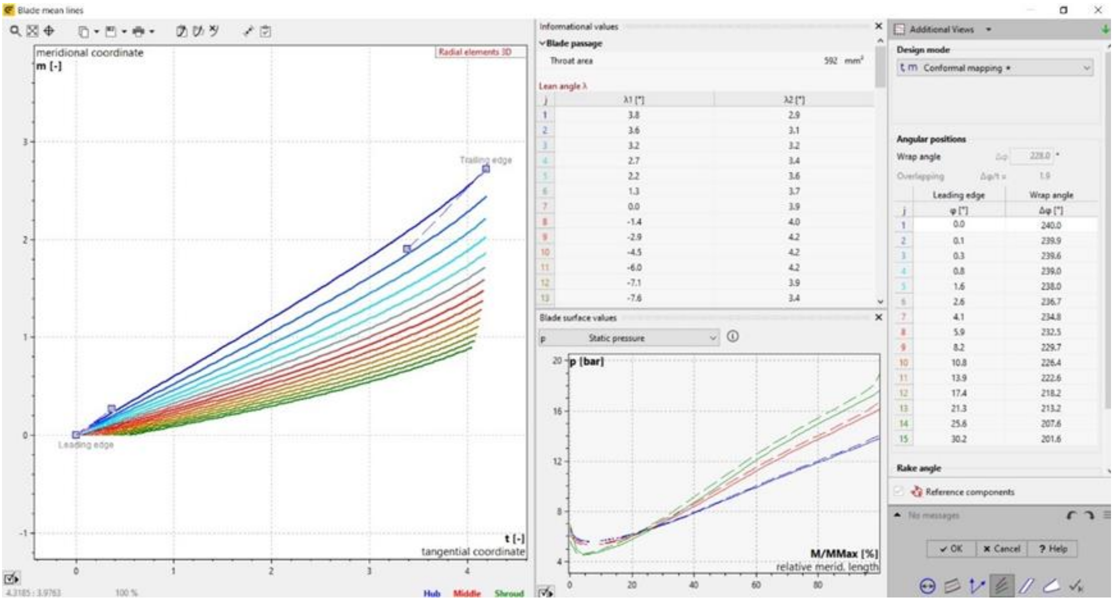

Picture 68 Blade configuration and design space with some criteria CFturbo program

Based on the solidity of the wing and the angles βB1 and βB2 at the middle distance of the wing, the recall δ was calculated. The relationship with which recall is calculated, is :

$$\delta = \left(2 + \frac{\beta B2 - \beta B2}{3}\right)\left(\frac{t}{l}\right)^{1/3}$$

First, the δ was 5° but it was corrected because for l/t =2.05 , βB2 = 30.4° and βB1 = 17.4° the δ = 4.99°. Because an incorrect estimate of δ was made, the corrected value was kept at 8 degrees, although normally it should have been at 5 degrees so that the whole design does not change.
The estimate was made at the average distance of the wing (at point 8) for the hub and for the Shroud.

Informational values

Blade angle βB

j	βB1 [°]	βB2 [°]	γ [°]
1	36.6	45.3	32.0
2	32.1	43.3	29.5
3	28.9	41.4	27.3
4	26.0	39.6	25.4
5	23.2	37.8	23.7
6	20.7	36.1	22.3
7	18.7	34.4	21.0
8	17.1	32.8	19.8
9	15.8	31.3	18.8
10	14.6	29.8	17.8
11	13.7	28.4	17.0
12	12.8	27.0	16.2
13	12.1	25.7	15.6
14	11.5	24.5	14.9
15	11.0	23.3	14.4

Blade angle in x-y βB,xy

Informational values

Blade solidity

j	l/t	lML/t	Δz/t	Δr/t
1	2.33	2.31	1.25	0.20
2	2.27	2.25	1.13	0.17
3	2.23	2.21	1.03	0.14
4	2.19	2.17	0.95	0.12
5	2.15	2.13	0.87	0.10
6	2.12	2.10	0.81	0.08
7	2.08	2.07	0.75	0.07
8	2.05	2.04	0.70	0.06
9	2.01	2.00	0.65	0.05
10	1.97	1.97	0.61	0.04
11	1.93	1.93	0.57	0.03
12	1.89	1.89	0.53	0.02
13	1.84	1.84	0.49	0.01
14	1.79	1.79	0.46	0.01
15	1.73	1.74	0.43	0.00

Other information

Picture 69 The entry and exit angles CFturbo program

Picture 70 Solidity of blade CFturbo program

No changes were made here

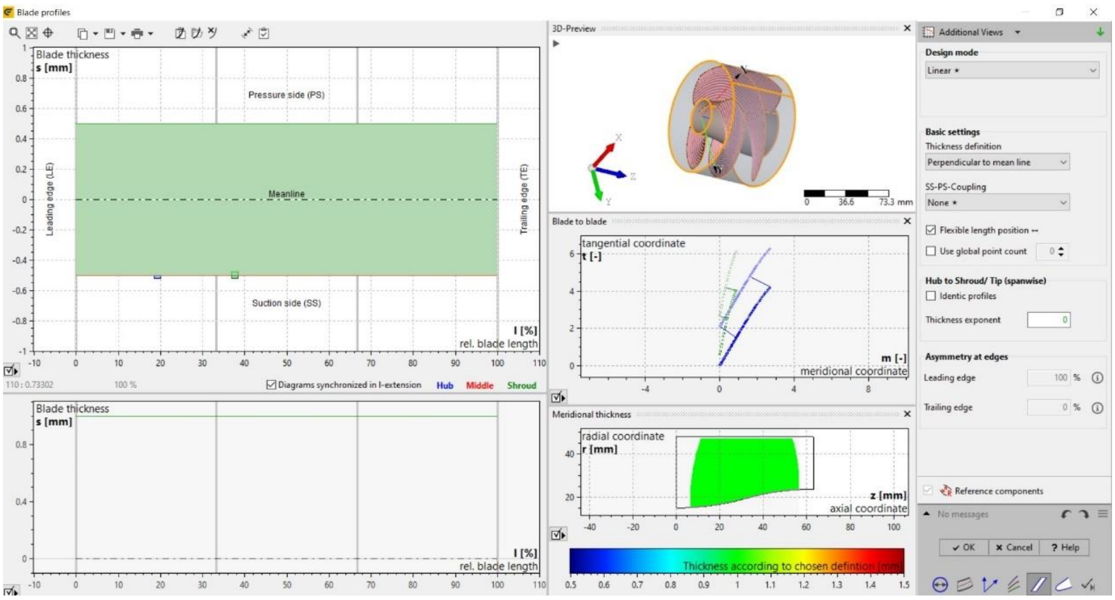

Picture 71 Blade profiles CFturbo program

Based on the pressure the elliptical nose adjusts to the ratio of 5 at the leading edge of the blade

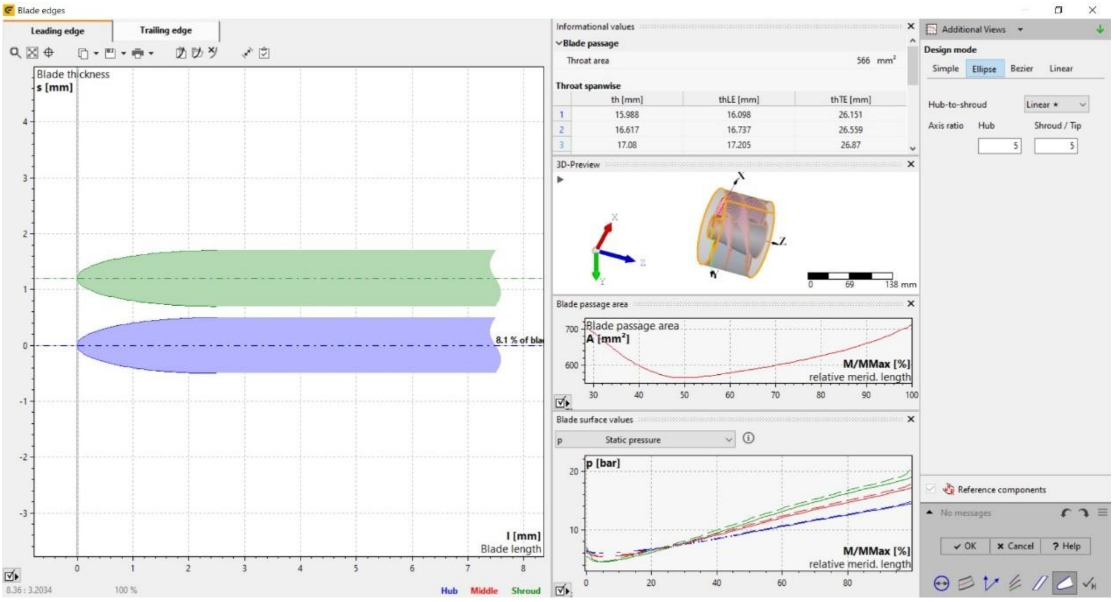

Picture 72 Blade leading edge CFturbo program

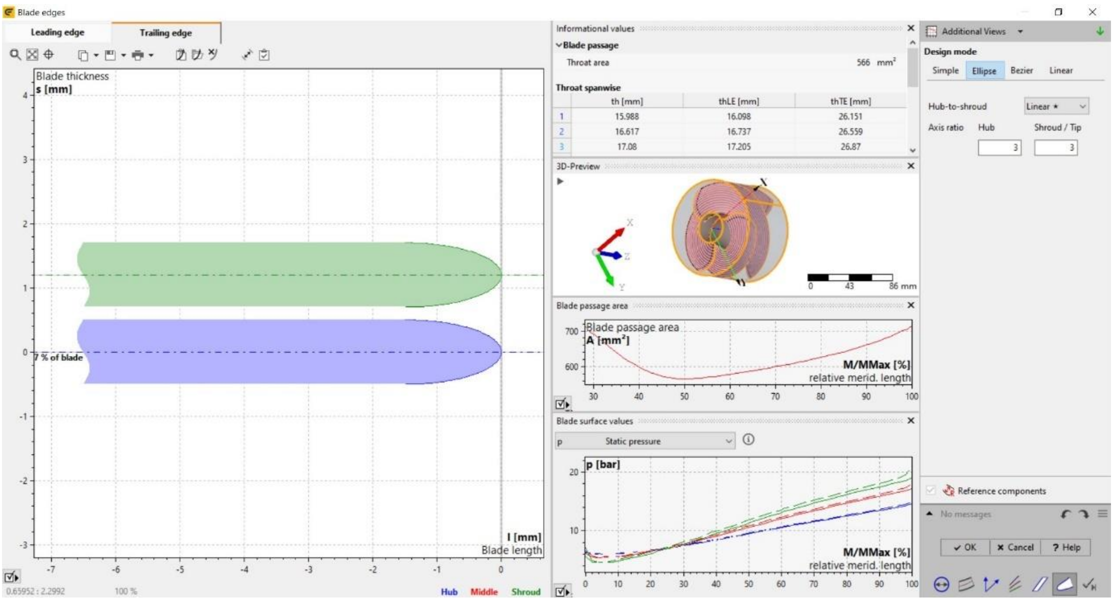

Picture 73 Blade trailing edge CFturbo program

4.1.2 Impeller

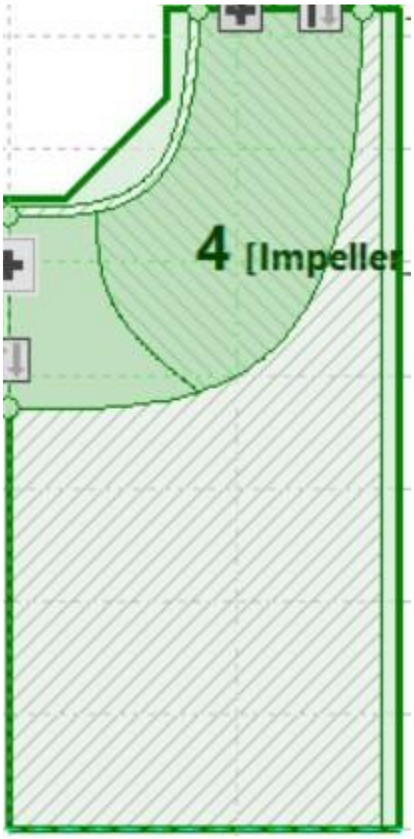

Picture74 Impeller CFturbo program

The impeller design was based on the head coefficient ψ, the ds/dh ratio, the b2/d2 ratio and the base diameter dH. The values were adjusted appropriately after several design iterations to have a retardation of the velocity W at each point of the blade

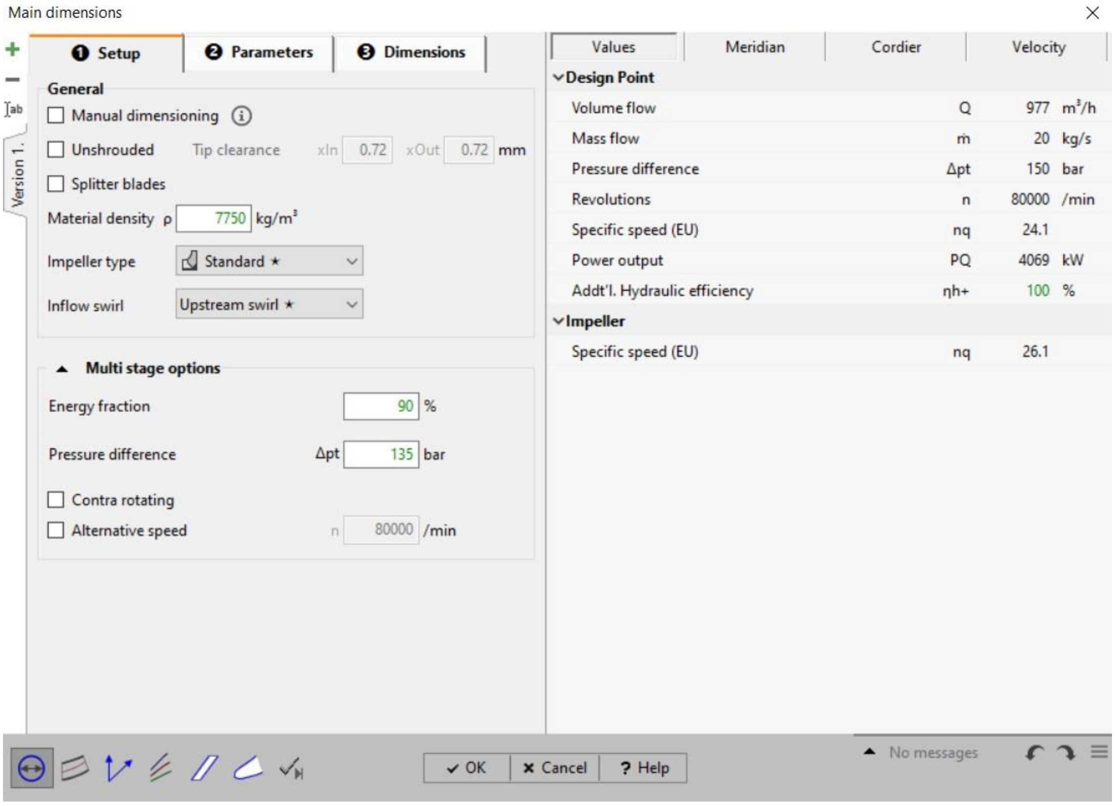

Picture 75 Start of set up of impeller CFturbo program

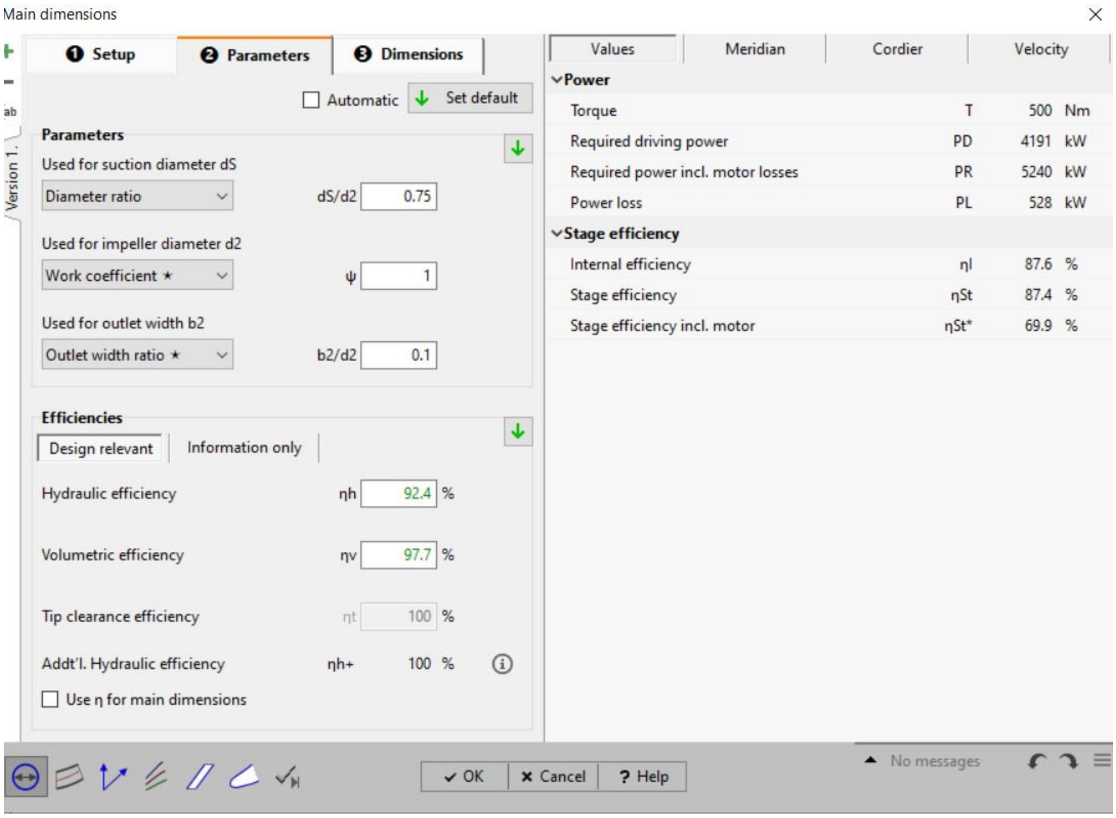

Picture 76 The design parameters CFturbo program

The coefficient ψ = 1 and other parameters were applied in order to where is retardation of the velocity W at each point of the blade. Also, the hub diameter dH = 74mm was set, based on the deceleration.

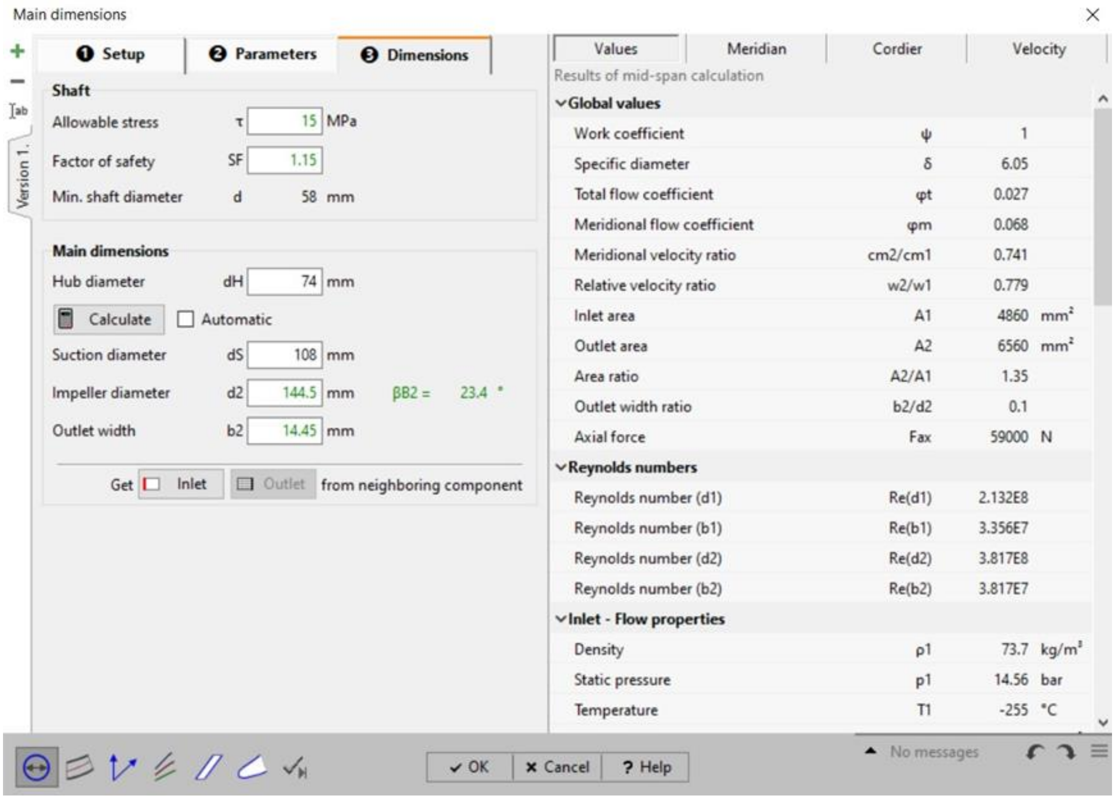

Picture 77 Input and output dimensions of the impeller and the all values CFturbo program

Below are the impeller inlet and outlet fluid characteristics, velocities and blade image.

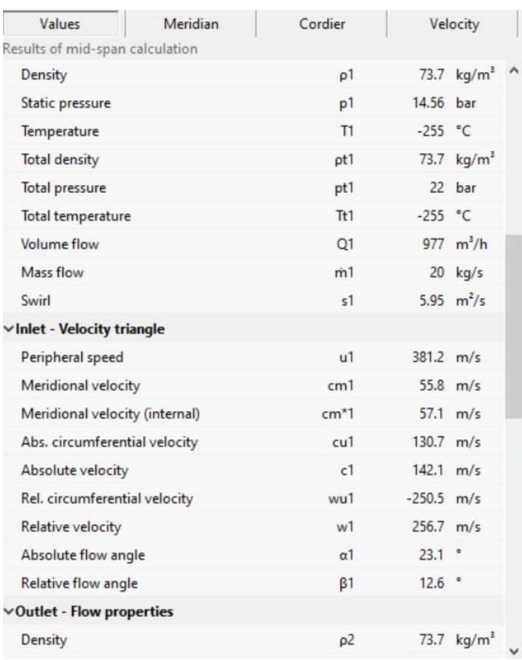

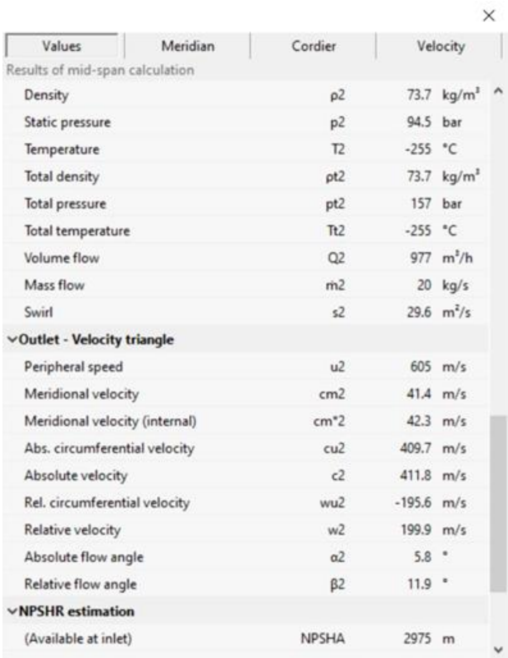

Picture 78 The values of all velocities, pressures and flow angles at the inlet and outlet of the impeller CFturbo program

Picture 79 The values of all velocities, pressures and flow angles at the inlet and outlet of the impeller CFturbo program

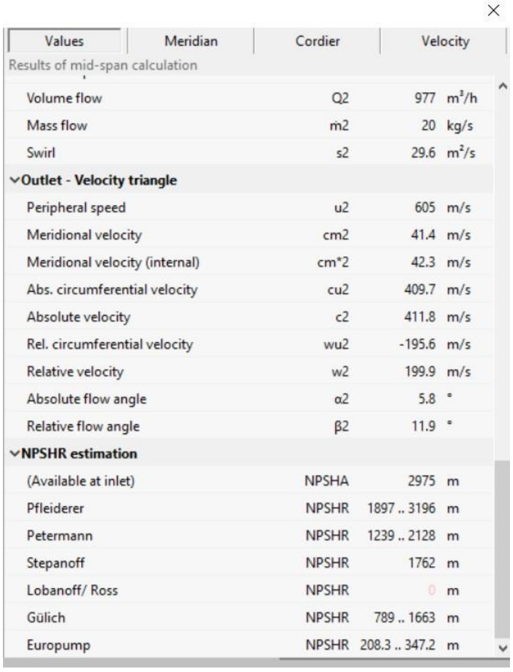

Values | Meridian | Cordier | Velocity

Results of mid-span calculation

Volume flow	Q2	977	m³/h
Mass flow	m2	20	kg/s
Swirl	s2	29.6	m²/s
Outlet - Velocity triangle			
Peripheral speed	u2	605	m/s
Meridional velocity	cm2	41.4	m/s
Meridional velocity (internal)	cm*2	42.3	m/s
Abs. circumferential velocity	cu2	409.7	m/s
Absolute velocity	c2	411.8	m/s
Rel. circumferential velocity	wu2	-195.6	m/s
Relative velocity	w2	199.9	m/s
Absolute flow angle	α2	5.8	°
Relative flow angle	β2	11.9	°
NPSHR estimation			
(Available at inlet)	NPSHA	2975	m
Pfleiderer	NPSHR	1897 .. 3196	m
Petermann	NPSHR	1239 .. 2128	m
Stepanoff	NPSHR	1762	m
Lobanoff/ Ross	NPSHR	0	m
Gülich	NPSHR	789 .. 1663	m
Europump	NPSHR	208.3 .. 347.2	m

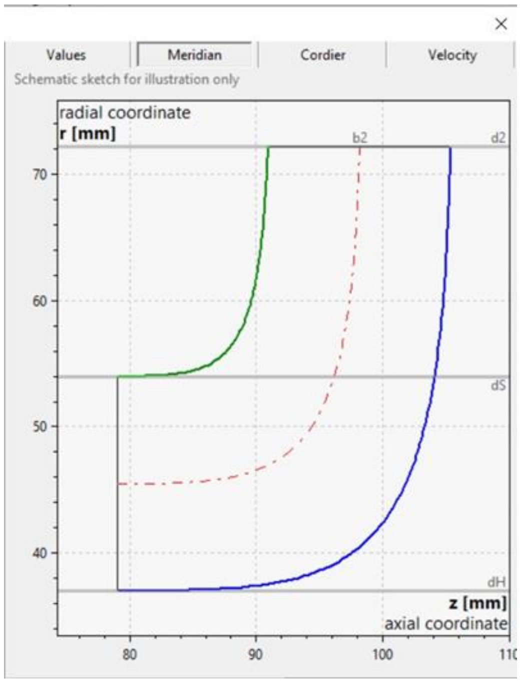

Picture 80 The values of all velocities, pressures and flow angles at the inlet and outlet of the impeller CFturbo program

Picture 81 Side view of blade CFturbo program

It is noted that :

- The NPSHA height is slightly less than the worst-case NPSHR value. Therefore there is a very small possibility of cavitation
- Angles β1 and β2 are very close in value although deceleration is achieved
- Typical values of head coefficient in turbopumps are from 0.5 to 0.8.

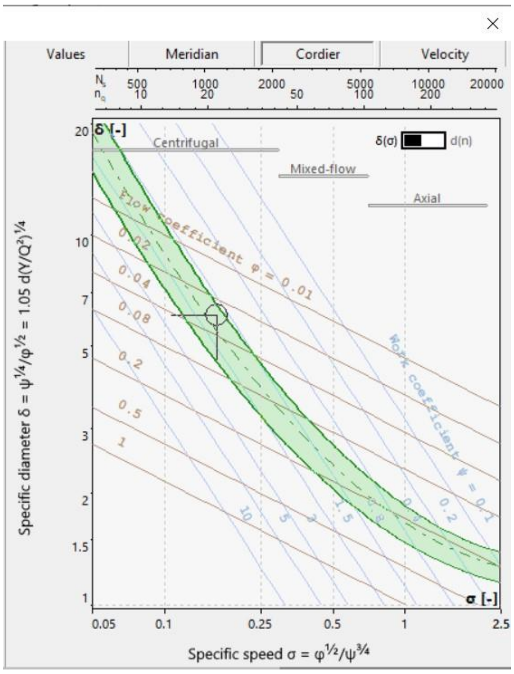

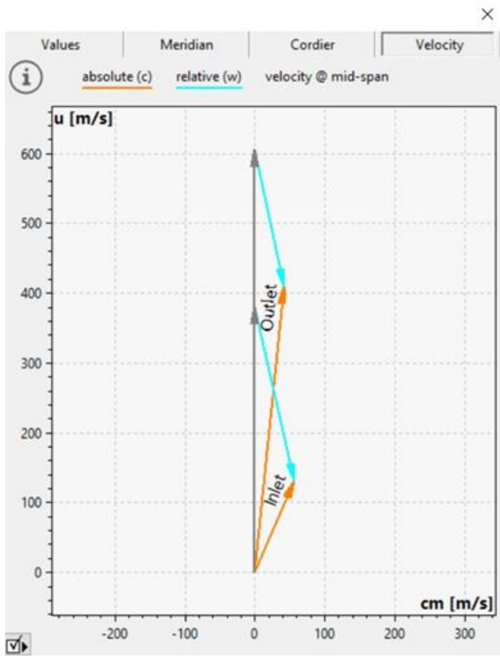

Picture 82 Inducer design point CFturbo program

Picture 83 Impeller input and output speed triangles CFturbo program

Below is the meridional contour. Minimal changes have been made with B-spline curves. shaped the aileron height to the default with ΔZ = 24mm and the leading edge of the wing with B-spline curves. The last diagramma shows the axial velocity distribution over blade.

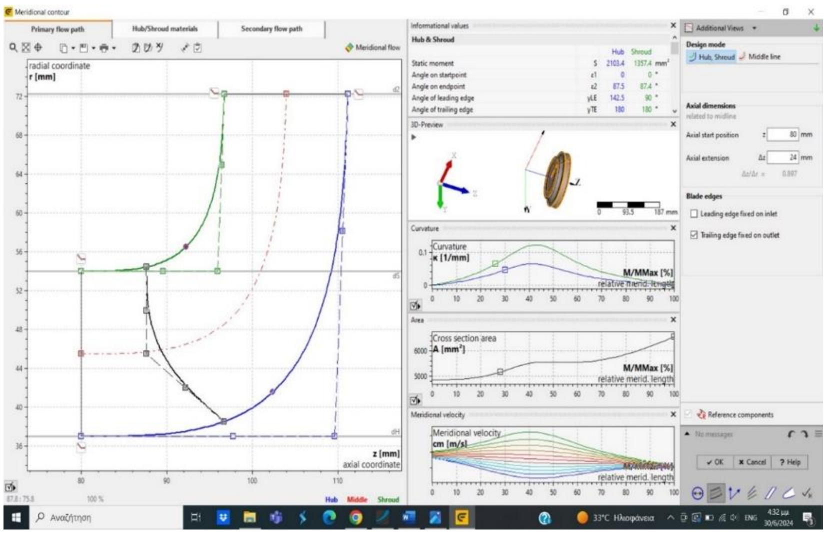

Picture 84 Meridian contour and B-spline configuration CFturbo program

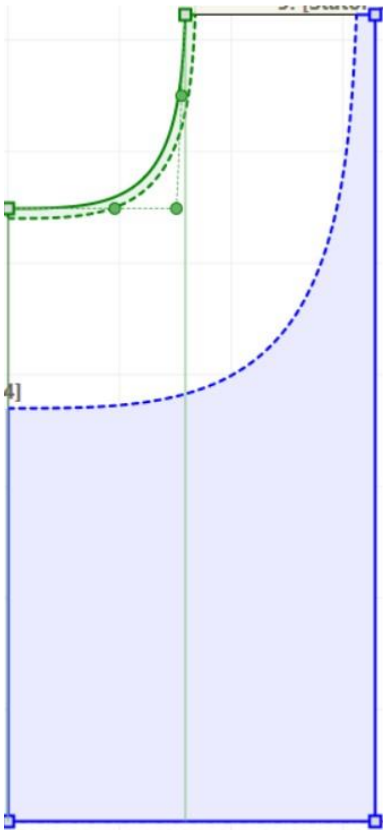

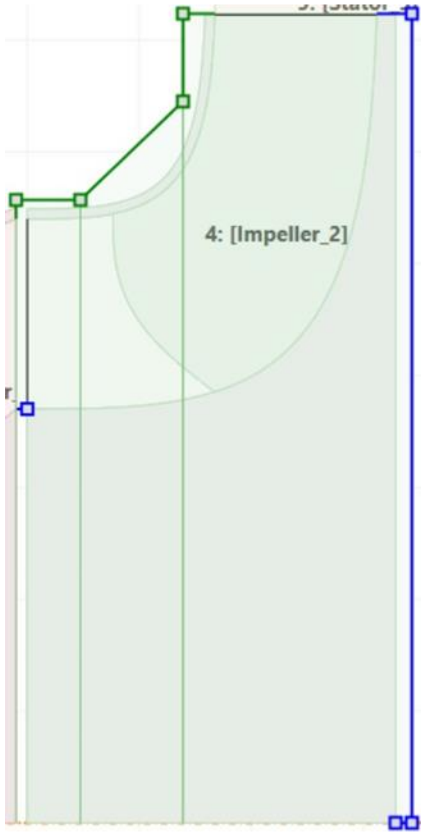

Picture 85 The material of the impeller shaft, disc and shroud CFturbo program

Picture 86 The impeller with an indicative static cover CFturbo program

With the methods Free-form 3D the shape of blade was made. The appeal is default and to control the shape of the vane, it was divided into 7 points. The number of vanes was determined by the relationship below :

$$Z = K_z \frac{d_2 + d_1}{d_2 - d_1} \sin\left(\frac{\beta_1 + \beta_2}{2}\right)$$

For K_z = 6,5 and the data from set up results in Z = 9,5. Therefore, 9 vanes are chosen. In water pumps, the ratio T is from 1.1 to 1.25. Based on this criterion the thickness of the blade is set. The thickness was set to 1.6 mm so that the T ratio is close to the value of 1.25[55] at the front of the impeller. The deviation angle was manually selected to the default of 10 degrees. Of course in the end because the fillet became very large, this ratio at the base of the wing exceeds the standard limit.

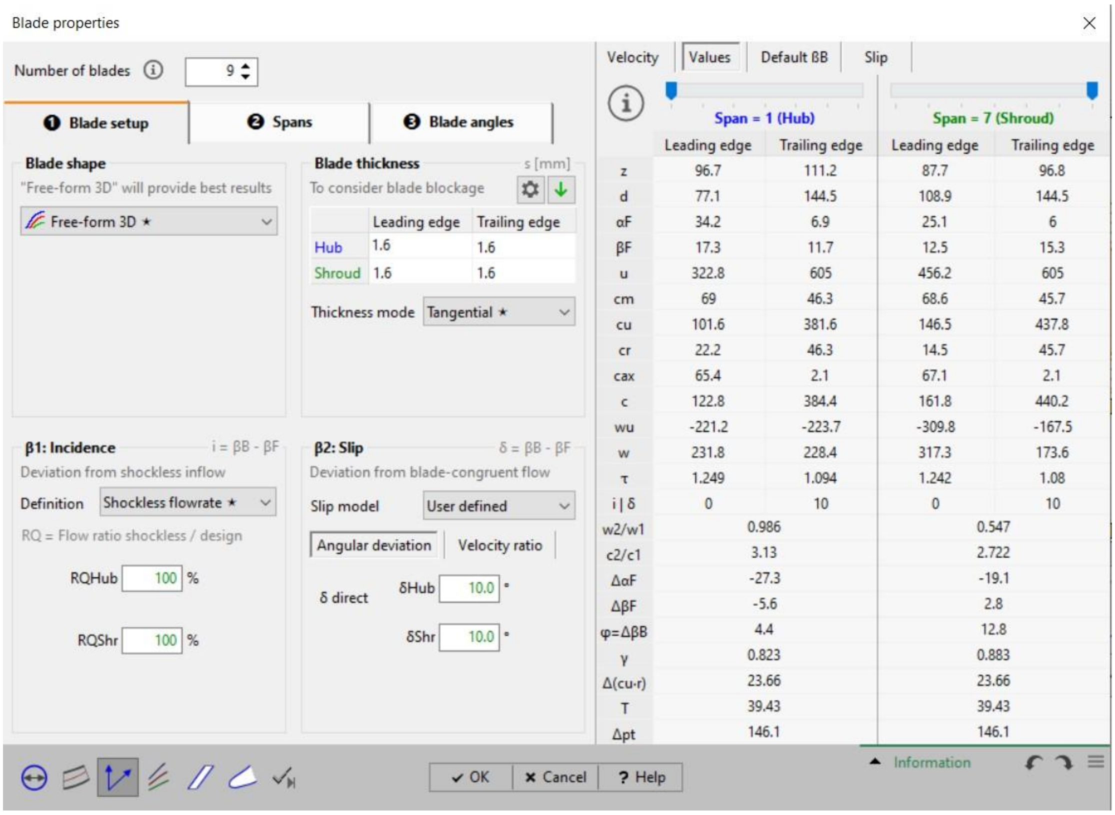

	Span = 1 (Hub) Leading edge	Span = 1 (Hub) Trailing edge	Span = 7 (Shroud) Leading edge	Span = 7 (Shroud) Trailing edge
z	96.7	111.2	87.7	96.8
d	77.1	144.5	108.9	144.5
αF	34.2	6.9	25.1	6
βF	17.3	11.7	12.5	15.3
u	322.8	605	456.2	605
cm	69	46.3	68.6	45.7
cu	101.6	381.6	146.5	437.8
cr	22.2	46.3	14.5	45.7
cax	65.4	2.1	67.1	2.1
c	122.8	384.4	161.8	440.2
wu	-221.2	-223.7	-309.8	-167.5
w	231.8	228.4	317.3	173.6
τ	1.249	1.094	1.242	1.08
i | δ	0	10	0	10
w2/w1	0.986		0.547	
c2/c1	3.13		2.722	
ΔαF	-27.3		-19.1	
ΔβF	-5.6		2.8	
φ=ΔβB	4.4		12.8	
γ	0.823		0.883	
Δ(cu·r)	23.66		23.66	
T	39.43		39.43	
Δpt	146.1		146.1	

Picture 87 Space for shape and wing design settings and corner deviations CFturbo program

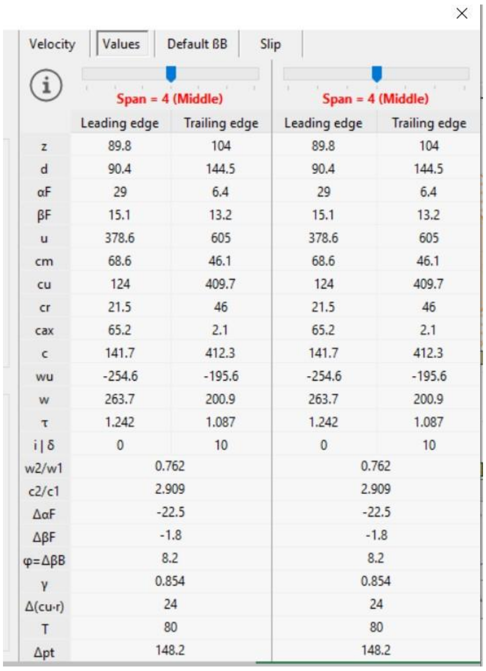

	Span = 4 (Middle) Leading edge	Span = 4 (Middle) Trailing edge	Span = 4 (Middle) Leading edge	Span = 4 (Middle) Trailing edge
z	89.8	104	89.8	104
d	90.4	144.5	90.4	144.5
αF	29	6.4	29	6.4
βF	15.1	13.2	15.1	13.2
u	378.6	605	378.6	605
cm	68.6	46.1	68.6	46.1
cu	124	409.7	124	409.7
cr	21.5	46	21.5	46
cax	65.2	2.1	65.2	2.1
c	141.7	412.3	141.7	412.3
wu	-254.6	-195.6	-254.6	-195.6
w	263.7	200.9	263.7	200.9
τ	1.242	1.087	1.242	1.087
i | δ	0	10	0	10
w2/w1	0.762		0.762	
c2/c1	2.909		2.909	
ΔαF	-22.5		-22.5	
ΔβF	-1.8		-1.8	
φ=ΔβB	8.2		8.2	
γ	0.854		0.854	
Δ(cu·r)	24		24	
T	80		80	
Δpt	148.2		148.2	

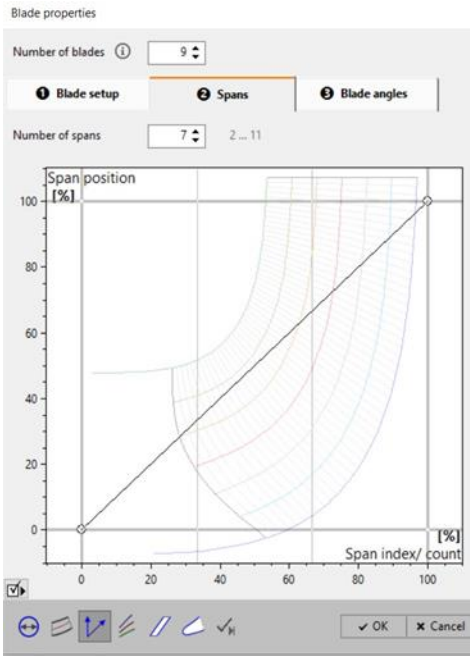

Picture 88 The values at the inlet and outlet of the impeller at the central point of the blade CFturbo program

Picture 89 Number of spans CFturbo program

These photos show the speeds, the corrected blade angles and the slip.

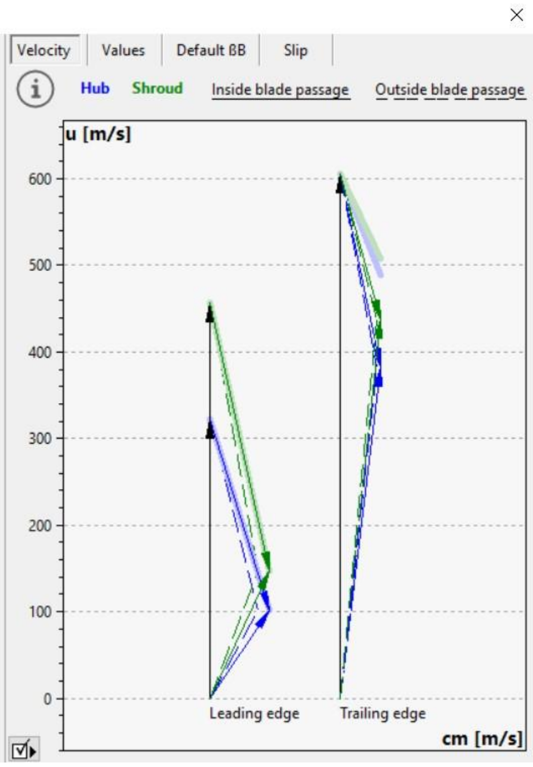


Velocity | Values | Default ßB | Slip

Default blade angles ßB [°] for main blade using "Free-form 3D" blade shape.
Based on:
- Shockless inflow for βB1 at leading edge
- Euler equation for βB2 at trailing edge

	βB1 [°]			βB2 [°]		
	optimal	current	ΔβB [°]	optimal	current	ΔβB [°]
1	17.3	17.3	0.0	17.8	21.7	3.9
2	16.6	16.6	0.0	19.1	22.2	3.1
3	15.9	15.9	0.0	20.7	22.7	2.0
4	15.1	15.1	0.0	22.7	23.2	0.5
5	14.2	14.2	0.0	25.3	23.9	-1.5
6	13.3	13.3	0.0	106.9	24.5	-82.3
7	12.5	12.5	0.0	123.7	25.3	-98.4

Picture 90 Velocity triangles at the inlet and outlet of the impeller with the deviation angles CFturbo program

Picture 91 The corrected inlet and outlet vane angle values CFturbo program

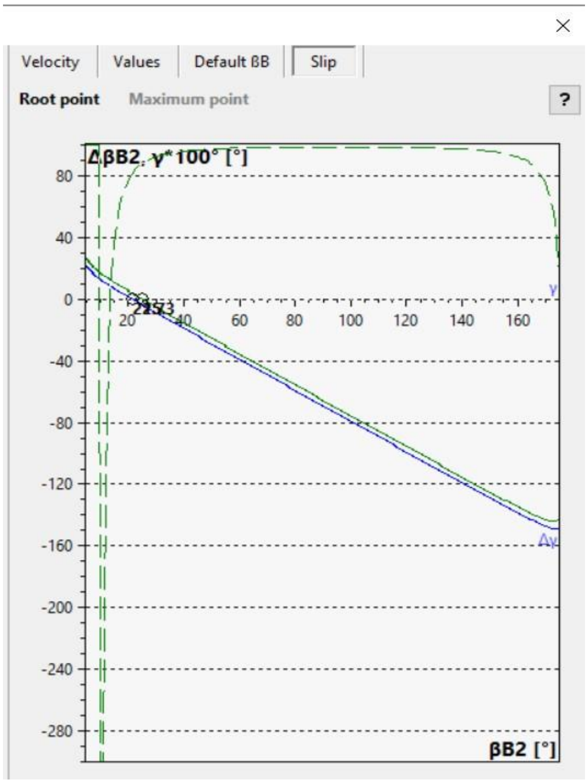

Picture 92 The slip CFturbo program

The fin was modeled based on the methods comfortable mapping. Appropriate meridional offsets were adjusted based on static pressure and by monitoring velocities. The scroll angle was left at the default ΔΦ =70º.

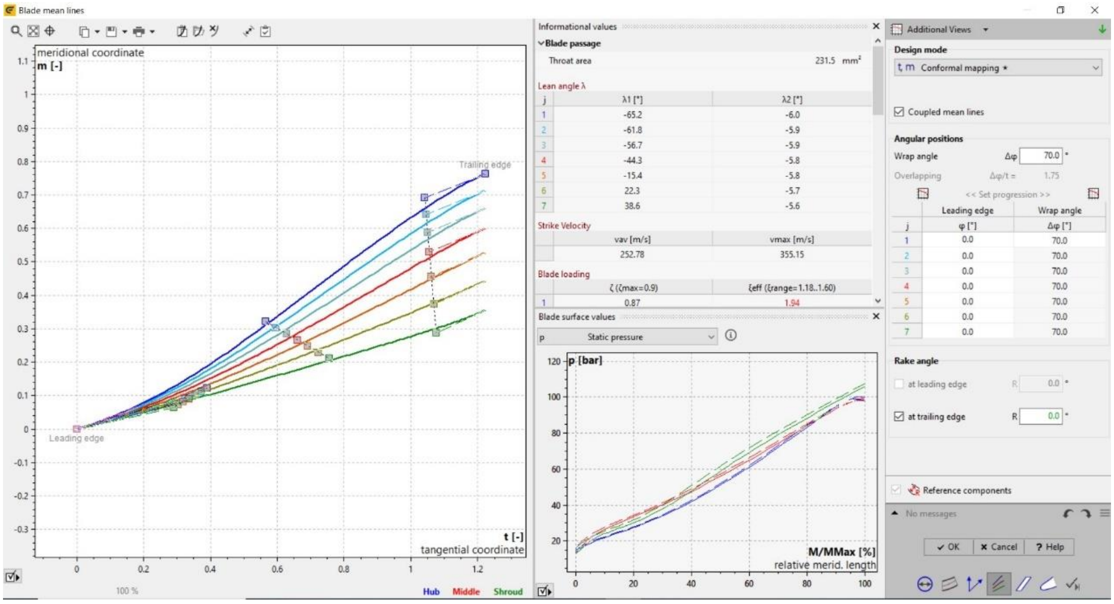

Picture 93 Blade configuration and design space with some criteria CFturbo program

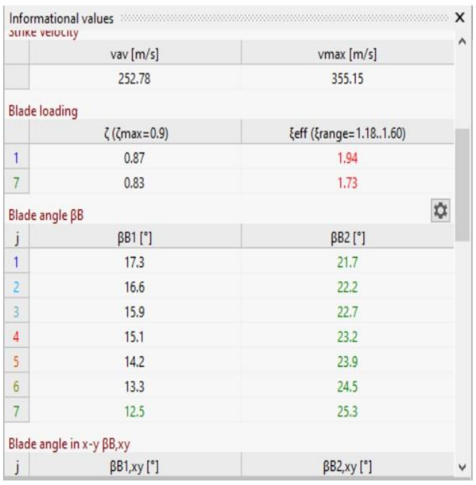

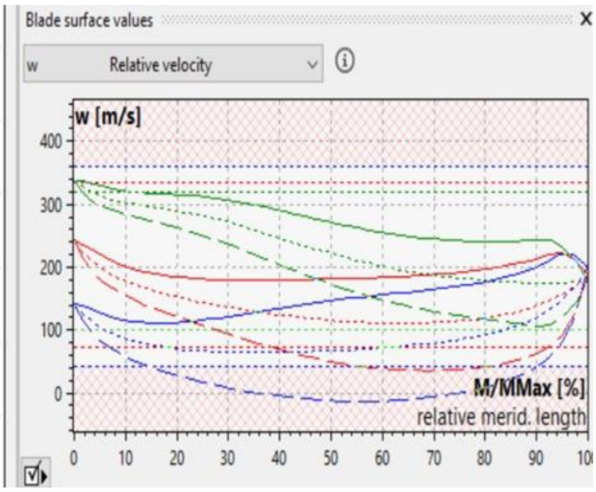

Picture 94 The entry and exit angles CFturbo program

Picture 95 The relative velocity distribution over the meridional length of the blade in percent CFturbo program

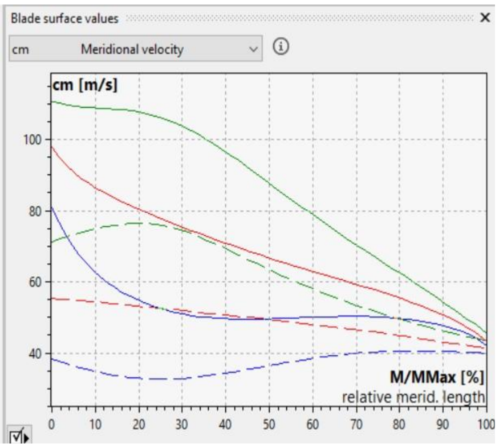

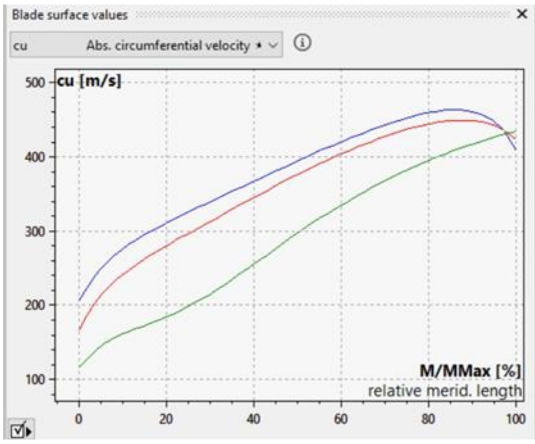

Picture 96 The meridional velocity distribution over the meridional length of the blade in percent CFturbo program

Picture 97 The absolute circumferential velocity distribution over the meridional length of the blade in percent CFturbo program

There are big appeals in the meridional velocity in the intel of impeller.

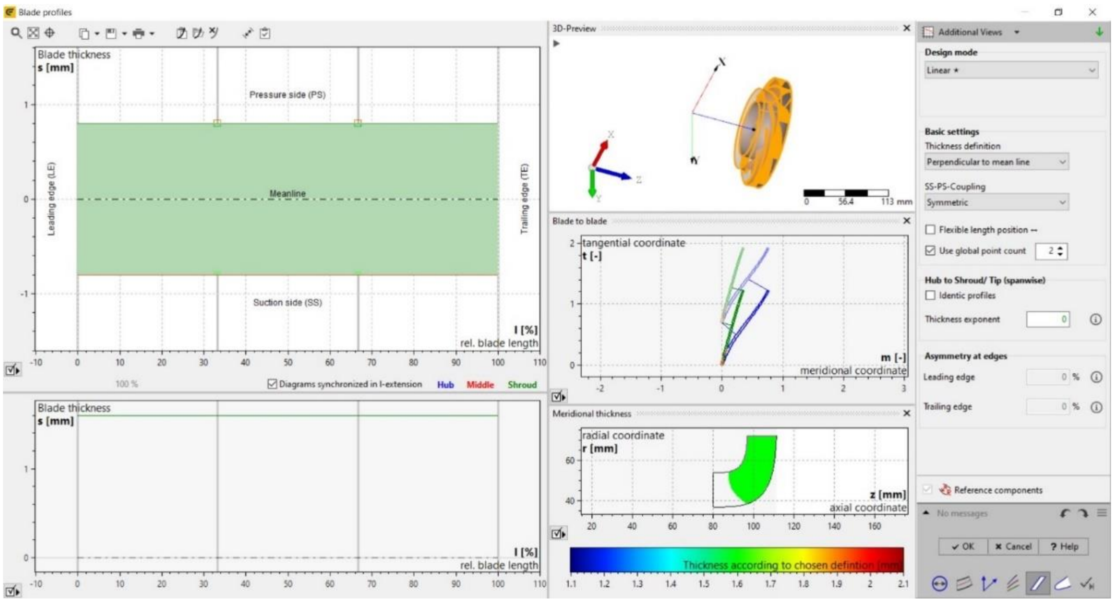

Picture 98 Blade profiles CFturbo program

Typically, the front tips of the impeller in turbopumps are elliptical with a ratio of 2 to 3[36]. Therefore, the default value of 3 was chosen based on the pressure.

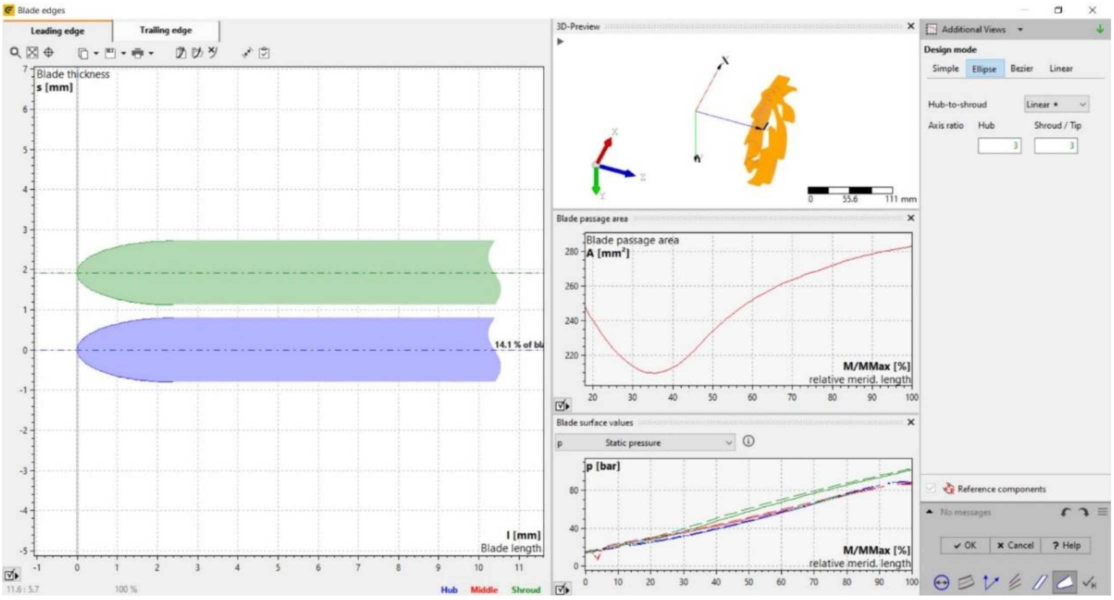

Picture 99 Blade leading edge CFturbo program

No changes were made to the rear of the impeller.

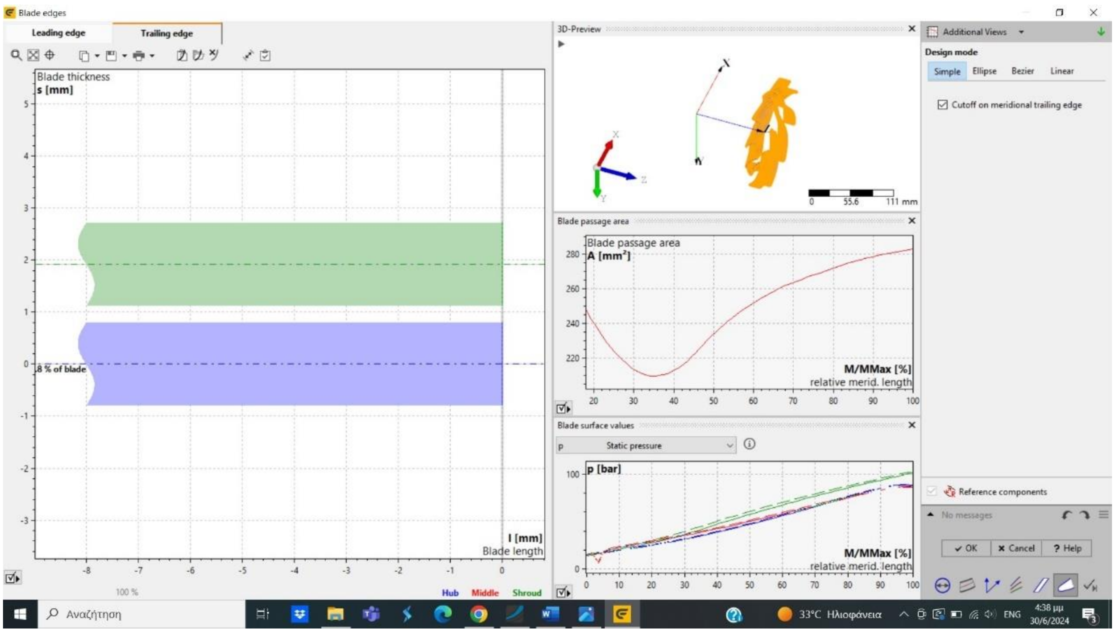

Picture 100 Blade trailing edge CFturbo program

4.1.3 Stator

Because the diameter of the commutator base and that of the impeller differ, a conical shaft was adapted to rotate inside a conical tube. This will bring additional hydraulic losses. Alternatively, fitting a diffuser would have been a better solution but was not used to simplify the CFD analysis. No design losses are taken.

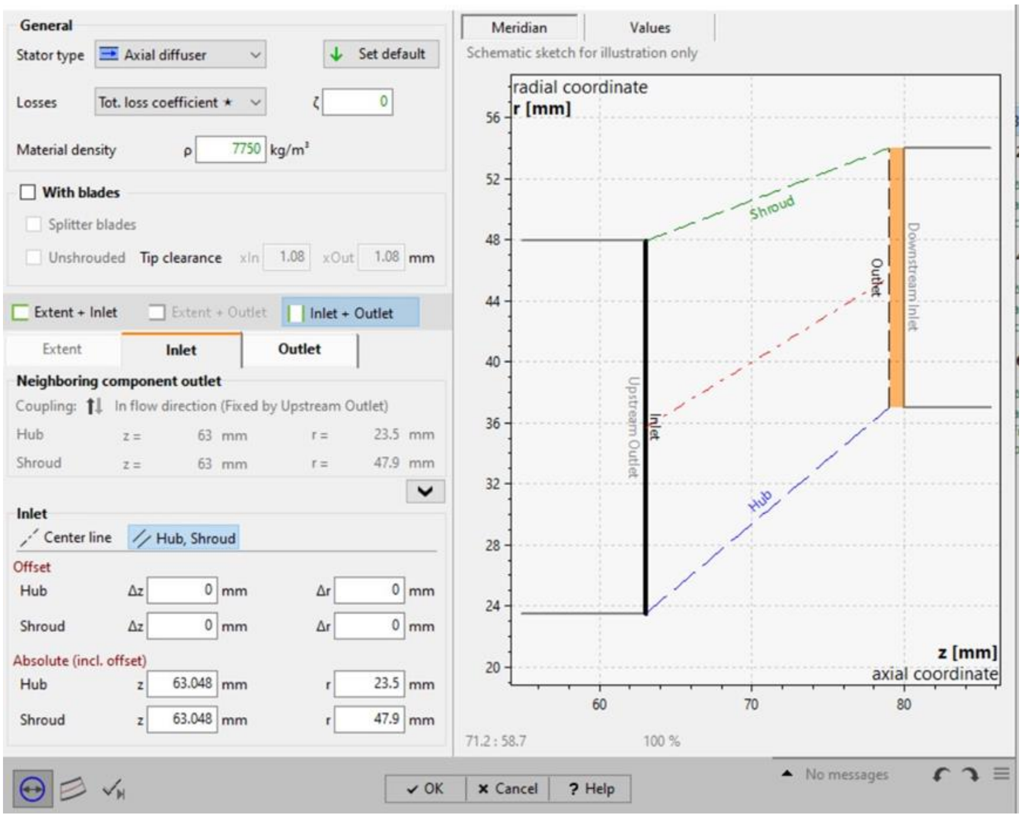

Picture 101 Conical stator input set up CFturbo program

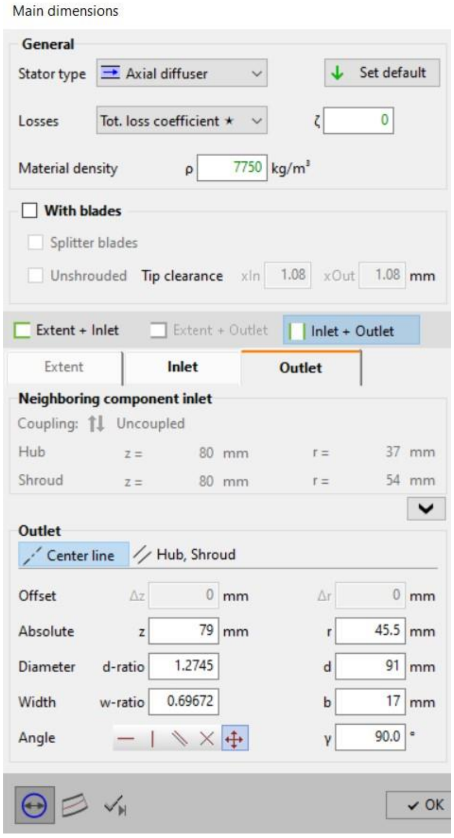

Picture 102 Conical stator output set up CFturbo program

Picture 103 Stator CFturbo program

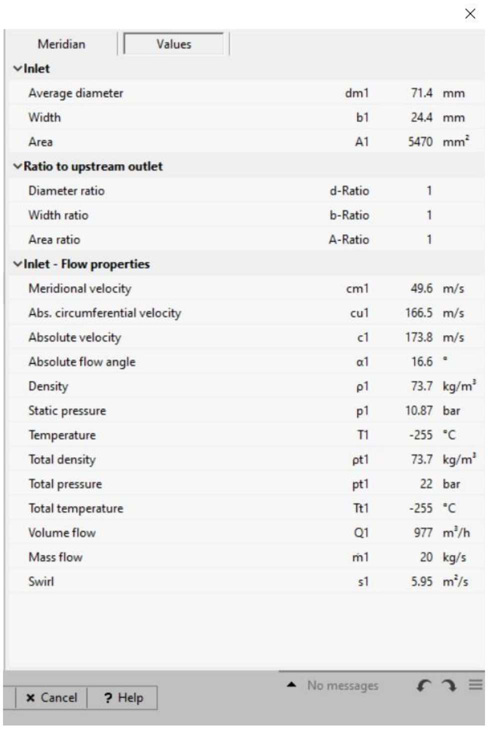

Picture 104 The values of all velocities, pressures and flow angles at the inlet of the stator CFturbo program

Picture 105 The values of all velocities, pressures and flow angles at the outlet of the stator CFturbo program

It is observed that the input and output data are different from those of the output of the inducer. In practice, the pressure will change very little and the velocity will be what comes out of the inducer.

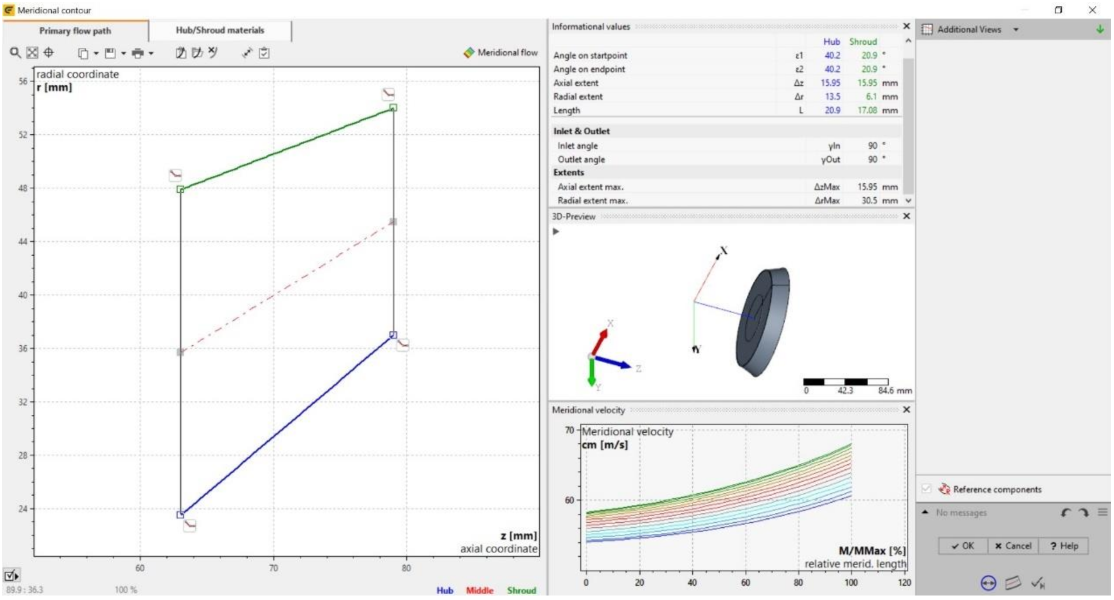

Picture 106 Meridian contour and B-spline configuration CFturbo program

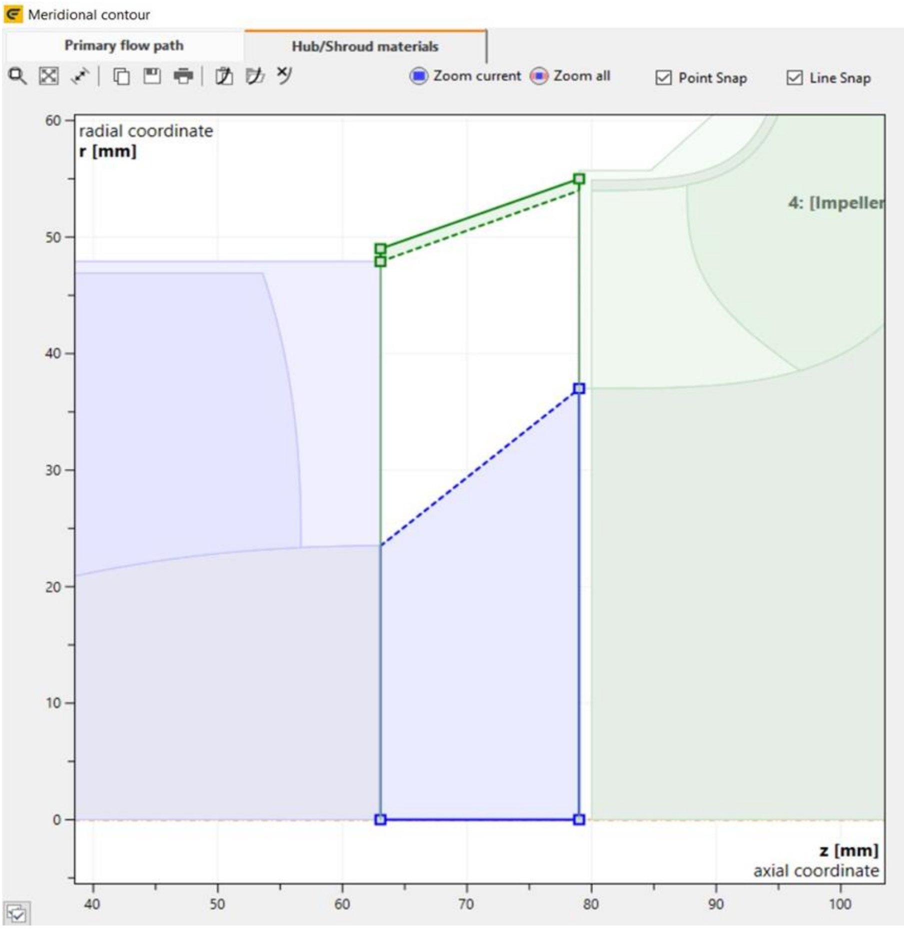

Picture 107 The material of the conic shaft and conic stator CFturbo program

4.1.4 Volute – Diffuser

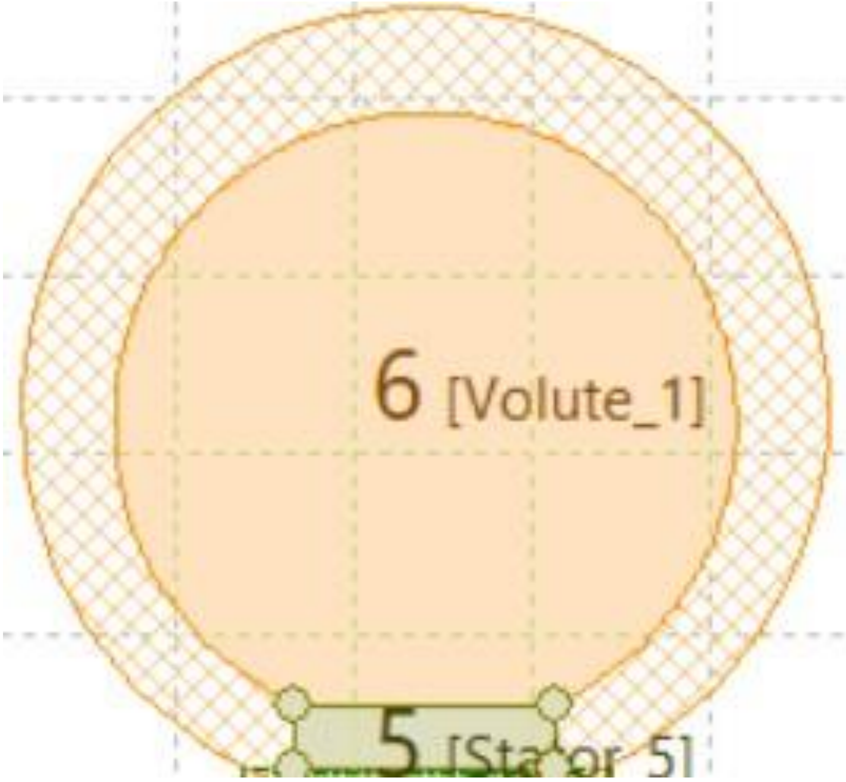

Picture 108 Volute - Diffuser

The distance from the volute - diffuser is usually very short and especially at high flows as in this case. In this case, the ration d_4/d_2 was chosen 1,05 and combined with the following function with the special number of revolutions comes out 1,06. The difference is small. The distance includes the distance between the impeller and the shell which is 0,1mm.

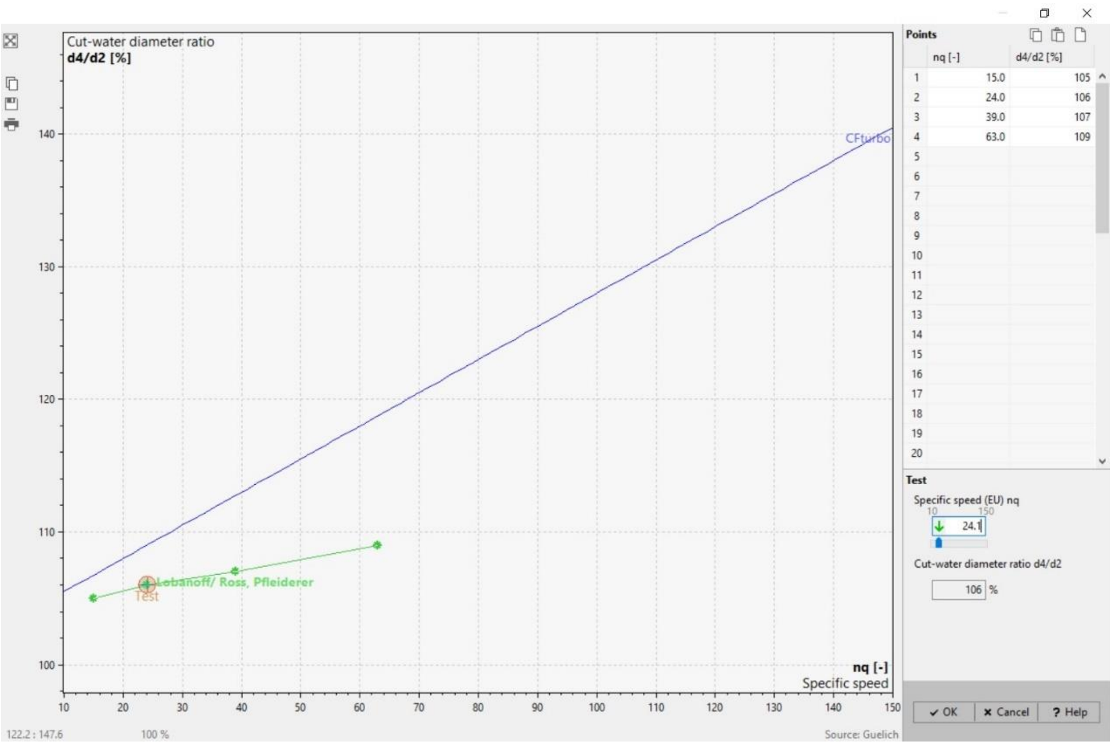

Picture 109 Function of the ratio d4/d2 with the specific speed number

For d_2 = 144,5mm (diameter impeller) $d_4 = 1{,}05d_2$ = 152mm.

In this way the distance Δr = 3.65mm was set together with the distance of the wall to the impeller which is 0.1mm

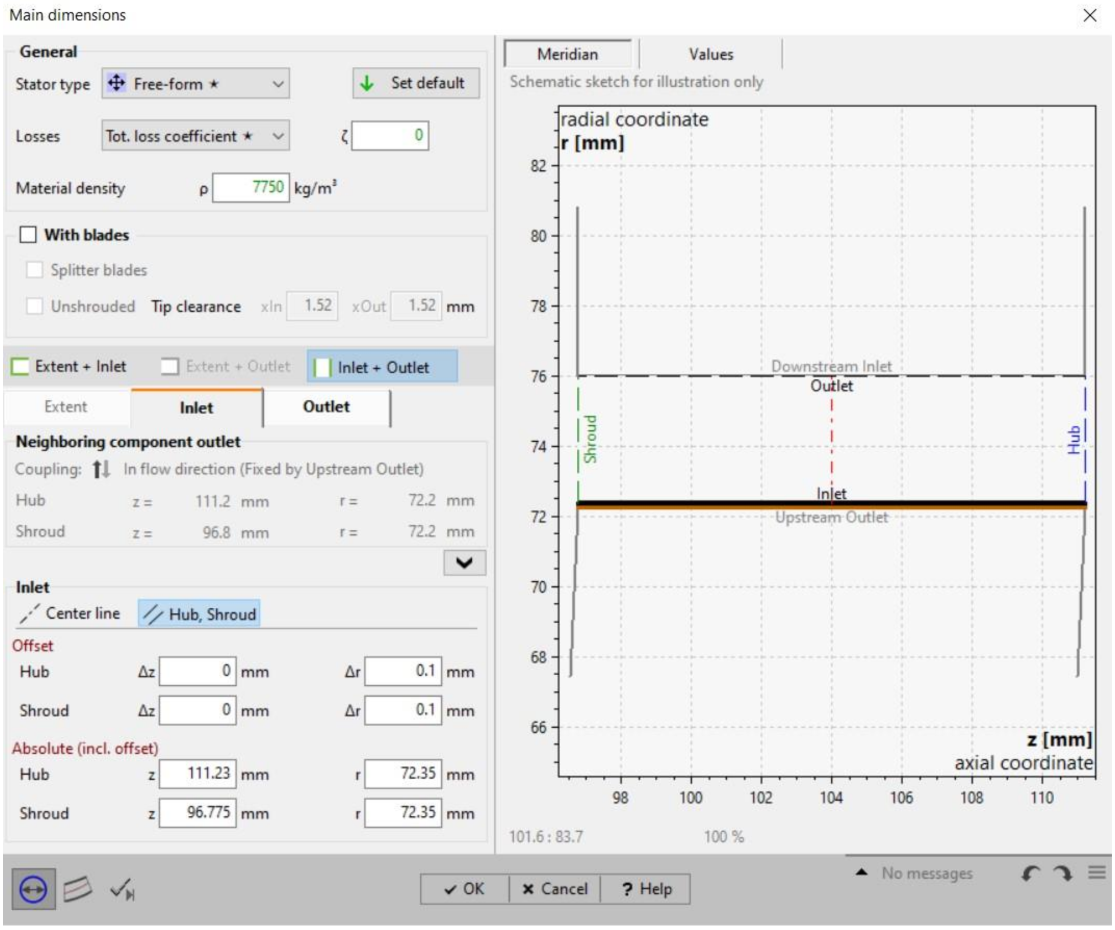

Picture 110 Stator input set up CFturbo program

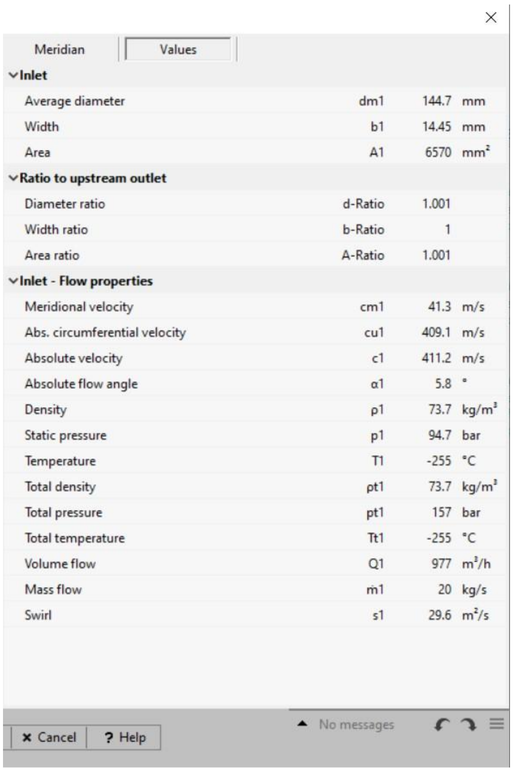

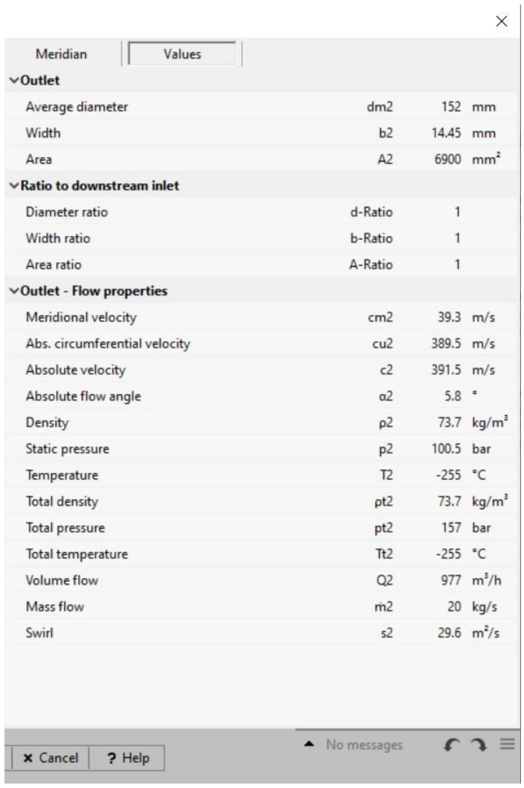

Picture 111 The values of all velocities, pressures and flow angles at the inlet of the stator CFturbo program

Picture 112 The values of all velocities, pressures and flow angles at the outlet of the stator CFturbo program

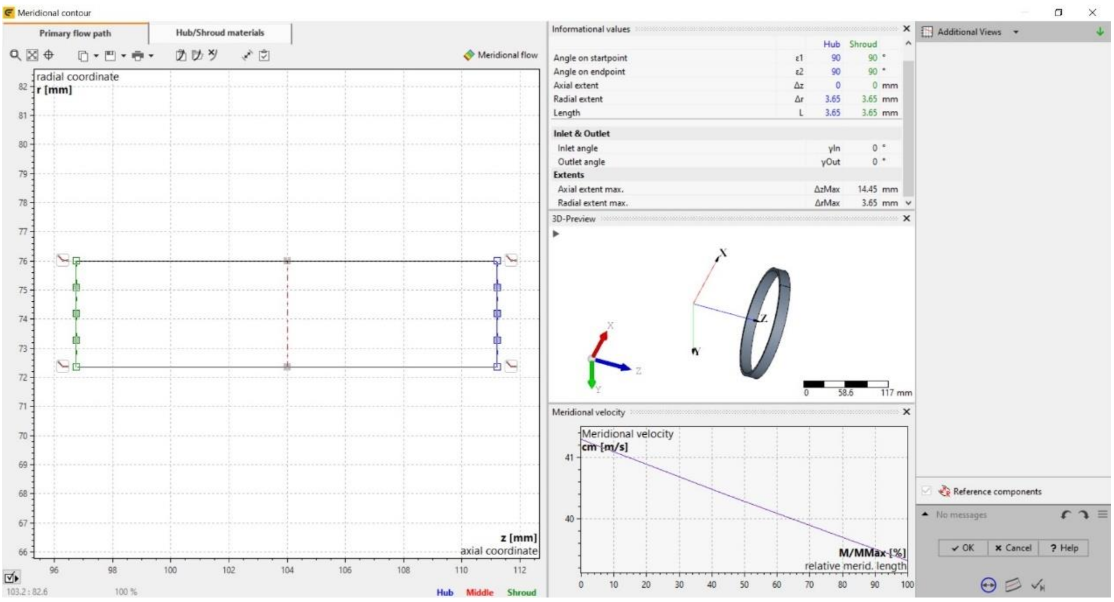

Picture 113 Meridian contour and B-spline configuration CFturbo program

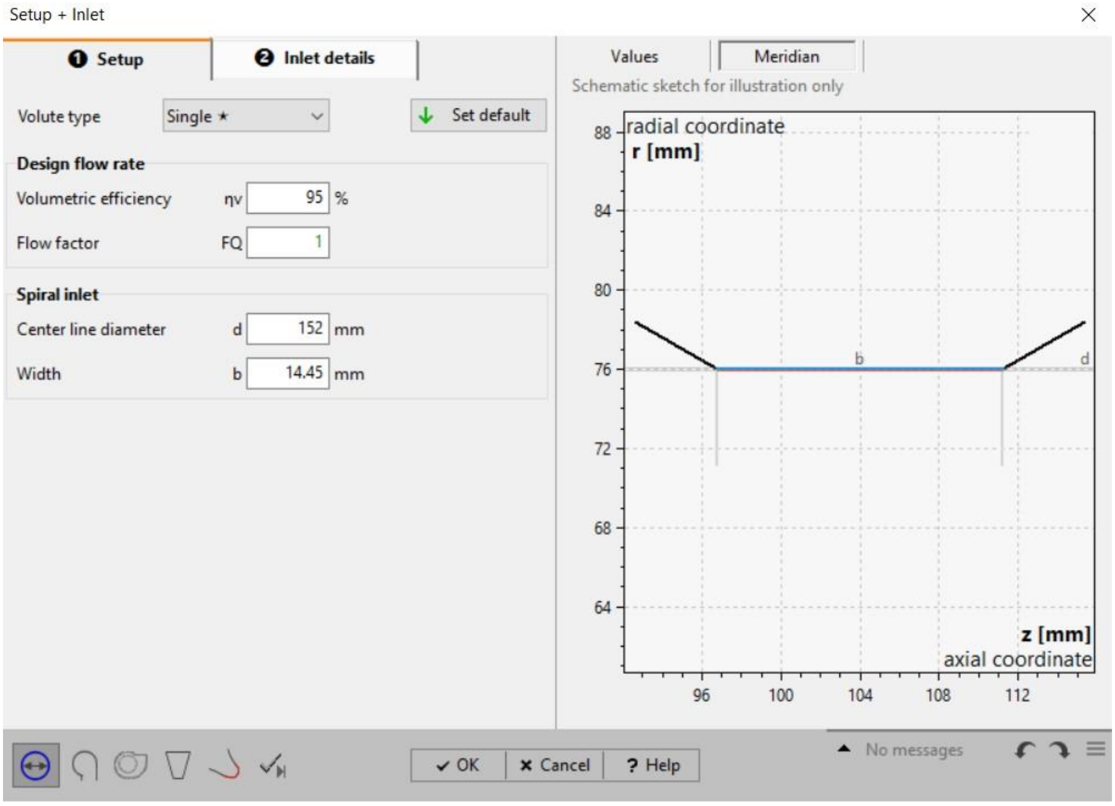

Picture 114 Start of set up of volute - diffuser CFturbo program

In general, no particular changes were made to the diffuser. The thickness was formed a little higher with 3 mm and the method designed is with the constant vorticity (x=1) where with this method we have a high hydraulic efficiency. By estimation, the hydraulic grade manually entered 95%. the diameter and height were adjusted so that we have an outlet pressure of about 130 bar.

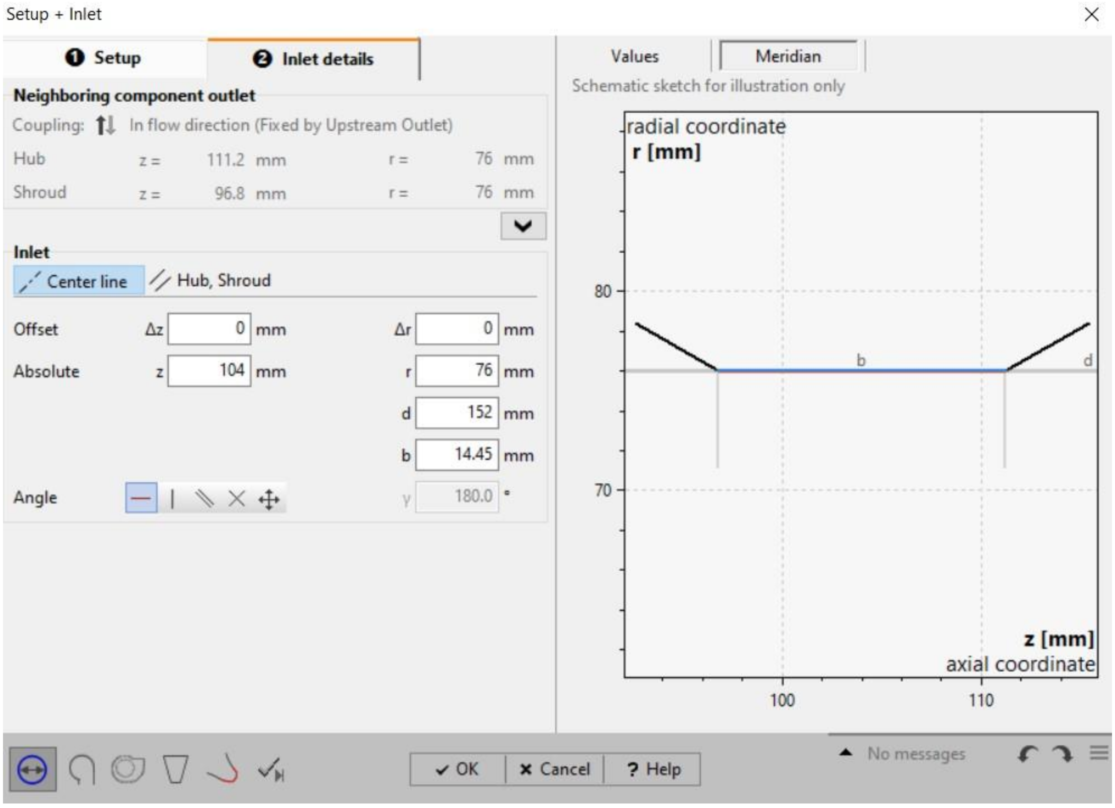

Picture 115 Entrance dimensions CFturbo program

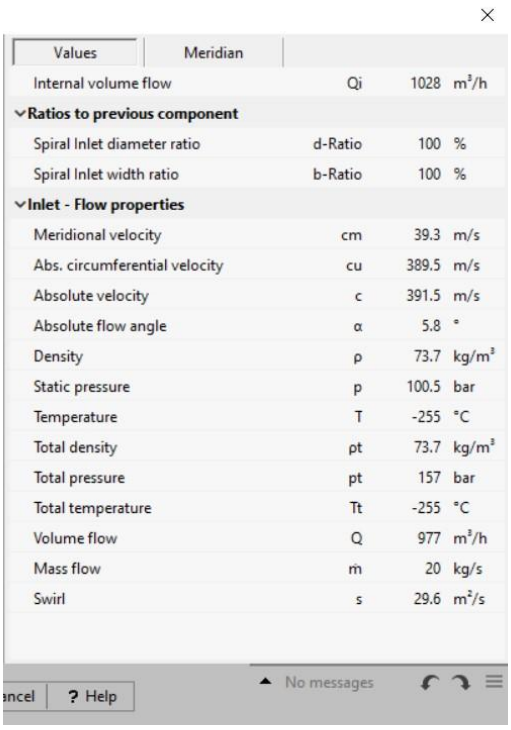

Picture116 The values of all velocities, pressures and flow angles at the inlet of the diffuser CFturbo program

It is noted that the stator added before the volute - diffuser is considered part of the diffuser. For this reason, d4/d2 = 105% and not 100% is mentioned in the set up.

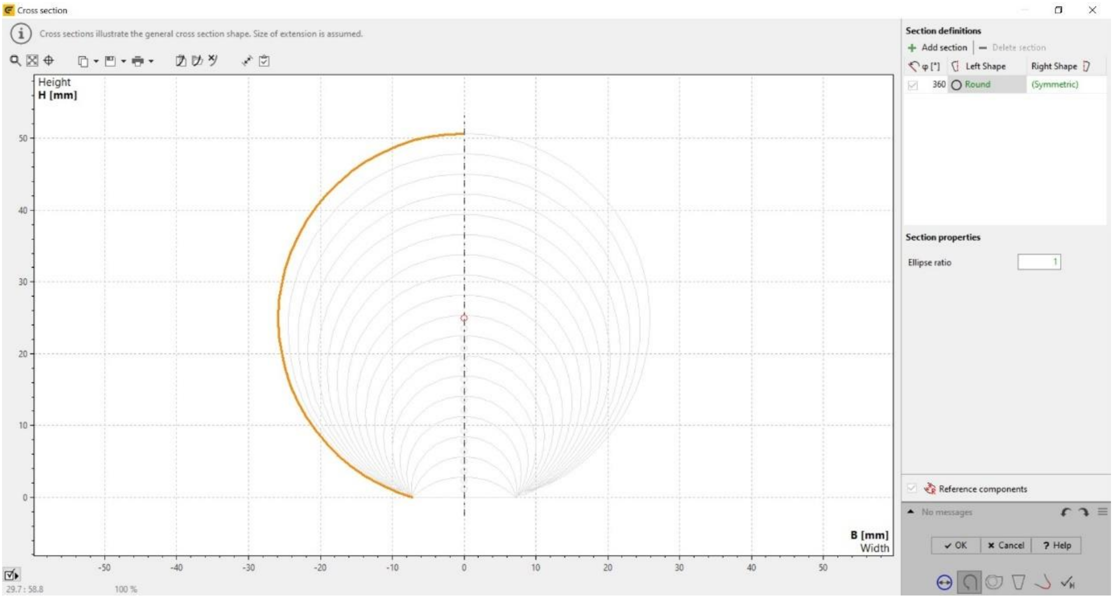

Picture 117 Configuration of spiral tube shape and size CFturbo program

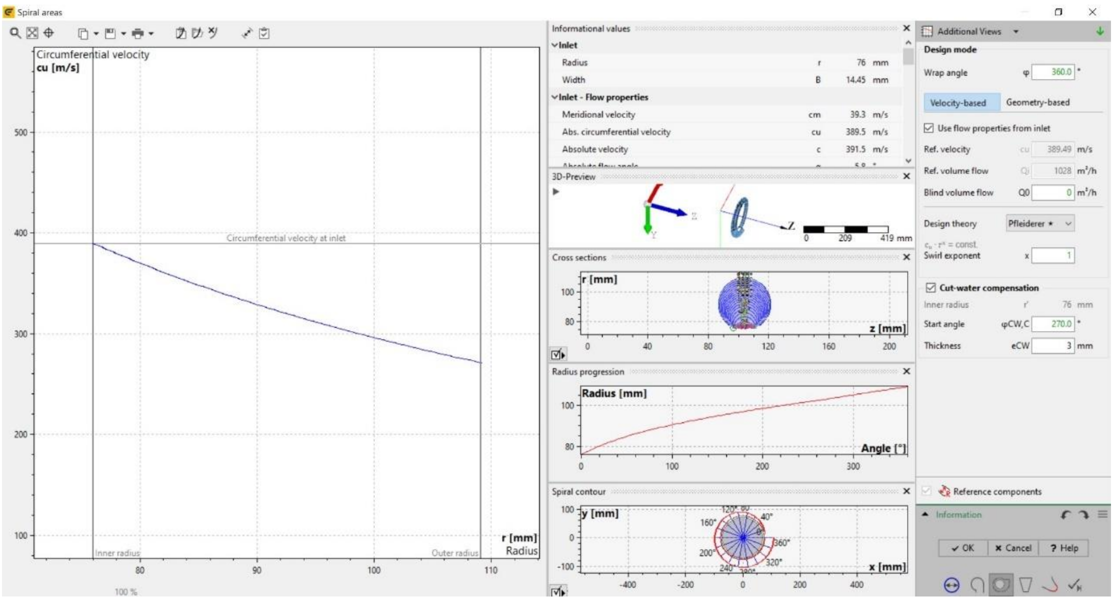

Picture 118 Spiral design space based on some criteria CFturbo program

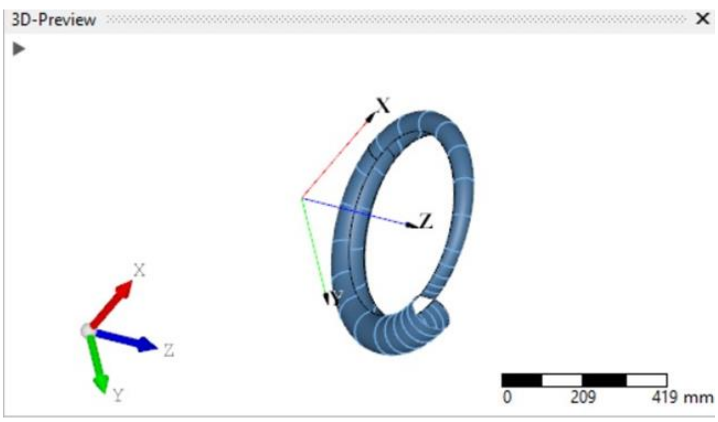

Picture 119 The spiral CFturbo program

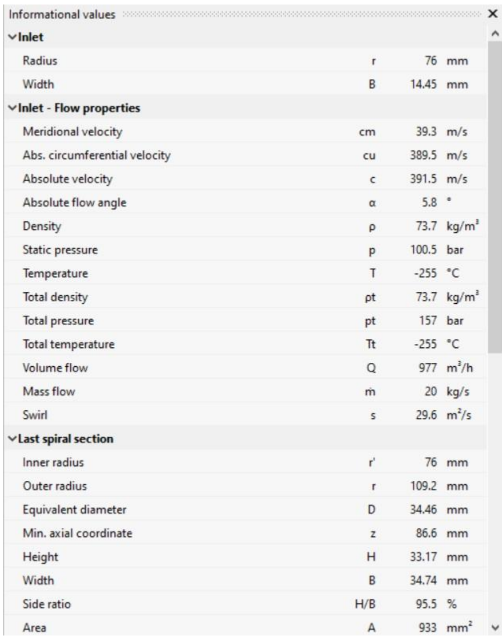

Informational values

Inlet			
Radius	r	76	mm
Width	B	14.45	mm
Inlet - Flow properties			
Meridional velocity	cm	39.3	m/s
Abs. circumferential velocity	cu	389.5	m/s
Absolute velocity	c	391.5	m/s
Absolute flow angle	α	5.8	°
Density	ρ	73.7	kg/m³
Static pressure	p	100.5	bar
Temperature	T	-255	°C
Total density	ρt	73.7	kg/m³
Total pressure	pt	157	bar
Total temperature	Tt	-255	°C
Volume flow	Q	977	m³/h
Mass flow	m	20	kg/s
Swirl	s	29.6	m²/s
Last spiral section			
Inner radius	r'	76	mm
Outer radius	r	109.2	mm
Equivalent diameter	D	34.46	mm
Min. axial coordinate	z	86.6	mm
Height	H	33.17	mm
Width	B	34.74	mm
Side ratio	H/B	95.5	%
Area	A	933	mm²

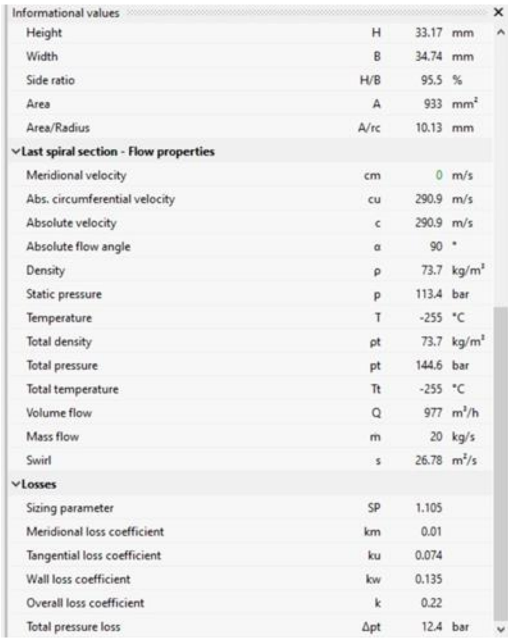

Informational values

Height	H	33.17	mm
Width	B	34.74	mm
Side ratio	H/B	95.5	%
Area	A	933	mm²
Area/Radius	A/rc	10.13	mm
Last spiral section - Flow properties			
Meridional velocity	cm	0	m/s
Abs. circumferential velocity	cu	290.9	m/s
Absolute velocity	c	290.9	m/s
Absolute flow angle	α	90	°
Density	ρ	73.7	kg/m³
Static pressure	p	113.4	bar
Temperature	T	-255	°C
Total density	ρt	73.7	kg/m³
Total pressure	pt	144.6	bar
Total temperature	Tt	-255	°C
Volume flow	Q	977	m³/h
Mass flow	m	20	kg/s
Swirl	s	26.78	m²/s
Losses			
Sizing parameter	SP	1.105	
Meridional loss coefficient	km	0.01	
Tangential loss coefficient	ku	0.074	
Wall loss coefficient	kw	0.135	
Overall loss coefficient	k	0.22	
Total pressure loss	Δpt	12.4	bar

Picture 120 The values of all velocities, pressures and flow angles at the inlet and the last spiral section CFturbo program

Picture 121 The values of all velocities, pressures and flow angles at the inlet and the last spiral section CFturbo program

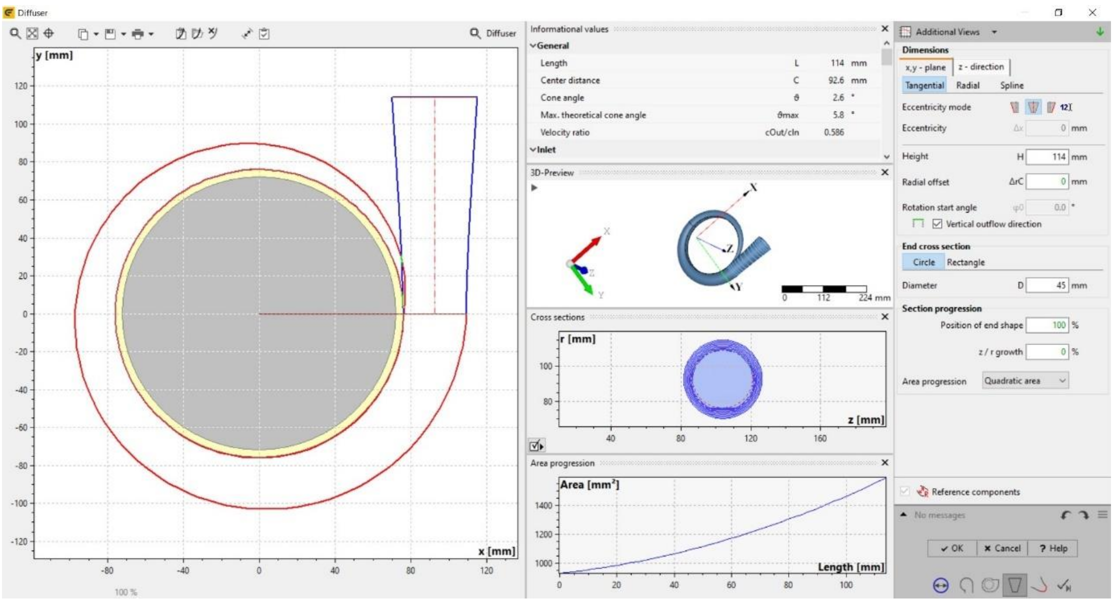

Picture 122 Configuration of conical diffuser at the outlet CFturbo program

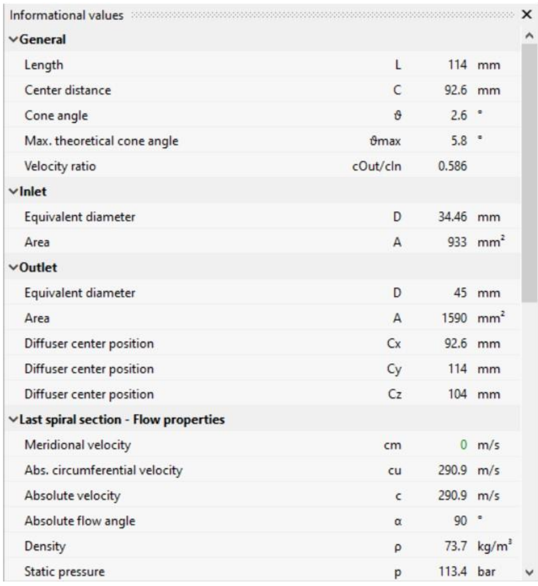

Informational values			
General			
Length	L	114	mm
Center distance	C	92.6	mm
Cone angle	θ	2.6	°
Max. theoretical cone angle	θmax	5.8	°
Velocity ratio	cOut/cIn	0.586	
Inlet			
Equivalent diameter	D	34.46	mm
Area	A	933	mm²
Outlet			
Equivalent diameter	D	45	mm
Area	A	1590	mm²
Diffuser center position	Cx	92.6	mm
Diffuser center position	Cy	114	mm
Diffuser center position	Cz	104	mm
Last spiral section - Flow properties			
Meridional velocity	cm	0	m/s
Abs. circumferential velocity	cu	290.9	m/s
Absolute velocity	c	290.9	m/s
Absolute flow angle	α	90	°
Density	ρ	73.7	kg/m³
Static pressure	p	113.4	bar

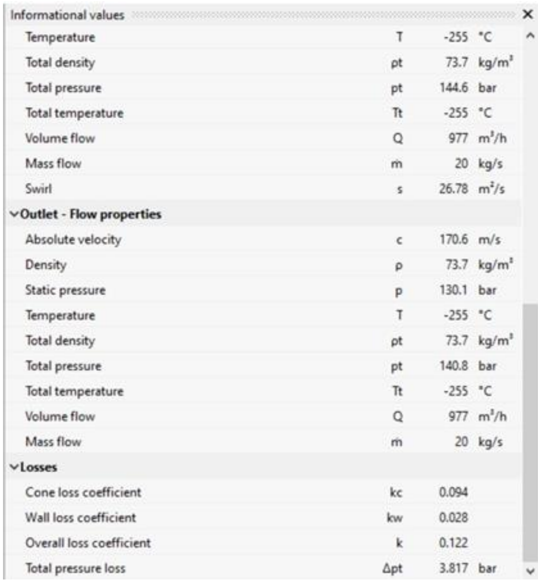

Informational values			
Temperature	T	-255	°C
Total density	ρt	73.7	kg/m³
Total pressure	pt	144.6	bar
Total temperature	Tt	-255	°C
Volume flow	Q	977	m³/h
Mass flow	ṁ	20	kg/s
Swirl	s	26.78	m²/s
Outlet - Flow properties			
Absolute velocity	c	170.6	m/s
Density	ρ	73.7	kg/m³
Static pressure	p	130.1	bar
Temperature	T	-255	°C
Total density	ρt	73.7	kg/m³
Total pressure	pt	140.8	bar
Total temperature	Tt	-255	°C
Volume flow	Q	977	m³/h
Mass flow	ṁ	20	kg/s
Losses			
Cone loss coefficient	kc	0.094	
Wall loss coefficient	kw	0.028	
Overall loss coefficient	k	0.122	
Total pressure loss	Δpt	3.817	bar

Picture 123 The values of all velocities, pressures and flow angles at the outlet of diffuser CFturbo program

Picture 124 The values of all velocities, pressures and flow angles at the outlet of diffuser CFturbo program

A curvature with a radius of 3mm was formed

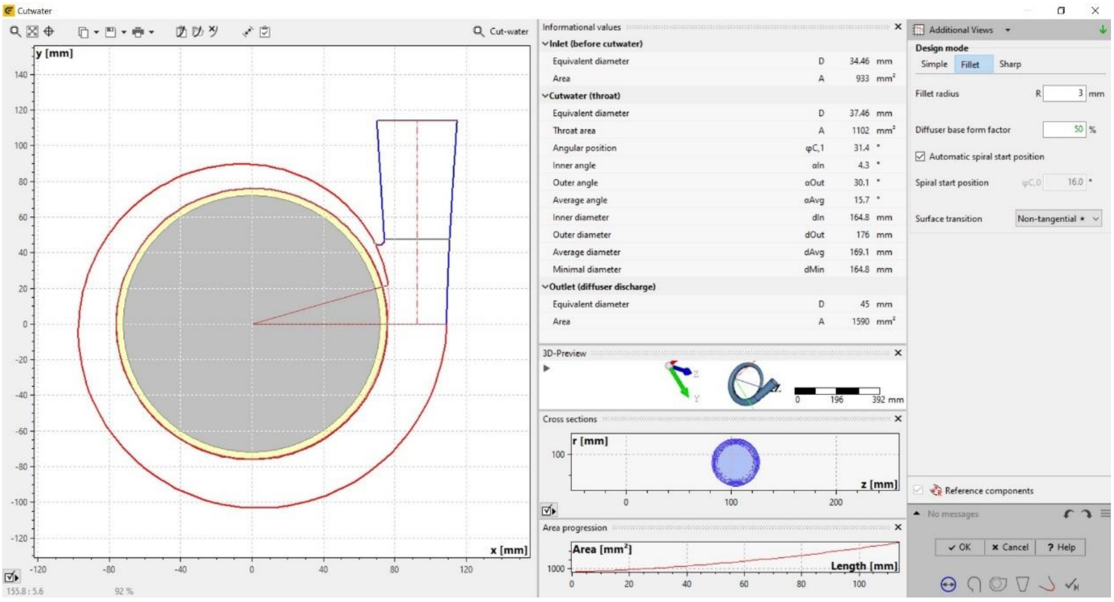

Picture 125 Curvature shaping space between conical diffuser and spiral CFturbo program

4.1.5 Rotary part of the inducer

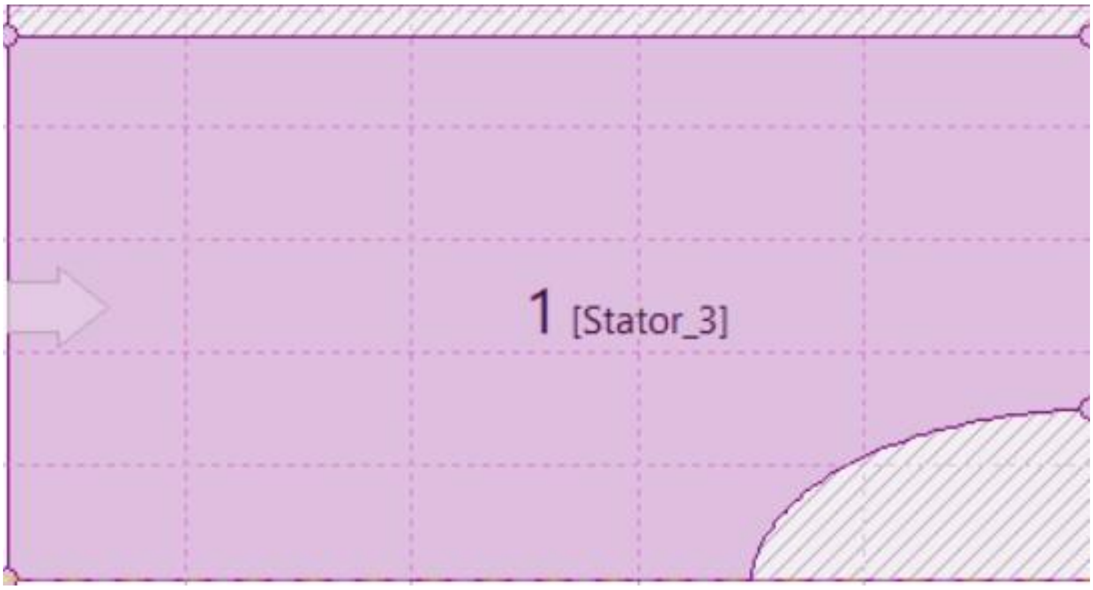

Picture 126 Rotary inducer nose & inducer input space CFturbo program

A distance almost equal to the inlet diameter was set. A rotary nose was designed in front of the inducer. This tip was designed with B-spline curves and shaped to smooth entry velocity. Its height is the same as the diameter of the inducer input hub.

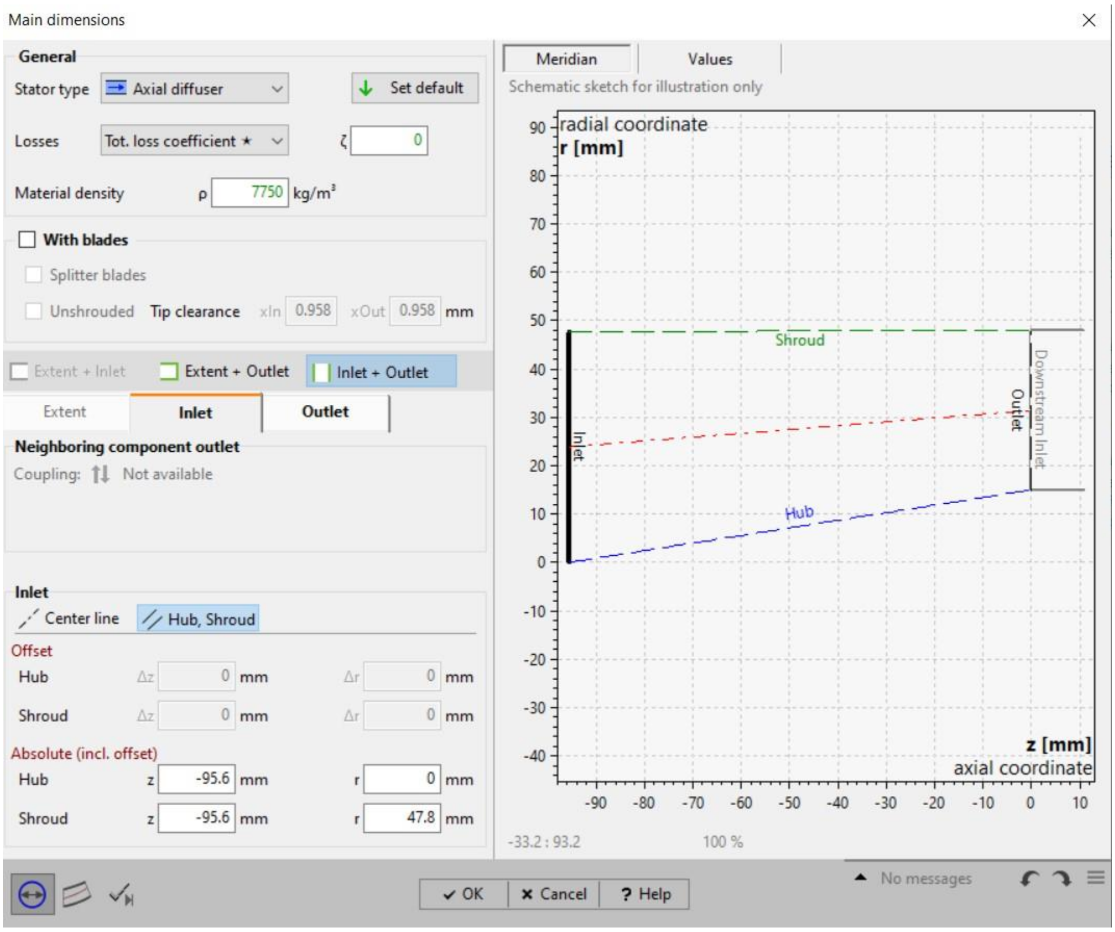

Picture 127 Set up the input area of the inducer CFturbo program

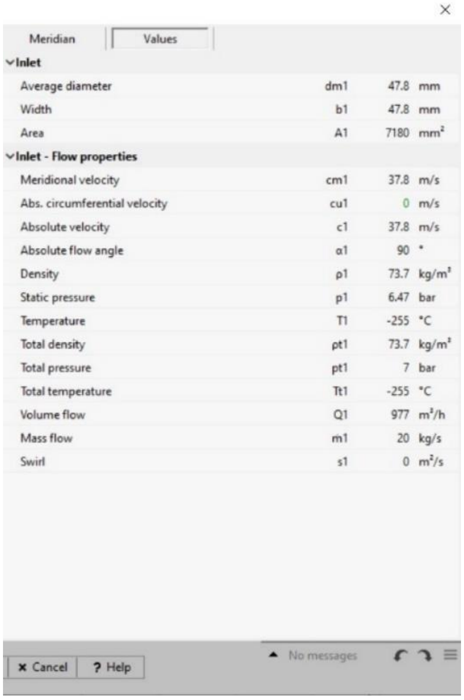

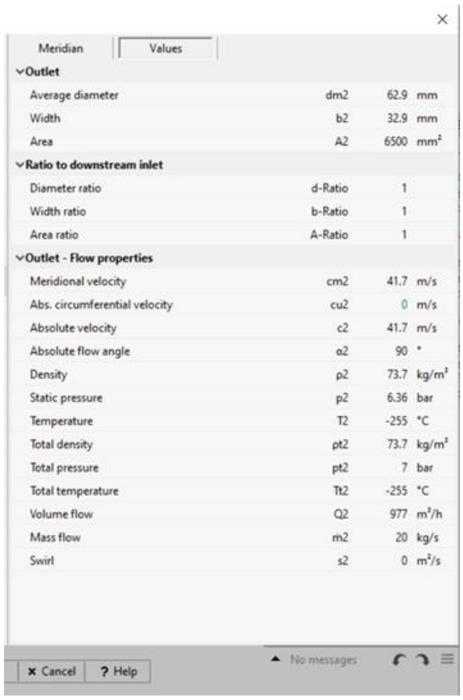

Picture 128 The values of all velocities, pressures and flow angles at the inlet CFturbo program

Picture 129 The values of all velocities, pressures and flow angles at the end of the rotary nose CFturbo program

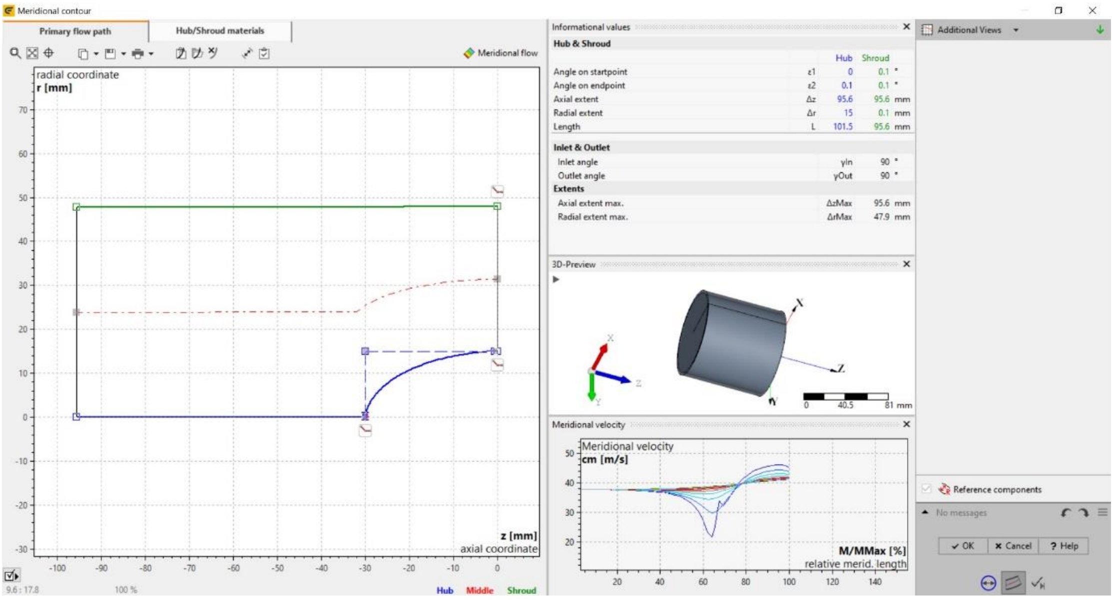

Picture 130 Meridian contour and B-spline configuration CFturbo program

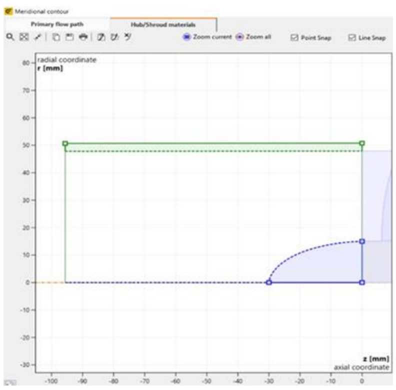

Picture 131 The material of the rotary nose CFturbo program

4.2 Oxidizer pump design

The usual oxidizer, liquid oxygen, was chosen. The theoretical combustion of oxygen with hydrogen is:

$$2H_2 + O_2 \rightarrow 2H_2O$$

But in the combustion chamber of the rocket engine, the hydrogen and oxygen are in liquid form and the speeds are very high. This means that the fuel and oxidizer do not remain long enough for the chemical reaction to be fully completed. For this reason, the real reaction is this:

$$5H_2 + O_2 \rightarrow 2H_2O + 3H_2$$

It follows that the mass ratio of liquid oxygen and hydrogen is 3,2 [55]. Therefore, the supply of the oxygen pump will be:

$$\dot{m}_{O2} = 3{,}2\dot{m}_{H2} = 64\ Kg/s$$

However, this ratio would actually change a bit as a small amount of fuel and oxidizer would also be consumed if combined in an open cycle gas generation. This also depends on the power of the turbine. It was just used to make a simple dissection to provide the oxidizer to start the design. The following procedure is the same as for the fuel pump design. With the criterion that the specific speed should be in the range of 1000 to 2000 to have a high efficiency, the total pressure difference and the number of revolutions were adjusted. A variation was made on liquid oxygen as it is required to be in fully liquid form. The following images show the design point

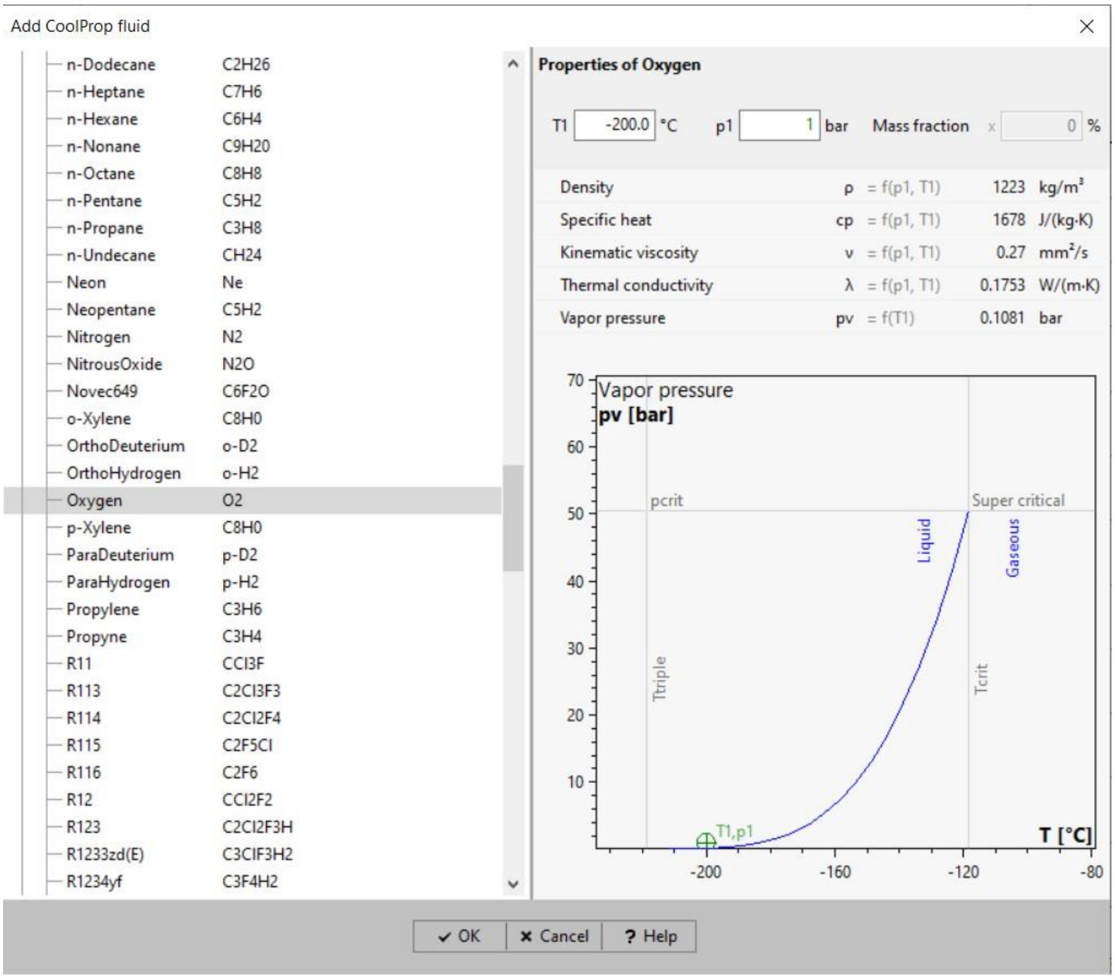

Picture 132 Formation space fluid material CFturbo program

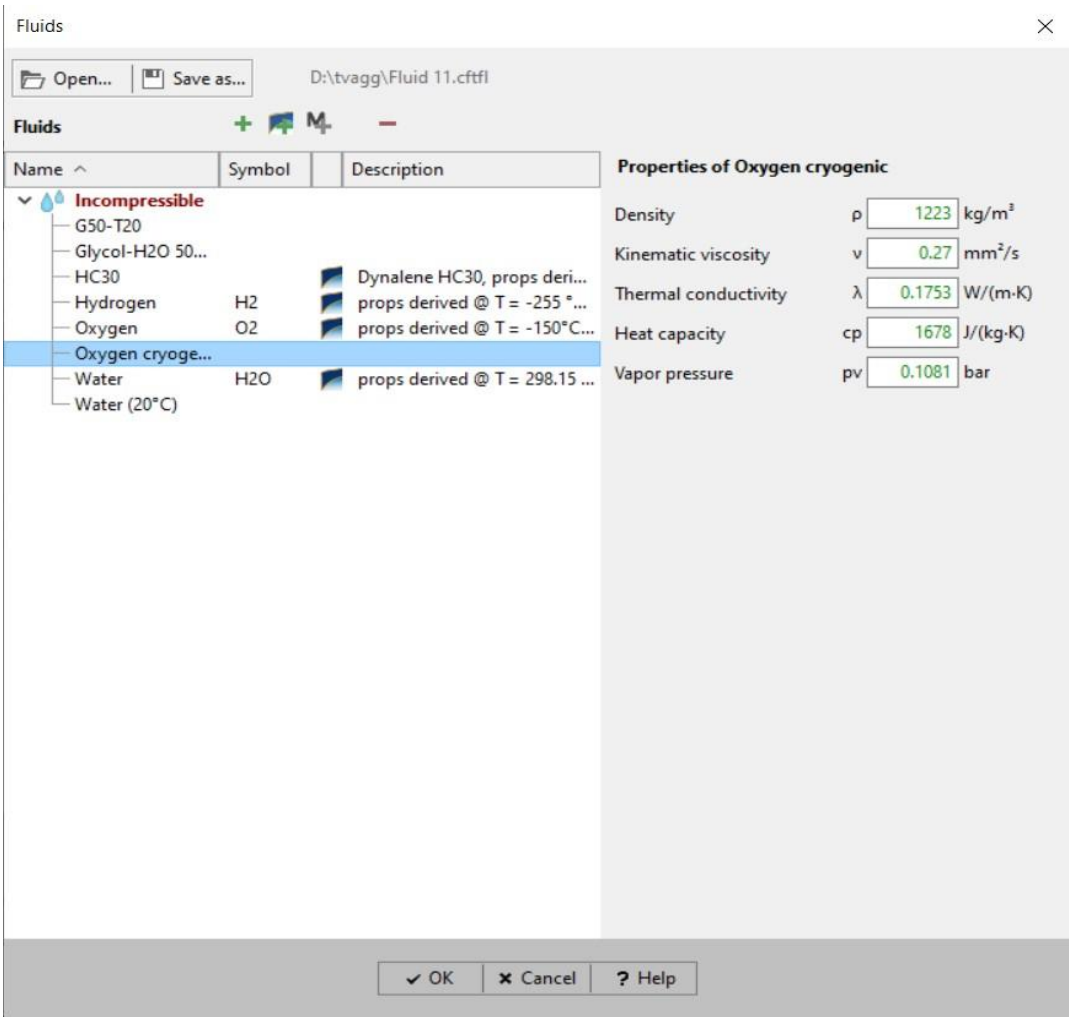

Picture 133 Properties of material fluid CFturbo program

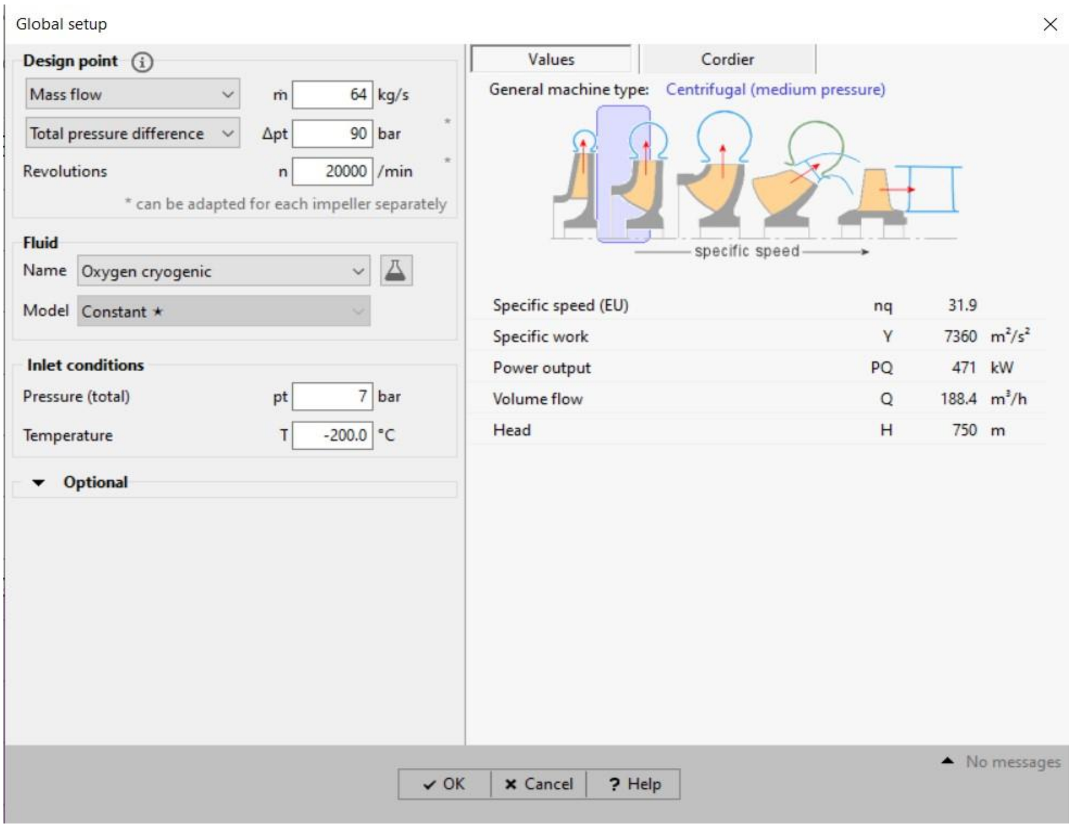

Picture 134 The design point of the LO_2 pump CFturbo program

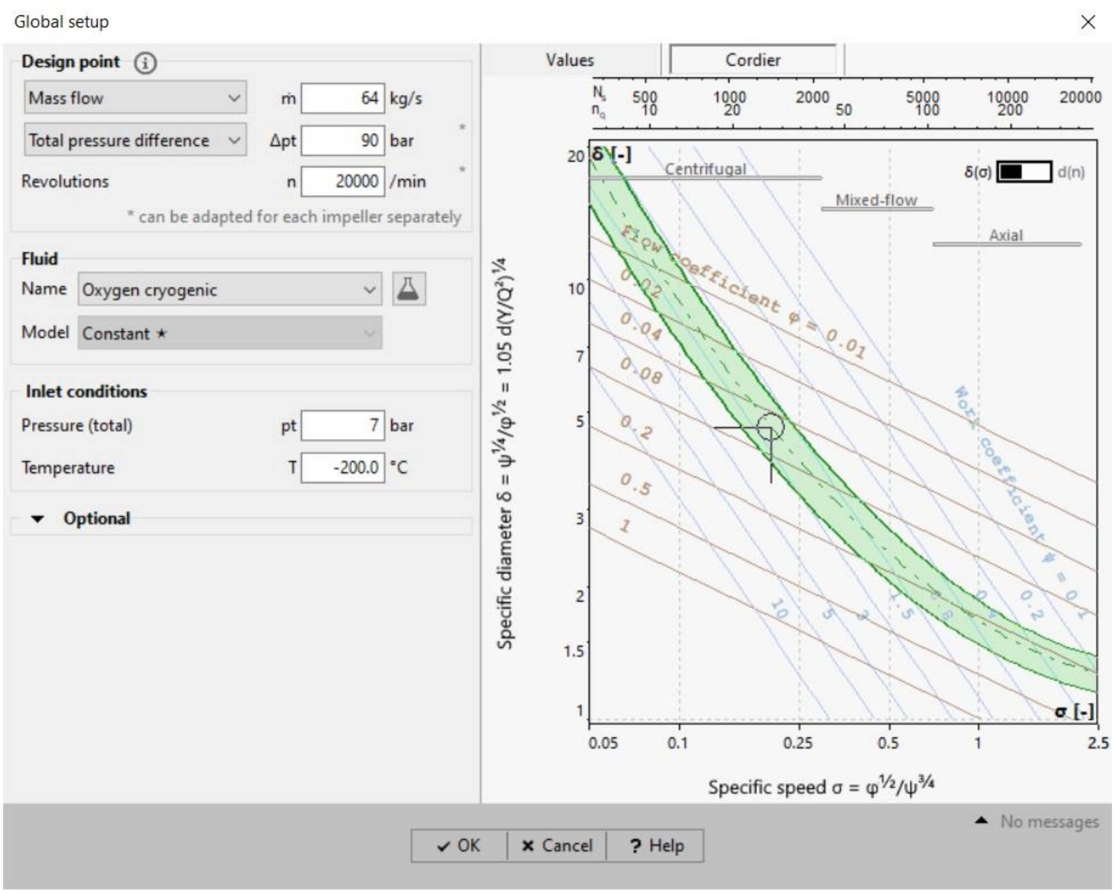

Picture 135 The design point of the LO_2 pump CFturbo program

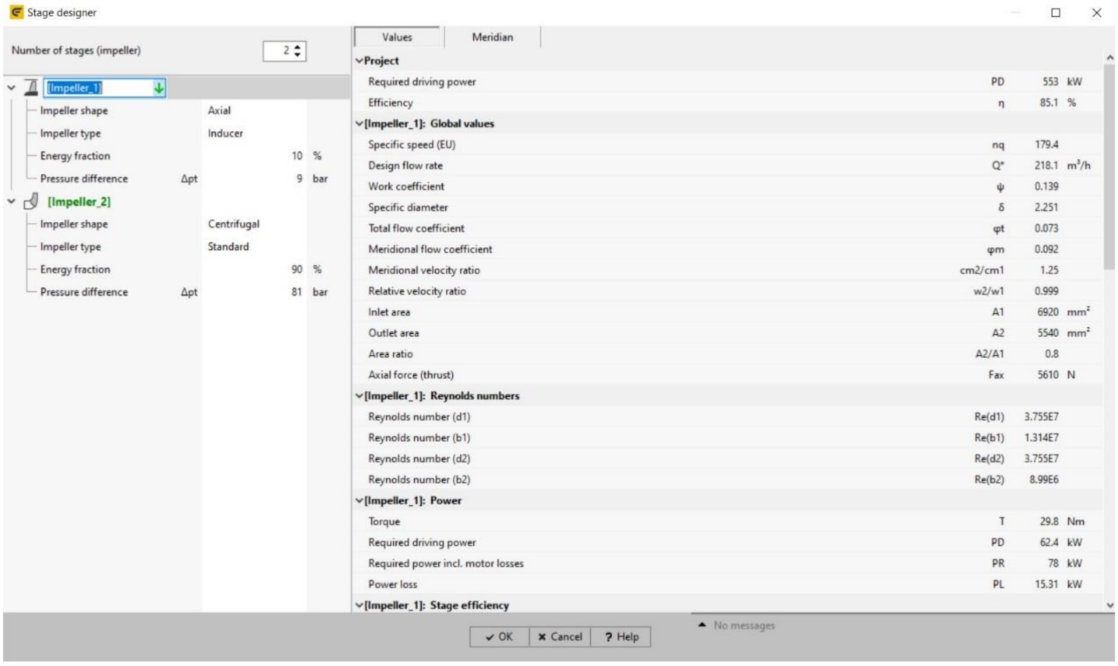

Picture 136 Pressure differential rates of the inducer and the impeller CFturbo program

4.2.1 Inducer

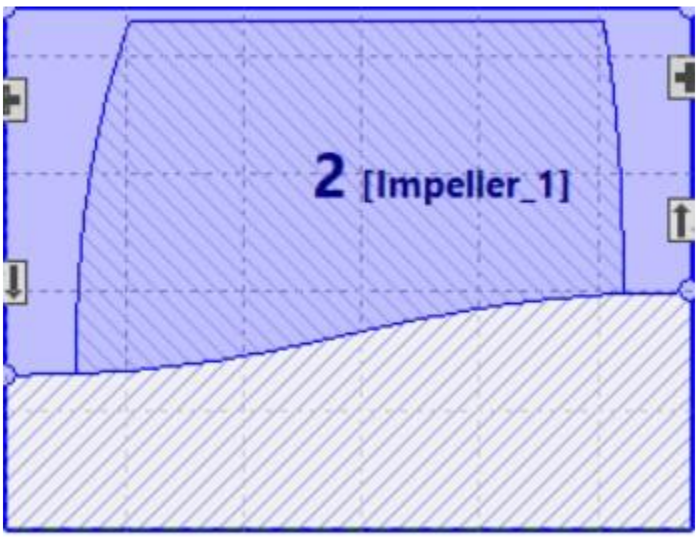

Picture 137 Inducer CFturbo program

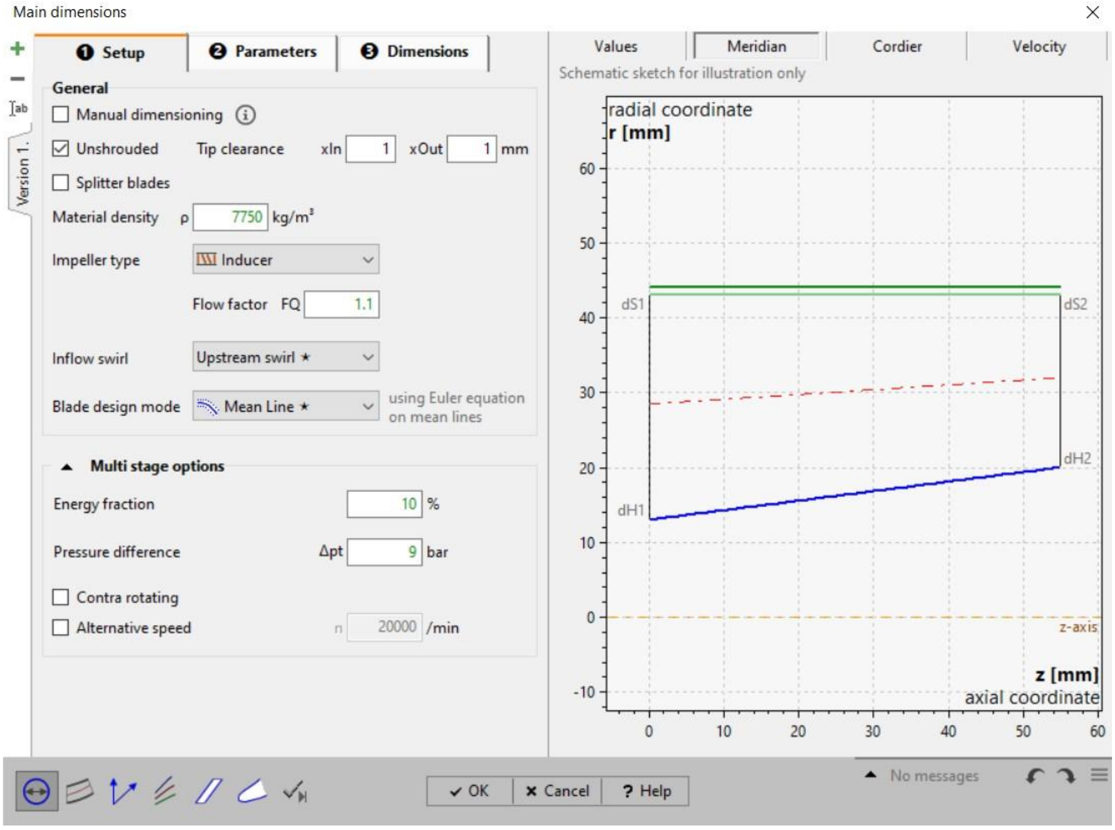

Picture 138 Start of set up of inducer CFturbo program

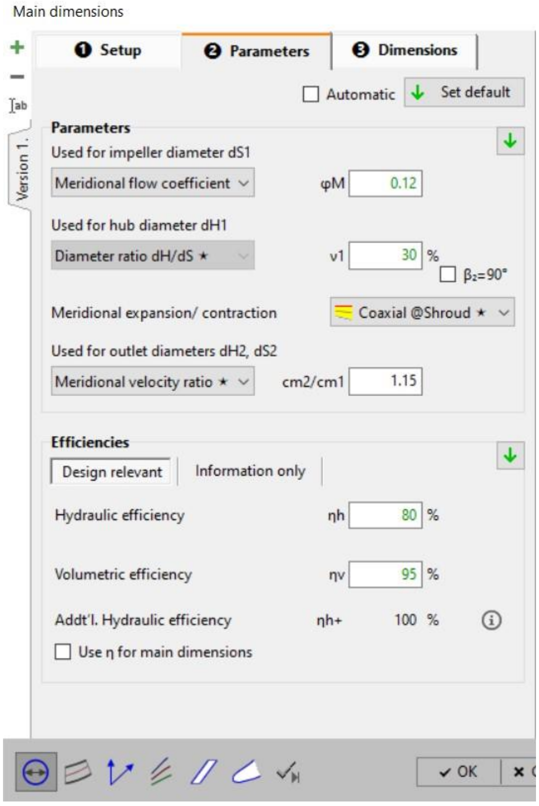

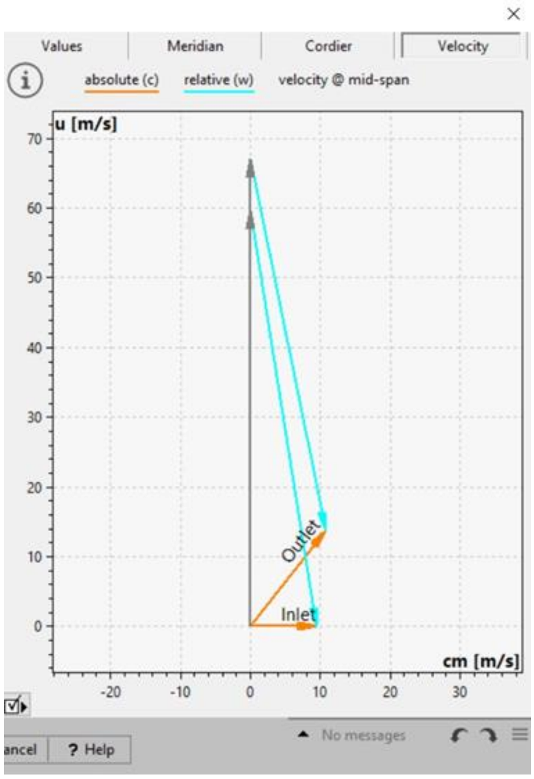

Picture 139 The design parameters CFturbo program

Picture 140 Inducer input and output speed triangles CFturbo program

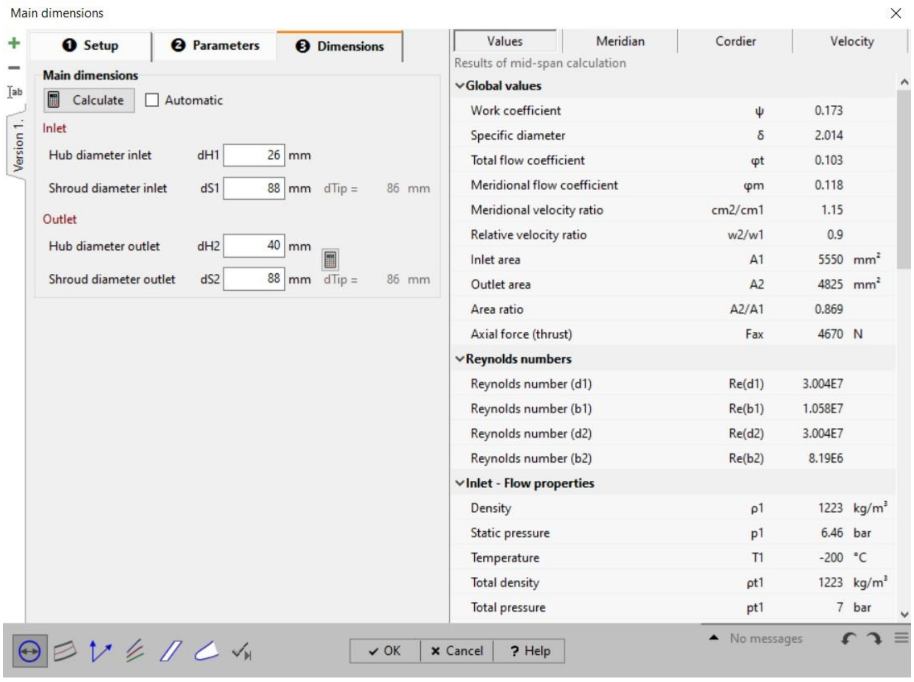

Picture 141 Input and output dimensions of the inducer and the all values CFturbo program

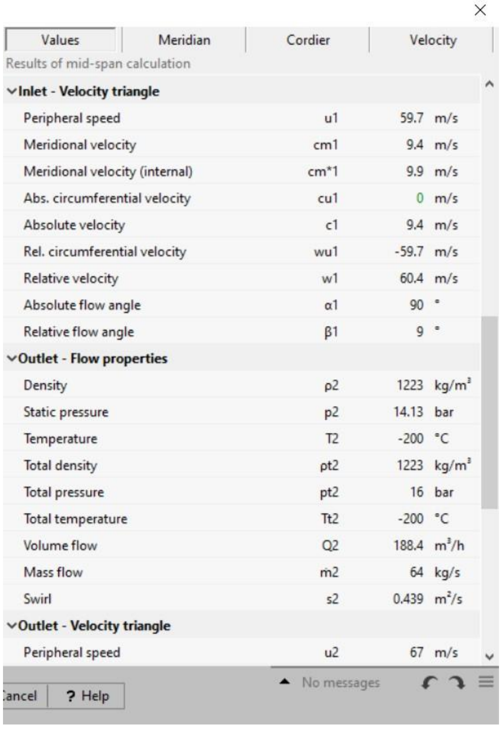

Values | Meridian | Cordier | Velocity

Results of mid-span calculation

Inlet - Velocity triangle			
Peripheral speed	u1	59.7	m/s
Meridional velocity	cm1	9.4	m/s
Meridional velocity (internal)	cm*1	9.9	m/s
Abs. circumferential velocity	cu1	0	m/s
Absolute velocity	c1	9.4	m/s
Rel. circumferential velocity	wu1	-59.7	m/s
Relative velocity	w1	60.4	m/s
Absolute flow angle	α1	90	°
Relative flow angle	β1	9	°
Outlet - Flow properties			
Density	ρ2	1223	kg/m³
Static pressure	p2	14.13	bar
Temperature	T2	-200	°C
Total density	ρt2	1223	kg/m³
Total pressure	pt2	16	bar
Total temperature	Tt2	-200	°C
Volume flow	Q2	188.4	m³/h
Mass flow	ṁ2	64	kg/s
Swirl	s2	0.439	m²/s
Outlet - Velocity triangle			
Peripheral speed	u2	67	m/s

No messages

Cancel | ? Help

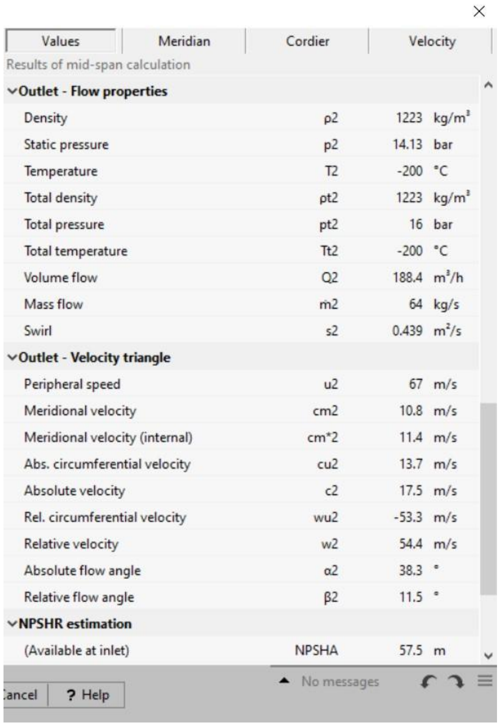

Values | Meridian | Cordier | Velocity

Results of mid-span calculation

Outlet - Flow properties			
Density	ρ2	1223	kg/m³
Static pressure	p2	14.13	bar
Temperature	T2	-200	°C
Total density	ρt2	1223	kg/m³
Total pressure	pt2	16	bar
Total temperature	Tt2	-200	°C
Volume flow	Q2	188.4	m³/h
Mass flow	ṁ2	64	kg/s
Swirl	s2	0.439	m²/s
Outlet - Velocity triangle			
Peripheral speed	u2	67	m/s
Meridional velocity	cm2	10.8	m/s
Meridional velocity (internal)	cm*2	11.4	m/s
Abs. circumferential velocity	cu2	13.7	m/s
Absolute velocity	c2	17.5	m/s
Rel. circumferential velocity	wu2	-53.3	m/s
Relative velocity	w2	54.4	m/s
Absolute flow angle	α2	38.3	°
Relative flow angle	β2	11.5	°
NPSHR estimation			
(Available at inlet)	NPSHA	57.5	m

No messages

Cancel | ? Help

Picture 143 The values of all velocities, pressures and flow angles at the inlet and outlet of the inducer CFturbo program

Picture 144 The values of all velocities, pressures and flow angles at the inlet and outlet of the inducer CFturbo program

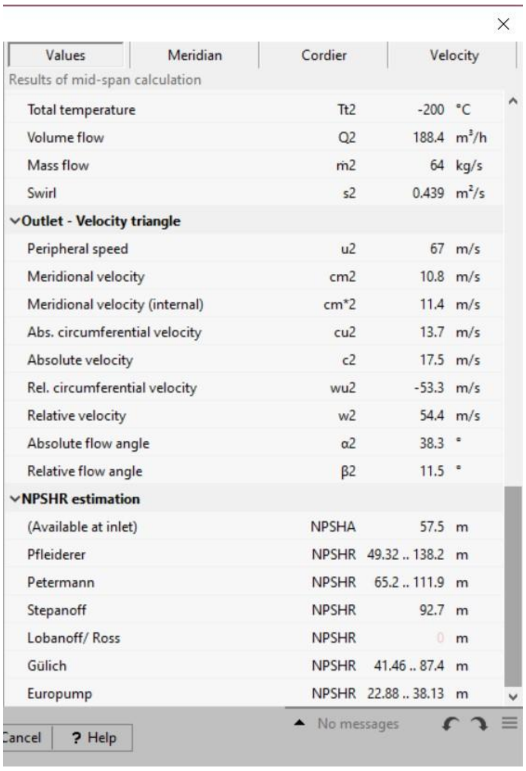

Values | Meridian | Cordier | Velocity

Results of mid-span calculation

Total temperature	Tt2	-200	°C
Volume flow	Q2	188.4	m³/h
Mass flow	ṁ2	64	kg/s
Swirl	s2	0.439	m²/s
Outlet - Velocity triangle			
Peripheral speed	u2	67	m/s
Meridional velocity	cm2	10.8	m/s
Meridional velocity (internal)	cm*2	11.4	m/s
Abs. circumferential velocity	cu2	13.7	m/s
Absolute velocity	c2	17.5	m/s
Rel. circumferential velocity	wu2	-53.3	m/s
Relative velocity	w2	54.4	m/s
Absolute flow angle	α2	38.3	°
Relative flow angle	β2	11.5	°
NPSHR estimation			
(Available at inlet)	NPSHA	57.5	m
Pfleiderer	NPSHR	49.32 .. 138.2	m
Petermann	NPSHR	65.2 .. 111.9	m
Stepanoff	NPSHR	92.7	m
Lobanoff/ Ross	NPSHR	0	m
Gülich	NPSHR	41.46 .. 87.4	m
Europump	NPSHR	22.88 .. 38.13	m

No messages

Cancel | ? Help

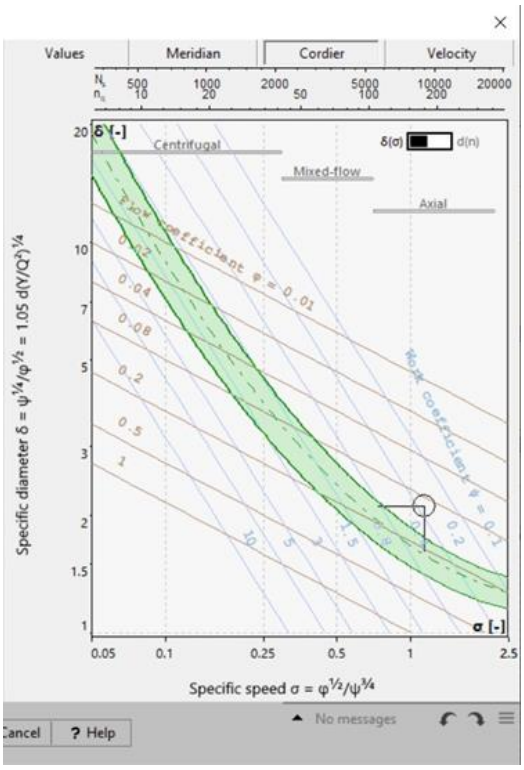

Picture 145 Input and output dimensions of the inducer and the all values CFturbo program

Picture 146 Inducer design point CFturbo program

Similar to the hydrogen pump, you also estimate the NSPHR height in this case

$$\mathrm{NPSHR} = \lambda_c \frac{C_{m1}^2}{2g} + \lambda_w \frac{W_1^2}{2g}$$

- For C_{m1} = 9,4m/s , λ_c = 1,1 , , λ_w = 0,03 and W_1 = 60,4m/s : NPSHR = 10,5m

- For C_{m1} = 9,4m/s , λ_c = 1,35, , λ_w = 0,06 and W_1 = 60,4m/s : NPSHR = 17 m

A range of NPSHR height was estimated for all cases. The available suction height is above these values. Therefore, the possibility of cavitation is very small.

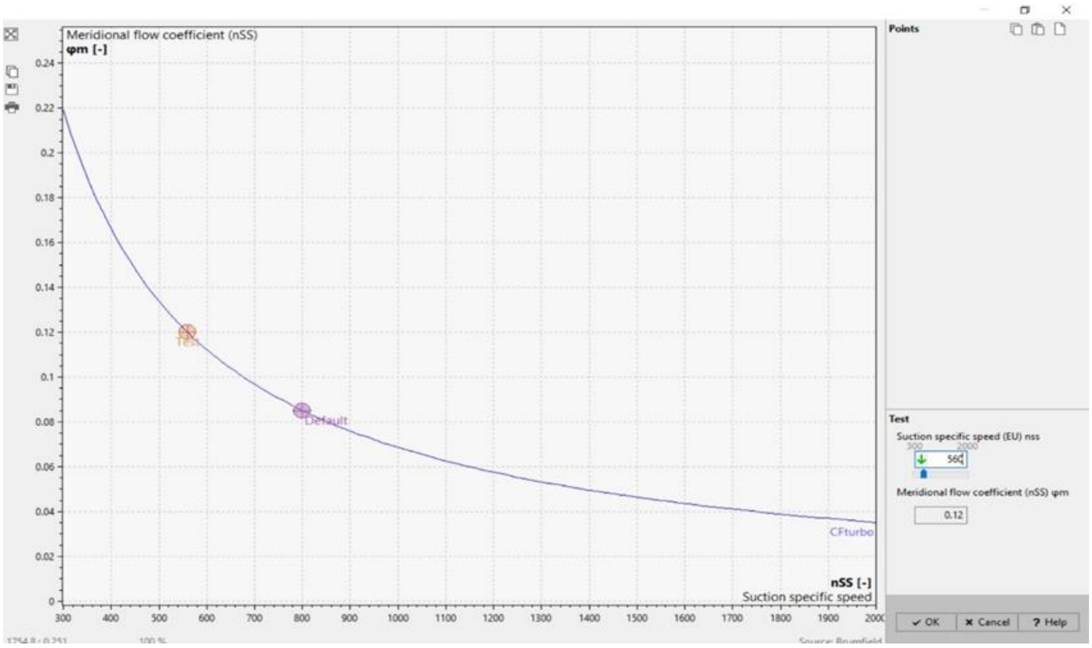

Picture 148 Flow coefficient function curve with specific speed number CFturbo program

From data and the function the NPSHR = 16,4m < NPSHA = 57,5 m

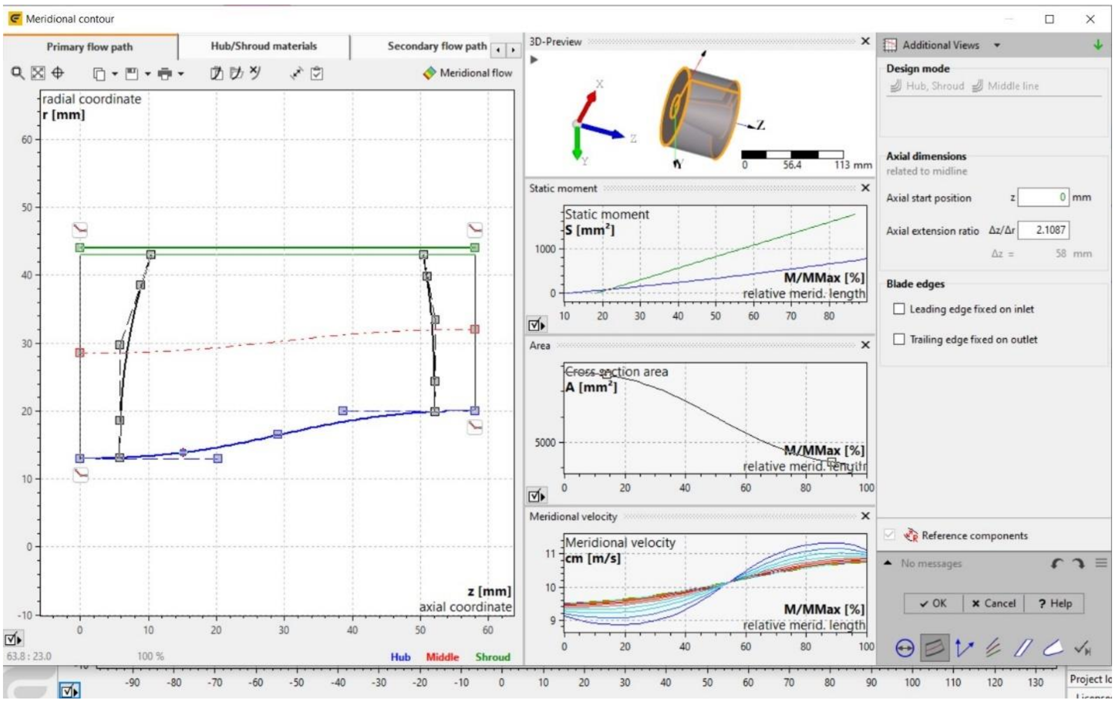

Picture 149 Meridian contour and B-spline configuration CFturbo program

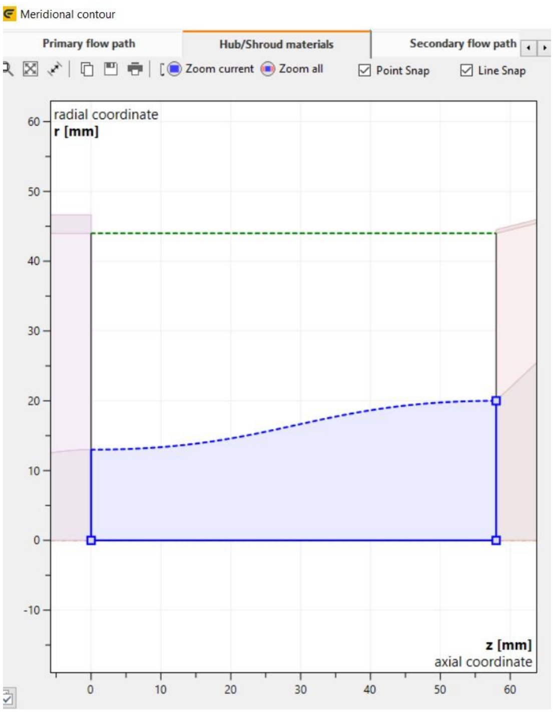

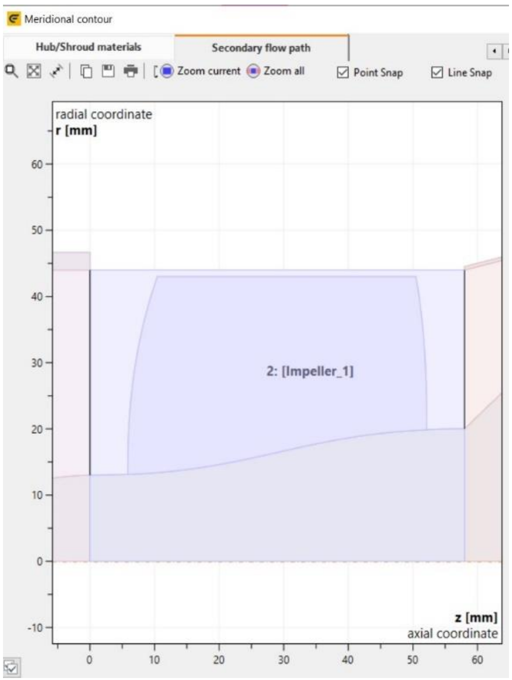

Picture 150 The shaft material (shaft shape) CFturbo program

Picture 151 Picture of inducer CFturbo program

The thickness in this case is 0.4 mm more than the default.

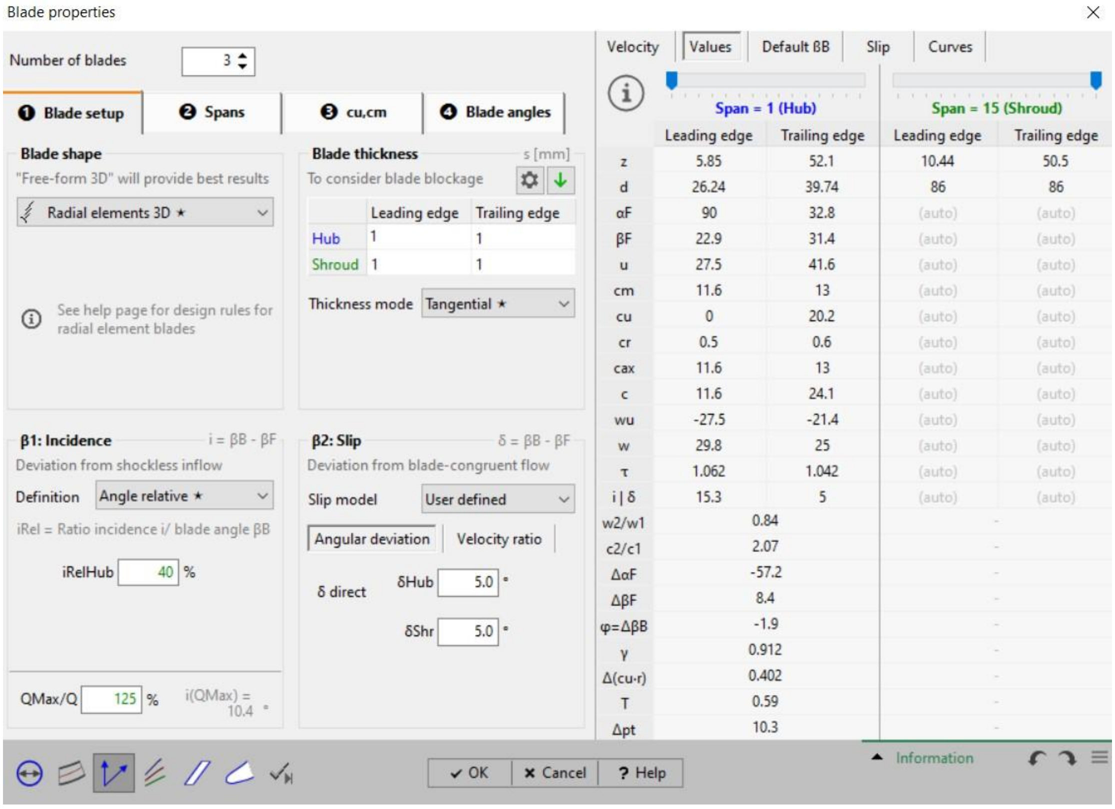

	Span = 1 (Hub) Leading edge	Span = 1 (Hub) Trailing edge	Span = 15 (Shroud) Leading edge	Span = 15 (Shroud) Trailing edge
z	5.85	52.1	10.44	50.5
d	26.24	39.74	86	86
αF	90	32.8	(auto)	(auto)
βF	22.9	31.4	(auto)	(auto)
u	27.5	41.6	(auto)	(auto)
cm	11.6	13	(auto)	(auto)
cu	0	20.2	(auto)	(auto)
cr	0.5	0.6	(auto)	(auto)
cax	11.6	13	(auto)	(auto)
c	11.6	24.1	(auto)	(auto)
wu	-27.5	-21.4	(auto)	(auto)
w	29.8	25	(auto)	(auto)
τ	1.062	1.042	(auto)	(auto)
i | δ	15.3	5	(auto)	(auto)
w2/w1	0.84		-	
c2/c1	2.07		-	
ΔαF	-57.2		-	
ΔβF	8.4		-	
φ=ΔβB	-1.9		-	
γ	0.912		-	
Δ(cu·r)	0.402		-	
T	0.59		-	
Δpt	10.3		-	

Picture 152   Space for shape and wing design settings and corner deviations CFturbo program

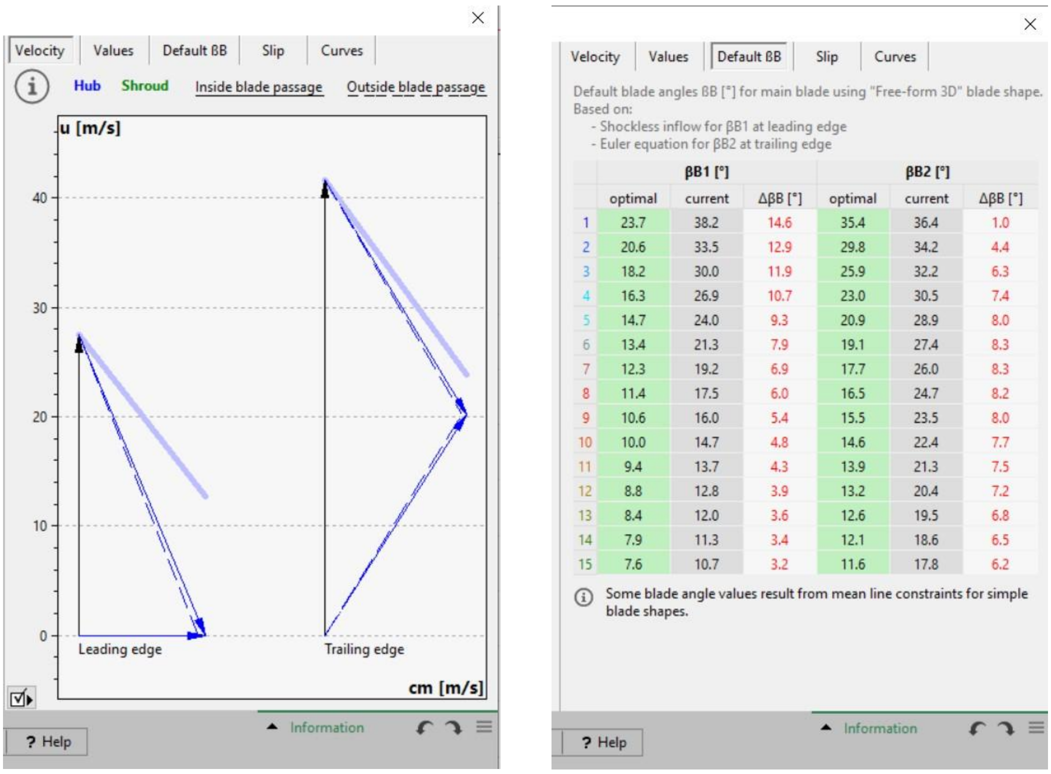

	βB1 [°] optimal	βB1 [°] current	βB1 ΔβB [°]	βB2 [°] optimal	βB2 [°] current	βB2 ΔβB [°]
1	23.7	38.2	14.6	35.4	36.4	1.0
2	20.6	33.5	12.9	29.8	34.2	4.4
3	18.2	30.0	11.9	25.9	32.2	6.3
4	16.3	26.9	10.7	23.0	30.5	7.4
5	14.7	24.0	9.3	20.9	28.9	8.0
6	13.4	21.3	7.9	19.1	27.4	8.3
7	12.3	19.2	6.9	17.7	26.0	8.3
8	11.4	17.5	6.0	16.5	24.7	8.2
9	10.6	16.0	5.4	15.5	23.5	8.0
10	10.0	14.7	4.8	14.6	22.4	7.7
11	9.4	13.7	4.3	13.9	21.3	7.5
12	8.8	12.8	3.9	13.2	20.4	7.2
13	8.4	12.0	3.6	12.6	19.5	6.8
14	7.9	11.3	3.4	12.1	18.6	6.5
15	7.6	10.7	3.2	11.6	17.8	6.2

Picture 153 Velocity triangles at the inlet and outlet of the inductor with the deviation angles CFturbo program

Picture 154 The corrected inlet and outlet vane angle values CFturbo program

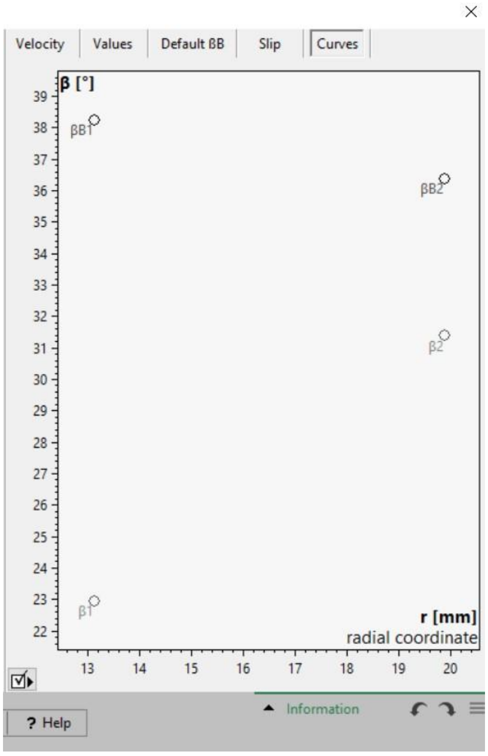

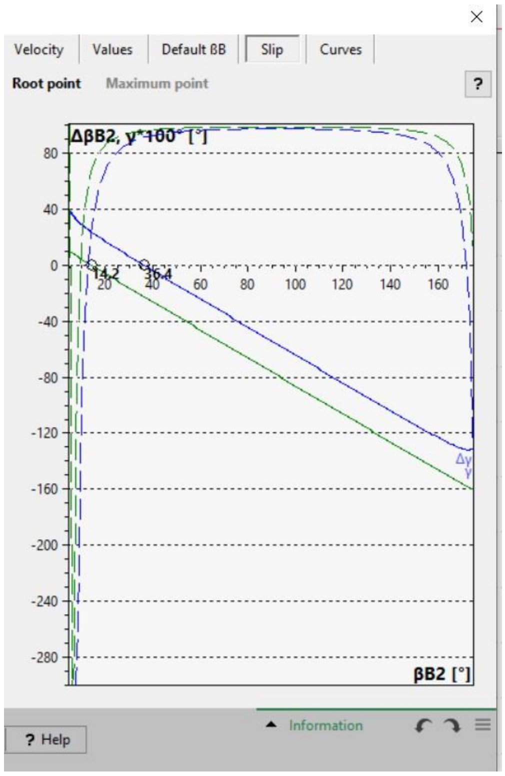

Picture 155 The slip of flow on blade CFturbo program

Picture 156 Angle distribution CFturbo program

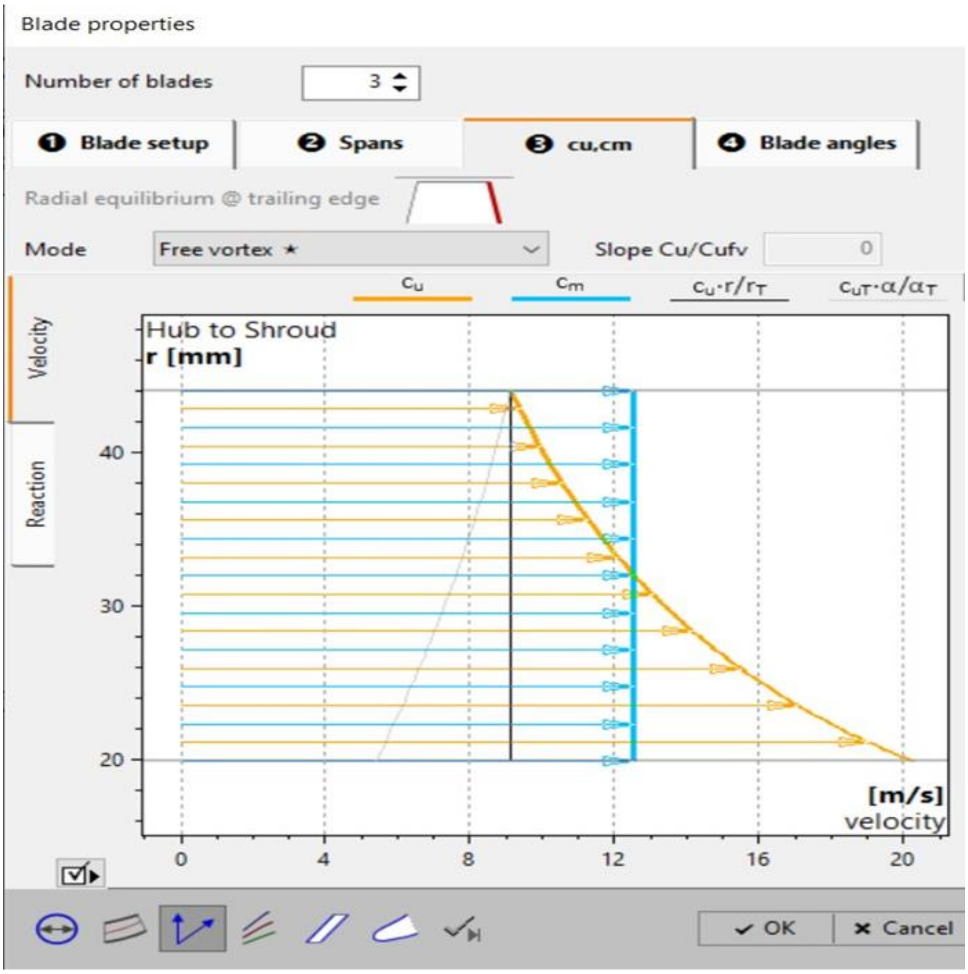

Picture 157 The radial distribution of Cu velocity with the free vorticity method CFturbo program

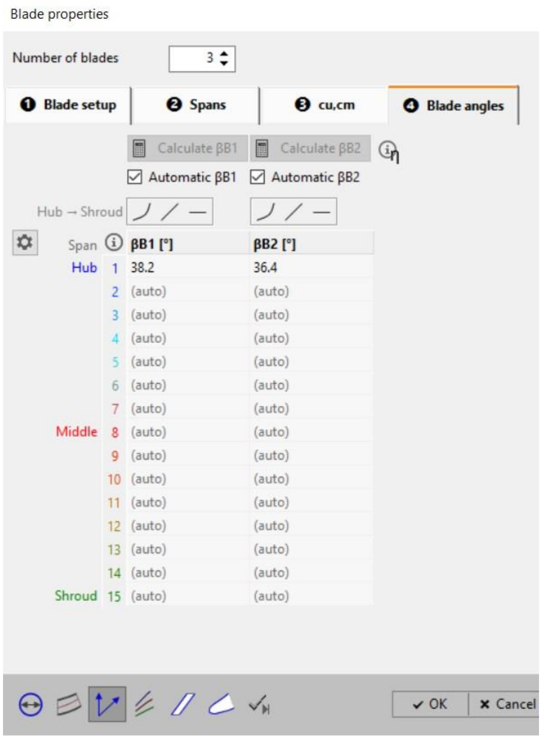

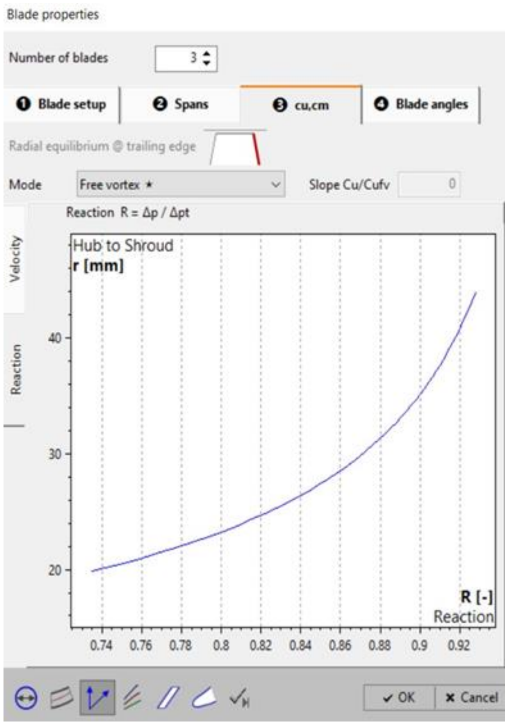

Picture 158 Automatic angle adjustment CFturbo program

Picture 159 The R ratio CFturbo program

The curvature of the wing lines and the wrap angle ΔΦ = 270° were adjusted with static pressure as the main criterion. It is noted that in the indicative diagrams for Cm and Cu velocities, there are large exclusions.

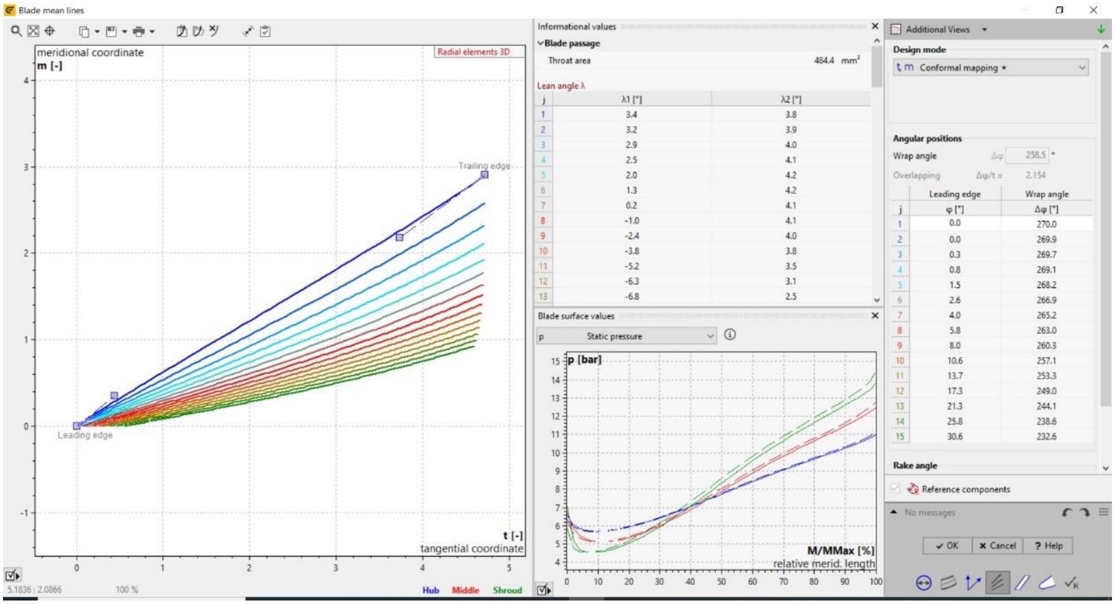

Picture 160 Blade configuration and design space with some criteria CFturbo program

In this case, the deviation for 5 degrees results in angles βB1 = 17.5° and βB2 = 24.7°, for degree of solidity of 2.29, δ = 3.33°. The difference is small. The estimate was made at the average distance of the wing (at point 8) for the hub and for the Shroud.

Informational values

j	βB1 [°]	βB2 [°]	γ [°]
1	38.2	36.4	30.8
2	33.5	34.2	28.1
3	30.0	32.2	25.8
4	26.9	30.5	23.8
5	24.0	28.9	22.1
6	21.3	27.4	20.6
7	19.2	26.0	19.3
8	17.5	24.7	18.2
9	16.0	23.5	17.2
10	14.7	22.4	16.2
11	13.7	21.3	15.4
12	12.8	20.4	14.7
13	12.0	19.5	14.0
14	11.3	18.6	13.4
15	10.7	17.8	12.9

Informational values

Blade solidity

j	l/t	lML/t	Δz/t	Δr/t
1	2.59	2.58	1.34	0.20
2	2.52	2.51	1.20	0.16
3	2.47	2.46	1.09	0.13
4	2.43	2.42	0.99	0.11
5	2.40	2.38	0.91	0.09
6	2.36	2.35	0.84	0.08
7	2.33	2.32	0.77	0.06
8	2.29	2.29	0.72	0.05
9	2.26	2.25	0.67	0.04
10	2.22	2.22	0.62	0.03
11	2.18	2.18	0.58	0.02
12	2.14	2.14	0.54	0.02
13	2.09	2.09	0.51	0.01
14	2.04	2.04	0.48	0.00
15	1.99	1.99	0.44	0.00

Picture 161 The entry and exit angles CFturbo program

Picture 162 Solidity of blade CFturbo program

\

Below are similar steps as in the previous inducer:

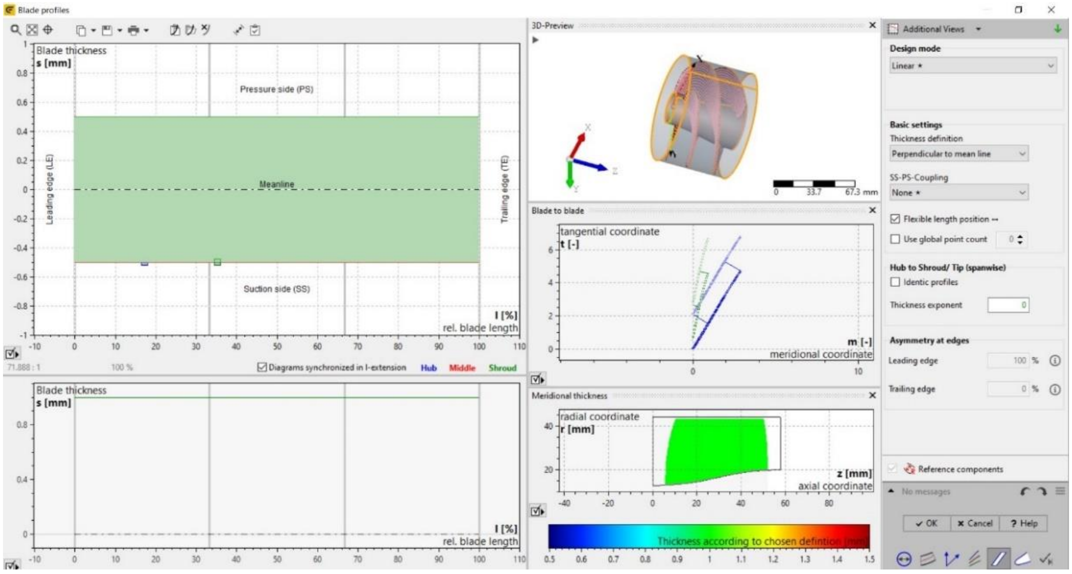

Picture 163 Blade profiles CFturbo program

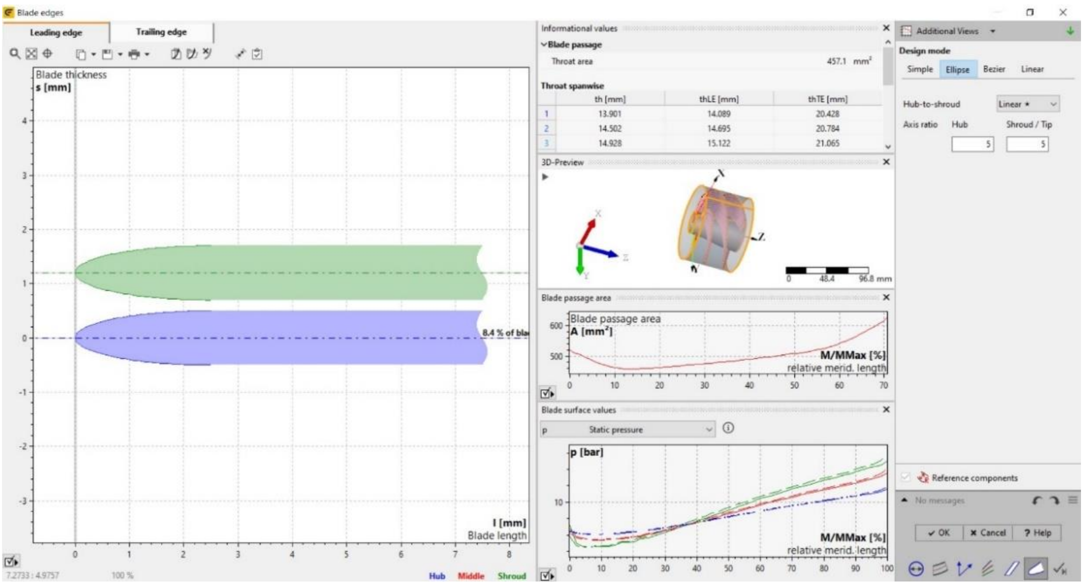

Picture 164 Blade leading edge CFturbo program

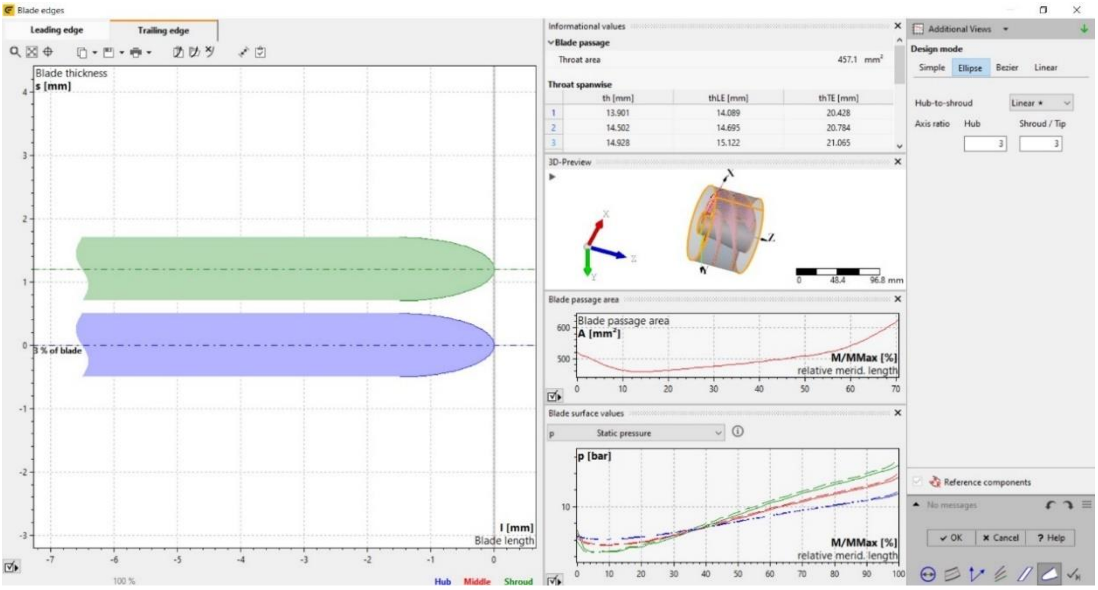

Picture 165 Blade trailing edge CFturbo program

4.2.2 Impeller

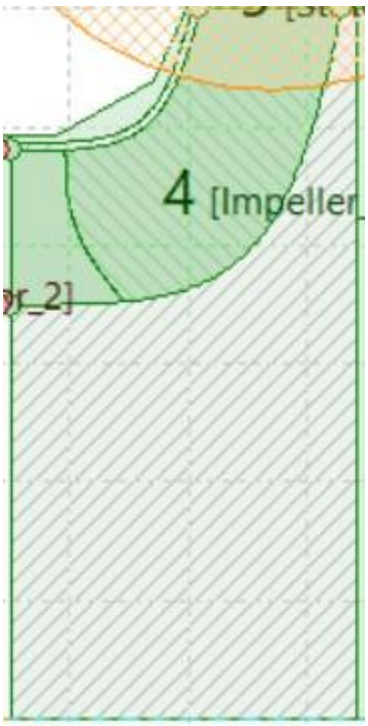

Picture 165 Impeller CFturbo program

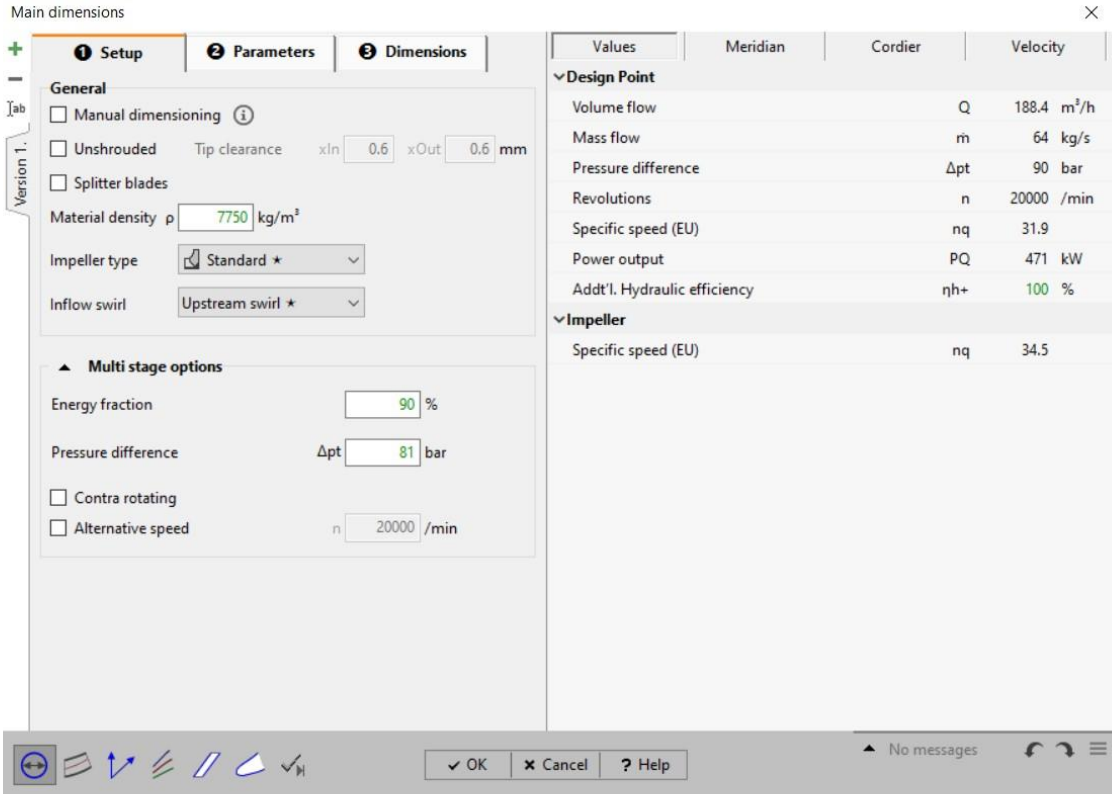

Picture 166 Start of set up of impeller CFturbo program

The method is exactly the same as in the previous impeller.

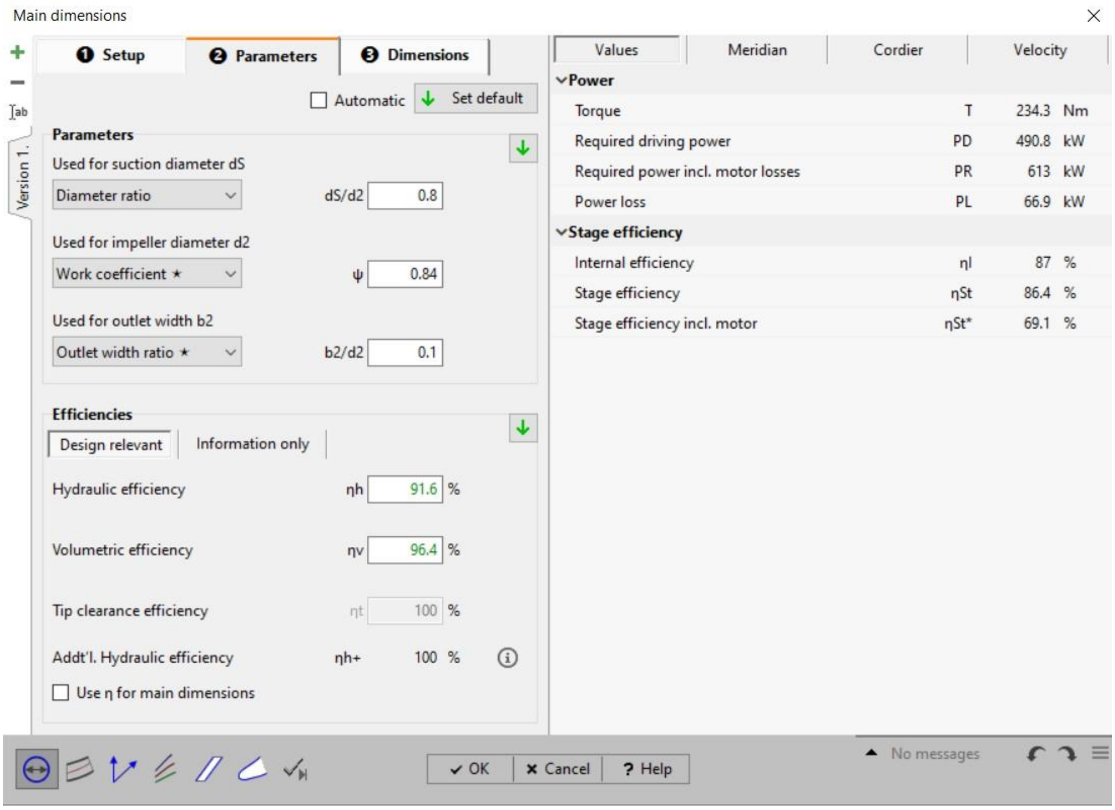

Picture167 The design parameters CFturbo program

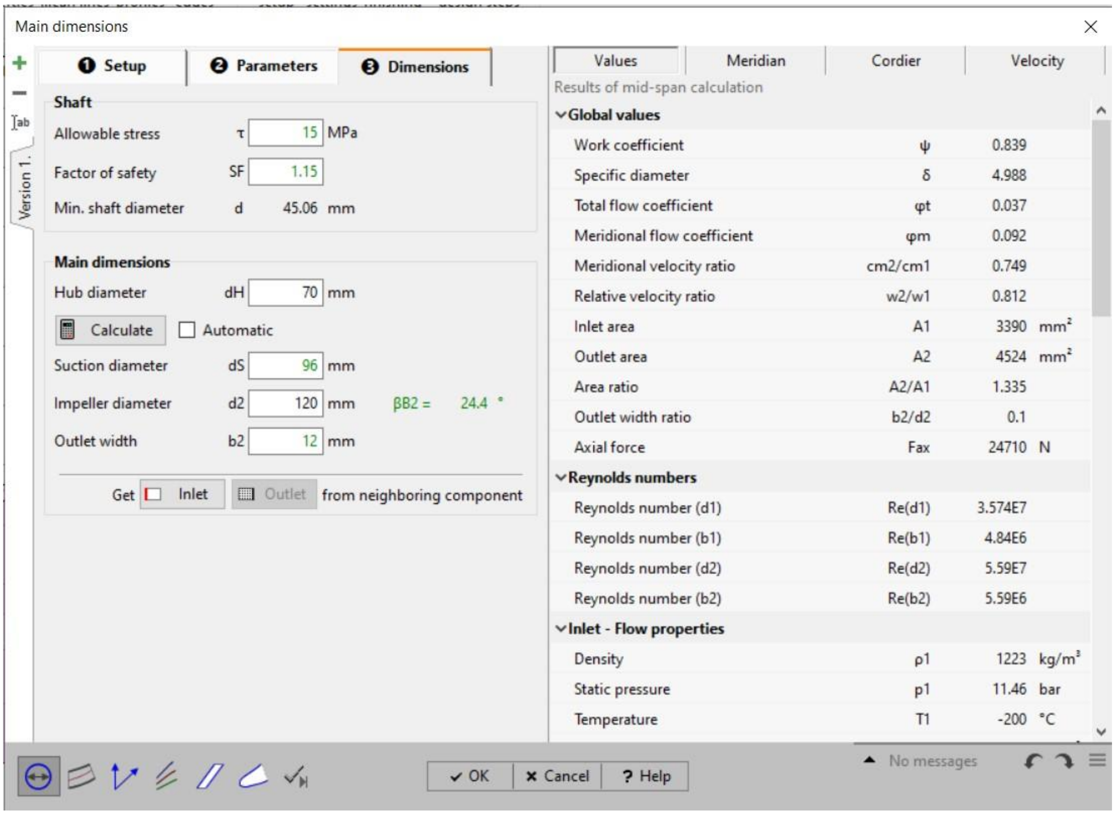

Picture 168 Input and output dimensions of the impeller and the all values CFturbo program

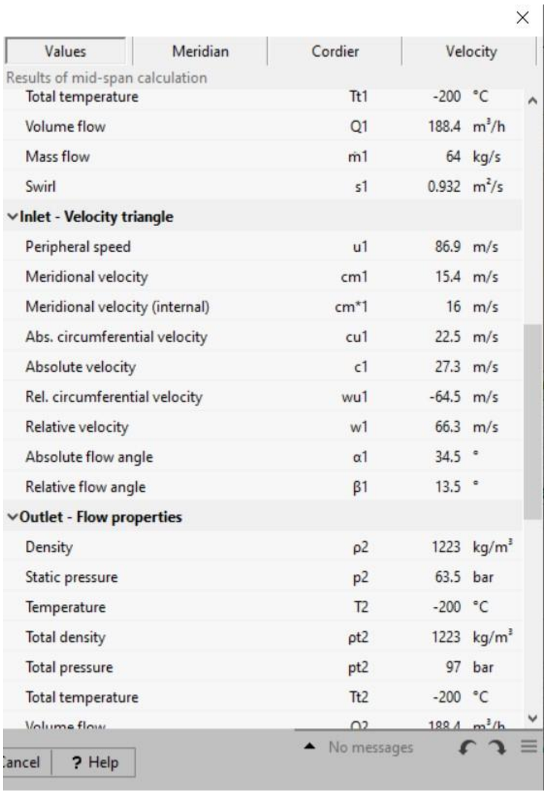

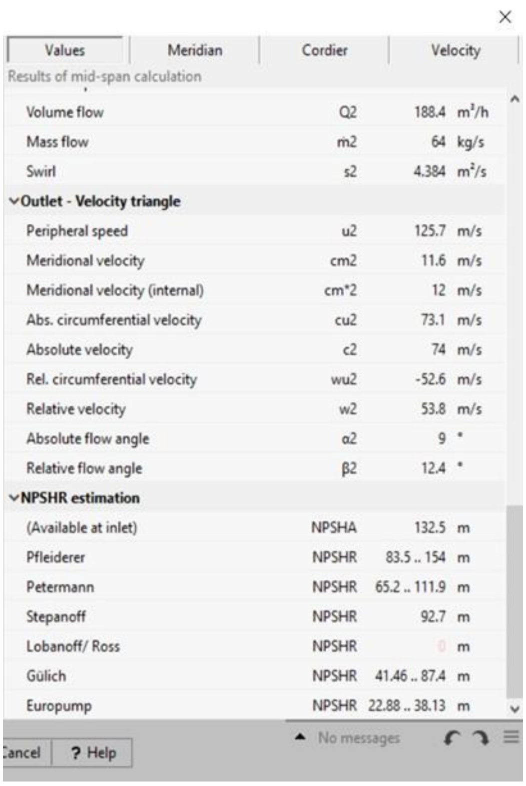

Picture 169 The values of all velocities, pressures and flow angles at the inlet and outlet of the impeller CFturbo program

Picture 170 The values of all velocities, pressures and flow angles at the inlet and outlet of the impeller CFturbo program

It is noted that :

- The NPSHA height is slightly less than the worst-case NPSHR value. Therefore, there is a very small possibility of cavitation.

- Angles β1 and β2 are very close in value although deceleration is achieved.

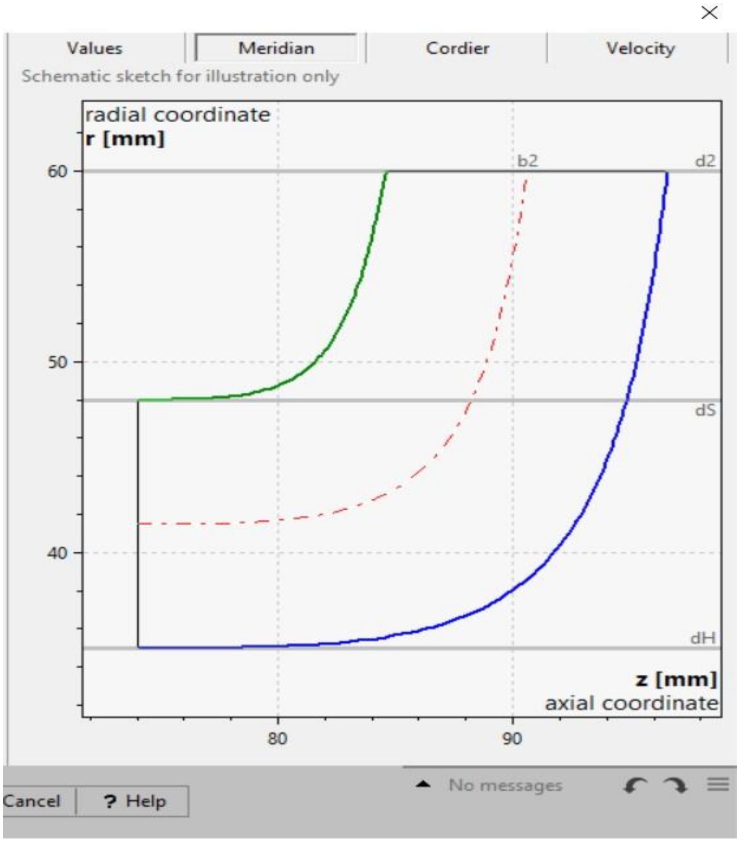

Picture 171 Side view of blade CFturbo program

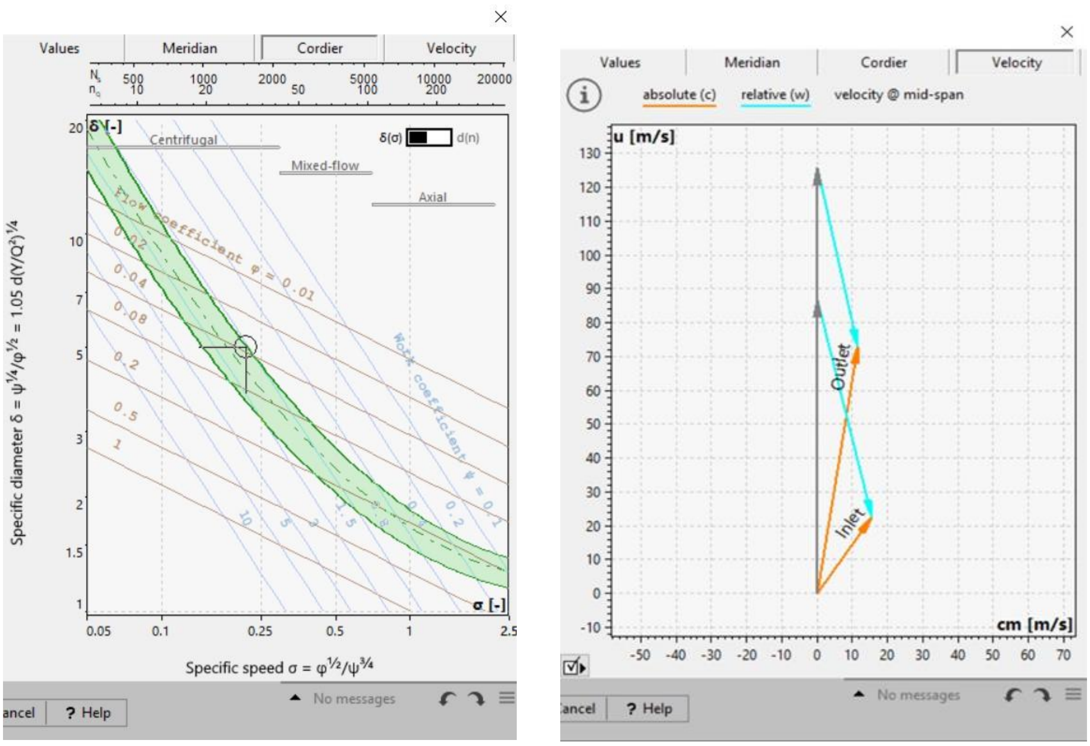

Picture 172 Inducer design point CFturbo program

Picture173 Impeller input and output speed triangles CFturbo program

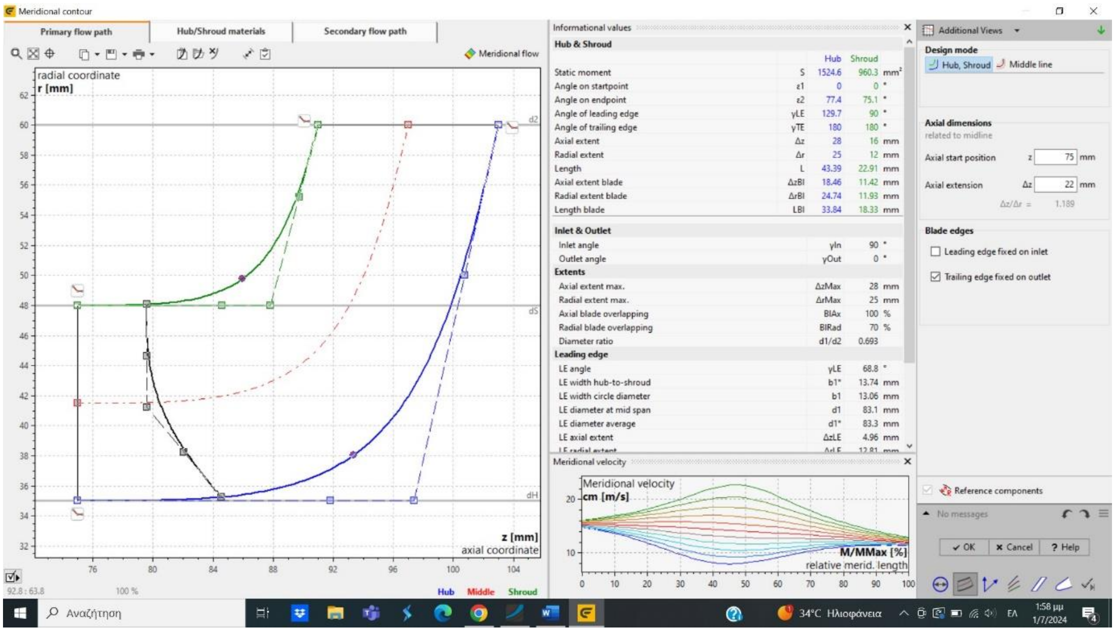

Picture 174 Meridian contour and B-spline configuration CFturbo program

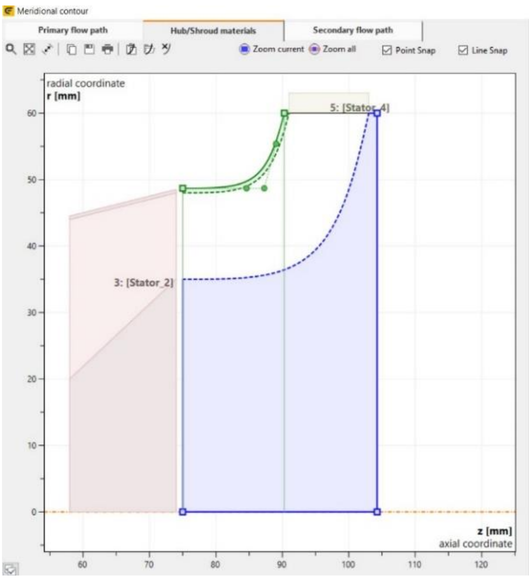

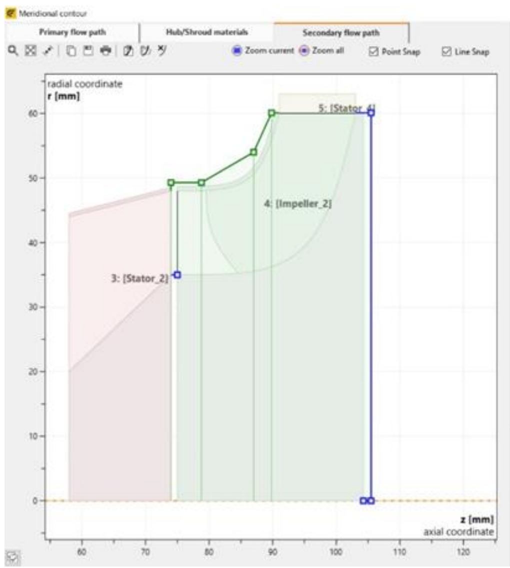

Picture 175 The material of the impeller shaft, disc and shroud CFturbo program

Picture 176 The impeller with an indicative static cover CFturbo program

Here the same methodology was applied with the previous one. The only difference is the coefficient k for estimating the number of fins. Because for K_z= 6.5, 13 fins come out, which caused a capacity issue. So, the coefficient became 5 and 10 fins were selected.

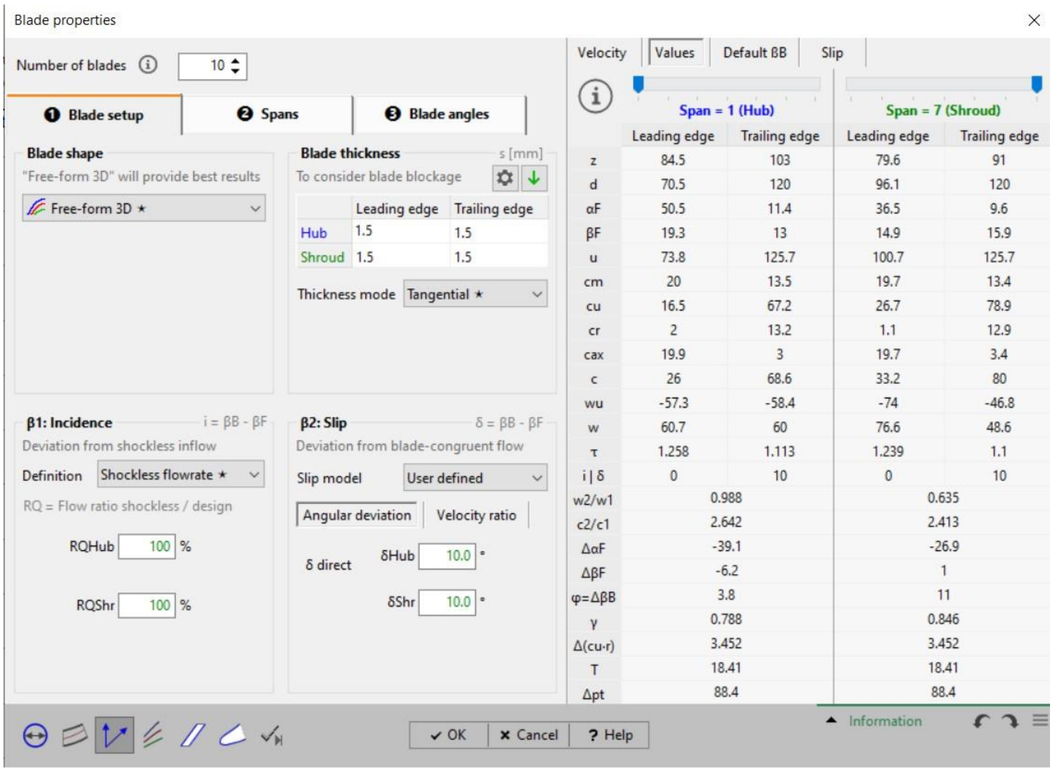

	Span = 1 (Hub) Leading edge	Span = 1 (Hub) Trailing edge	Span = 7 (Shroud) Leading edge	Span = 7 (Shroud) Trailing edge
z	84.5	103	79.6	91
d	70.5	120	96.1	120
αF	50.5	11.4	36.5	9.6
βF	19.3	13	14.9	15.9
u	73.8	125.7	100.7	125.7
cm	20	13.5	19.7	13.4
cu	16.5	67.2	26.7	78.9
cr	2	13.2	1.1	12.9
cax	19.9	3	19.7	3.4
c	26	68.6	33.2	80
wu	-57.3	-58.4	-74	-46.8
w	60.7	60	76.6	48.6
τ	1.258	1.113	1.239	1.1
i | δ	0	10	0	10
w2/w1	0.988		0.635	
c2/c1	2.642		2.413	
ΔαF	-39.1		-26.9	
ΔβF	-6.2		1	
φ=ΔβB	3.8		11	
γ	0.788		0.846	
Δ(cu·r)	3.452		3.452	
T	18.41		18.41	
Δpt	88.4		88.4	

Picture 177 Space for shape and wing design settings and corner deviations CFturbo program

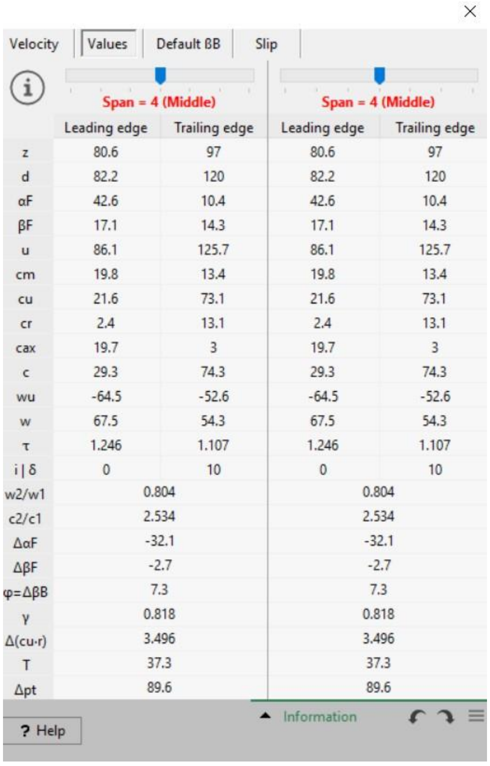

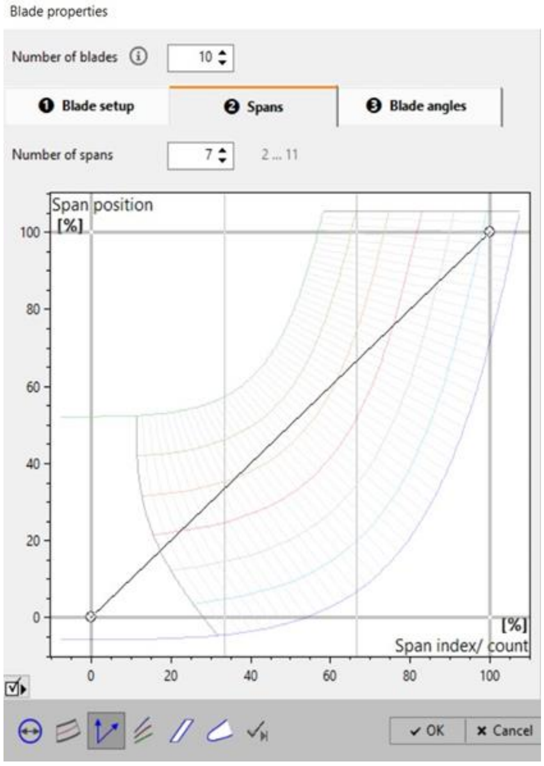

Picture 178 The values at the inlet and outlet of the impeller at the central point of the blade CFturbo program

Picture 179 Number of spans CFturbo program

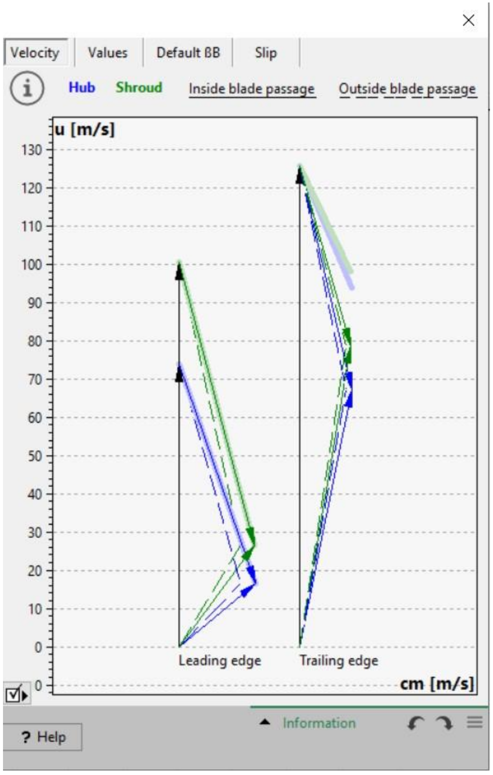

Picture 180 Velocity triangles at the inlet and outlet of the impeller with the deviation angles CFturbo program

Picture 181 The corrected inlet and outlet vane angle values CFturbo program

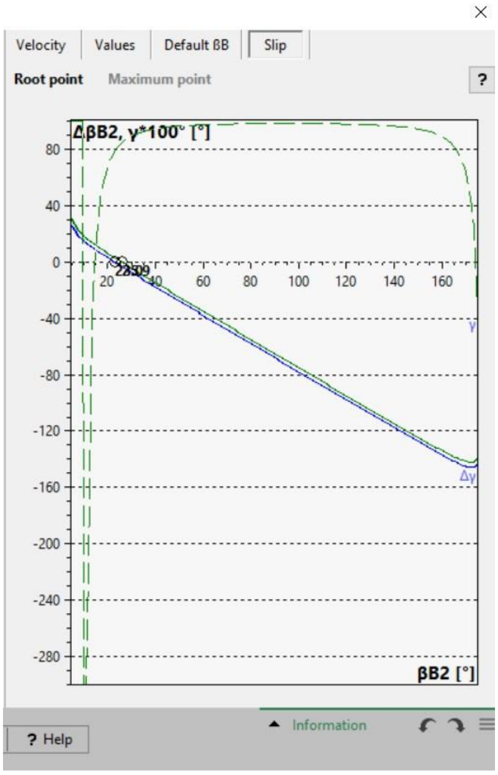

Picture 182 The slip CFturbo program

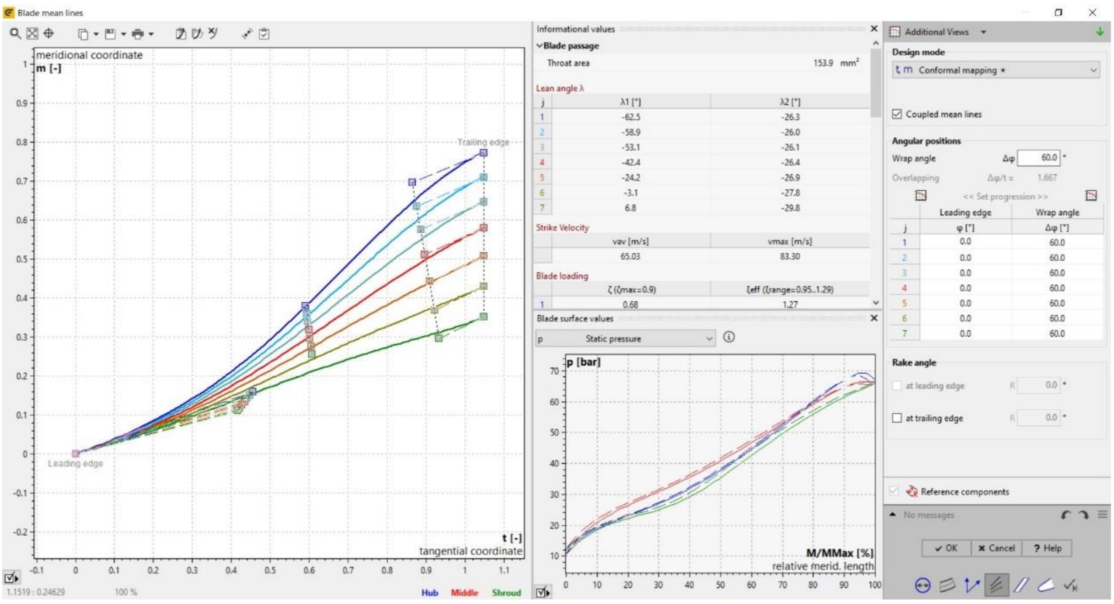

Picture 183 Blade configuration and design space with some criteria CFturbo program

Informational values

Blade loading

	ζ (ζmax=0.9)	ξeff (ξrange=0.95..1.29)
1	0.68	1.27
7	0.67	1.20

Blade angle βB

j	βB1 [°]	βB2 [°]
1	19.3	23.0
2	18.5	23.4
3	17.8	23.9
4	17.1	24.3
5	16.3	24.8
6	15.6	25.4
7	14.9	25.9

Blade angle in x-y βB,xy

j	βB1,xy [°]	βB2,xy [°]
1	2.0	22.5
2	2.8	22.9
3	2.7	23.4

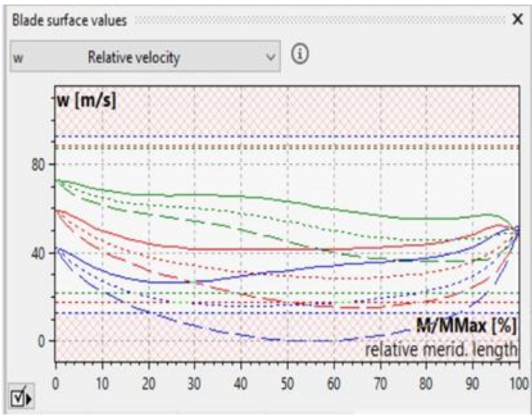

Picture184 The entry and exit angles CFturbo program

Picture 185 The relative velocity distribution over the meridional length of the blade in percent CFturbo program

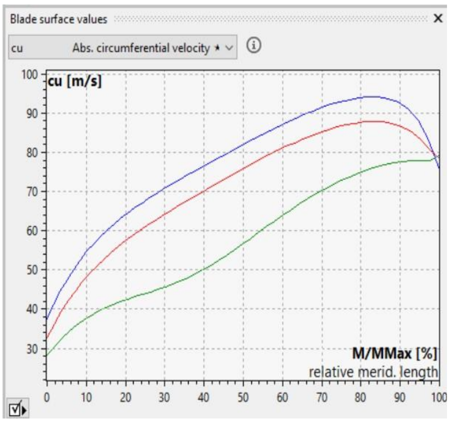

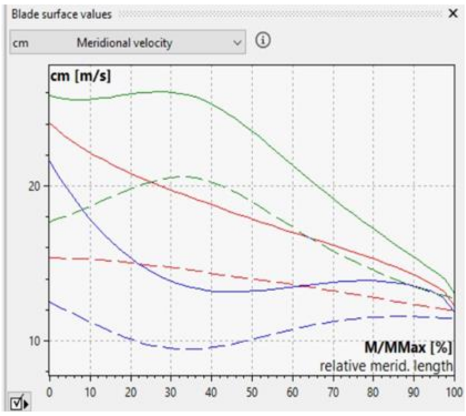

Picture 186 The absolute circumferential velocity distribution over the meridional length of the blade in percent CFturbo program

Picture 187 The meridional velocity distribution over the meridional length of the blade in percent CFturbo program

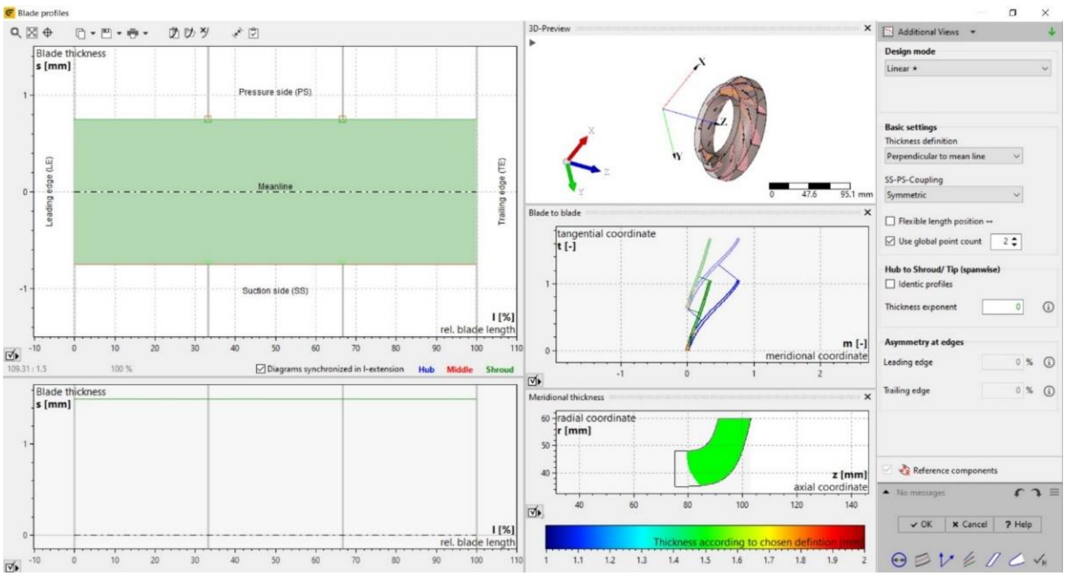

Picture 188 Blade profiles CFturbo program

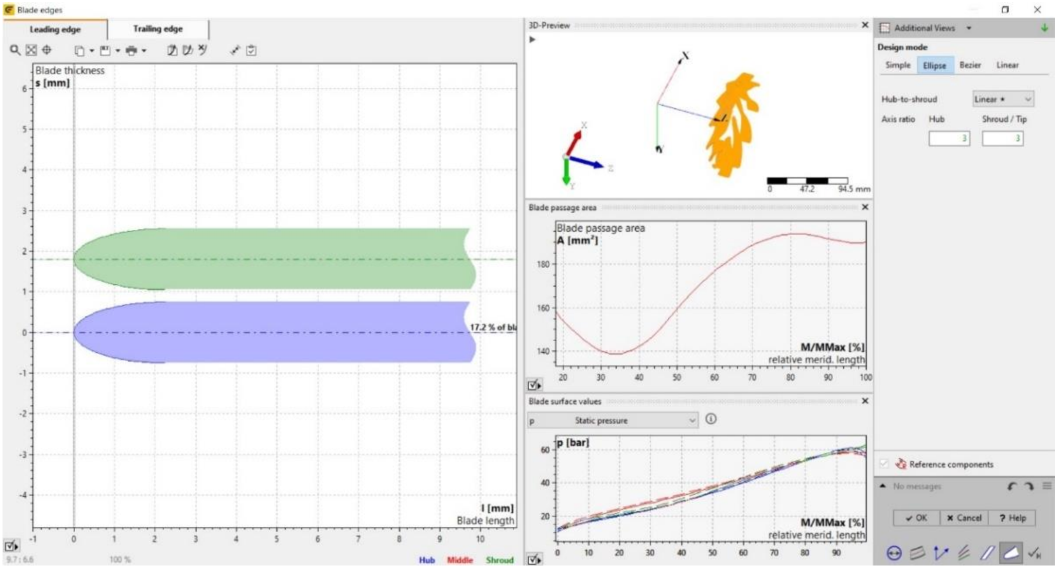

Picture 189 Blade leading edge CFturbo program

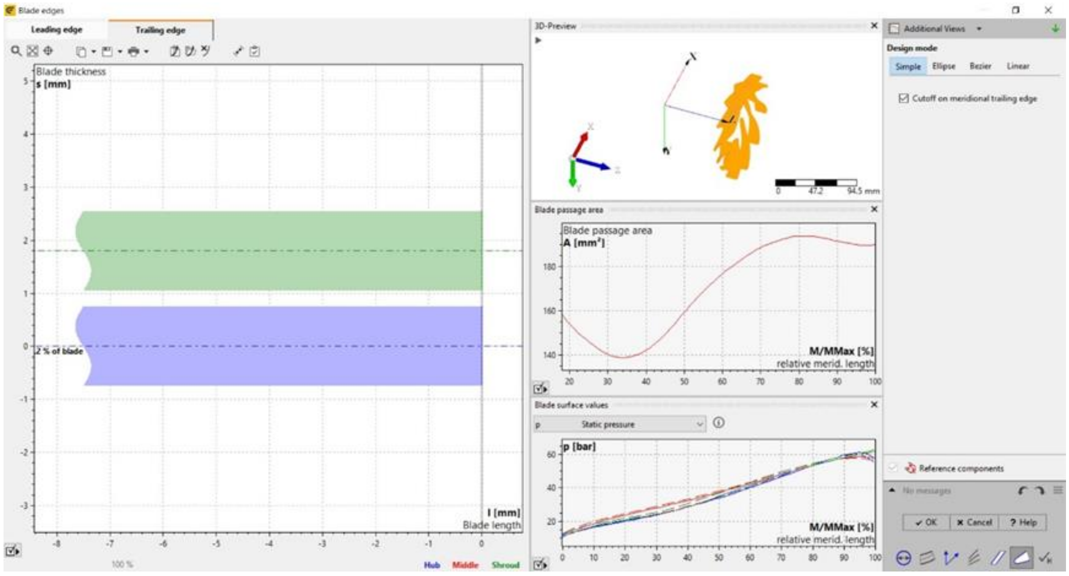

Picture 190 Blade trailing edge CFturbo program

4.2.3 Stator

Likewise, here is a suitably pre-drilled tapered shaft that rotates in a tapered rotor:

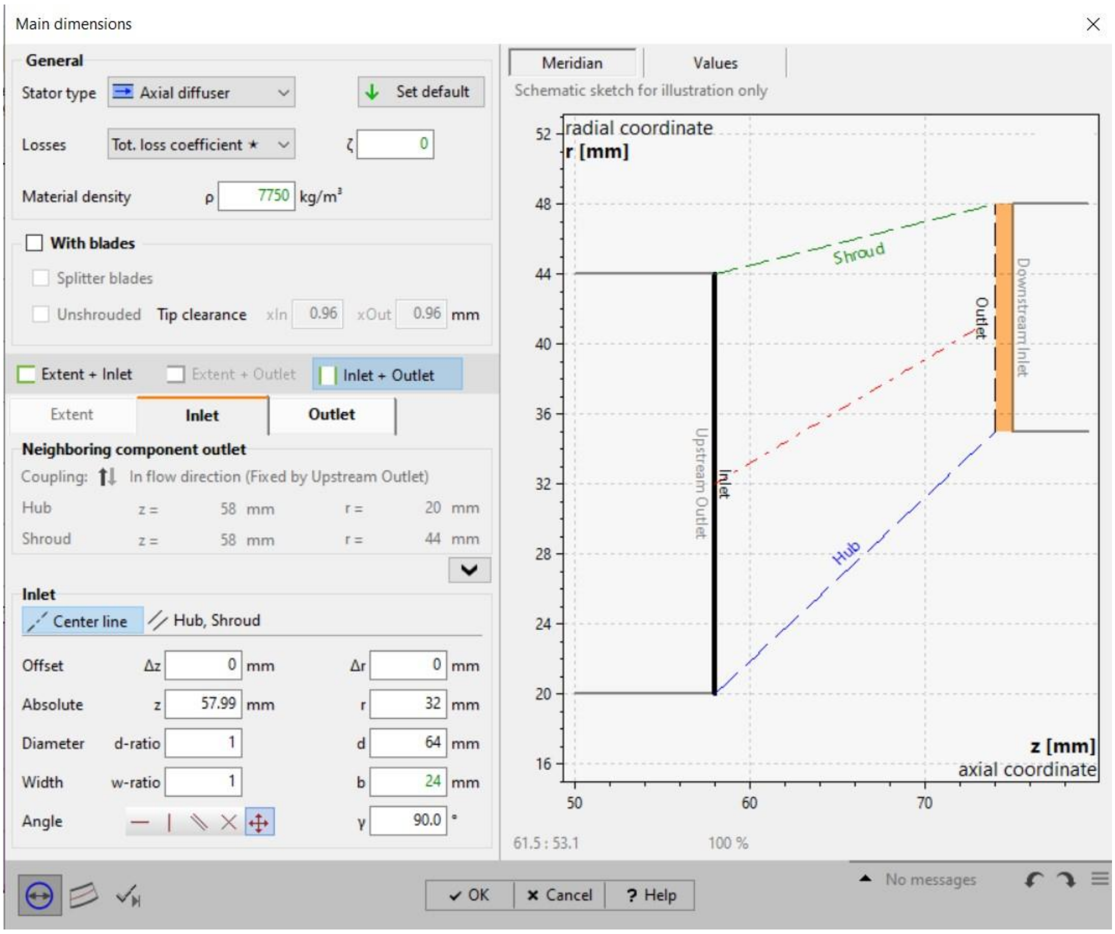

Picture 191Conical stator input set up CFturbo program

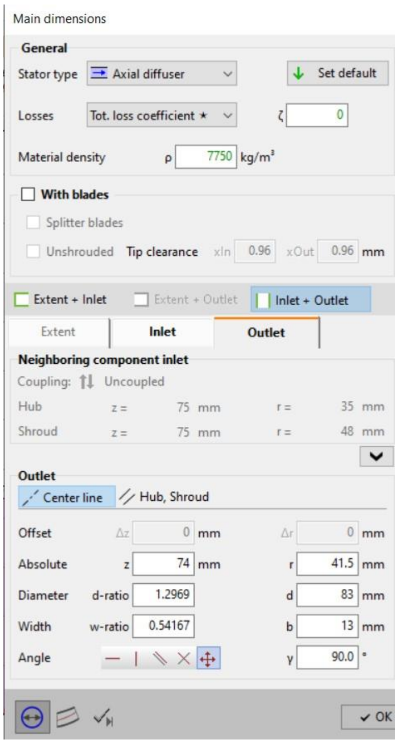

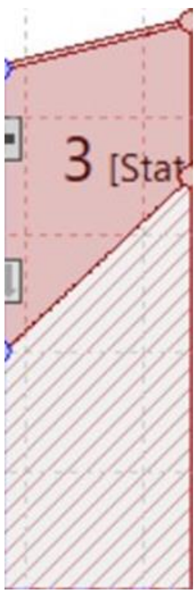

Picture 192 Conical stator output set up CFturbo program

Picture 193 Stator CFturbo program

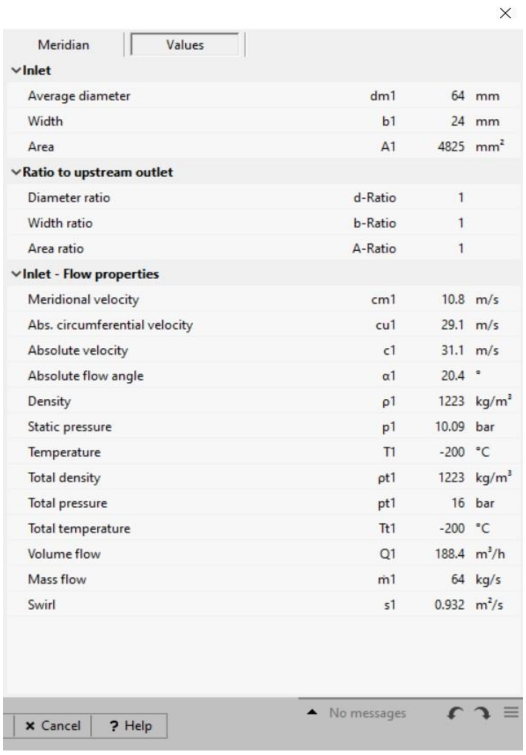

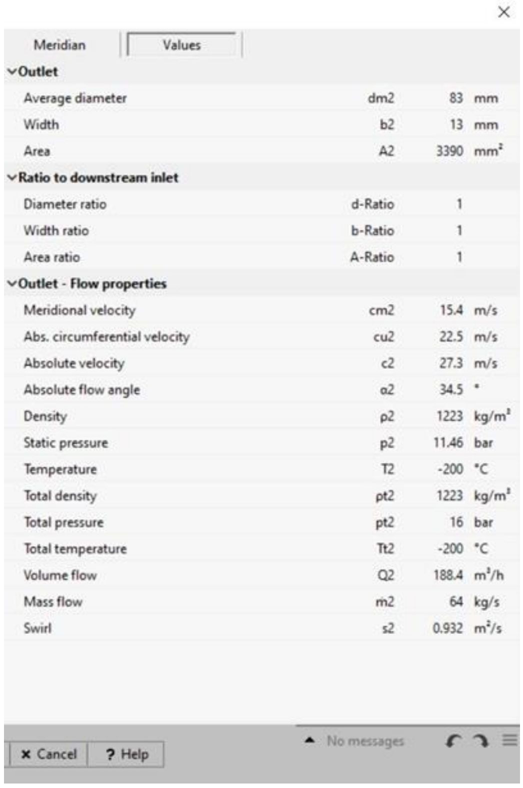

Picture 194 The values of all velocities, pressures and flow angles at the inlet of the stator CFturbo program

Picture 195 The values of all velocities, pressures and flow angles at the outlet of the stator CFturbo program

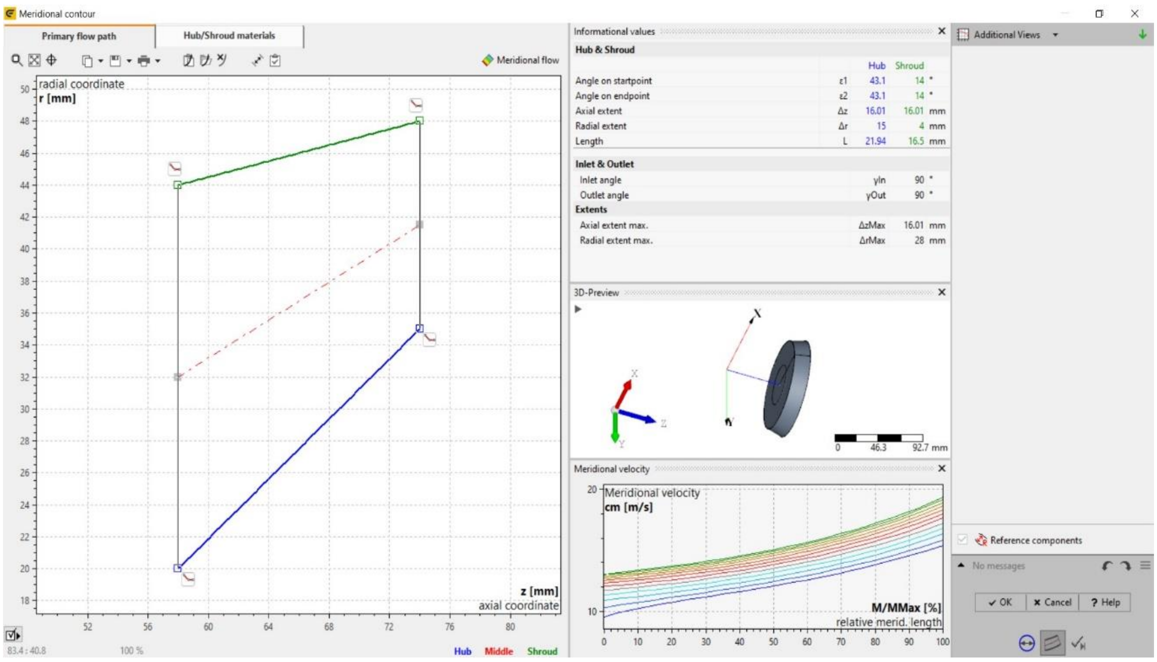

Picture 196 Meridian contour and B-spline configuration CFturbo program

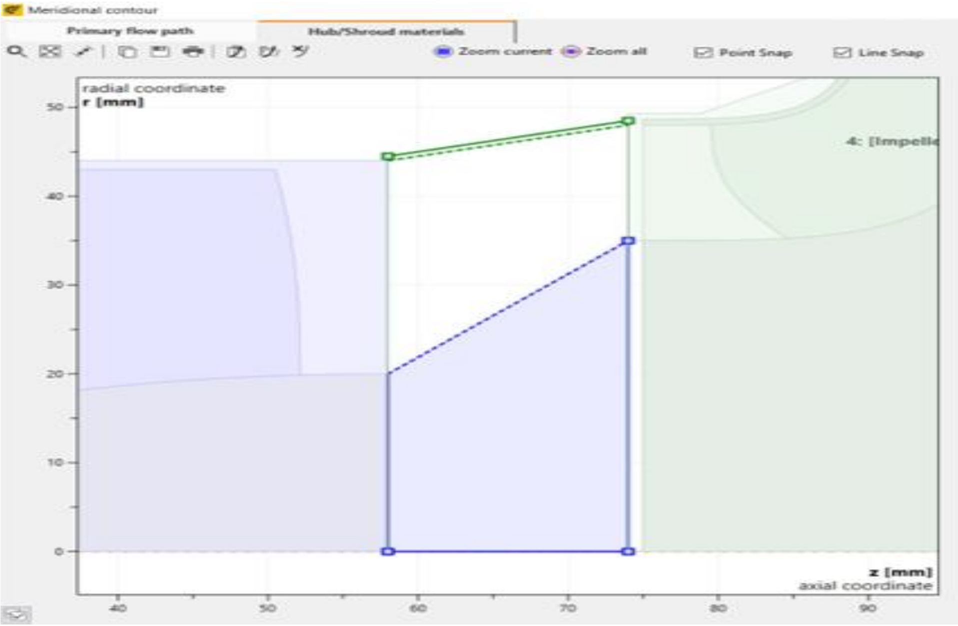

Picture 197 The material of the conic shaft and conic stator CFturbo program

4.2.4 Volute-Diffuser

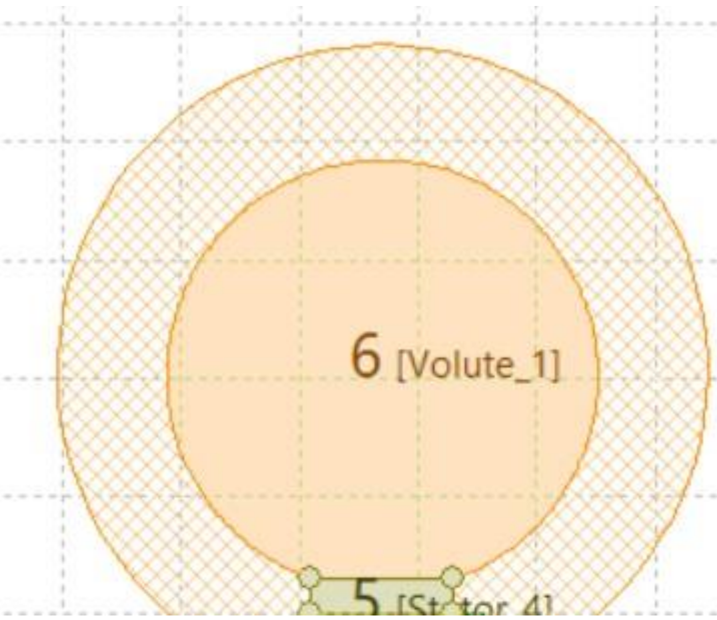

Picture 198 Volute - Diffuser

In this case, the ration d_4/d_2 was chosen 1.05 and combined with the following function with the special number of revolutions comes out 1.065. The difference is small. The distance includes the distance between the impeller and the shell which is 0.1mm.

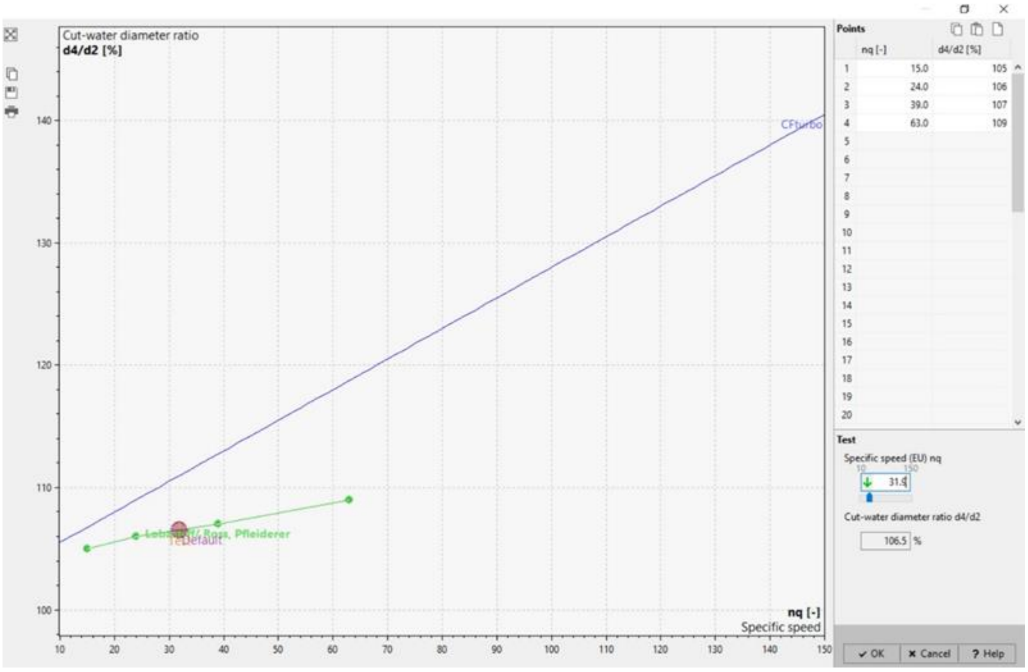

Picture 199 Function of the ratio d4/d2 with the specific speed number CFturbo program

The distance Δr was similarly defined.

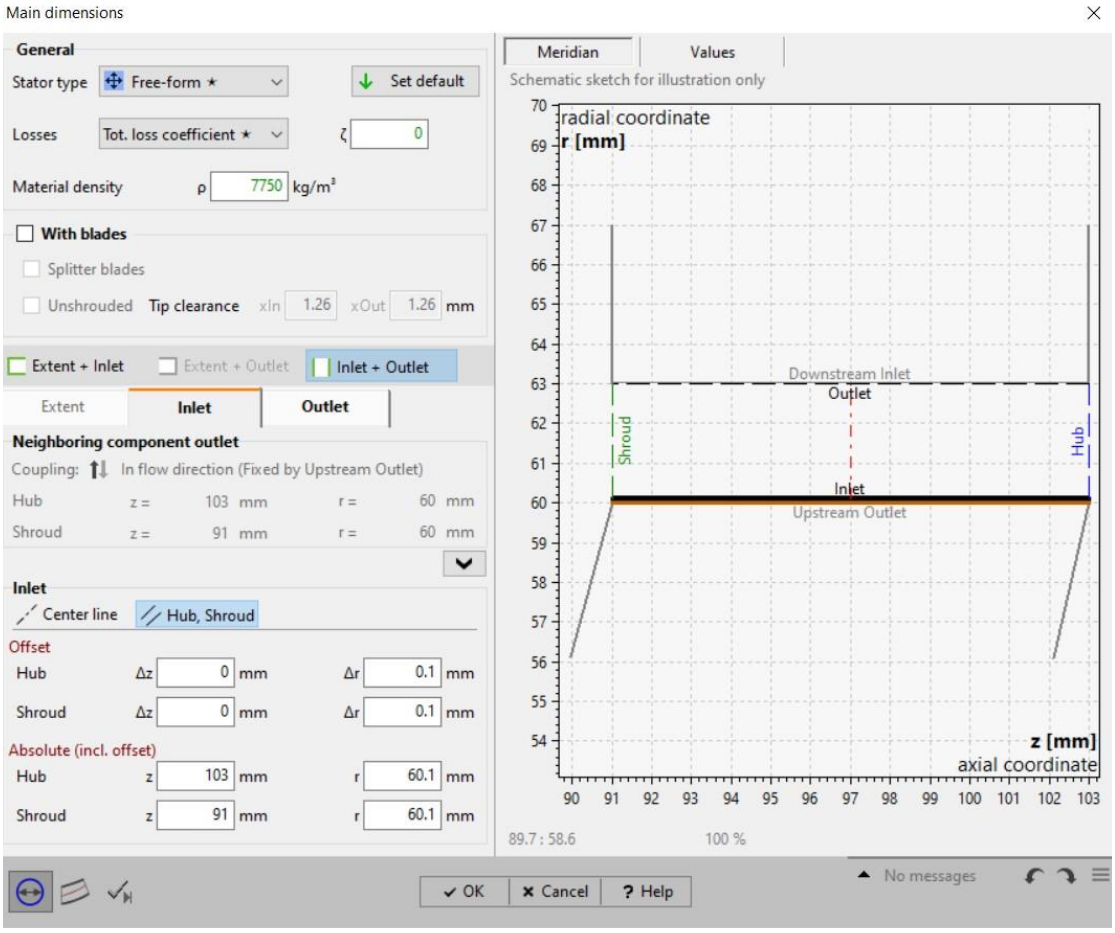

Picture 200 Stator input set up CFturbo program

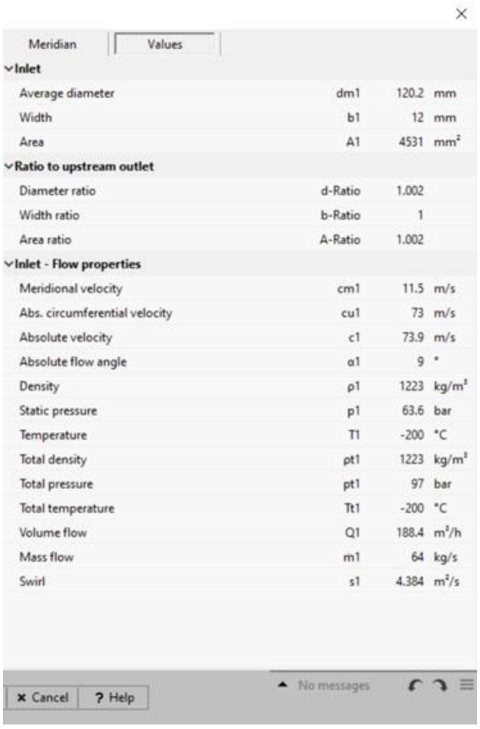

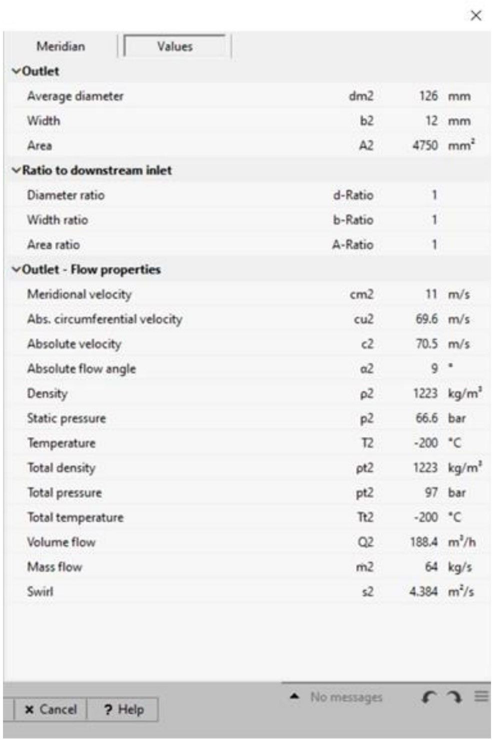

Picture 201 The values of all velocities, pressures and flow angles at the inlet of the stator CFturbo program

Picture 202 The values of all velocities, pressures and flow angles at the outlet of the stator CFturbo program

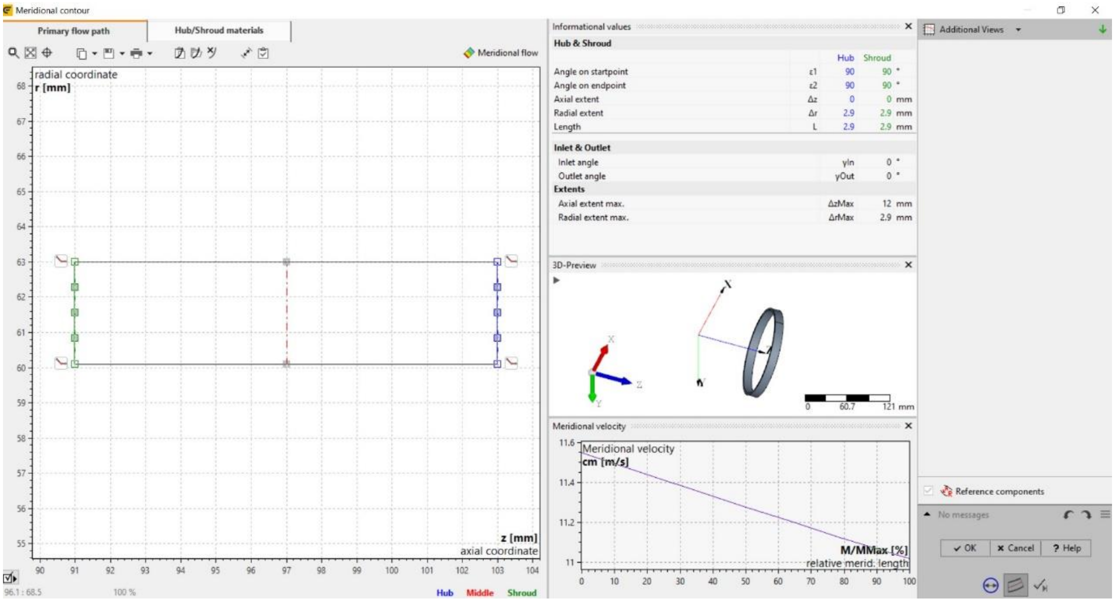

Picture 203 Meridian contour and B-spline configuration CFturbo program

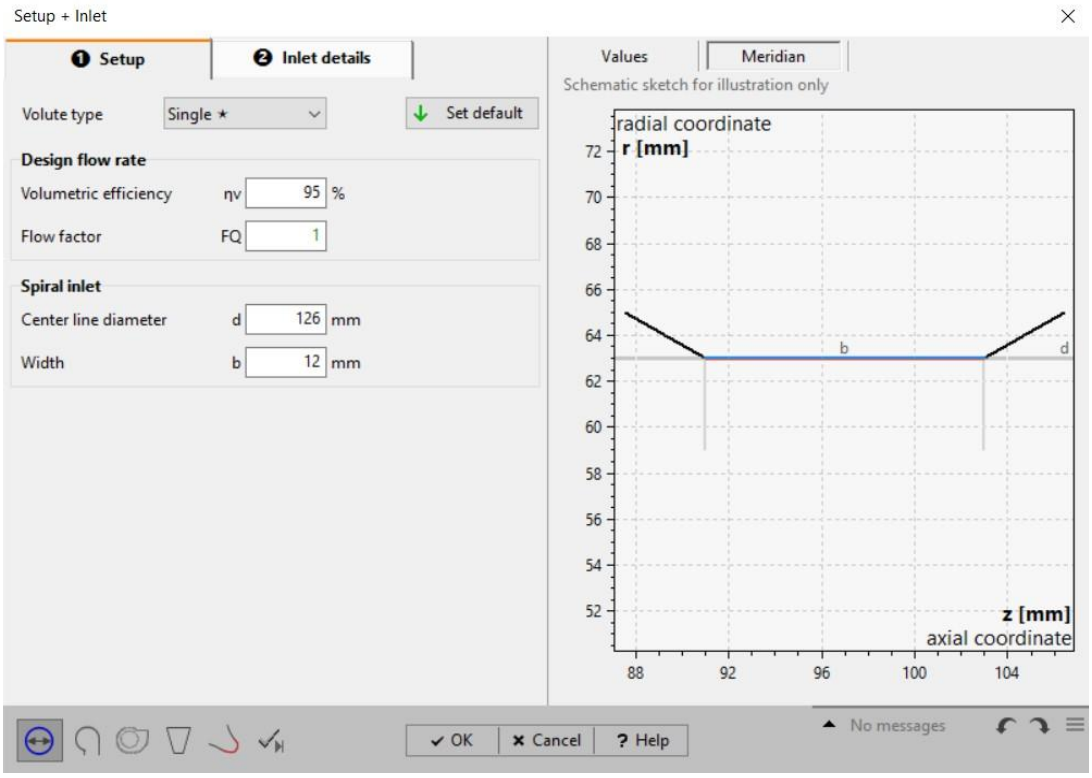

Picture 204 Start of set up of volute - diffuser CFturbo program

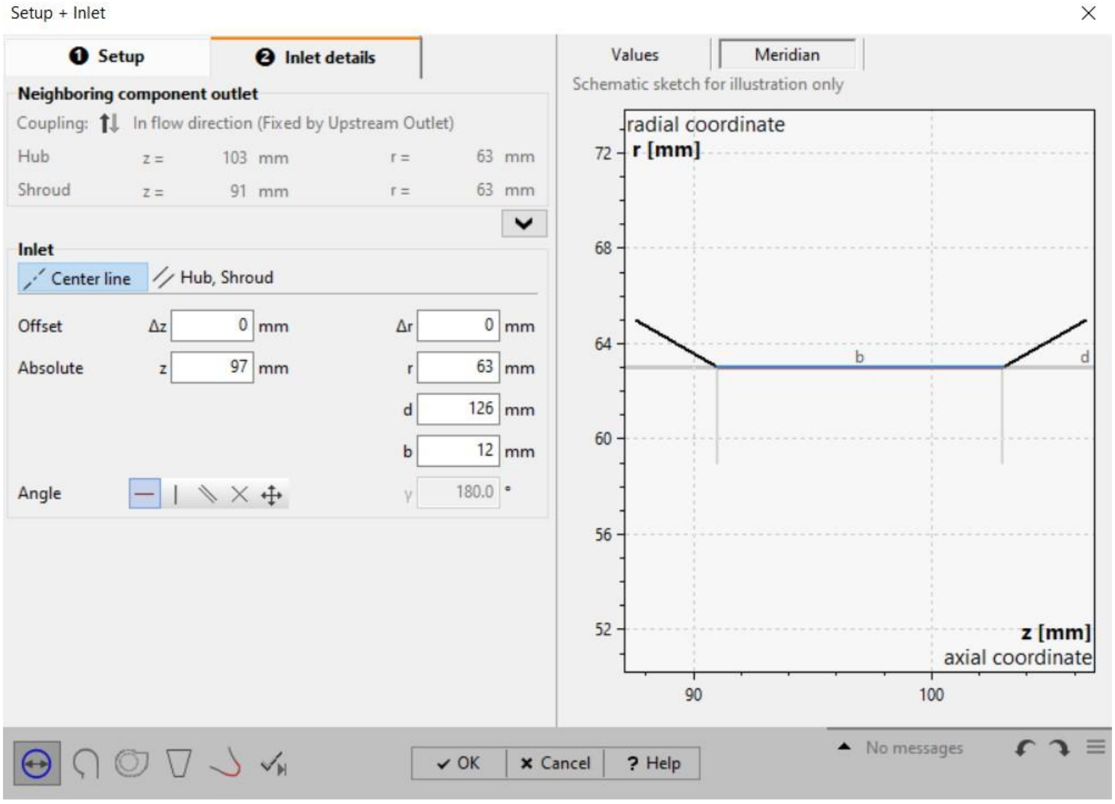

Picture 205 Entrance dimensions CFturbo program

The thickness was formed a little higher, with 2.5 mm, and the method designed is with the constant vorticity (x=1), whereas with this method, we have a high hydraulic efficiency. By estimation, the hydraulic grade manually entered 95%. The diameter and height were adjusted so that we have an outlet pressure of about 86 bar.

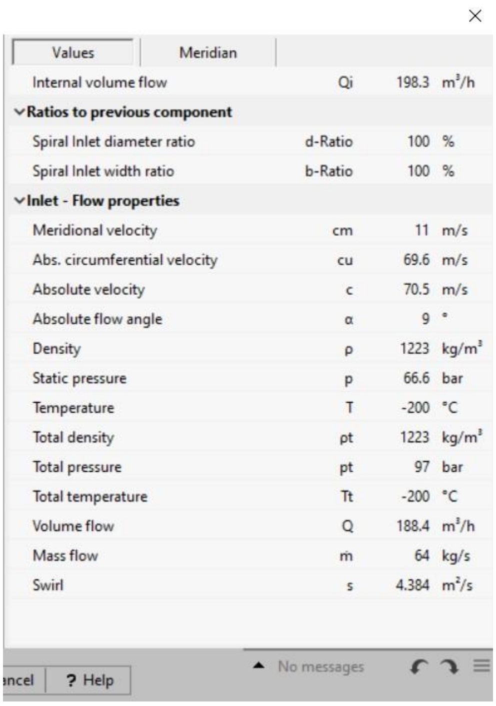

Picture 206 The values of all velocities, pressures and flow angles at the inlet of the volute - diffuser CFturbo program

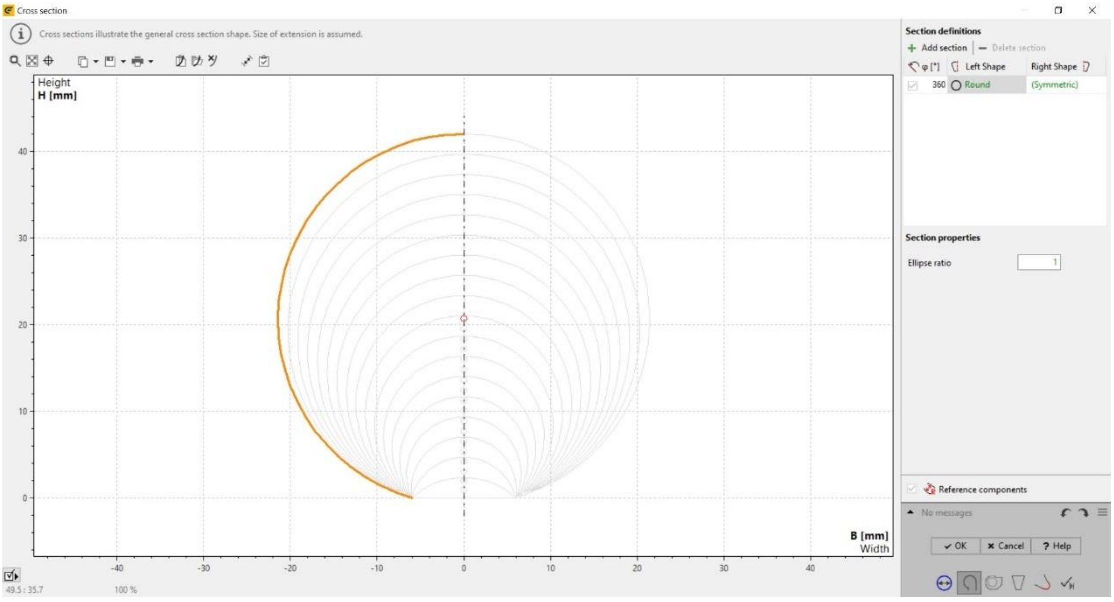

Picture 207 Configuration of spiral tube shape and size CFturbo program

It is noted that the stator added before the diffuser is considered part of the diffuser. For this reason, d4/d2 = 105% and not 100% is mentioned in the set up.

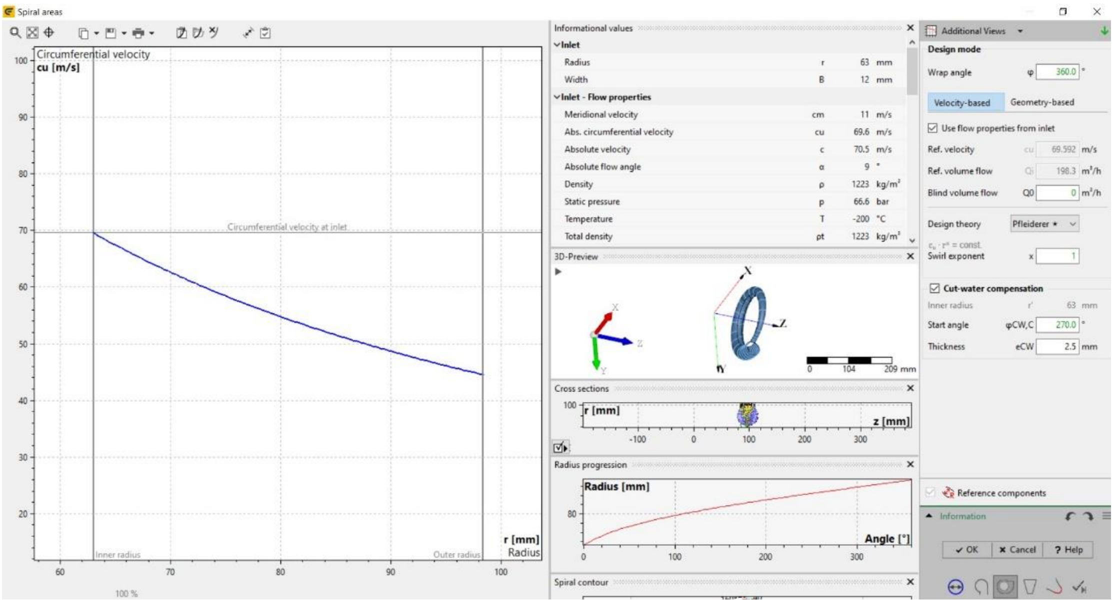

Picture 208 Spiral design space based on some criteria CFturbo program

Informational values

Inlet			
Radius	r	63	mm
Width	B	12	mm
Inlet - Flow properties			
Meridional velocity	cm	11	m/s
Abs. circumferential velocity	cu	69.6	m/s
Absolute velocity	c	70.5	m/s
Absolute flow angle	α	9	°
Density	ρ	1223	kg/m³
Static pressure	p	66.6	bar
Temperature	T	-200	°C
Total density	ρt	1223	kg/m³
Total pressure	pt	97	bar
Total temperature	Tt	-200	°C
Volume flow	Q	188.4	m³/h
Mass flow	m	64	kg/s
Swirl	s	4.384	m²/s
Last spiral section			
Inner radius	r'	63	mm
Outer radius	r	98.4	mm
Equivalent diameter	D	36.3	mm
Min. axial coordinate	z	78.8	mm
Height	H	35.42	mm
Width	B	36.44	mm
Side ratio	H/B	97.2	%

Informational values

Width	B	36.44	mm
Side ratio	H/B	97.2	%
Area	A	1035	mm²
Area/Radius	A/rc	12.88	mm
Last spiral section - Flow properties			
Meridional velocity	cm	0	m/s
Abs. circumferential velocity	cu	50.6	m/s
Absolute velocity	c	50.6	m/s
Absolute flow angle	α	90	°
Density	ρ	1223	kg/m³
Static pressure	p	75.9	bar
Temperature	T	-200	°C
Total density	ρt	1223	kg/m³
Total pressure	pt	91.5	bar
Total temperature	Tt	-200	°C
Volume flow	Q	188.4	m³/h
Mass flow	m	64	kg/s
Swirl	s	4.063	m²/s
Losses			
Sizing parameter	SP	1.079	
Meridional loss coefficient	km	0.024	
Tangential loss coefficient	ku	0.054	
Wall loss coefficient	kw	0.102	
Overall loss coefficient	k	0.181	
Total pressure loss	Δpt	5.49	bar

Picture 209 The values of all velocities, pressures and flow angles at the inlet and the last spiral section CFturbo program

Picture 210 The values of all velocities, pressures and flow angles at the inlet and the last spiral section CFturbo program

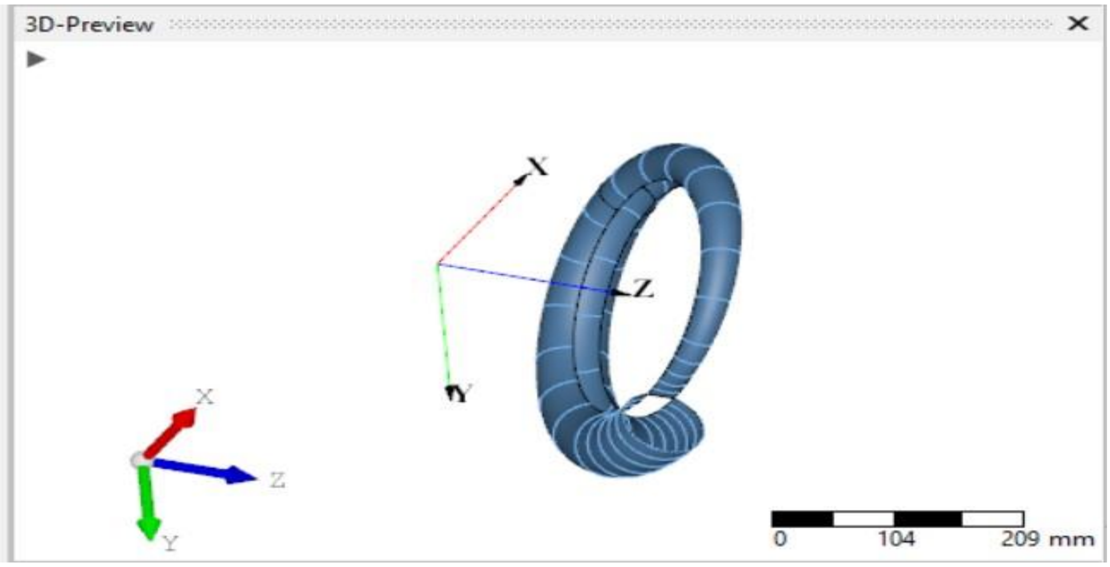

Picture 211 The spiral CFturbo program

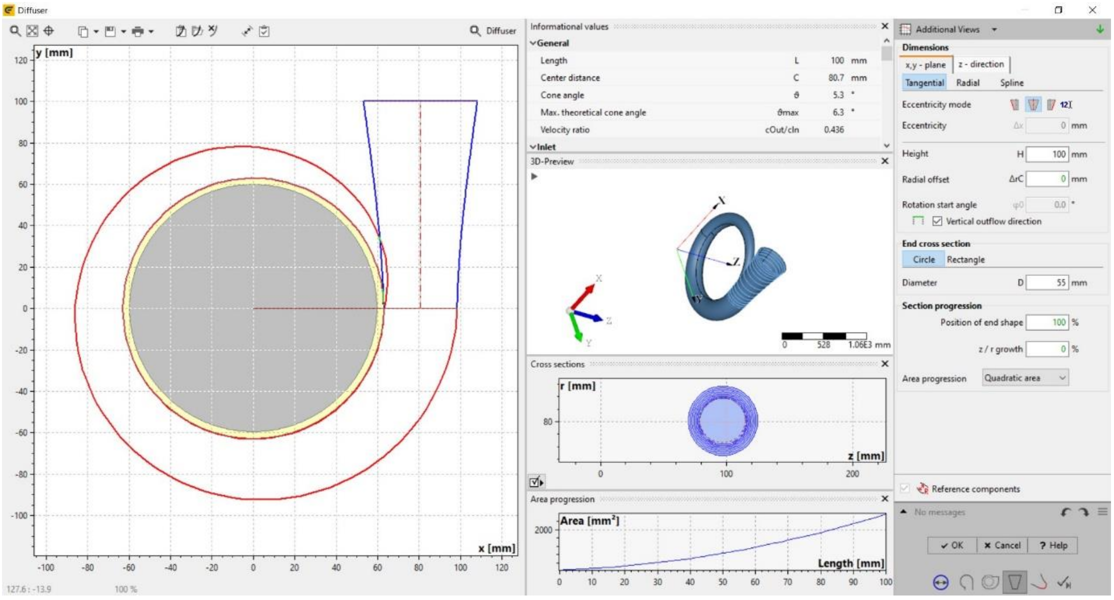

Picture 212 Configuration of conical diffuser at the outlet CFturbo program

Informational values			
General			
Length	L	100	mm
Center distance	C	80.7	mm
Cone angle	ϑ	5.3	°
Max. theoretical cone angle	ϑmax	6.3	°
Velocity ratio	cOut/cIn	0.436	
Inlet			
Equivalent diameter	D	36.3	mm
Area	A	1035	mm²
Outlet			
Equivalent diameter	D	55	mm
Area	A	2376	mm²
Diffuser center position	Cx	80.7	mm
Diffuser center position	Cy	100	mm
Diffuser center position	Cz	97	mm
Last spiral section - Flow properties			
Meridional velocity	cm	0	m/s
Abs. circumferential velocity	cu	50.6	m/s
Absolute velocity	c	50.6	m/s
Absolute flow angle	α	90	°
Density	ρ	1223	kg/m³
Static pressure	p	75.9	bar
Temperature	T	-200	°C
Total density	ρt	1223	kg/m³

Informational values			
Density	ρ	1223	kg/m³
Static pressure	p	75.9	bar
Temperature	T	-200	°C
Total density	ρt	1223	kg/m³
Total pressure	pt	91.5	bar
Total temperature	Tt	-200	°C
Volume flow	Q	188.4	m³/h
Mass flow	ṁ	64	kg/s
Swirl	s	4.063	m²/s
Outlet - Flow properties			
Absolute velocity	c	22	m/s
Density	ρ	1223	kg/m³
Static pressure	p	85.8	bar
Temperature	T	-200	°C
Total density	ρt	1223	kg/m³
Total pressure	pt	88.8	bar
Total temperature	Tt	-200	°C
Volume flow	Q	188.4	m³/h
Mass flow	ṁ	64	kg/s
Losses			
Cone loss coefficient	kc	0.164	
Wall loss coefficient	kw	0.011	
Overall loss coefficient	k	0.175	
Total pressure loss	Δpt	2.74	bar

Picture 213 The values of all velocities, pressures and flow angles at the outlet of diffuser CFturbo program

Picture 214 The values of all velocities, pressures and flow angles at the outlet of diffuser CFturbo program

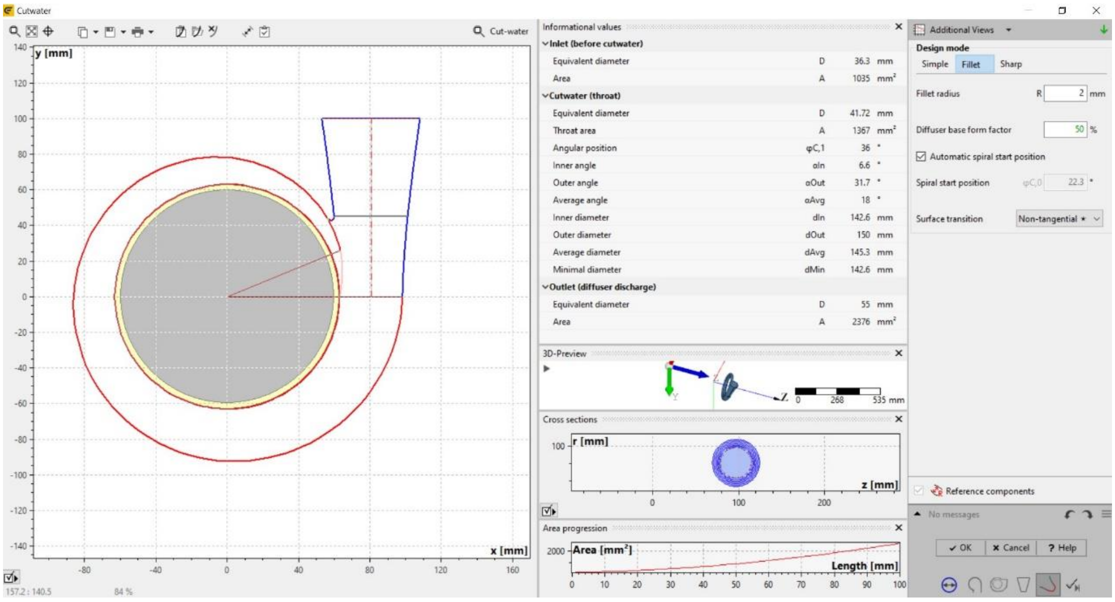

Picture 215 Curvature shaping space between conical diffuser and spiral CFturbo program

4.2.5 Rotary part of the inducer

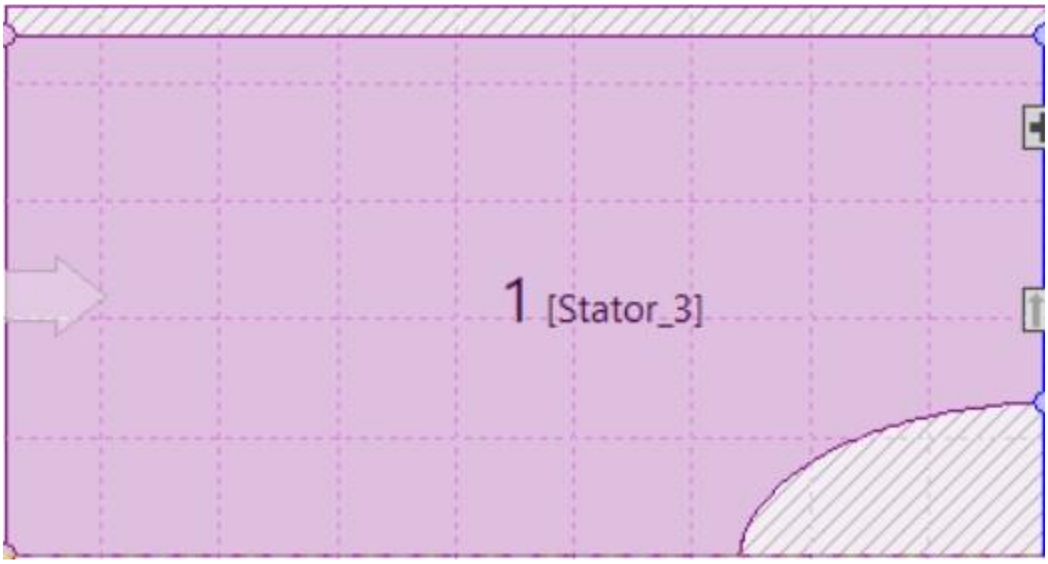

Picture 216 Rotary inducer nose & inducer input space CFturbo program

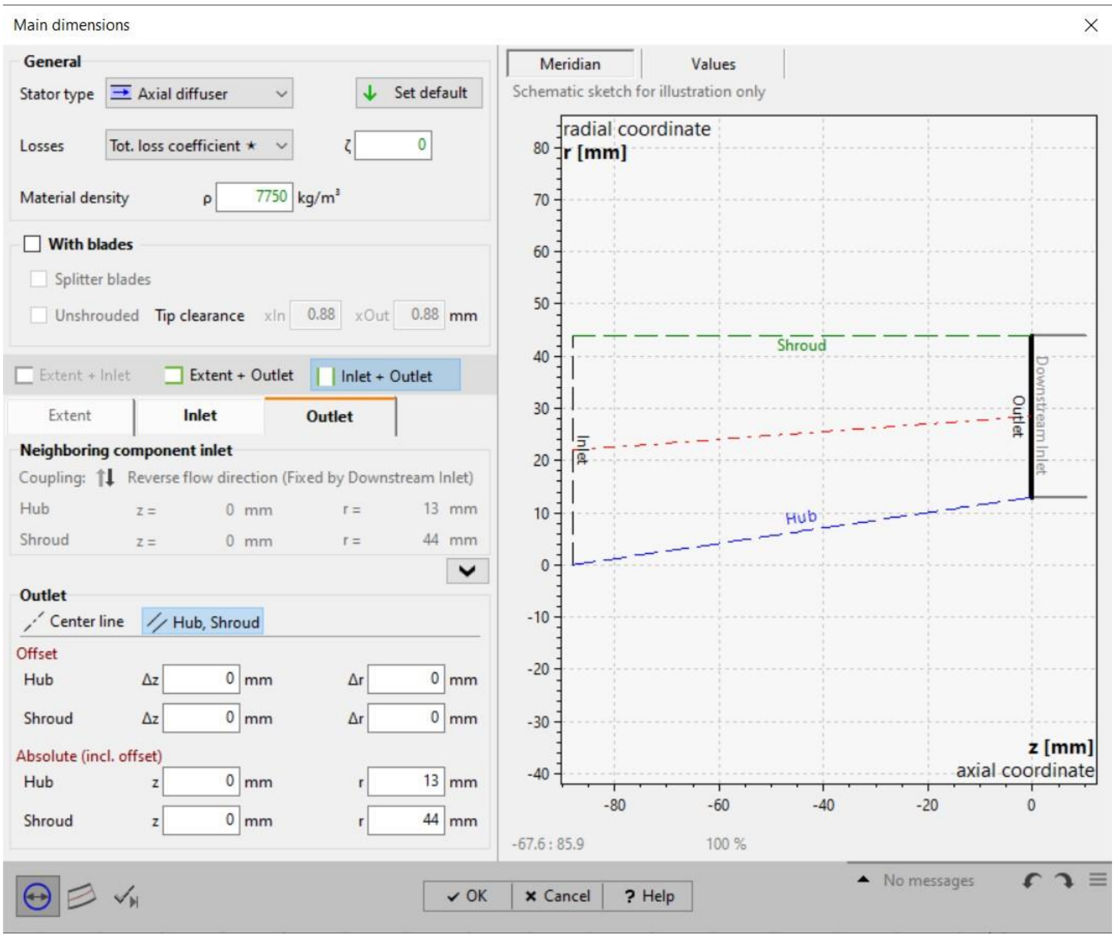

Picture217 Set up the input area of the inducer CFturbo program

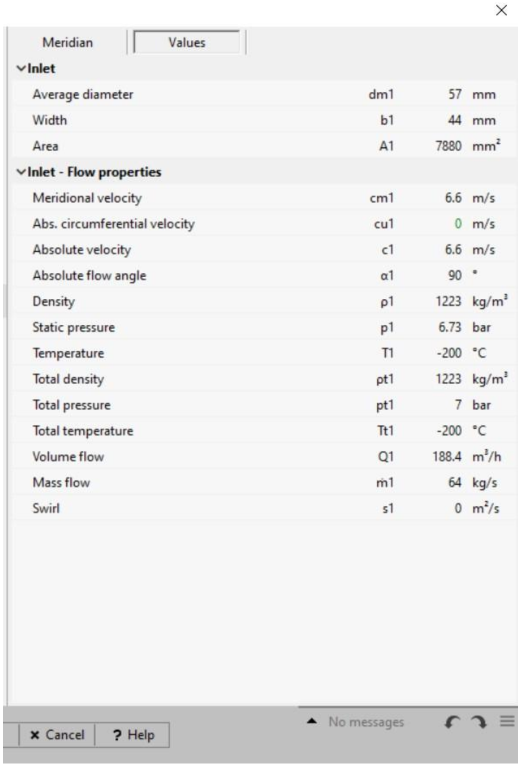

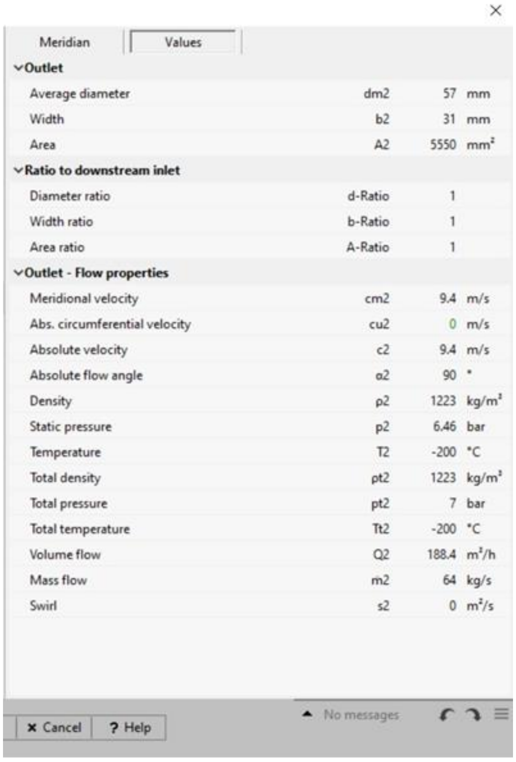

Picture218 The values of all velocities, pressures and flow angles at the inlet CFturbo program

Picture 219 The values of all velocities, pressures and flow angles at the end of the rotary nose CFturbo program

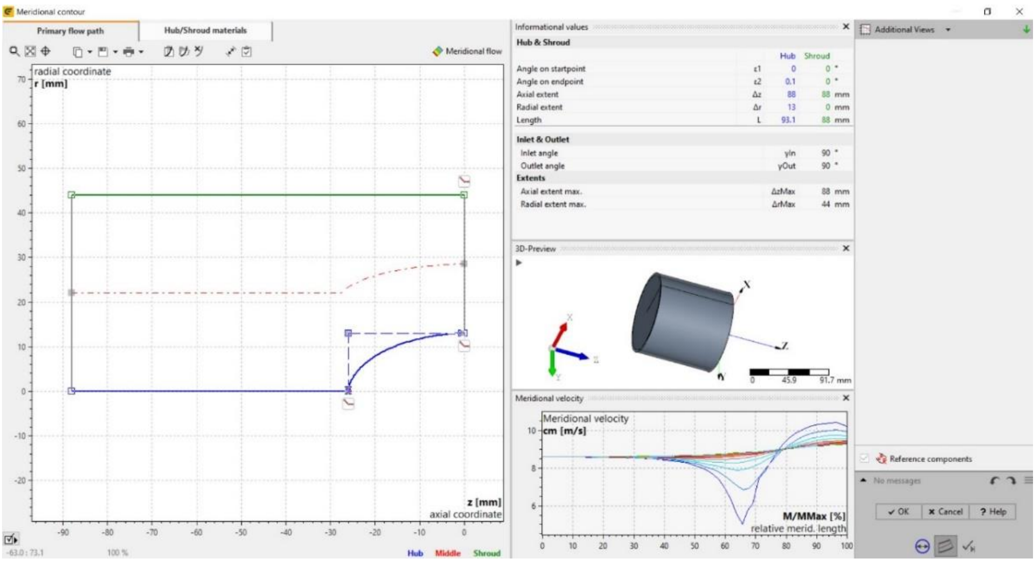

Picture 220 Meridian contour and B-spline configuration CFturbo program

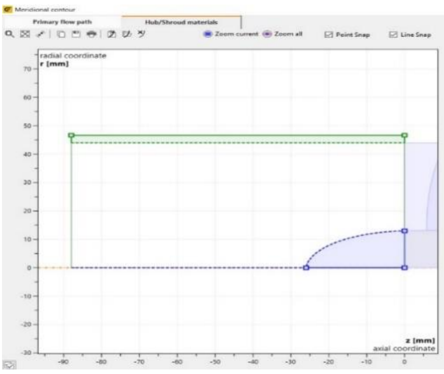

Picture 221 The material of the rotary nose CFturbo program

4.3 CFD analysis

Since the design has been completed, appropriate preparation was made for its export to the Simscale program. First, the housing where you find the impeller was deleted to simplify the CFD. Then, a 0.5mm fillet and a fillet in the impeller, equal to 1.5 times the thickness of the fin [36], were made in the inducer. Then, the flow extension of the diffuser was set 4 times the exit diameter. Finally, the flow volume was defined and with the grid extension of the Rotating Zone 0.5mm. The pictures below show the actions taken for the hydrogen pump. Exactly the same happened with the oxygen pump.

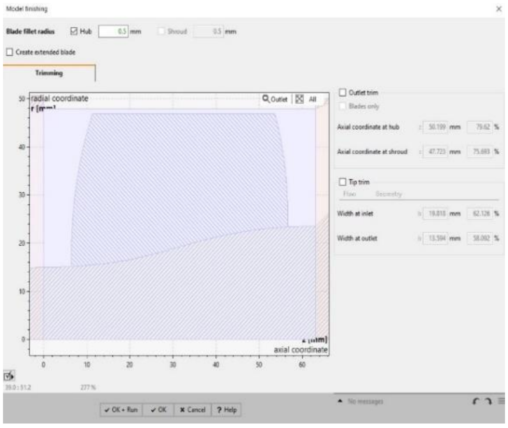

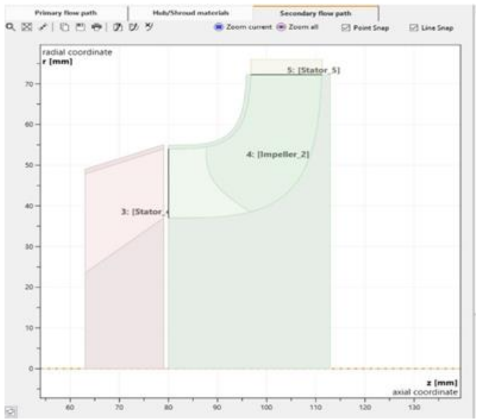

Picture 222 Fillet of inducer CFturbo program

Picture 223 Impeller without the curve CFturbo program

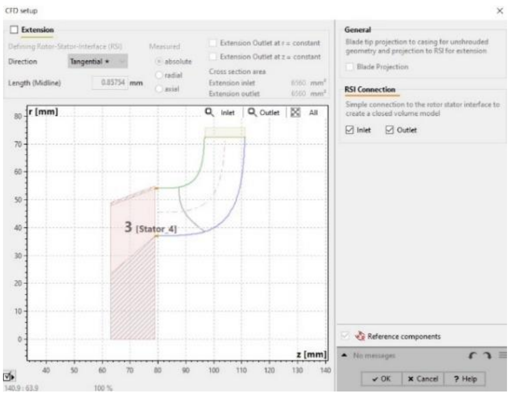

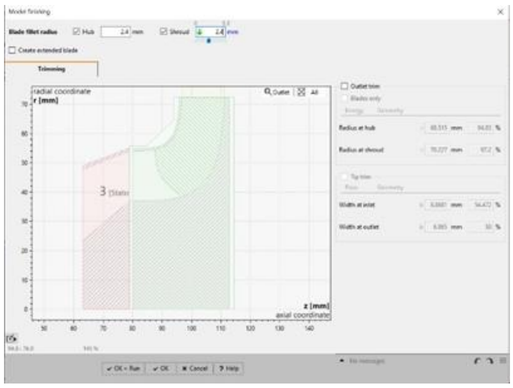

Picture 224 CFD impeller setup CFturbo program

Picture 225 Fillet of inducer CFturbo program

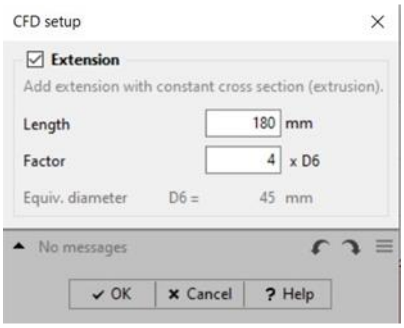

Picture 226 CFD extension to diffuser outlet CFturbo program

4.3.1 Simulation settings for CFD analysis

Initially, before exporting to Simscale ,the flow volume was set automatically by the CFturbo program and a 0.5 mm mesh extension was made in the rotating zones of the inductor and impeller. Then, using an API key from Simscale, the model was exported in STEP file format. Finally, the model was imported into the Simscale program.

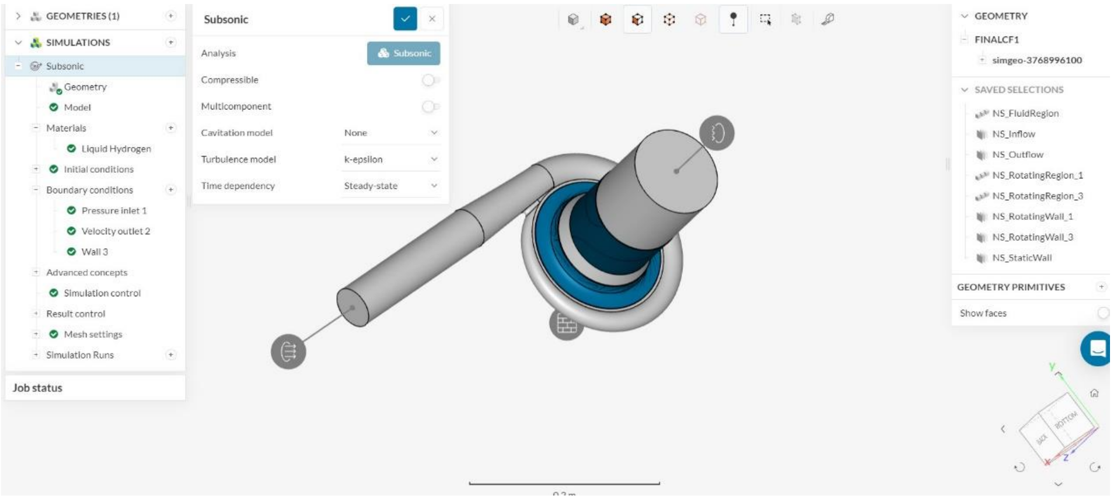

Picture 227 Simscale program environment Simscale program

In the next step, all the necessary settings for the simulation were made. The following images show all the necessary simulation settings. The material, the rotating walls, the rotating zone, the inlet pressure, the outlet flow, the simulation control, the output data measurements, total pressure difference, torque, force and the mesh. Exactly the same settings were made for the oxygen pump for an inlet pressure of 7 bar, outlet flow of 64 Kg/s and number of revolutions of 20000 rpm. The flow chosen is Subsonic because in this case the velocities are very high. Also, to simplify the analysis we assume that there is no heat flow from the walls and the flow is incompressible.

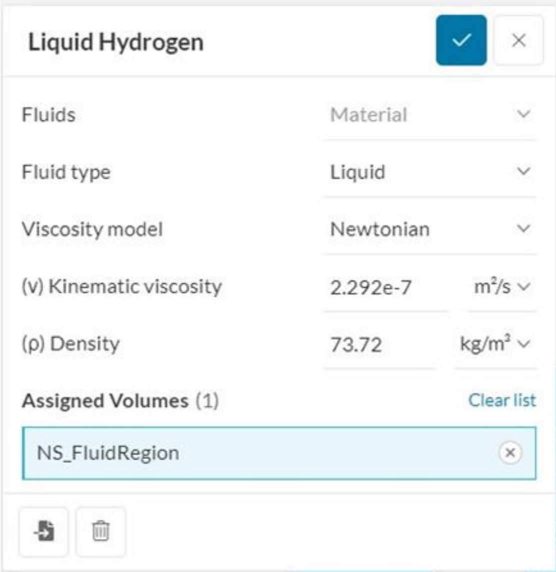

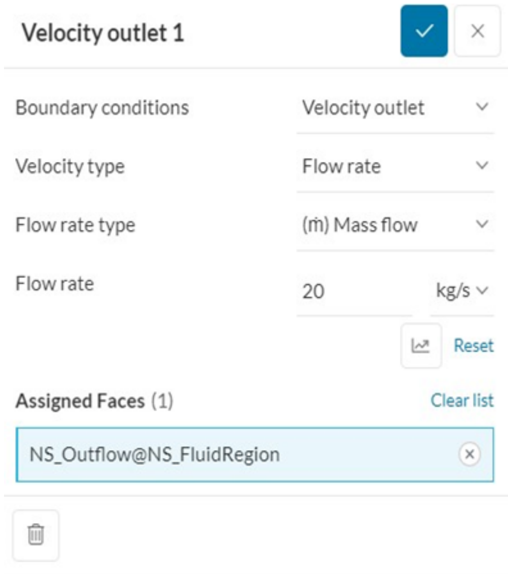

Picture 228 Properties of material Simscale program

Picture 229 Output mass flow Simscale program

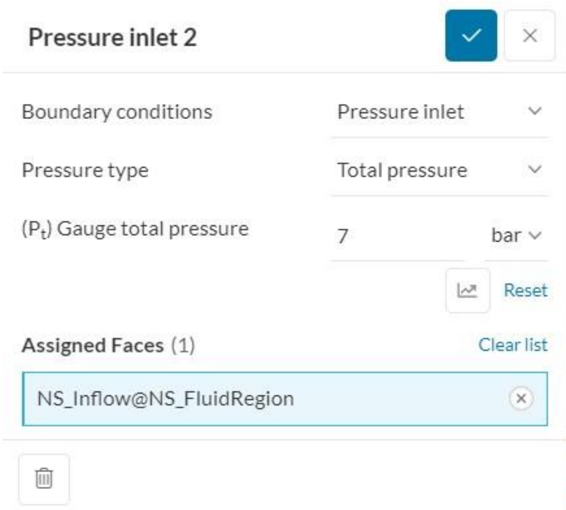

Picture 230 Total inlet pressure Simscale program

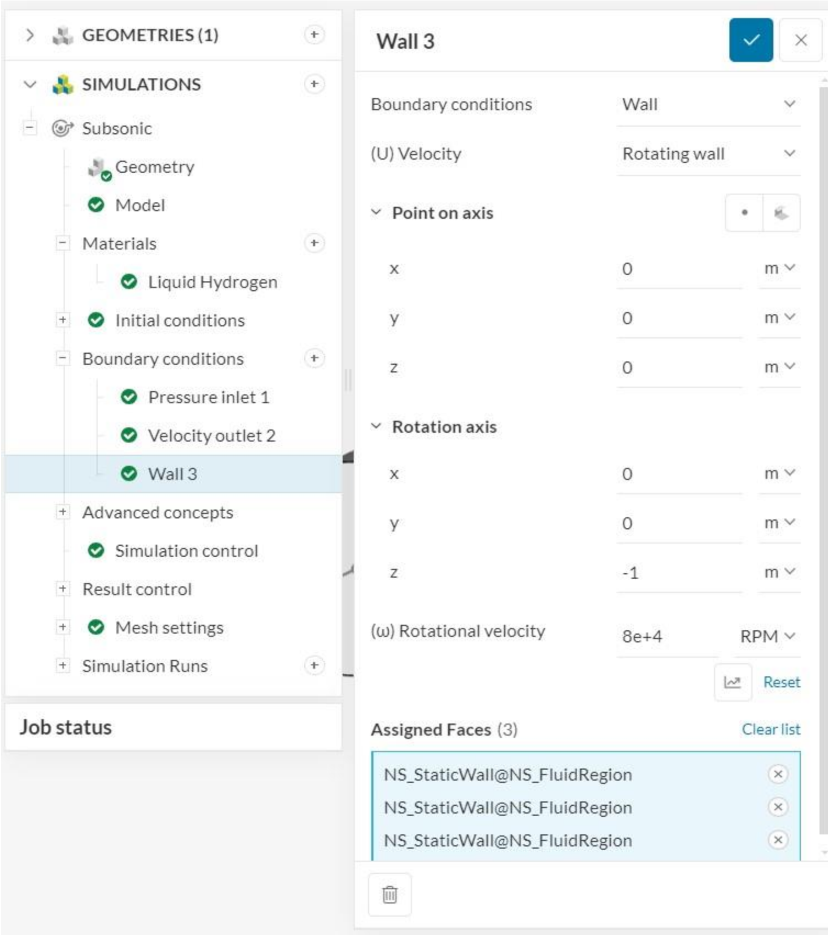

Picture 231 Setting up rotating walls Simscale program

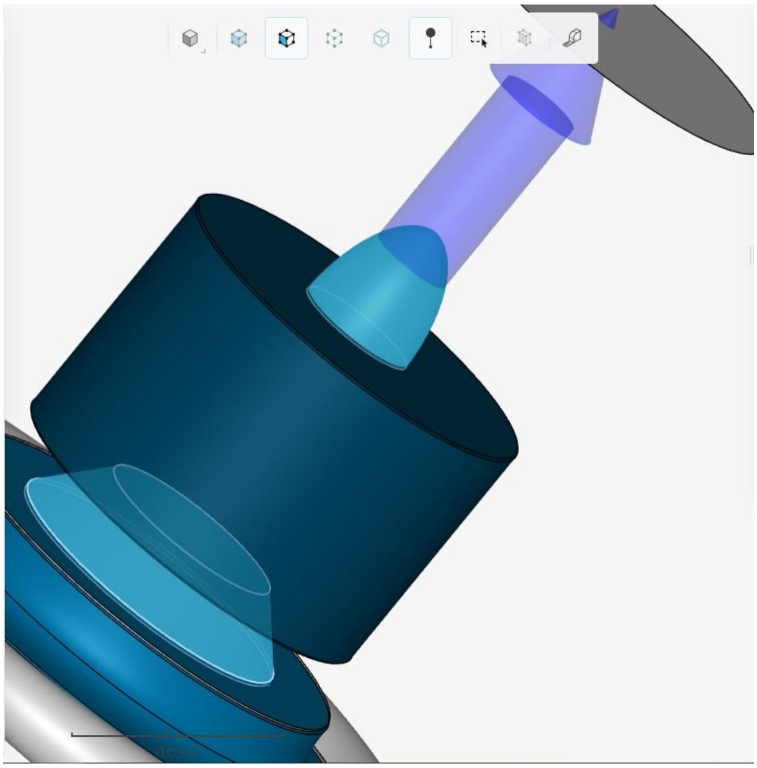

Picture 232 Rotating walls Simscale program

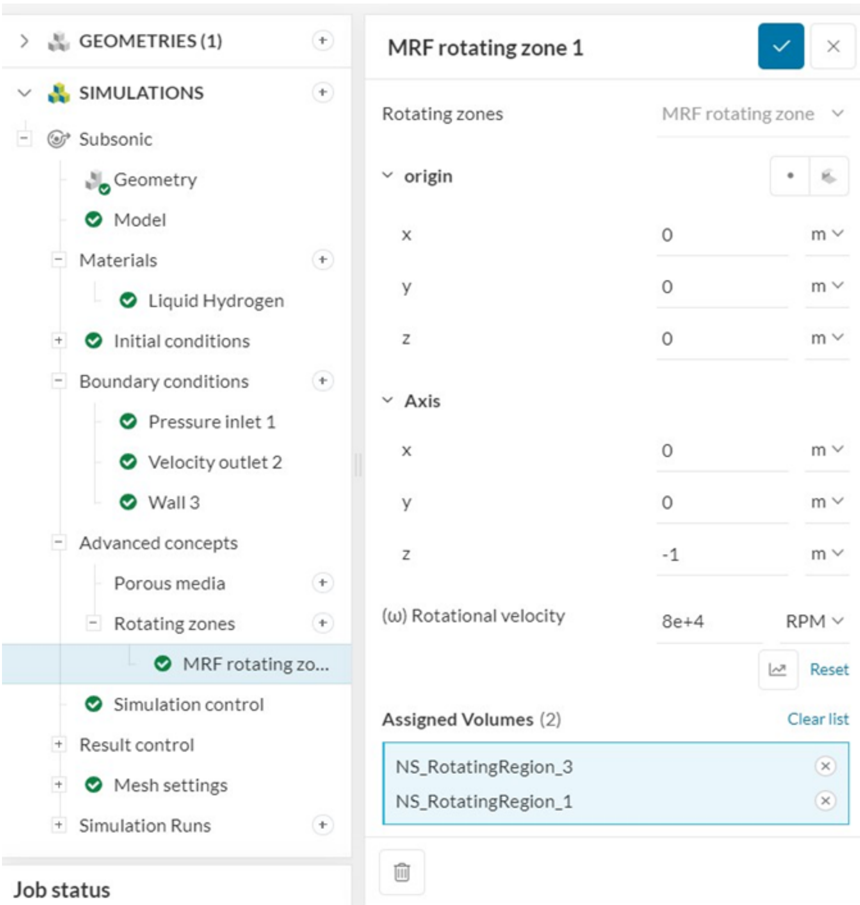

Picture 233 Setting up rotating zones Simscale program

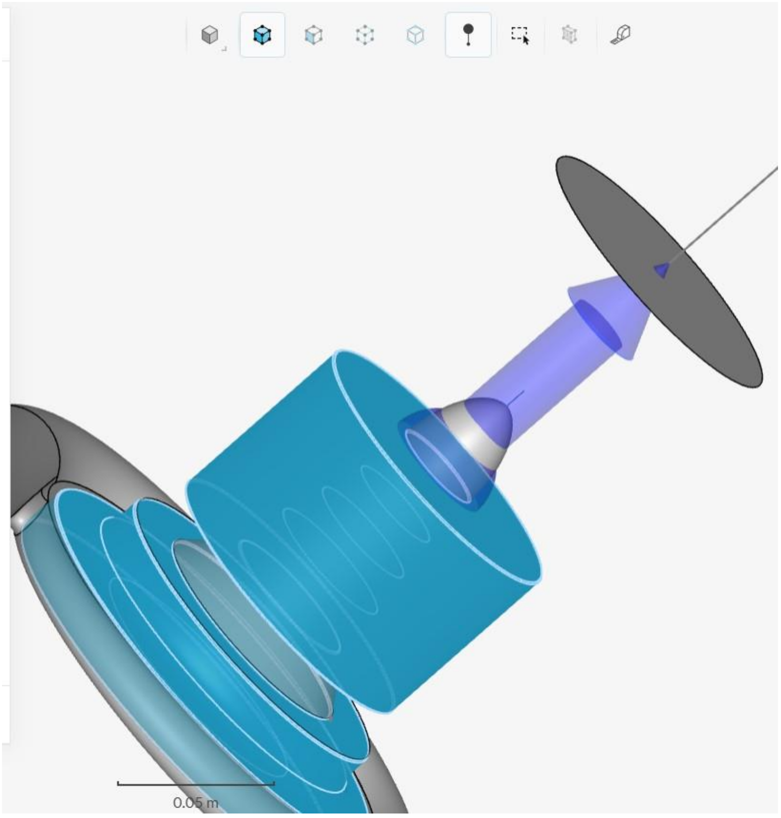

Picture 234 Rotating zones Simscale program

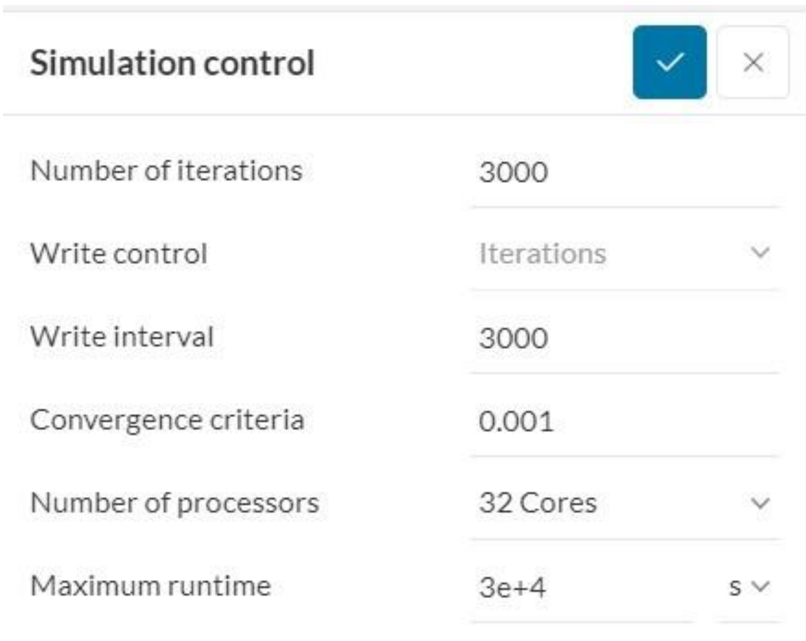

Picture 235 Simulation control setup Simscale program

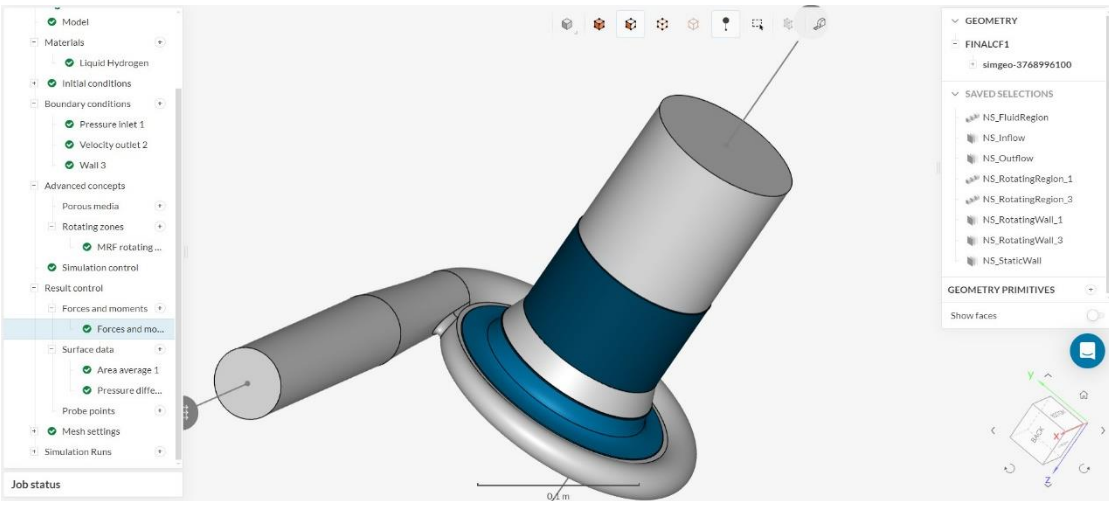

Picture 236 The model and enter result control settings Simscale program

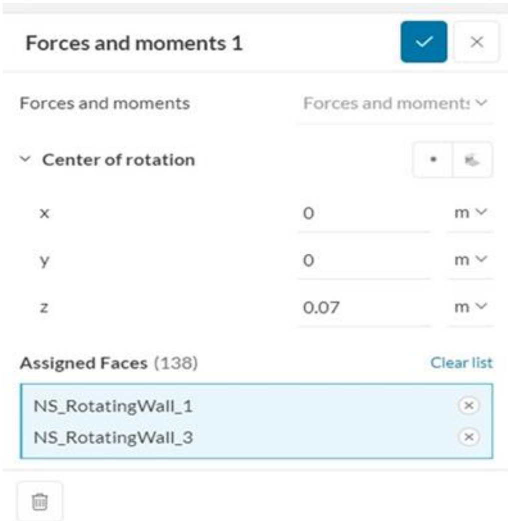

Picture 237 Force and torque measurement setup Simscale program

The center of mass was roughly defined. However, experimentally, it was found that it does not affect the results to a large extent.

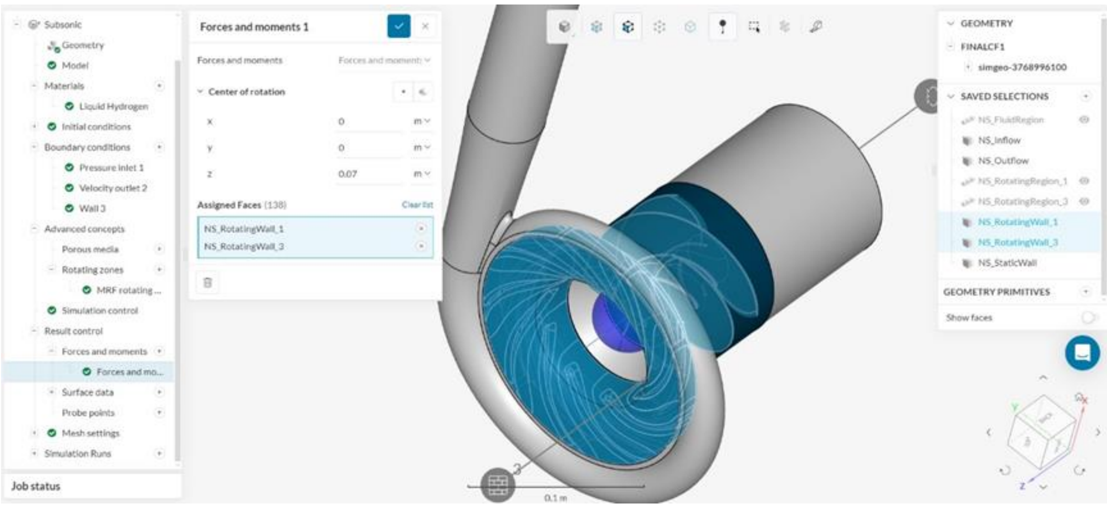

Picture 238 The center of mass of the model and the rotating walls from the rotation zones Simscale program

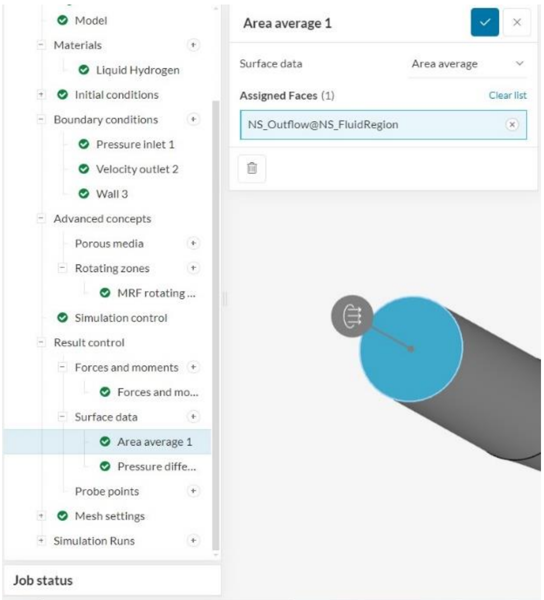

Picture 239 Setting average value measurements at the output Simscale program

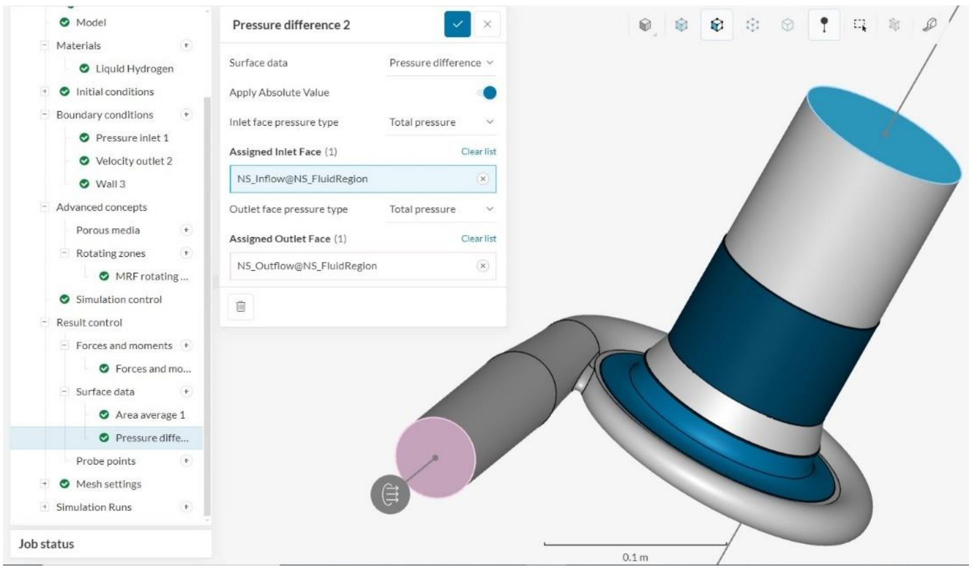

Picture 240 Setting up total pressure difference measurements Simscale program

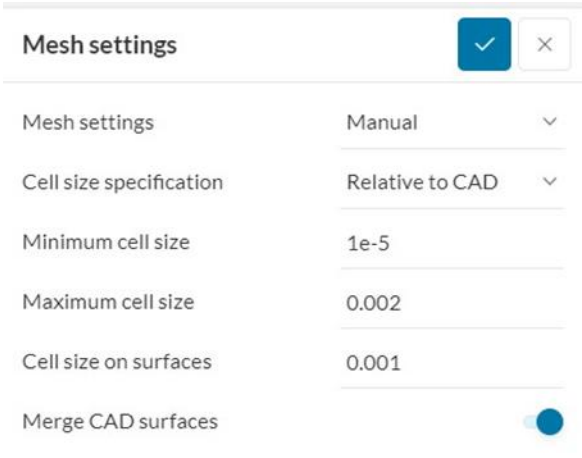

Picture 241 Manual setting of mesh Simscale program

4.3.2 Results of CFD analysis

The figures below show the effects of speed and total pressure on the impeller and commutator on the liquid hydrogen and liquid oxygen pumps.

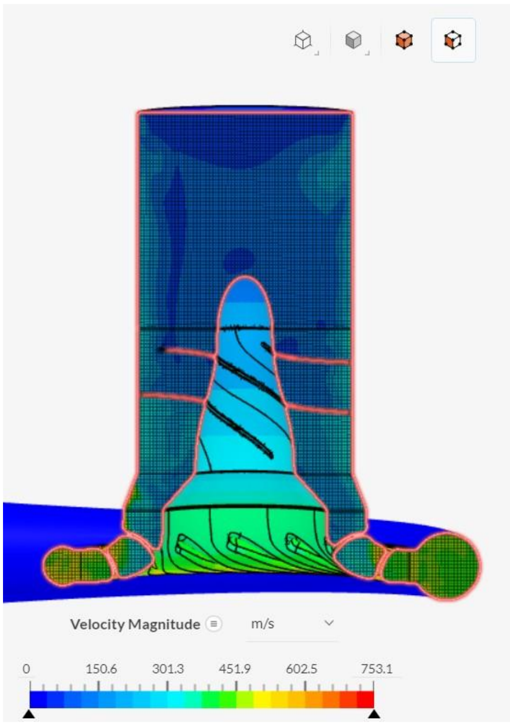

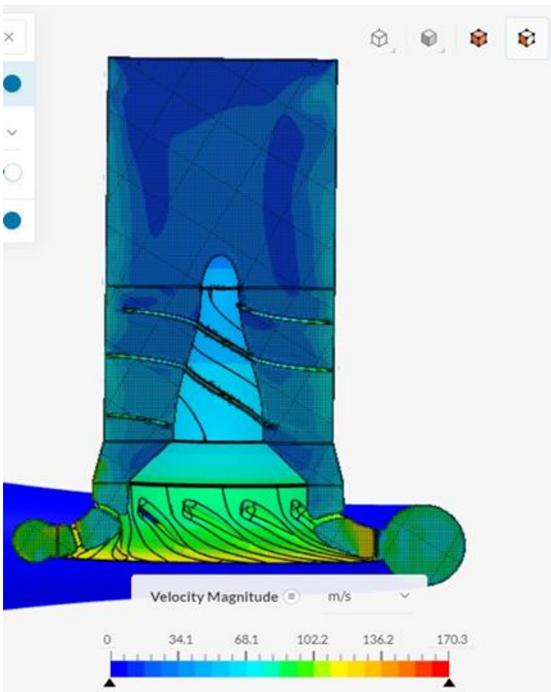

Picture 242 Velocity Magnitude on the XZ level of pump LH_2 Simscale program

Picture 243 Velocity Magnitude on the XZ level of pump LO_2 Simscale program

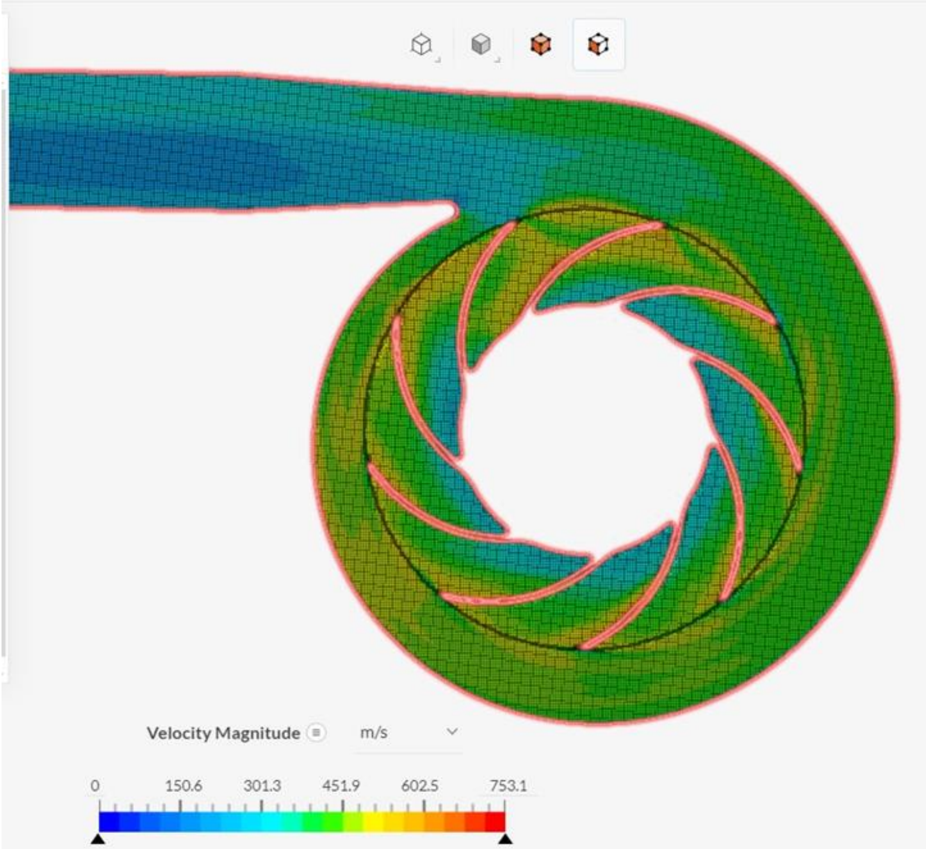

Picture244 Velocity Magnitude on the pump impeller LH_2 Simscale program

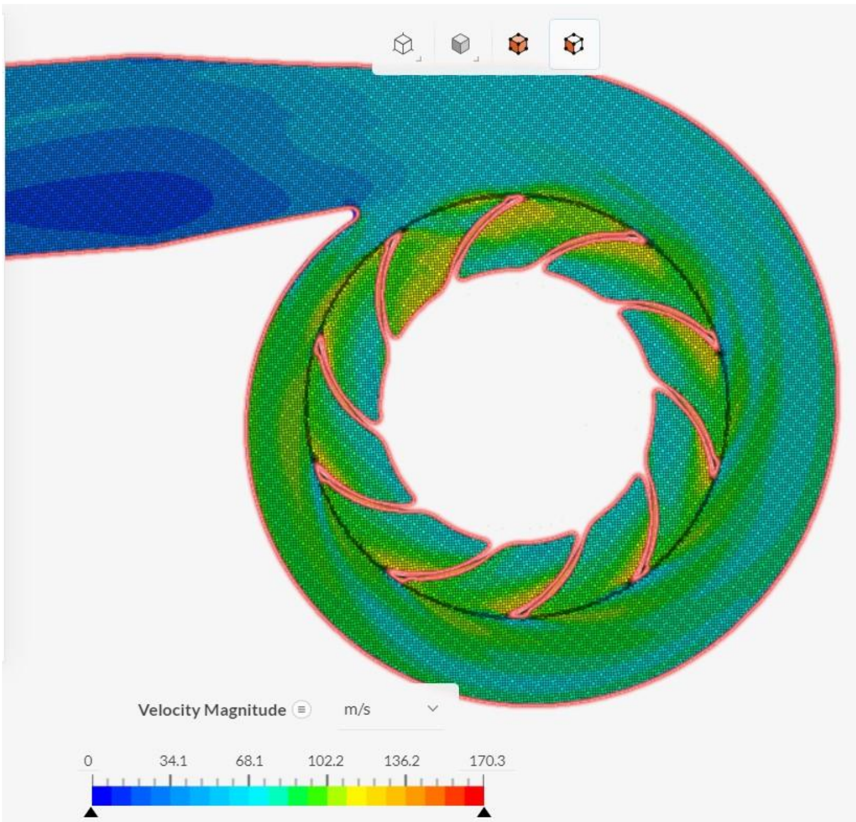

Picture 245 Velocity Magnitude on the pump impeller LO_2 Simscale program

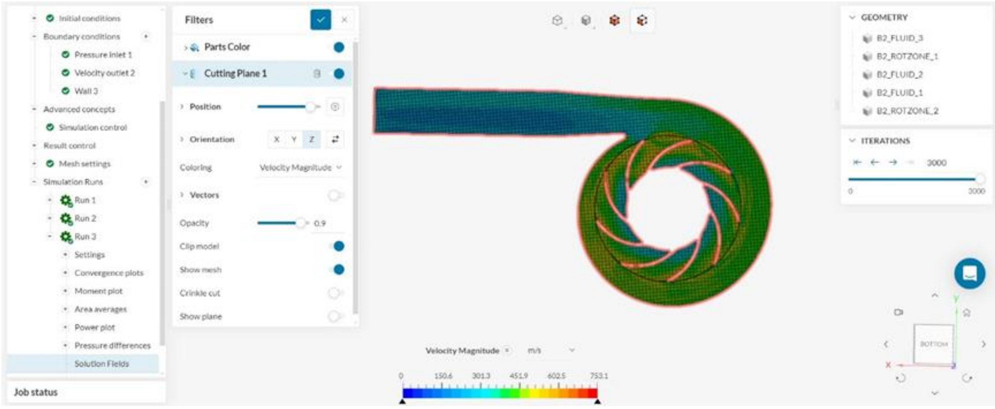

Picture 246 Velocity Magnitude on the pump impeller LH_2 (the whole picture) Simscale program

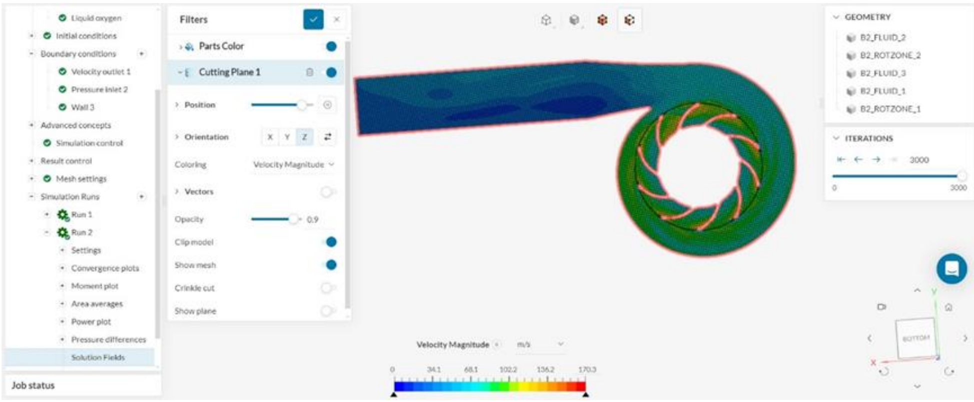

Picture 247 Velocity Magnitude on the pump impeller LO_2 (the whole picture) Simscale program

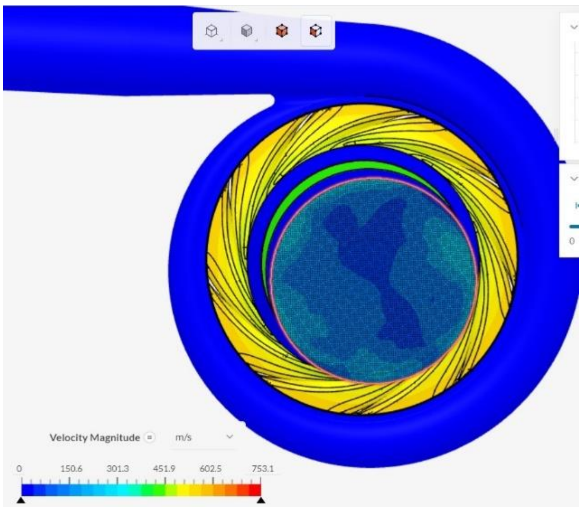

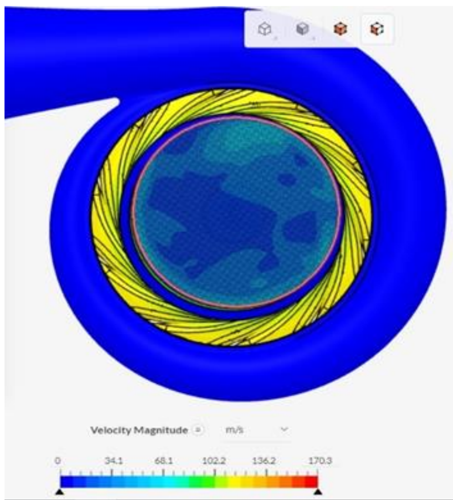

Picture 248 Velocity Magnitude on the pump LH_2 at the input Simscale program

Picture 249 Velocity Magnitude on the pump LO_2 at the input Simscale program

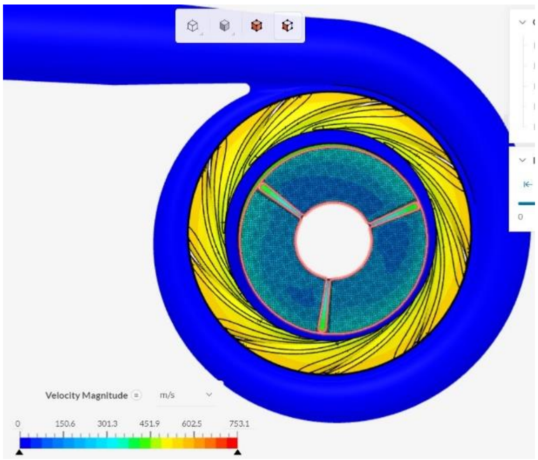

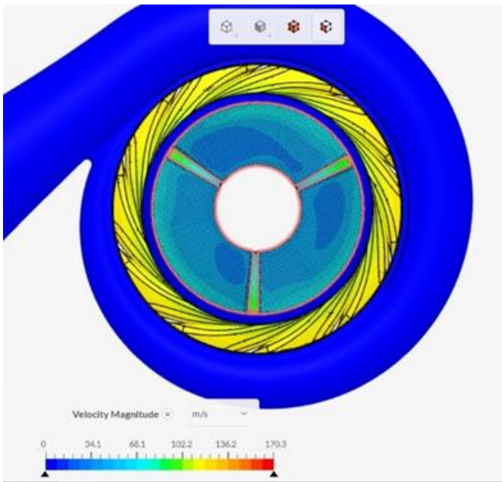

Picture 250 Velocity Magnitude on the pump inducer LH_2 Simscale program

Picture 251 Velocity Magnitude on the pump inducer LO_2 Simscale program

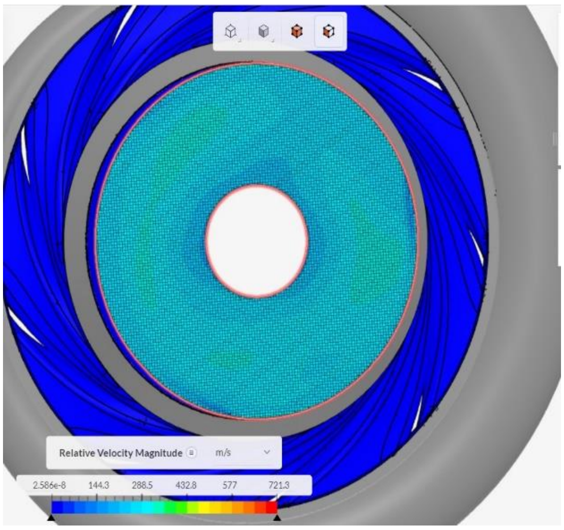

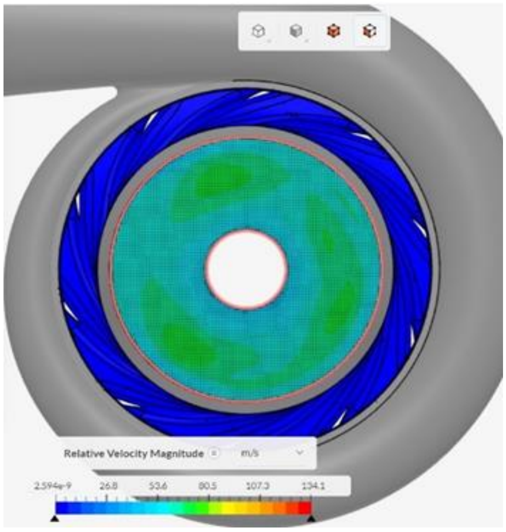

Picture 2523 Relative Velocity Magnitude at the inducer input LH_2 Simscale program

Picture 253 Relative Velocity Magnitude at the inducer input LO_2 Simscale program

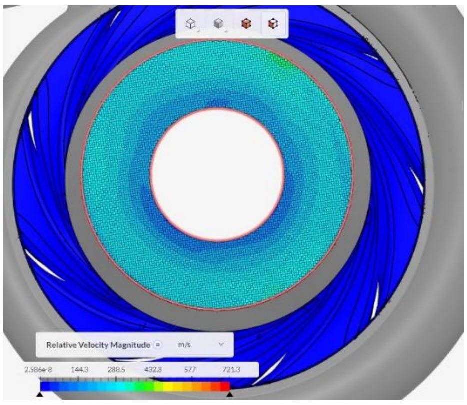

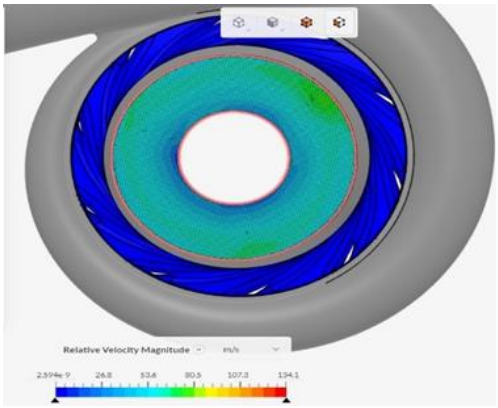

Picture 254 Relative Velocity Magnitude at the inducer output LH_2 Simscale program

Picture 255 Relative Velocity Magnitude at the inducer output LO_2 Simscale program

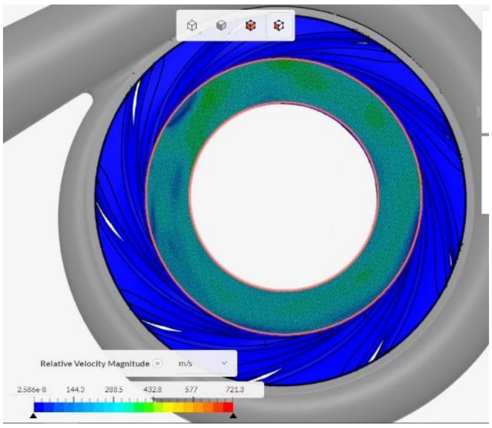

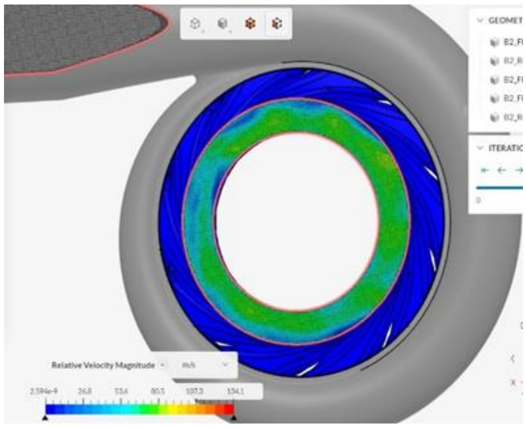

Picture 256 Relative Velocity Magnitude at the impeller input LH_2 Simscale program

Picture 257 Relative Velocity Magnitude at the impeller input LO_2 Simscale program

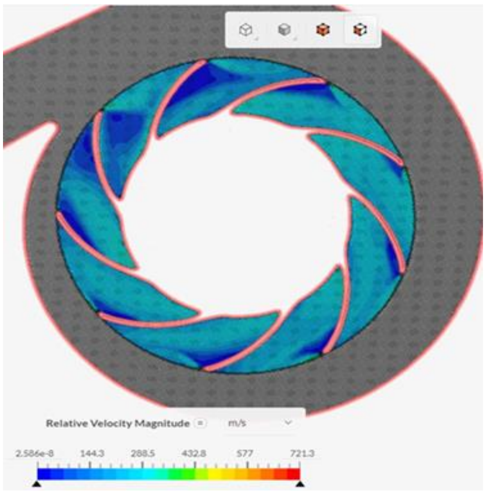

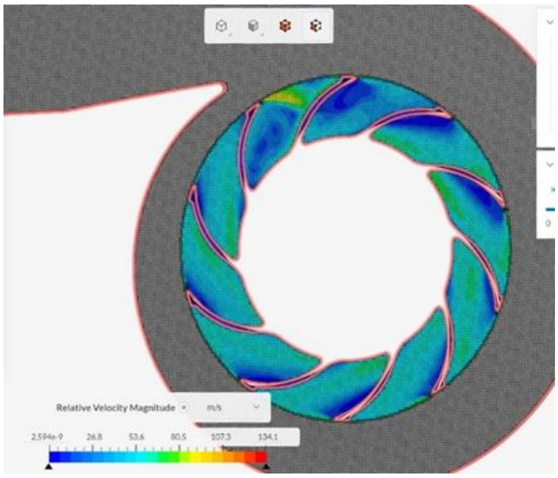

Picture 258Relative Velocity Magnitude at the impeller LH_2 Simscale program

Picture 259 Relative Velocity Magnitude at the impeller LO_2 Simscale program

From the above photos of the velocities, strong eddies and flow reversals are observed at the inlet. The speed increase in the inducer and impeller is also observed. This is followed by normalization and velocity reduction in the diffuser. Finally, there are the relative speed decelerations that occur in the inductor and the impeller. Below are the pressures.

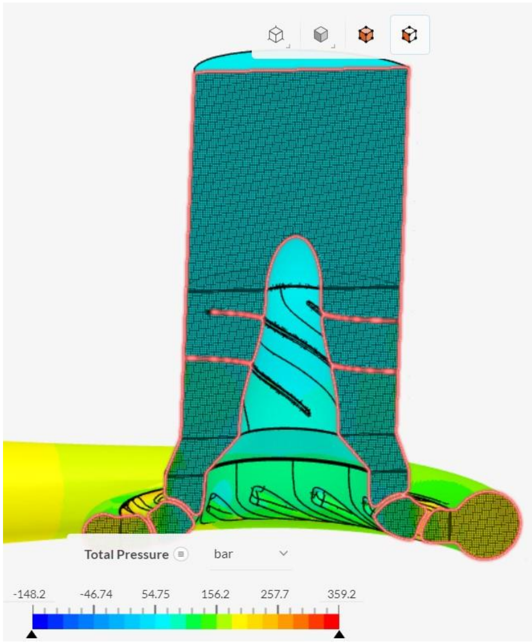

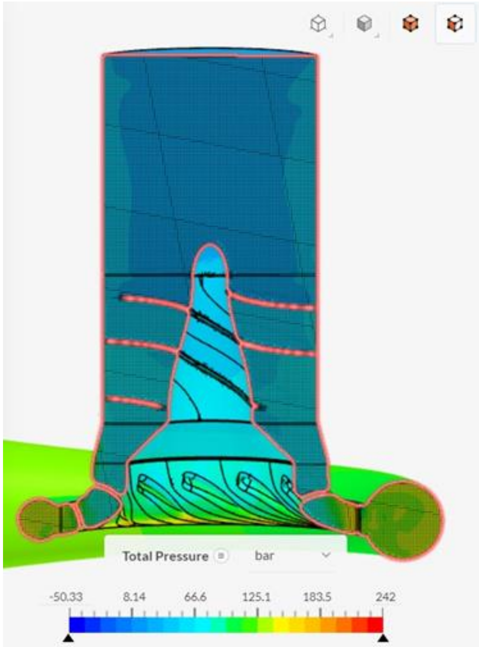

Picture 260 Total Pressure on the XZ level of pump LH_2 Simscale program

Picture 261 Total Pressure on the XZ level of pump LO_2 Simscale program

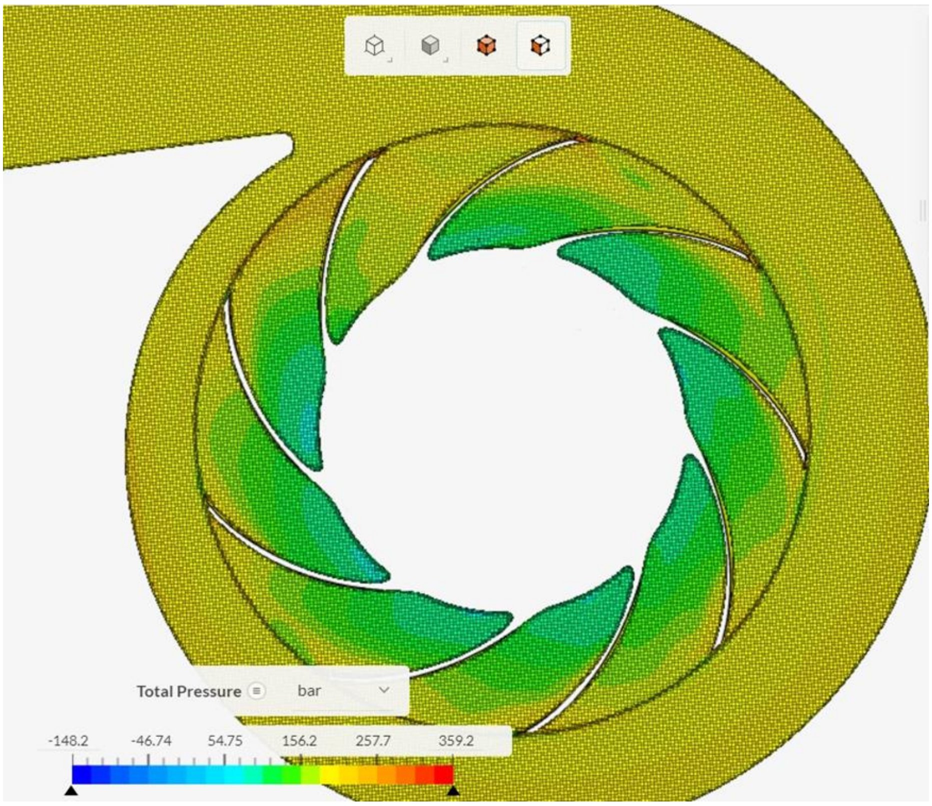

Picture 262 Total Pressure on the pump impeller LH_2 Simscale program

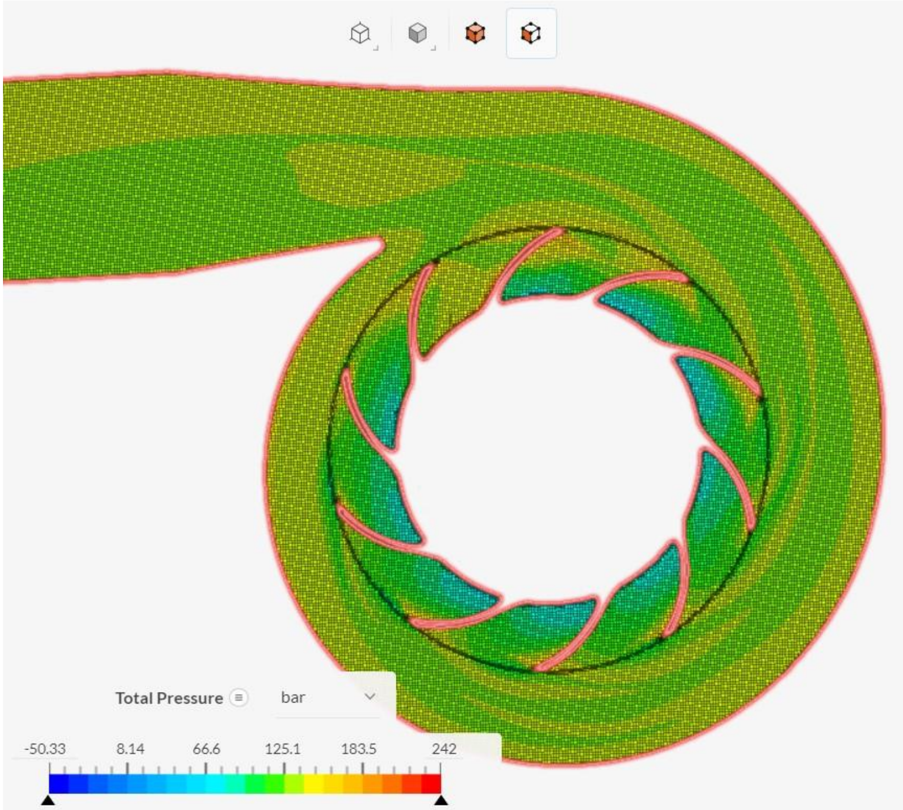

Picture 263 Total Pressure on the pump impeller LO_2 Simscale program

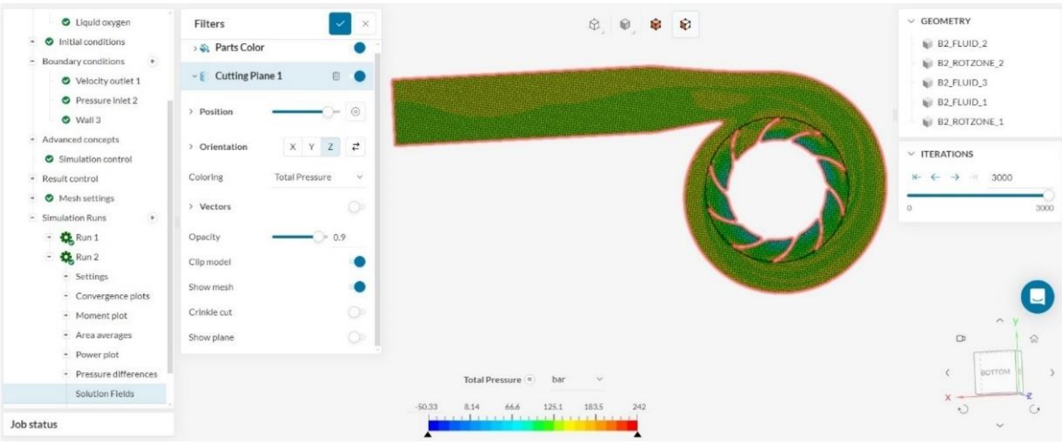

Picture 264 Total Pressure on the pump impeller LH_2 (the whole picture) Simscale program

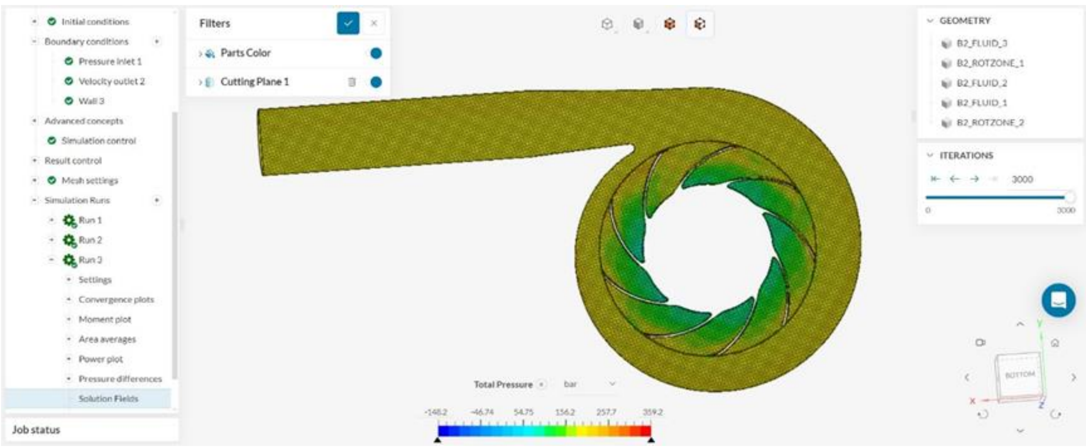

Picture 265 Total Pressure on the pump impeller LO_2 (the whole picture) Simscale program

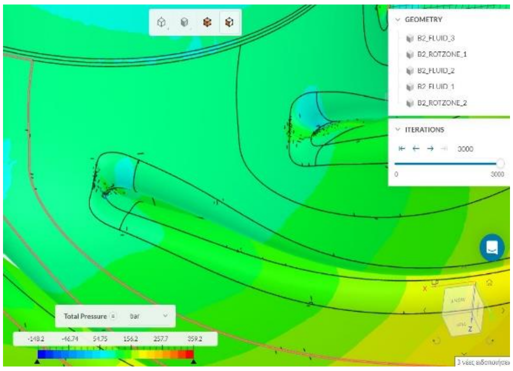

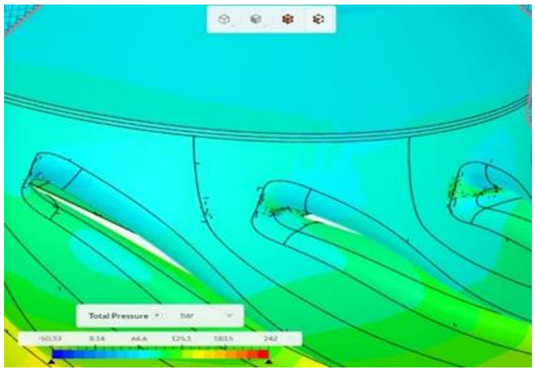

Picture 266 Development of small cavitation at the hub of the wings (pump LH_2) Simscale program

Picture 267 Development of small cavitation at the hub of the wings (pump LO_2) Simscale program

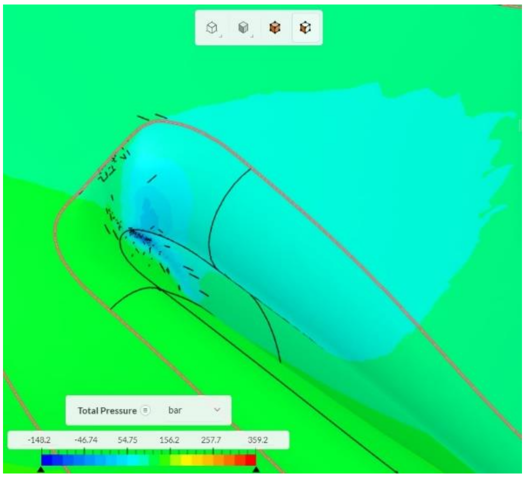

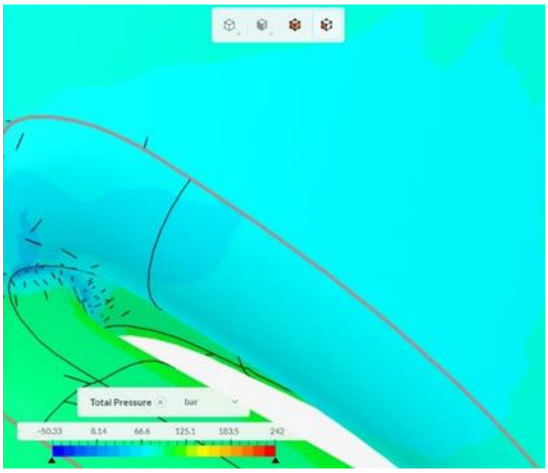

Picture 268 The blade in which intense cavitation develops (pump LH_2) Simscale program

Picture 269 The blade in which intense cavitation develops (pump LO_2) Simscale program

From the results, it can be seen that the cavitation is developing locally. However, intense cavitation was detected only on one wing locally on the leading edge. In addition, the cavitation is more pronounced in the hydrogen pump. Here a small development of cavitation at the base of the wing is observed. This may be due to hydraulic pressure losses between the rotating conical shaft and the walls. It can also be caused by the excessive inlet speed of the impeller. Excessive cavitation development is observed locally on the front side of the inducer blade. This is shown in the results below where the images are 3D.

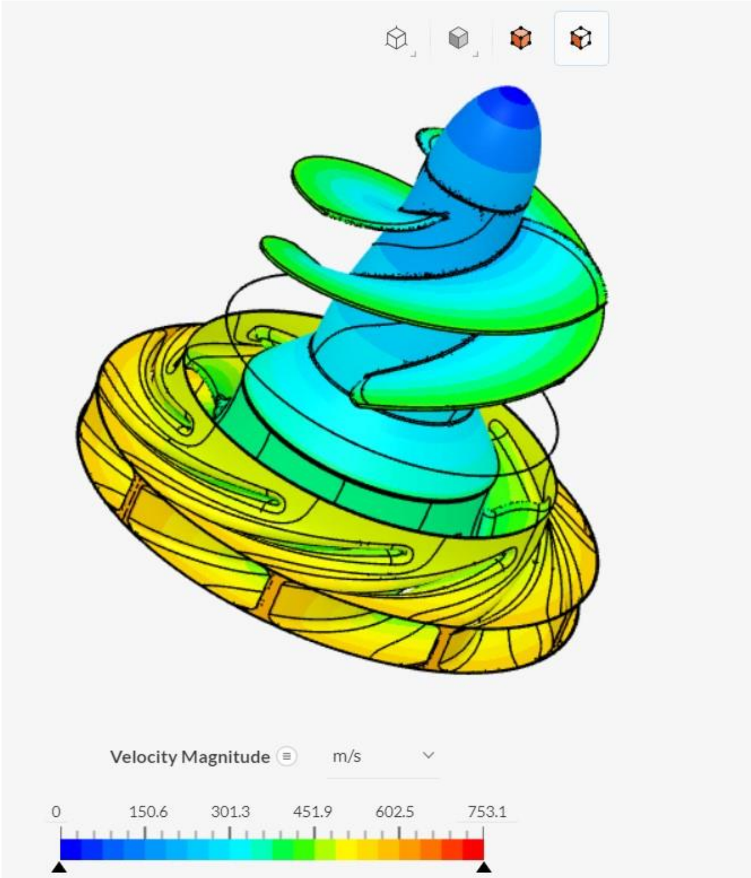

Picture 270 Velocity Magnitude 3D on the inducer and impeller of pump LH_2 Simscale program

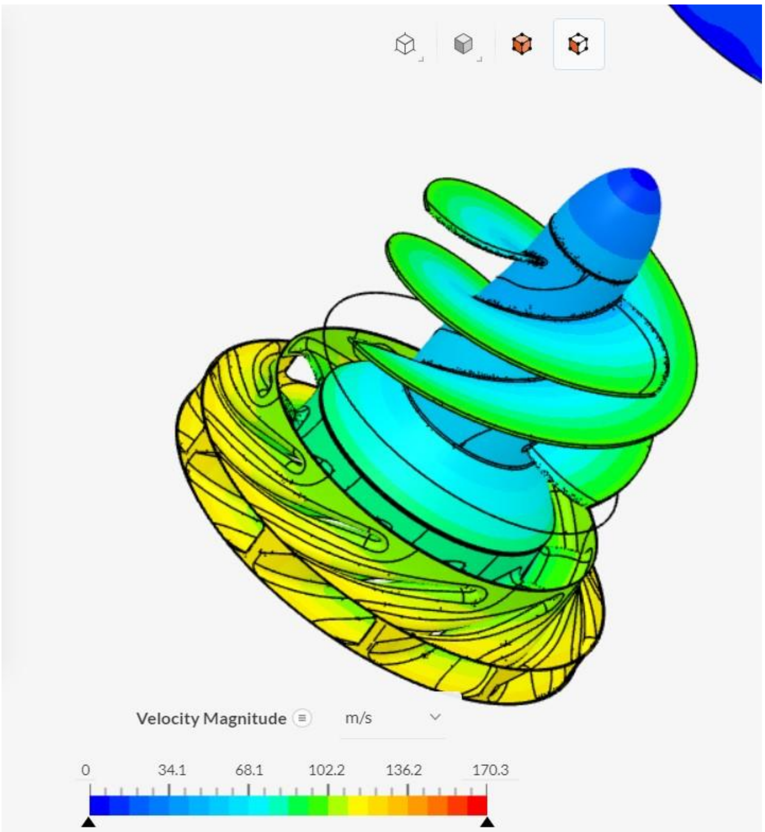

Picture 271 Velocity Magnitude 3D on the inducer and impeller of pump LO_2 Simscale program

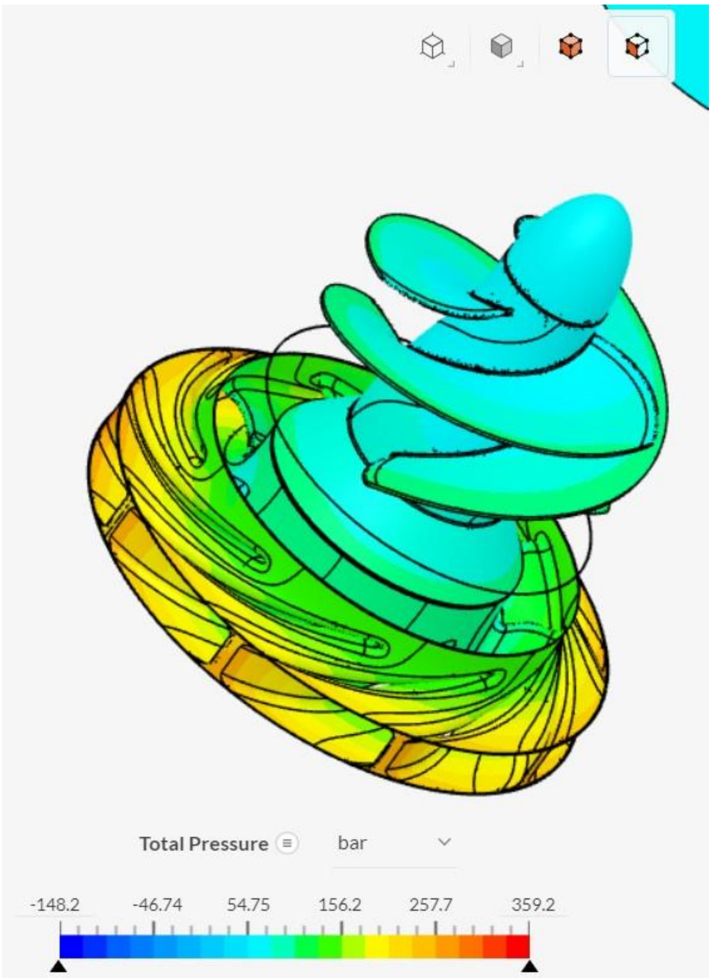

Picture 272 Total pressure 3D on the inducer and impeller of pump LH_2 Simscale program

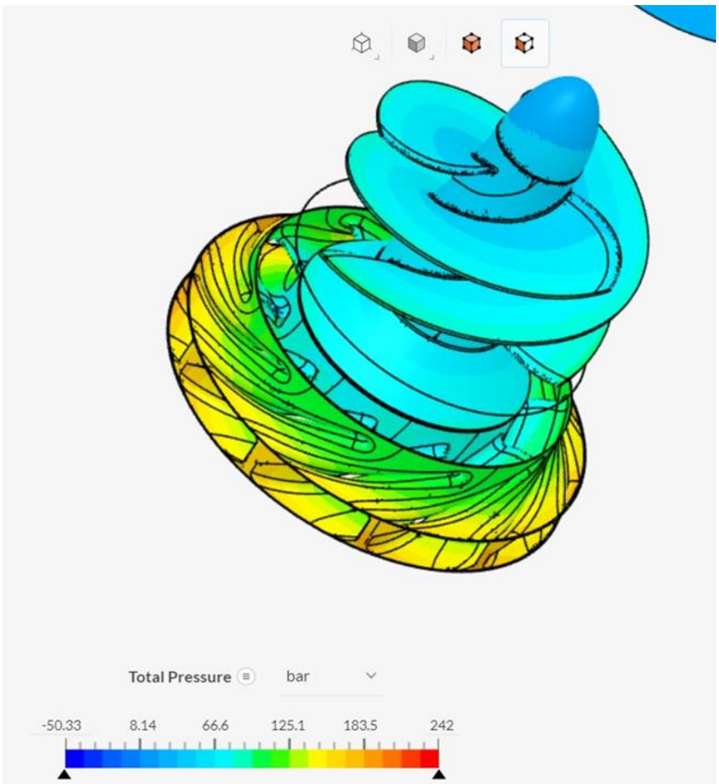

Picture 273 Total pressure 3D on the inducer and impeller of pump LO_2 Simscale program

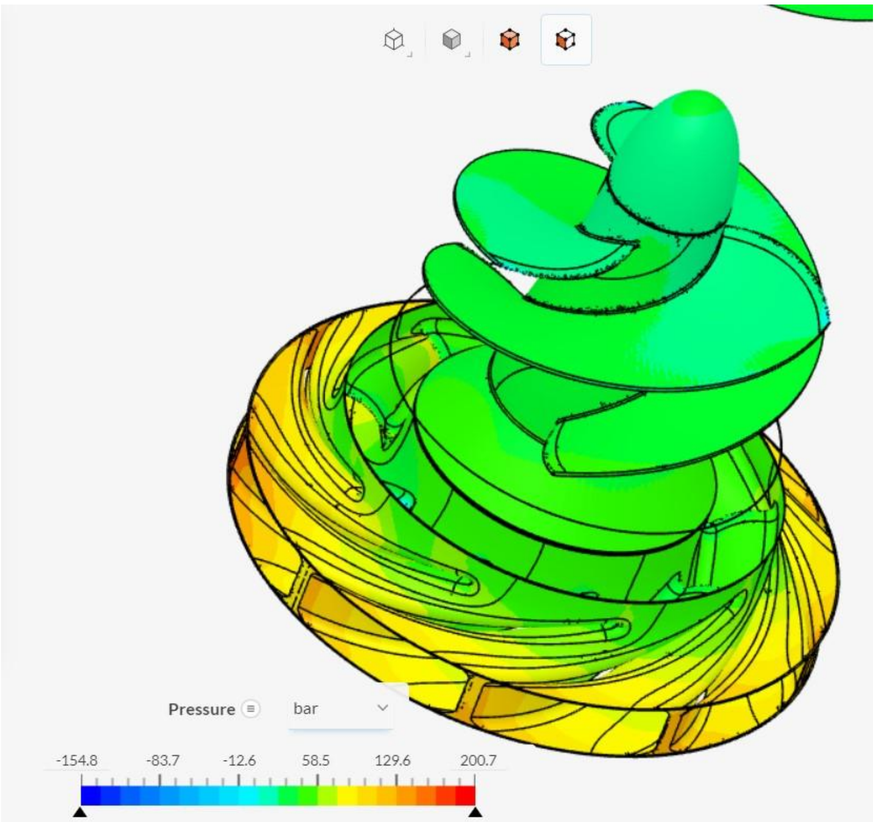

Picture 274 Static pressure 3D on the inducer and impeller of pump LH_2 Simscale program

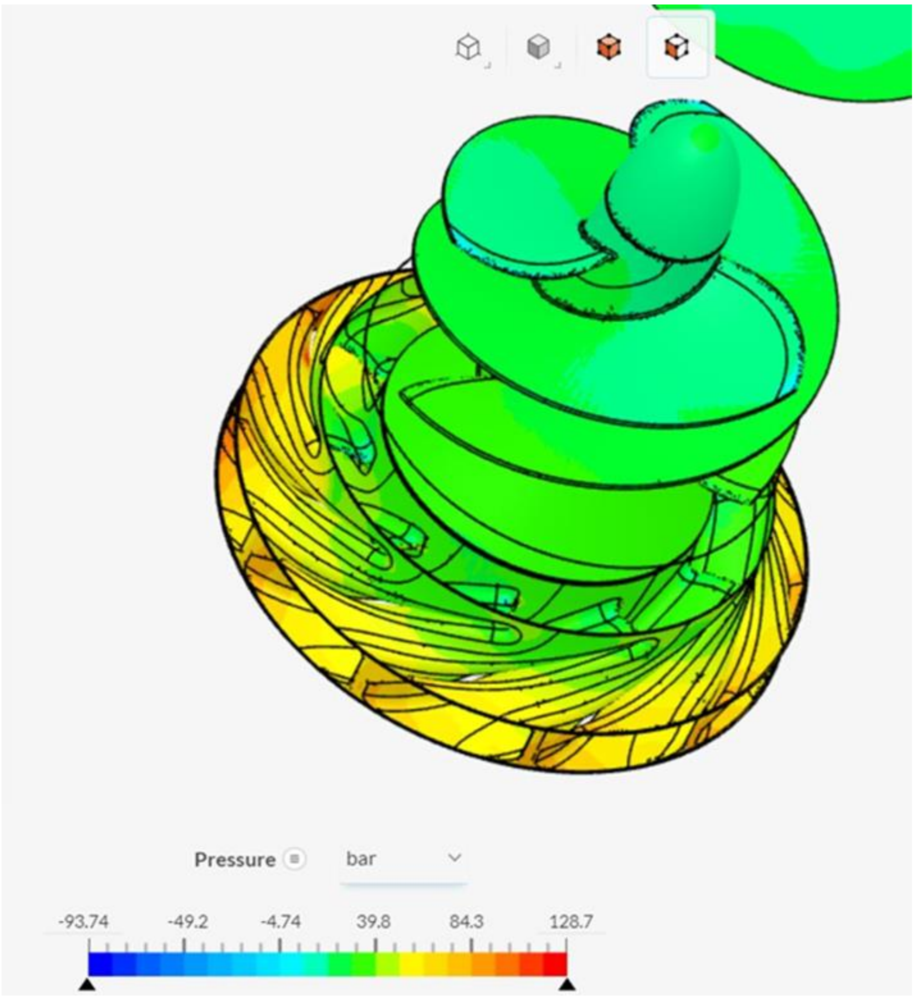

Picture 275 Static pressure 3D on the inducer and impeller of pump LO_2 Simscale program

Below are the results of the output values of the two pumps, the mesh characteristics, the efficiency and the power of the pumps.

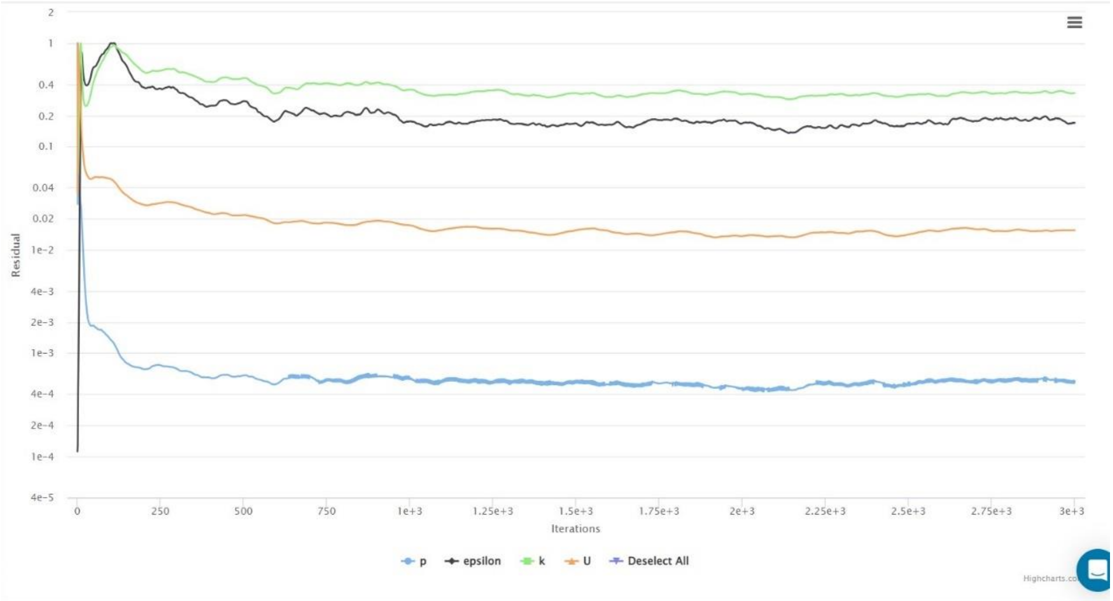

Picture 276 The turbulence model coefficients (pump LH_2) Simscale program

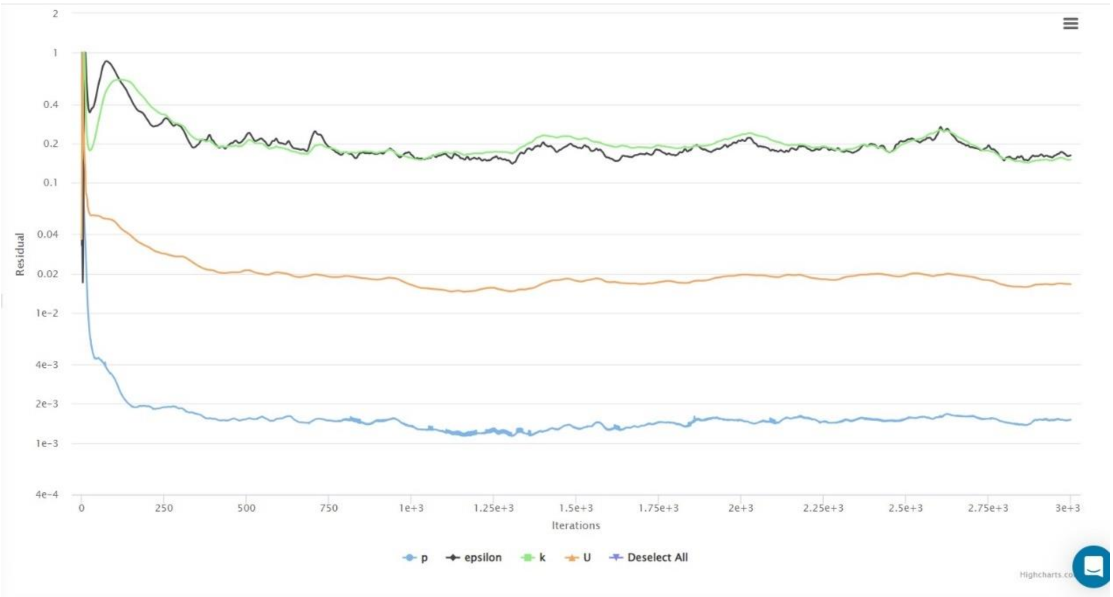

Picture 277 The turbulence model coefficients (pump LO_2) Simscale program

Here we notice that the coefficients of the K-e turbulent model are balanced.

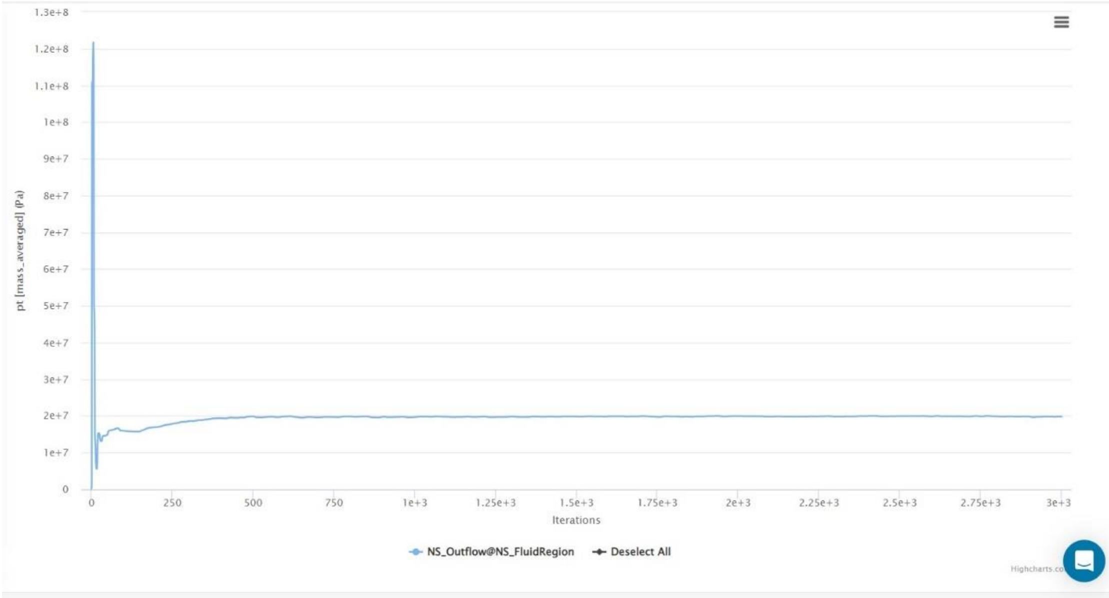

Picture 278 Average outlet pressure of pump LH_2 Simscale program

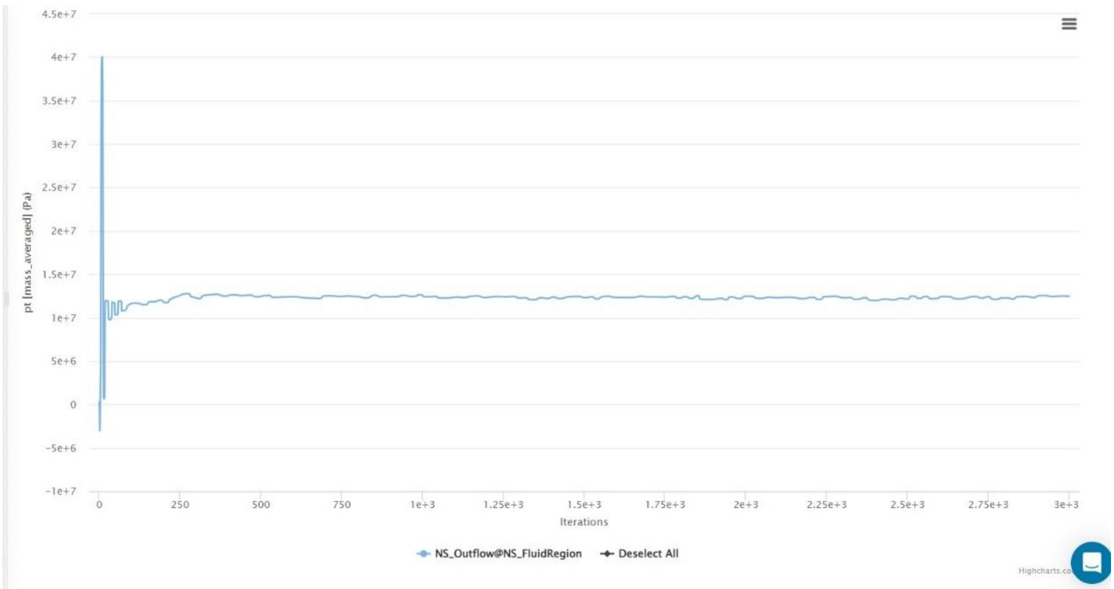

Picture 279 Average outlet pressure of pump LO_2 Simscale program

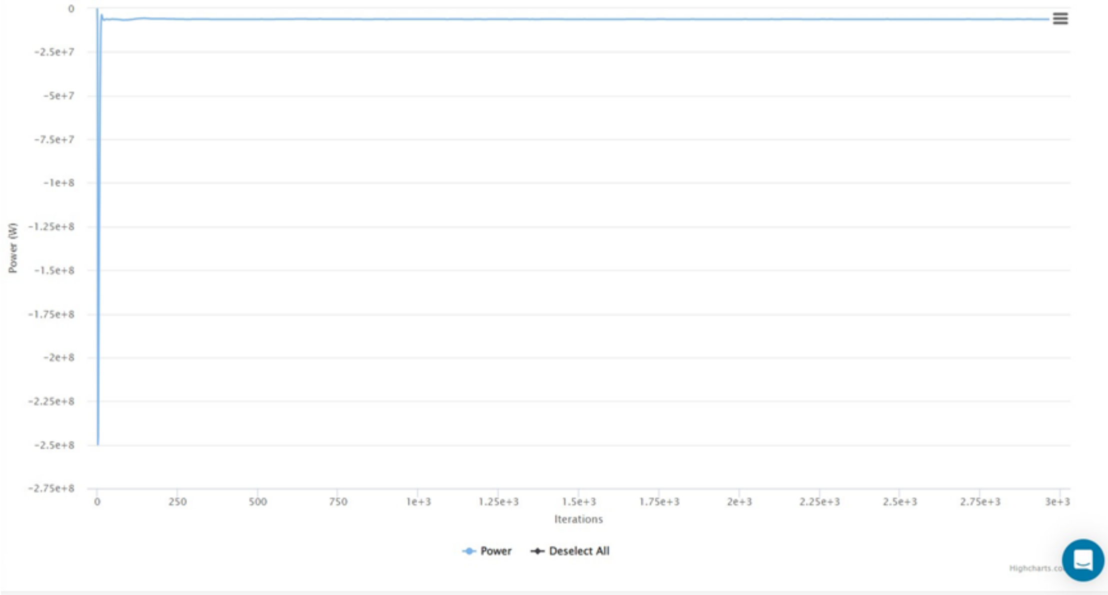

Picture280 Input power of pump LH_2 Simscale program

Picture 281 Input power of pump LO_2 Simscale program

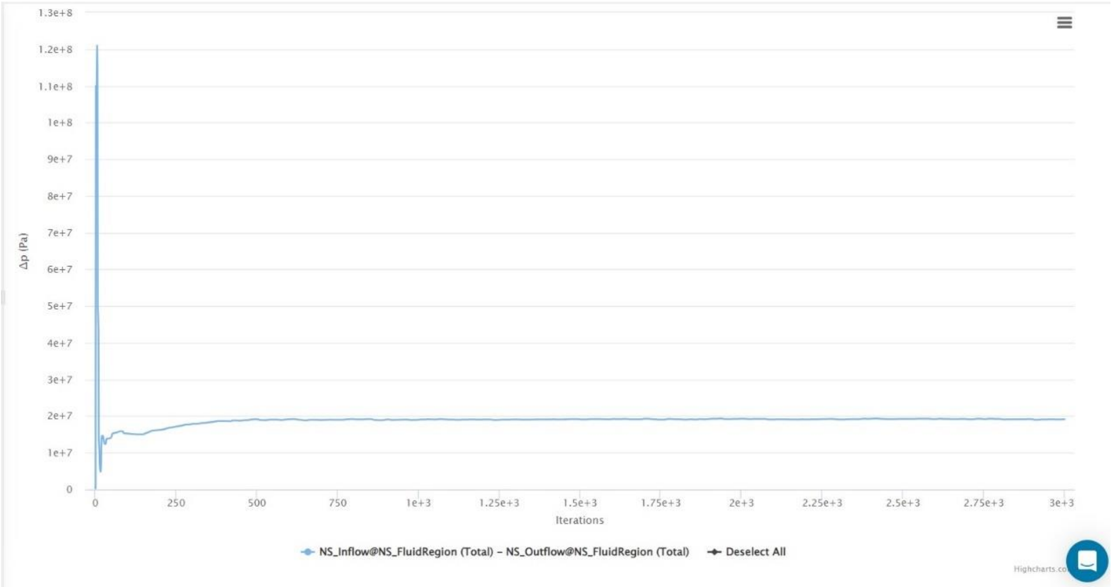

Picture 282 Total pressure difference of pump LH_2 Simscale program

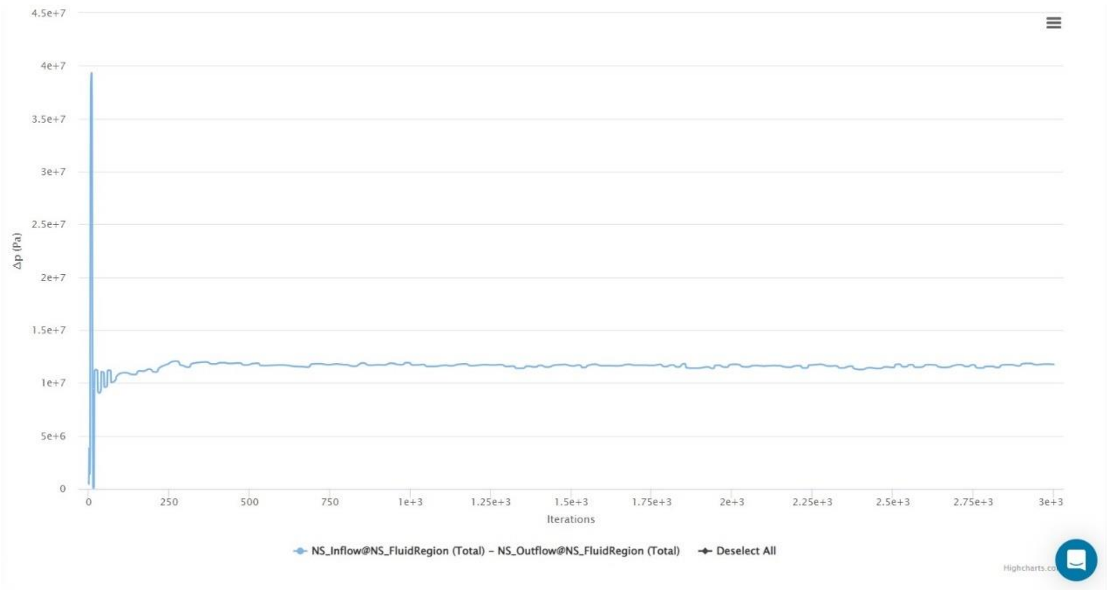

Picture 283 Total pressure difference of pump LO_2 Simscale program

Picture 284 Torque of pump LH_2 Simscale program

Picture 285 Torque of pump LO_2 Simscale program

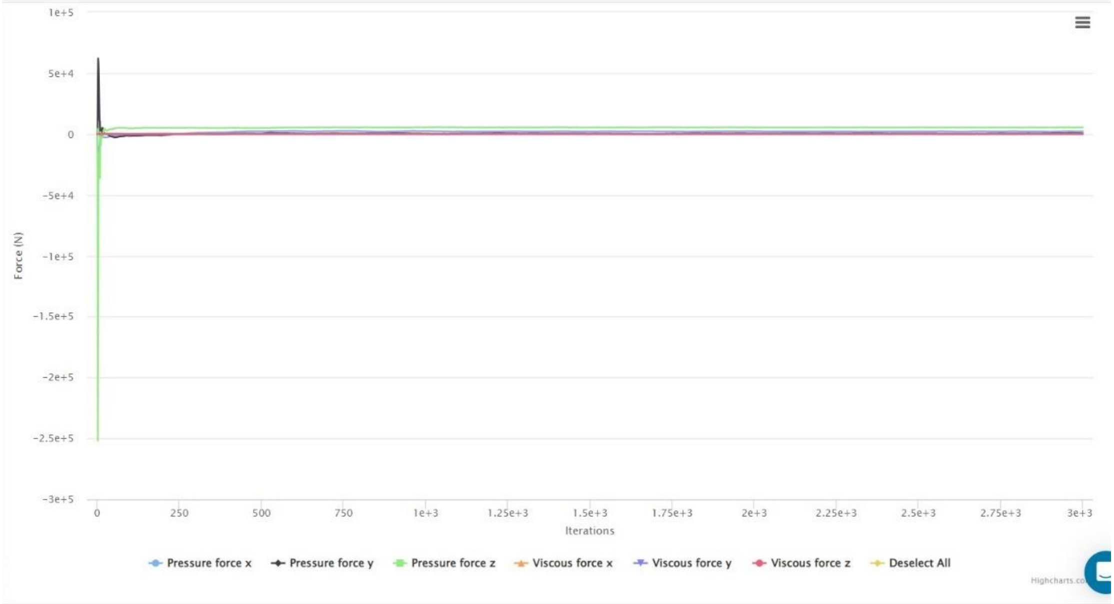

Picture 286 Force of pump LH_2 Simscale program

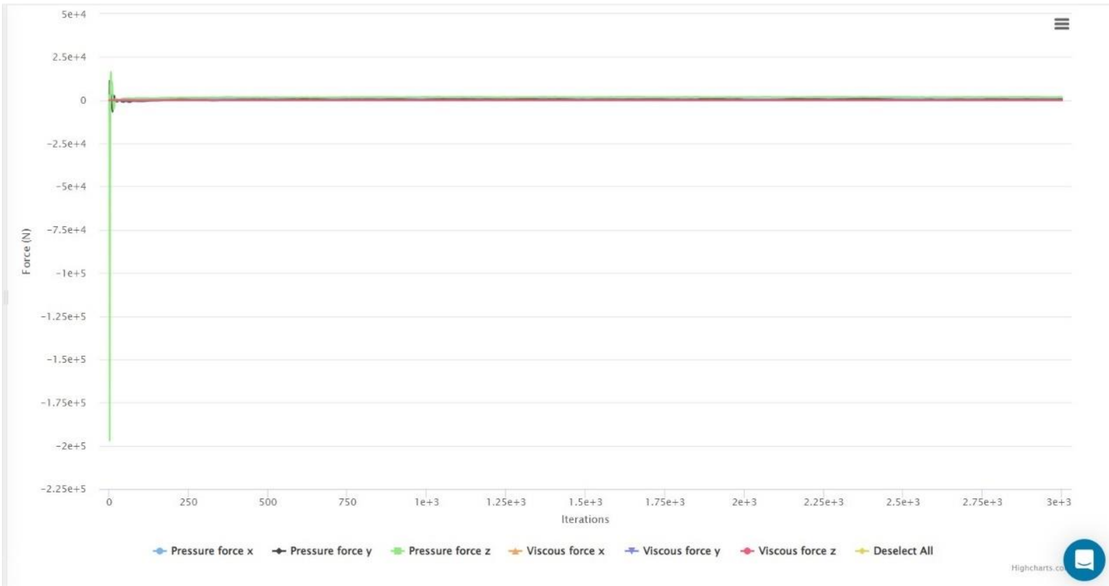

Picture 287 Force of pump LO_2 Simscale program

From the results it is found that the outlet pressure and the pump torque are above the design point. The tables below show the characteristics of the two pumps, the conditions under which they operated and the grid characteristics.

TABLE 1 PUMP TECHNICAL CHARACTERISTICS		
Size	Pump LH_2	Pump LO_2
Inlet pressure (bar)	7	7
Outlet pressure total (bar)	198	124,6
Input Power (MW)	6,25	0,761
Mass flow (Kg/s)	20	64
Volume flow (m3/s)	0,27129	0,05223
Pressure totaldifference (bar)	191,5	117,6
Number of revolutions (rpm)	80000	20000
Hydraulic efficiency (%)	83	80,7

TABLE 2 CHARACTERISTICS OF MESH		
Size	Pump LH_2	Pump LO_2
Minimum (relative to CAD) cell size	0,00001	0,00001
Cell size on surface (relative to CAD)	0,001	0,001
Maximum (relative to CAD) cell size	0,002	0,002
Number of vertices	9726819	8158698
Number of cells	7398816	6221598
Number of volumes	5	5
Number of cell sets	5	5
Number of faces	25037810	21028755
Number of face sets	172	200

The hydraulic efficiency is very large and is very close to the corresponding efficiency curves with respect to the specific speed number nq.

Preferred construction materials are shown in the table below. They are two common materials used to make these pumps. Many examples are cited from NASA reports of the use of these materials.

PUMP	MATERIAL
LH_2	✓ Ti-5AL-2,5Sn
LO_2	✓ Inconel-718

What remains to be designed with more stringent requirements is the material, the canopy and the disk at the back of the impeller in order to be tested in a stressful analysis. This part is not considered in this thesis.

FINAL MODELS

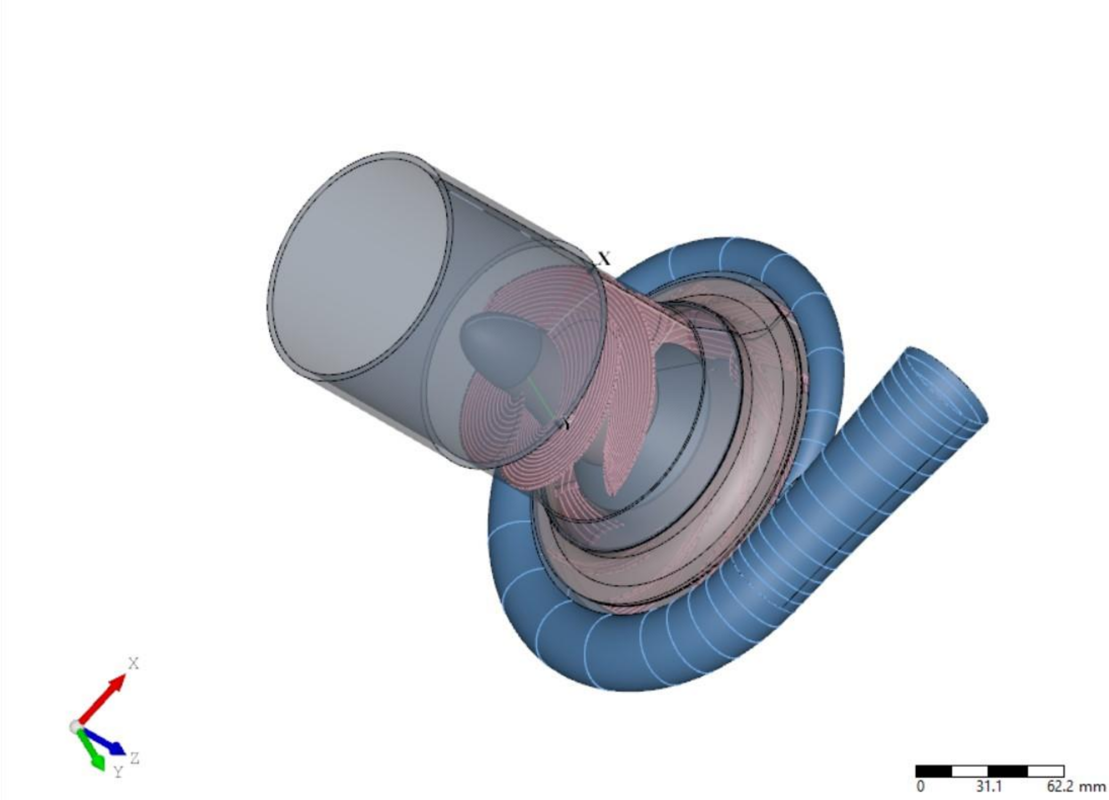

Picture 288 3D-mdel LH_2 CFturbo program

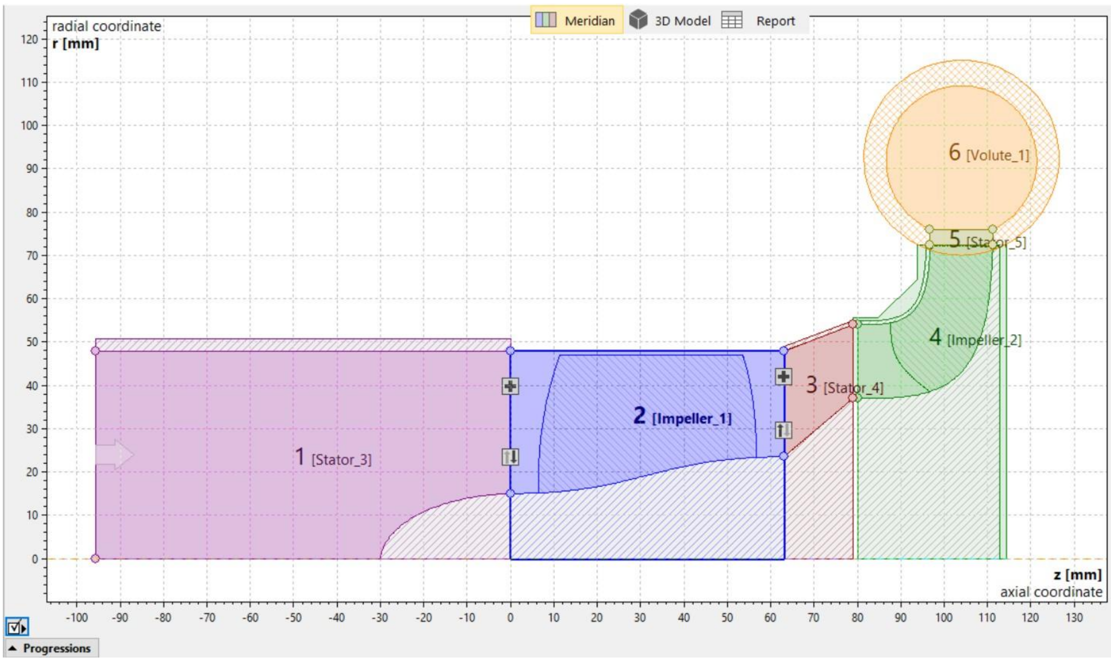

Picture 289 Side view of model LH_2 CFturbo program

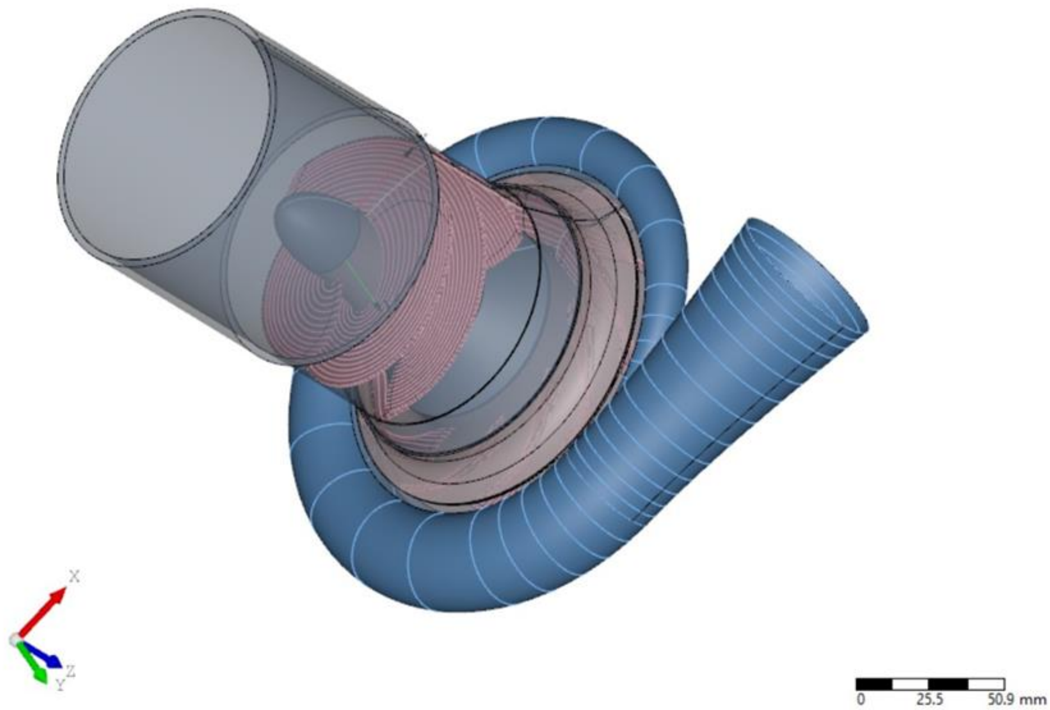

Picture 290 3D-mdel LO_2 CFturbo program

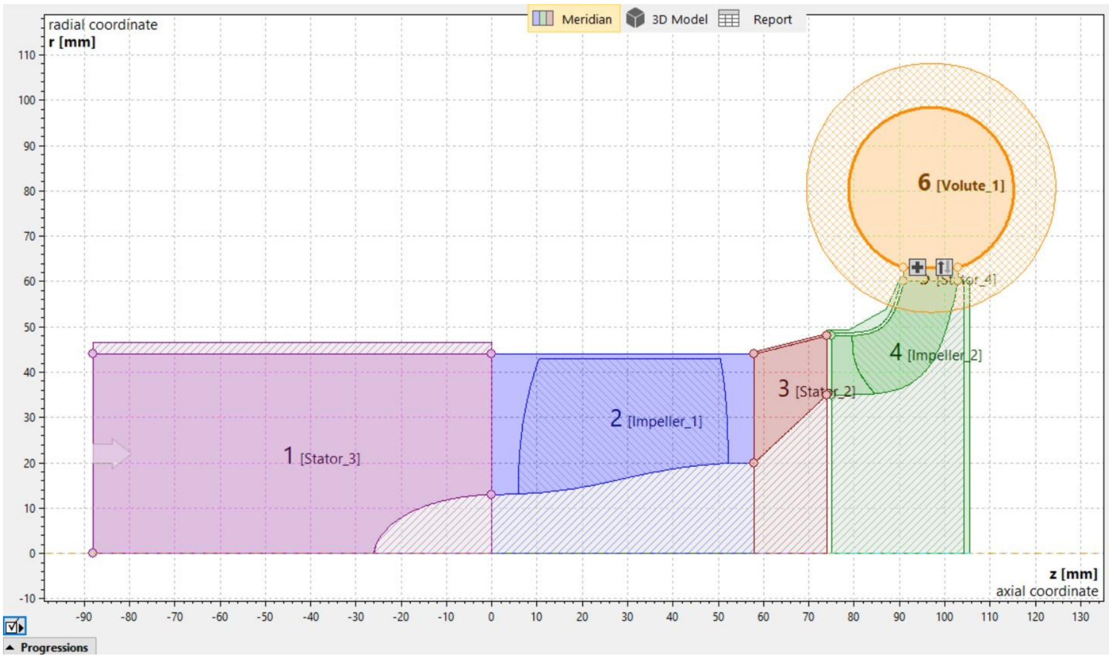

Picture 291 Side view of model LO_2 CFturbo program

Unit 5 Observations and conclusions

The design of the two pumps for liquid hydrogen and liquid oxygen was completed and successfully tested in a simple CFD simulation. If data were available on the cryogenic fluids at that temperature, a more accurate cavitation simulation could be made. However, there is a lot of room for improvement and corrections for the design of the pumps.

- Start designing the pumps with smaller mass flow. Thus, the hydraulic losses are reduced and the flow would be more controlled.

- Set the design point so that the inducer outlet and the impeller inlet intersect geometrically. By itself, there would be no need for the conical rotor with the conical stator which makes the construction more complicated, and brings hydraulic losses

- Design a finned diffuser between the inducer and the impeller so that the fluid that exits from the inducer, is the same as the fluid inlet of the impeller.

- Use different criteria for the design of the impeller such as those based on the inlet angle.

- Use the automatic model of the deviation angle of the inducer, rather than manually.

- Thin the inducer fin at the leading edge. In this way, the flow is smoother, hydraulic losses are reduced and cavitation possibilities are reduced.

In general, the design of a turbopump for both normal and cryogenic rocket engines is very difficult. However, software has been developed with which engineers cannot only design the components very quickly but they can also redesign the entire pump-turbine system if the desired criteria are not met. Nevertheless, the prediction of unstable cavitation has not been fully understood by engineers. Also, there is no universal method to avoid cavitation during design. Therefore, cavitation remains a big problem for engineers, which they try to tackle with advanced design software, with CFD simulations, with real experiments and with their experience.

BIBLIOGRAPHY

[1] A. Dhara, P. M. Kishan, και V. V. Kannah, 'Design of Regenerative Cooled Cryogenic Rocket Engine', v. 29, ed. 10, 2020.

[2] 'F-1 Rocket Engine | National Air and Space Museum'. Access date: 18 July 2024. [Digital edition]. Available at: https://airandspace.si.edu/collection-objects/rocket-engine-liquid-fuel-f-1/nasm_A19700271000

[3] 'Space Launch System RS-25 Core Stage Engine - NASA'. Access date: 22 July 2024. [Digital Edition]. Available at: https://www.nasa.gov/reference/space-launch-system-rs-25-core-stage-engine/

[4] 'What Was the Space Shuttle? (Grades 5-8) - NASA'.Access date: 26 July 2024. [Digital Edition]. Available at: https://www.nasa.gov/learning-resources/for-kids-and-students/what-was-the-space-shuttle-grades-5-8/

[5] 'U.S. military tracking unguided re-entry of large Chinese rocket – Spaceflight Now'. Access date: 19 July 2024. [Digital edition]. Available at: https://spaceflightnow.com/2020/05/09/u-s-military-tracking-large-chinese-rocket-reentry/

[6] 'Pumps and Tanks', Glenn Research Center | NASA.Access date: 28 July 2024. Digital edition]. Available at: https://www1.grc.nasa.gov/historic-facilities/rockets-systems-area/pumps-and-tanks/

[7] 'Rocket Parts', Glenn Research Center | NASA. Access date: 19 July 2024. [Έκδοση σε ψηφιακή μορφή]. Available at: https://www1.grc.nasa.gov/beginners-guide-to-aeronautics/rocket-parts/

[8] A. Ruiz, 'Unsteady Numerical Simulations of Transcritical Turbulent Combustion in Liquid Rocket Engines'.

[9] 'Internal structure of the external space shuttle tank'. Access date: 20 July 2024. [Digital edition]. Available at: https://shellbuckling.com/presentations/nonCylinders/pages/page_85.html

[10] P. Rachov, 'ELECTRIC FEED SYSTEMS FOR LIQUID PROPELLANT ROCKET ENGINES'.

[11] R. Krishnamurthy, 'Turbopumps - A Unique Rotating Machine', GridPro Blog. Access date: 20 July 2024. [Digital edition]. Available at: https://blog.gridpro.com/turbopumps-in-liquid-rocket-engines/

[12] J. Bae, H. D. Kwak, και C. Choi, 'Study on the Mechanical Face Seal Performance for a 7-ton-Class Turbopump', *Tribol. Lubr.*, v. 32, ed. 5, pg. 154–159, July 2016, doi: 10.9725/KSTLE.2016.32.5.154.

[13] 'SSME'. Access date: 20 July 2024. [Digital edition]. Available at: https://www.enginehistory.org/Rockets/SSME/ssme.shtml

[14] 'Dr. Robert H. Goddard, American Rocketry Pioneer - NASA'. Access date: 22 July 2024. [Digital edition]. Available at: https://www.nasa.gov/dr-robert-h-goddard-american-rocketry-pioneer/

[15] 'Turbopumps, a Historical Perspective | Joint Propulsion Conferences'. Access date: 22 July 2024. [Digital edition]. Available at: https://arc.aiaa.org/doi/abs/10.2514/6.2006-5033

[16] R. J. Dalby, 'A4 / V2 Rocket in detail: Turbopump', V2 Rocket History. Access date: 22 July 2024. [Digital edition]. Available at: https://v2rockethistory.com/v2-turbopump-and-walter-hydrogen-peroxide-steam-generator-plant-video-overview/

[17] 'V-2 Rockets and Rocket Motors | Historic Spacecraft'. Access date: 20 July 2024. [Digital edition]. Available at: https://historicspacecraft.com/Rockets_V-2.html

[18] 'The A-4 (V-2) ballistic missile'. Access date: 20 July 2024. [Digital edition]. Available at: https://www.russianspaceweb.com/a4.html

[19] 'Space Program Pumps Up Turbomachinery | NASA Spinoff'. Access date: 20 July 2024. [Digital edition]. Available at: https://spinoff.nasa.gov/Space-Program-Pumps-Up-Turbomachinery

[20] P. Pempie και H. Vernin, 'Multi Purposes Reusable LOX/CH4 Bleed Rocket Engine'.

[21] 'Inducer Design Considerations and its Effect on Turbopump Cavitation | Turbomachinery blog'. Access date: 25 July 2024. [Digital edition]. Available at: https://blog.softinway.com/inducer-design-considerations-and-its-effect-on-turbopump-cavitation/

[22] C. Wang, L. Xiang, Y. Tan, H. Chen, και K. Xu, 'Experimental investigation of thermal effect on cavitation characteristics in a liquid rocket engine turbopump inducer', *Chin. J. Aeronaut.*, v. 34, ed. 8, pg. 48–57, August 2021, doi: 10.1016/j.cja.2021.03.035.

[23] P. Marcalík, L. Zavadil, M. Kozubková, and J. Jablonská, 'Inducer with Variable Pitch', *EPJ Web Conf.*, τ. 269, σ. 01035, 2022, doi: 10.1051/epjconf/202226901035.

[24] C. J. Farquhar, 'Centrifugal Pumps for Rocket Engines'.

[25] 'Turbopump systems for liquid rocket engines'. 1 August 1974. Access date: 21 July 2024. [Digital edition]. Available at: https://ntrs.nasa.gov/citations/19750012398

[26] 'Study on inducer and impeller of a centrifugal pump for a rocket engine turbopump'. Access date: 20 July 2024. [Digital edition]. Available at: https://journals.sagepub.com/doi/epub/10.1177/0954406212449939

[27] J. C. Williams και R. R. Boyer, 'Opportunities and Issues in the Application of Titanium Alloys for Aerospace Components', *Metals*, τ. 10, τχ. 6, σ. 705, May 2020, doi: 10.3390/met10060705.

[28] 'Radial Type Centrifugal Pump Impeller with Overhung Inducer | 3D CAD Model Library | GrabCAD'. Access date: 20 July 2024. [Digital Edition]. Available at: https://grabcad.com/library/radial-type-centrifugal-pump-impeller-with-overhung-inducer-1

[29] 'Volute', Corrosionpedia. Access date: 27 July 2024. [Digital edition]. Available at: https://www.corrosionpedia.com/definition/6933/volute

[30] 'Diffusers - an overview | ScienceDirect Topics'. Access date: 27 July 2024. [Digital edition]. Available at: https://www.sciencedirect.com/topics/engineering/diffusers

[31] H. Lee, E. Jeong, P. Park, S. Yoon, και J. Kim, 'Effect of Shroud Split on the Performance of a Turbopump Turbine Rotor', in *Journal of the Korean Society of Propulsion Engineers*, August 2013, pg. 25–31. doi: 10.6108/KSPE.2013.17.4.025.

[32] J. Min, D. Harris, και J. Ting, 'Advances in Ceramic Matrix Composite Blade Damping Characteristics for Aerospace Turbomachinery Applications', στο *52nd AIAA/ASME/ASCE/AHS/ASC Structures, Structural Dynamics and Materials Conference*, Denver, Colorado: American Institute of Aeronautics and Astronautics, April 2011. doi: 10.2514/6.2011-1784.

[33] 'Common Challenges in Rocket Engine Rotor/Bearing Systems | Turbomachinery blog'. Access date: 20 July 2024. [Digital edition]. Available at: https://blog.softinway.com/common-challenges-in-rocket-engine-rotor-bearing-systems/

[34] 'Turbopump Modeling Software Propels Fluid-Flow Simulations | NASA Spinoff'. Access date: 20 July 2024. [Digital edition]. Available at: https://spinoff.nasa.gov/Spinoff2020/it_7.html

[35] 'Liquid rocket engine turbopump gears'. 1 March 1974. Access date: 23 July 2024. [Digital edition]. Available at: https://ntrs.nasa.gov/citations/19750002094

[36] 'Liquid rocket engine centrifugal flow turbopumps'. 1 December 1973. Access date: 21 July 2024. [Digital edition]. Available at: https://ntrs.nasa.gov/citations/19740020848

[37] 'A Comparison of Different Rocket Engine Cycles Throughout the Years | Turbomachinery blog'. Access date: 20 July 2024. [Digital edition]. Available at: https://blog.softinway.com/a-comparison-of-different-rocket-engine-cycles-throughout-the-years/

[38] D. Thorpe, 'Design of an Expander Cycle Engine with J-2 Equivalent Thrust', στο *45th AIAA/ASME/SAE/ASEE Joint Propulsion Conference & Exhibit*, Denver, Colorado: American Institute of Aeronautics and Astronautics, August 2009. doi: 10.2514/6.2009-4908.

[39] 'Space Shuttle Turbopumps'. Access date: 27 July 2024. [Digital edition]. Available at: https://www.aerospaceonline.com/doc/space-shuttle-turbopumps-0001

[40] ‘SpaceX Raptor – SpaceX | Spaceflight101’.
Access date: 27 Ιούλιος 2024. [Digital edition]. Available at: https://spaceflight101.com/spx/spacex-raptor/
[41] ‘RD-170 engine’. Access date: 20 July 2024. [Digital Edition]. Available at: https://www.russianspaceweb.com/rd170.html
[42] ‘RD-170’. Access date: 27 July 2024. [Digital Edition]. Available at: http://www.astronautix.com/r/rd-170.html
[43] ‘Rocket Engine, Liquid Fuel, H-1 | National Air and Space Museum’. Access date: 20 July 2024. [Digital edition]. Available at https://airandspace.si.edu/collection-objects/rocket-engine-liquid-fuel-h-1/nasm_A19700284000
[44] ‘60 Years Ago: First Launch of a Saturn Rocket - NASA’. Access date: 25 July 2024. [Digital edition]. Available at: https://www.nasa.gov/history/60-years-ago-first-launch-of-a-saturn-rocket/
[45] ‘H1rockengi 010509142633 | Download Free PDF | Rocket Propellant | Combustion’, Scribd. Access date: 27 July 2024. [Digital Edition]. Available at: https://www.scribd.com/document/199392301/H1rockengi-010509142633
[46] J. K. Jakobsen και R. B. Keller, ‘Liquid rocket engine turbopump inducers’. 1 May 1971. Access date: 21 July 2024. [Digital Edition]. Available at: https://ntrs.nasa.gov/citations/19710025474
[47] F. Wislicenus, ‘Preliminary Design of Turbopumps and Related Machinery’.
[48] ‘CFturbo’. Access date: 22 July 2024. [Digital edition]. Available at: https://manual.cfturbo.com/en/index.html?cfturbo.html
[49] G. Nautiyal, ‘Design of Turbopumps’.
Access date: 26 July 2024. [Digital edition]. Available at: https://blog.adtechnology.com/design-of-turbopumps
[50] ‘lecture_26.pdf | Rocket Propulsion | Aeronautics and Astronautics’, MIT OpenCourseWare. Access date: 22 July 2024. [Digital edition]. Available at: https://ocw.mit.edu/courses/16-512-rocket-propulsion-fall-2005/resources/lecture_26/
[51] H. I. Kim, T.-S. Roh, H. Huh, και H. J. Lee, ‘Development of Ultra-Low Specific Speed Centrifugal Pumps Design Method for Small Liquid Rocket Engines’, *Aerospace*, v. 9, ed. 9, pg. 477, August 2022, doi: 10.3390/aerospace9090477.
[52] P. Adhikari, U. Budhathoki, S. R. Timilsina, S. Manandhar, και T. R. Bajracharya, ‘A Study on Developing Pico Propeller Turbine for Low Head Micro Hydropower Plants in Nepal’, *J. Inst. Eng.*, τ. 9, τχ. 1, pg. 36–53, Ιουνίου 2014, doi: 10.3126/ jie.v9i1.10669.
[53] W. Huang, K. Yang, X. Guo, J. Ma, J. Wang, και J. Li, ‘Prediction Method for the Complete Characteristic Curves of a Francis Pump-Turbine’, *Water*, v. 10, ed. 2, pg. 205,
February 2018, doi: 10.3390/w10020205.
[54] V. P. Sompoliński, ‘Alloy 718, 2.4668, UNS N07718, Inconel® 718 - Nickel Alloy’, Virgamet. Access date: 22 July 2024. [Digital Edition]. Available at: https://virgamet.com/alloy-inconel-718-2-4668-n07718-bs2901-na51-ncf718-chn55mbju
[55] Δημήτρη Γ. Παπανίκας (2012). ΡΕΥΣΤΟΔΥΝΑΜΙΚΕΣ ΜΗΧΑΝΕΣ ΣΧΕΔΙΑΣΜΟΣ, ΕΠΙΛΟΓΗ, ΕΓΚΑΤΑΣΤΑΣΕΙΣ : Αντλίες – Ανεμιστήρες – Συμπιεστές – Υδροστρόβιλοι – Ανεμοκινητήρες – Ατμοστρόβιλοι – Αεριοστρόβιλοι – Πυραυλοκινητήρες – Μικρομηχανές – Ειδικές μηχανές ΑΘΗΝΑ: 3η ΕΚΔΟΣΗ

[56] S.L. DIXON / C.A. HALL (2014). Στροβιλομηχανές ΡΕΥΣΤΟΜΗΧΑΝΙΚΗ ΚΑΙ ΘΕΡΜΟΔΥΝΑΜΙΚΗ ΣΤΡΟΒΙΛΟΜΗΧΑΝΩΝ – ΘΕΩΡΙΑ ΚΑΙ ΕΦΑΡΜΟΓΕΣ 7η ΕΚΔΟΣΗ, ΑΘΗΝΑ: FOUNTAS

[57] Luca d’Agosstino, Maria Vittoria Salvetti (2007). Fluid Dynamics of Cavitation and Cavitating Turbopumps. CLSM Courses and Lectures vol.496. New York: Springer Wien

[58] ΓΙΑΝΝΗΣ Δ. ΧΡΥΣΟΥΛΑΚΗΣ , ΔΗΜΗΤΡΗΣ Ι. ΠΑΝΤΕΛΗΣ (2008). ΕΠΙΣΤΗΜΗ ΚΑΙ ΤΕΧΝΟΛΟΓΙΑ ΤΩΝ ΜΕΤΑΛΛΙΚΩΝ ΥΛΙΚΩΝ, 2η ΕΚΔΟΣΗ. ΑΘΗΝΑ : ΠΑΠΑΣΩΤΗΡΙΟΥ